

COLLAPSE BEHAVIOUR OF STEEL COLUMNS IN FIRE

by

Olawale, Aderemi Olayiwola

A thesis submitted to the Department of Civil
and Structural Engineering in partial fulfilment
of the requirements for the Degree of Doctor of
Philosophy.

University of Sheffield.

September, 1988

DEDICATION
To God and my family

ACKNOWLEDGEMENT

The author is indebted to Drs. R.J. Plank and I.W. Burgess who supervised this work for their assistance and support. The support of the computer centre staff is appreciated. I shall like to acknowledge the assistance provided by Professor Hanna in deferring my admission twice before I could secure sponsorship. The author is grateful to the Association of Commonwealth Universities in providing fund and sponsorship for this project.

Finally, the support of God on my family is acknowledged.

SYNOPSIS

The three years' work undertaken in this project is a purely numerical analysis of the inelastic behaviour of steel columns in fire. This is made up of three main parts, each devoted to the development and use of a numerical technique to study the behaviour of steel columns in fire. The first two chapters report on the state of the art on plate analysis, plasticity theories, column behaviour at room temperature, finite strip method and the behaviour of columns at elevated temperature.

Part 1, consisting of Chapters 3 to 5, reports on the development of the small deflection finite strip method which includes the effect of plastification of component plates using deformation theory of plasticity. The validity of the method is tested by comparing with published test data on steel columns at ambient and elevated temperature. The comparisons show that the method gives good correlation with test data. Parametric studies have been carried out to assess the effects of slenderness ratios, different stress-strain-temperature representations, residual stresses, eccentricity of loading and local buckling of columns. In addition the inelastic behaviour of an H-section under uniform end couples is studied.

Part 2, consisting of Chapters 6 and 7, reports on the development of a finite element method which includes the effect of thermal gradients over the member cross-section. The method is compared with test data on both uniformly and non-uniformly heated columns. This shows a good correlation between the method and experiment. Parametric studies have been carried out to assess the effects of initial out-of-straightness, different end conditions, thermal gradients

and interaction of eccentricity of loading with thermal gradients on columns. In addition a simple Shanley's column theory is utilised to demonstrate the interaction effect of eccentricity of loading with thermal gradients on columns.

Part 3, consisting of Chapter 8, reports on the development of a large deflection finite strip method which includes flow theory of plasticity. The method has not been used for any parametric study.

Finally, general conclusions and recommendations for future works are presented in Chapter 9. It is hoped that the valuable information provided in this thesis will be useful in providing a better understanding on the real behaviour of steel columns in fire.

LIST OF FIGURES

- Fig. 2.1 The buckling modes of I-section
- Fig. 2.2 Load-slenderness ratio curve for interaction buckling
- Fig. 2.3a Tresca yield criterion
- Fig. 2.3b Von Mises yield criterion
- Fig. 2.4 Membrane displacement of a strip
- Fig. 2.5 Typical temperature distribution along column length
- Fig. 3.1 A basic plate showing compressive stress, edge forces and displacement system
- Fig. 3.2 Comparison between stress-strain relationships of BS5950 Pt. 8 and present method
- Fig. 3.3 Flow chart for elevated temperature buckling analysis
- Fig. 4.1 Comparison of FSM with Horsley and Strymowicz test results
- Fig. 4.2 Comparison of FSM with column test results of European wide flange shape
- Fig. 4.3 Comparison of FSM with Dibley test results
- Fig. 4.4 Comparison of FSM with Vandamme and Janss test results
- Fig. 4.5 Comparison of FSM with Danish test results
- Fig. 4.6 Comparison of FSM with Aasen test results
- Fig. 4.7 Comparison of FSM with BAM (West Germany) test results
- Fig. 4.8 Comparison of FSM with Hoffend test results
- Fig. 5.1 Variation of critical stress with slenderness ratio at increasing temperature (Ramberg-Osgood with BS5950 expressions)
- Fig. 5.2 Variation of critical stress with temperature

- (Ramberg-Osgood with BS5950 expressions)
- Fig. 5.3 Variation of critical stress (relative to ambient temperature critical stress) with temperature
- Fig. 5.4 Variation of critical temperature with slenderness ratio
- Fig. 5.5 Variation of critical stress with slenderness ratio at increasing temperature (Bilinear with BS5950 expressions)
- Fig. 5.6 Variation of critical stress with temperature (Bilinear with BS5950 expressions)
- Fig. 5.7 Variation of critical stress with slenderness ratio at increasing temperature (Ramberg-Osgood with ECCS expressions)
- Fig. 5.8 Variation of critical stress with temperature (Ramberg-Osgood with ECCS expressions)
- Fig. 5.9 Variation of critical stress with slenderness ratio at increasing temperature (Bilinear with ECCS expressions)
- Fig. 5.10 Variation of critical stress with temperature (Bilinear with ECCS expressions)
- Fig. 5.11 Variation of critical stress with slenderness ratio at increasing temperature (Ramberg-Osgood with CTICM expressions)
- Fig. 5.12 Variation of critical stress with temperature (Ramberg-Osgood with CTICM expressions)
- Fig. 5.13 Variation of critical stress with slenderness ratio at increasing temperature (Bilinear with CTICM expressions)
- Fig. 5.14 Variation of critical stress with temperature

(Bilinear with CTICM expressions)

- Fig. 5.15 Comparison of column response using different strength expressions with Ramberg-Osgood representation
- Fig. 5.16 Comparison of column response using different strength expressions with bilinear representation
- Fig. 5.17 Comparison of column response using Ramberg-Osgood and bilinear representations with different strength property expressions (BS5950, ECCS and CTICM)
- Fig. 5.18 Variation of critical stress with temperature at increasing residual stress
- Fig. 5.19 Variation of critical stress (relative to ambient temperature critical stress) with temperature at different residual stress level
- Fig. 5.20 Variation of critical temperature with slenderness ratio at increasing residual stress
- Fig. 5.21 Variation of critical stress with temperature at increasing eccentricity of loading
- Fig. 5.22 Variation of critical stress (relative to ambient temperature critical stress) with temperature at different eccentricity level
- Fig. 5.23 Variation of critical temperature with slenderness ratio at increasing eccentricity of loading
- Fig. 5.24 Variation of critical stress with wavelength
- Fig. 5.25 Variation of critical stress with temperature for different half wavelength
- Fig. 5.26 Variation of critical temperature with wavelength
- Fig. 5.27 Variation of critical bending stress with slenderness ratio

at increasing temperature

Fig. 5.28 Variation of critical bending stress with temperature

Fig. 5.29 Variation of critical bending stress (relative to ambient temperature critical bending stress) with temperature

Fig. 5.30 Variation of critical temperature with slenderness ratio

Fig. 5.31 Blocked in web column

Fig. 5.32a Variation of critical stress with slenderness ratio for bare and blocked in web columns

at increasing temperature

Fig. 5.32b Variation of critical stress with slenderness ratio for bare and blocked in web columns

at increasing time

Fig. 5.33 Critical stress (relative to ambient temperature critical stress) - temperature relationship for bare and blocked columns

Fig. 5.34 Variation of critical temperature with slenderness ratio for bare and blocked in web columns

Fig. 6.1 Thermal bowing deflection for simply supported beam

Fig. 6.2 Local nodal displacement system

Fig. 6.3 Displacement configuration of the finite element model with thermal bowing superimposed

Fig. 6.4 Comparison between finite strip and finite element methods at ambient temperature

Fig. 6.5 Comparison between finite strip and finite element method at elevated temperature

- Fig. 6.6a Comparison of FEM with Danish test results**
- Fig. 6.6b Comparison of FEM with Belgian test results**
- Fig. 6.7 Comparison of the temperature-deflection characteristics of finite element with Test 3 of Fire Research Station**
- Fig. 6.8 Comparison of the temperature-deflection characteristics of finite element with British Steel test SH/RS/3664/3/83/B**
- Fig. 7.1 Variation of failure stress with temperature at increasing level of initial imperfection**
- Fig. 7.2 Variation of failure stress (relative to ambient temperature failure stress) with temperature at different initial imperfection levels**
- Fig. 7.3 Variation of critical temperature with slenderness ratio at increasing levels of initial imperfection**
- Fig. 7.4 Variation of failure stress with slenderness ratio for different end conditions**
- Fig. 7.5 Variation of failure stress with temperature for different end conditions**
- Fig. 7.6 Variation of failure stress (relative to ambient temperature failure stress) with temperature for fixed end condition**
- Fig. 7.7 Variation of critical temperature with slenderness ratio for different end conditions**
- Fig. 7.8 Failure stress-thermal gradient relationship with maximum temperature set at 500°C**
- Fig. 7.9 Variation of failure stress with slenderness at increasing gradient**

- Fig. 7.10** Variation of failure stress with centre line temperature at increasing thermal gradient
- Fig. 7.11** Variation of failure stress with maximum temperature
- Fig. 7.12** Load-eccentricity of loading relationship with thermal gradient
- Fig. 7.13** Load-eccentricity of loading relationship at increasing thermal gradient
- Fig. 7.14** Shanley column model with thermal gradient
- Fig. 7.15** Average stress-deflection relationship with thermal gradient and eccentricity of loading

NOTATION

b	Strip width
b_r, b_r^t	Width and transformed width of a plate region respectively
l	Length of the beam element
l_r	Plate region length
q_i	Displacement parameters
$\{\Delta r\}$	Assembled vector of incremental nodal displacement
t	Strip thickness
t_k	Plate segment thickness
A^t	Transformed area
E_{20}, E_θ	Young's and effective moduli respectively
$E_s, E_s(\theta)$	Secant moduli at ambient and elevated temperature respectively
$E_t, E_t(\theta)$	Tangent moduli at ambient and elevated temperature respectively
$[F]$	Elastic and elasto-plastic matrix
J_2	Von Mises yield condition(stress tensor)
$[K_i]$	In-plane stiffness matrix for a strip
$[K_o]$	Out-of-plane stiffness matrix for a strip
$[K_T]_G$	Element tangential stiffness matrix
$[K_T]$	Assembled tangential stiffness matrix
M, M^*, N	Stress resultants
M_e, M_i	External and internal moment
P, P_1, P_2, P_t	Axial and tangent loads

$\{Q\}$	External load vector
$\{\Delta R_e\}_G$	Element unbalanced force vector
$\{\Delta R\}$	Assembled unbalanced force vector
$[S_i]$	In-plane stability matrix for a strip
$[S_o]$	Out-of-plane stability matrix for a strip
S_{ij}	Deviatoric stress vector
U, V, W	Displacement functions for a strip
U_o, V_o	Displacement functions relative to reference axes for a beam element
Z_c	Distance from the centroid of a section
$\{\chi\}$	Curvature
$\{\chi_i\}$	Displacement variables
κ	Column end rotation
γ	Orientation of the cartesian coordinate relative to global system
α	Coefficient of thermal expansion
θ	Temperature variable
λ	Length of a strip
ϵ_x	Total axial strain
ϵ_i, ϵ_o	In-plane and out-of-plane strain vectors
$\epsilon_{bi}, \epsilon_{bo}$	In-plane and out-of-plane membrane strain vectors
ϵ_{ij}	Total strain vector
ϵ_{ij}^e	Elastic strain vector
ϵ_{ij}^p	Plastic strain vector
ϵ_{ij}^t	Thermal strain vector

σ_e	Von Mises effective stress
σ_{ii}	Hydrostatic stress
σ_{ij}	Stress vector
$\sigma_{y,20}, \sigma_{y\theta}$	Yield stress and effective stress
σ_z	Total axial stress
δ_i, δ_o	In-plane and out-of-plane displacement parameters for a strip
δ_{ij}	Kronecker delta

Contents

1	INTRODUCTION	2
2	LITERATURE REVIEW	6
2.1	Plate Buckling Review	6
2.1.1	Historical Background	6
2.1.2	Plate Buckling Behaviour	8
2.2	Column Buckling At Ambient Temperature	13
2.3	Theory Of Plasticity Review	20
2.4	Finite Strip Method	27
2.5	Column Buckling At Elevated Temperature	32
3	FINITE STRIP METHOD	44

3.1	Theoretical Basis Of Finite Strip Method	44
3.2	Extension To Elevated Temperature Structural Response . . .	53
3.3	Computer Program	54
3.3.1	The Substrip Total Stress	55
3.3.2	The Nonlinear Material Properties	56
3.3.3	The Strip Stiffness Matrix	56
3.3.4	The Strip Stability Matrix	57
3.3.5	Impose Boundary Condition	57
3.3.6	Transformation and Assembly of the Global Matrix and Solution	58
4	COMPARISON WITH TEST DATA	59
4.1	Ambient Temperature Comparison	59
4.2	Elevated Temperature Comparison	62
5	PARAMETRIC STUDIES	67
5.1	Effect of slenderness ratio	69
5.2	Effect of stress-strain relationships	72

5.2.1	Comparison between bilinear and continuous stress-strain-temperature representation(BS5950)	74
5.2.2	Comparison between bilinear and continuous stress-strain-temperature representation(ECCS)	76
5.2.3	Comparison between bilinear and continuous stress-strain-temperature representations(CTICM)	78
5.2.4	Comparison between different continuous stress-strain-temperature representations	79
5.2.5	Comparison between different bilinear stress-strain-temperature representations	80
5.2.6	Summary of comparisons	81
5.3	Effect of residual stress	82
5.4	Effect of eccentricity of loading	85
5.5	Effect of local buckling phenomenon	88
5.6	Sections under uniform bending	90
5.7	Behaviour of blocked in web columns	92

6 THE EFFECT OF THERMAL GRADIENT ON STEEL COLUMNS

6.1	Theoretical Development Of The Finite Element Method . . .	98
6.1.1	Evaluation Of Tangential Stiffness $(K_T)_{ij}$	111
6.1.2	Evaluation of the incremental stress resultant vector for the inelastic element	114
6.2	Validation Of The Finite Element Method	115
7	PARAMETRIC STUDIES	119
7.1	Effect of initial out-of-straightness	120
7.2	Effect of different end conditions	123
7.3	Effect of thermal gradient	125
7.4	Effect of eccentricity of loading with thermal gradient	127
7.5	The Shanley column model	129
8	NONLINEAR ANALYSIS OF PLATE USING FLOW THE- ORY OF PLASTICITY	136
9	CONCLUSIONS AND RECOMMENDATIONS	150
9.1	Scope of the work	150
9.1.1	Uniformly heated columns	151

9.1.2 Columns under thermal gradients	154
9.2 Recommendations for future work	155
BIBLIOGRAPHY	157
Appendix A	177
Appendix B	181
Appendix C	186

Chapter 1

INTRODUCTION

The effect of fire on structural steel is quite detrimental to its performance in that it loses strength and stiffness with increasing temperature. This leads to collapse when its stiffness and material properties have degraded to such an extent that the steelwork is unable to support the applied load. The temperature at which such collapse occurs can be referred to as the failure temperature. This is often assumed to be about 550°C for the purpose of design. Since this temperature is very quickly reached in a standard fire it has major implications for fire protection requirements as incorporated in many building regulations. Thus in order to prevent the rapid decline in stiffness and strength some form of fire protection in the form of insulation to the steelwork is often utilised. This ensures a reduced rate of temperature increase and hence the fire resistance of the steelwork, that is the time to collapse, is improved. However, the application of fire protection increases the cost of construction. According to one survey carried out by the British Steel Corporation on multi-storey

steel frames the increase in construction cost can be about 30%. Despite this the provision of protection is often based on a simplified approach which fails to take into account the real behaviour of steelwork in fire. It may be that columns under different conditions will exhibit different failure temperatures. If this is so the type and quantity of protection needed should reflect these factors in order to ensure economy.

Fire protection materials are often applied to cover the whole surface area of the steelwork. However, some forms of construction offer partial protection to the steelwork. These include steel beams supporting a concrete slab which provides protection to the top flanges of the beams, shelf angle floor construction, columns built into masonry walls and blocked in web columns, where the blockwork is provided specifically to give partial protection to the steelwork. It has been established experimentally that such forms of construction result in a temperature gradient over the member cross-sections and hence sustain applied load for longer periods of time.

It is highly desirable for more work to be done experimentally to establish the behaviour of steel columns under various conditions in fire. Unfortunately this cannot be readily accomplished. This is due to the high cost and time involved in full-scale fire resistance tests and the scarcity of suitable facilities. In United Kingdom, for example, the only furnace available for testing columns is at Fire Insurer Research and Testing Organisation (FIRTO). This is basically a vertical cylinder with natural gas burners in both vertically-split halves. This cannot be used without modifications for eccentric loading or non-uniform heating tests on columns.

Because of the problems of an expensive experimental investigation there is clearly a role for numerical and analytical studies to be employed to provide data at relatively low cost. Thus the present study is a purely numerical investigation of steel column behaviour in fire. The possibility of including many parameters in theoretical studies enables ~~an~~ extensive parametric studies to be undertaken with relative ease. However, as with any theoretical approach it is necessary to validate the method with available test data. Hence the work is compared wherever possible with published results.

OBJECTIVES AND SCOPE

The scope of this research is divided into three main parts. The first is concerned with the development and use of a finite strip method for elevated temperature structural analysis. Small deflection theory is used with deformation theory of plasticity applied. The uniaxial stress-strain-temperature representation is modelled as a series of continuous curves. The method is then used for parametric studies on the inelastic behaviour of steel columns in fire. The second phase involves the development of a finite element method capable of handling thermal gradients across the section. The original development of this approach was meant for ambient temperature ultimate strength analysis of multi-storey steel frames. Extensive remodelling of the method has been necessary in order to include thermal gradients. This is subsequently used for some parametric studies on the inelastic behaviour of steel columns. The final part involves a large deflection finite strip method in which flow theory of plasticity is utilised with von Mises's yield criterion incorporated. This has not been used for any parametric studies as some further work is needed to fully establish it.

The parametric studies include consideration of slenderness ratio, different stress-strain-temperature representations, residual stress, eccentricity of loading, local buckling, initial out-of-straightness, thermal gradient, interaction of eccentricity of loading with thermal gradient and different end conditions. In addition the behaviour of blocked in web columns and sections under uniform end couples are studied.

The information generated represents a step forward towards the development of an improved fire engineering system. Up to the present moment only a little research has been done to study the inelastic behaviour of columns in fire. Thus this research will provide some valuable information that may be of use in this context.

Chapter 2

LITERATURE REVIEW

2.1 Plate Buckling Review

2.1.1 Historical Background

The first work on plate buckling analysis dates back to 1766 when Euler[1] formulated the first mathematical theory of plates based on the analogy of two systems of stretched strings perpendicular to each other. His work included the vibrational problem of rectangular and circular membranes. Bernoulli[2] in 1789 employed a grid work analogy to develop the partial differential equation governing the small deflections. This was an extension to Euler's analogy for plates. Between 1811 and 1820 Lagrange and Navier arrived at the correct partial differential equation for the small deflections of an isotropic plate under surface load. Saint Venant(1833) included the in-plane forces applied

at the edges to complement Navier and Lagrange's work. In 1891 a simply supported plate was analysed by Bryan[3]. He subjected the plate to in-plane compressive load. The energy criterion of stability was first applied to the solution of the plate buckling problem. By 1907, Timoshenko[4] had determined the critical stresses of plates with different support conditions using Bryan's approach. Reissner (1909)[6] independently presented the solution for an edge - compressed rectangular plate with two edges clamped, one edge clamped and the other one free. Between 1910 and 1913 Timoshenko[5] applied the ideas of Rayleigh and Ritz to the stability problems and thus solved a stiffened plate problem for the first time. Bleich[7] in 1924 extended the theory of plate stability to include inelastic considerations by accounting for anisotropy of a plate with varying modulus of elasticity. This approach constitutes an elastic theory with varying modulus. Between 1935 and 1946 Krollbrunner[8] tested large scale plates under edge compression. The buckling behaviour of plates was investigated in both elastic and inelastic ranges. The development of the large deflection theory of plates was initiated by Kirchhoff in 1877. Foppl (1907)[9] introduced the use of stress functions to simplify the form of the governing differential equation. Von Karman (1910)[22] for the first time established the partial differential equation of the large deflections in its current form. Marguerre in 1910 extended von Karman's equations to include initial deflection.

2.1.2 Plate Buckling Behaviour

The evaluation of the critical buckling stresses of a plate has been attempted by many researchers as documented by Timoshenko and Gere (1960)[10], Bulson (1970)[11] and Allen and Bulson (1980)[12].

Solutions for plates under transverse loading have been obtained by many researchers, among them Kaiser[13] who obtained the finite difference solution for a simply supported plate under transverse pressure. The same problem was solved by Way[14] with slightly more complexity in the boundary conditions. Levy[15] attempted to obtain a more general solution for a rectangular plate under in-plane loading using a double Fourier series with restricted boundary conditions.

Most of the early work on the investigation of plate behaviour neglected the effect of membrane forces due to bending. Thus these analyses were limited to bending stiffness reduction due to the in-plane stress. The effect of combinations of loading on the plate behaviour was studied by Levy[18] by extending his method to include the combination of lateral pressure and in-plane compression. This method was later extended further by Woolley et al[19] in studying the behaviour of a clamped long rectangular plate under lateral in-plane compression. The incapability of the Timoshenko[20] method to allow for the effect of the in-plane boundary conditions has placed restrictions on the approach of approximate solution for combined loading using Fourier series. Bleich[21] extended plate theory to include the effect of pressure by deriving a cubic equation in terms of plate deflections and transverse pressure.

The application of large deflection theory to analyse plates was first undertaken by Wang[16]. Later Basu and Chapman[17] extended Wang's method to obtain large deflection solution for a wide range of isotropic plates. The inclusion of initial imperfections in the large deflection analysis of plate has been undertaken by many researchers. The early work includes von Karman's [22] in which some sets of equations were developed. These equations were generalised by Marguerre[23] to allow the inclusion of initial imperfections. In 1946 Hu et al[24] extended Levy's method for plates under compression to include initial imperfections and Coan[25], using the same approach, combined different forms of applied compression with the unloaded edges allowed to distort. Yamaki [26] obtained solutions for rectangular plates with clamped or simply supported edges and provided data for the ultimate loads of square plates by defining the yield limit. In 1963 Bauer and Reiss[27] transformed the von Karman equations into two simultaneous pairs. These equations were solved using a finite difference scheme to provide information on the postbuckling behaviour of plates under in-plane compression.

The arrival of digital computers led to a breakthrough in the analysis of plates. This led to the advancement and development of many numerical methods such as finite element, dynamic relaxation and recently the finite strip method. The finite element method has been widely applied to obtain elastic and inelastic solutions for plates[28][29][30][31]. This is a general solution method which has no restrictions on the mode of buckling but is approximate in the sense that it is based on assumed displacement functions.

In order to simulate sophisticated plate behaviour, many parameters have to be

accounted for, such as the large deflection behaviour, spread of yield through the volume of plate, the inclusion of both the initial geometric imperfection and residual stresses. An ultimate strength analysis would provide designers with a more efficient design analysis than elastic post buckling analysis.

The ultimate strength of plates has been widely studied both experimentally and numerically. Since 1960 a comprehensive study on the ultimate strength of plates has been carried out at Cambridge University[32][33][34][35][36][37] and also at Imperial College[38][39]. The theoretical studies of elasto-plastic large-deflection buckling and post-buckling behaviour of plates have received attention from many researchers. In Imperial college Frieze et al[38] and Harding[39] have used the dynamic relaxation method to analyse an isolated plate in the elasto-plastic range using flow theory of plasticity. In the two studies undertaken the major differences have been in the loading, yield criterion and representation of residual stresses. Frieze et al[38] studied the plate under uniaxial and biaxial compression with the Ilyushin criterion of a single-layer of sudden plastification at any section occurring over the full depth. Uniaxial residual stress was taken into account. Harding et al[39] considered complex loading such as compression, shear and in-plane bending. The plate thickness was divided into layers with the von Mises yield criterion applied to each layer. Biaxial residual stresses were included. Many researchers have applied the Rayleigh-Ritz energy method to analyse the compressive strength of plates with simply supported boundary condition and both residual stresses and initial imperfection have been taken into account. Little[40] applied a live energy method to analyse accurately the collapse behaviour of simply supported rectangular plates loaded uniaxially or biaxially (in-plane). He used

the flow theory of plasticity which allows for elastic unloading. The effects of residual stresses and initial imperfections were considered. This approach was later applied to analyse 960 different simply supported rectangular plates under longitudinal compression[41]. The actual plate panels of a box-girder bridge were modelled by carefully controlling the transverse displacement function, the longitudinal in-plane boundary conditions and the aspect ratio. It was concluded that the critical aspect ratio for a simply supported plate in the inelastic range is not unity as suggested by the classical elastic buckling analysis. In most cases the minimum plate strength was shown to occur at an aspect ratio of 0.6 while Dwight[33] suggested a critical aspect ratio of 0.875. Little suggested that this disparity was due to small initial imperfections and limited boundary conditions used by Dwight[33] (i.e the unloaded edge was free to pull in). Little[41] concluded that the maximum effect of the longitudinal boundary conditions on the plate strength was less than 7 %. Crisfield[42] applied the finite element method to analyse the collapse behaviour of plates. In his analysis two approaches were considered viz: the volume and area approaches. The volume approach was based on the flow theory of plasticity with von Mises yield criterion applied. The area approach was based on the use of the approximate yield criterion given by Ilyushin[43] which relates to the six generalised stress resultants in a shell with sudden plastification of the plate section. The area approach is much economical but less accurate than the volume approach. In his later work[44] Crisfield modified the area approach to allow for the spread of yield through the fibres before full plastification of the section sets in. A detailed review of plasticity theory is presented in a later section 2.3.

In the present decade more sophisticated work has been undertaken on the analysis of plates. Among this Kaldas and Dickinson[45] applied the finite difference method to predict the in-plane residual stresses induced by welding heat. The plate's critical stress was determined using the Rayleigh-Ritz energy approach. Dow and Smith[46] studied extensively the effect of localised initial imperfections on the compressive strength of long rectangular plates using a general purpose finite element package in which large-displacement effects are handled using an updated Lagrangian formulation. The plasticity effect is represented by assuming the von Mises yield criterion and the associative Prandtl-Reuss flow rule. Bradfield and Stonor[47] applied a simplified elasto-plastic approach to predict load-shortening characteristics of plates under uniaxial in-plane compression. The Ilyushin yield criterion was applied to set the limiting condition on the plate response. In this approach both the initial imperfection and welding induced residual stresses were accounted for. This method compared favourably with many numerical methods and test data. Dawe and Grondin[48] investigated the inelastic buckling of plates experimentally by simulating simply supported web and flange outstands. In their investigation four sets of inelastic material properties were examined. The unsatisfactory behaviour of plates with these material properties led to the development of a new set of semi-empirical material properties which resulted in accurate prediction of inelastic plate behaviour.

Voyiadjis et al[49] investigated the effect of transverse shear strain on the plate behaviour. The governing differential bending equations of a plate were recast into the form involving the average transverse displacement function to account for the influence of transverse normal strain. The resulting sixth order

differential equations were solved using the Levy type of plate with various boundary conditions considered in the direction orthogonal to the simply supported direction. Very recently Mahendran and Murray[50] studied the elastic response of plates under complex loading (compression, bending and shear) using the finite strip method. Although this work is limited to elastic response, an insight into the effect of combination of loading could be gained. Gradzki and Kowal-Michalska[51] also studied the post-buckling behaviour of plates using the Raleigh-Ritz variational principle with the flow theory of plasticity. The von Mises effective stress was used as a proportional limit. The ultimate load of the plate was determined as the the load at which the load-shortening curve reaches a maximum or has a long plateau.

Inelastic analysis of plates has become very popular with many researchers. The material nonlinearity is given preference to the elastic nonlinear analysis. Effort has been directed towards combinations of elasto-plastic material response with the large displacement theory. This ensures better representation of the plate constitutive equations for studying its behaviour.

2.2 Column Buckling At Ambient Temperature

Historically, the first work on metal columns dates back to 1729 and 1759 when Euler published his treatise on the elastic buckling of columns. For the critical load of a perfect column in the inelastic range, two well-known formulae have been proposed. The tangent modulus theory known as Engesser theory and

the reduced or double modulus theory known as the Considere-Engesser theory. The reduced modulus theory provided the basis for the column buckling concepts in the inelastic range.

The reduced modulus theory had been accepted as the correct buckling theory for columns in the inelastic range for many years. It was in 1947 when Shanley [52] reported that the buckling load of a centrally loaded column was actually the tangent modulus load. He pointed out for a simplified column that bending will begin as soon as the tangent-modulus load is exceeded and that the maximum column load will be reached at a load less than reduced-modulus load. This concept has since been investigated by many researchers.

The buckling mode of a steel column can be of the local, interactive or overall type as shown in Fig. 2.1. The critical mode depends on the geometry of the cross-section, slenderness ratio, the geometric initial imperfection, residual stresses and the eccentricity of loading. The local buckling effect may cause premature overall buckling in thin-walled sections, while on the other hand failure might be delayed beyond the local buckling load. This phenomenon is usually common for column sections whose component plates have large width-thickness ratio and small slenderness ratio. It is usually assumed that the cross-section of a structural member buckling in the overall mode remains undistorted. The interactive buckling mode involves distortion in both local and overall modes. This is critical for structural elements of intermediate length with large width-thickness ratio of their component plates. Fig. 2.2 shows the various buckling modes associated with columns.

Bijlaard and Fisher[53] were the first to study the behaviour of I-sections

and hollow-sections in the post-local buckling range. They tested aluminium columns which had minimal initial geometric imperfection and found that these columns buckled in a flexural mode at a load higher than the local buckling load when this load is less than the Euler buckling load. Since then a considerable amount of work has been reported on the stability problem of columns. Theoretical and experimental investigations have been carried out on members with different cross-sections. Most of this work is limited to the elastic response of the component plates using small deflection theory.

Locally buckled column behaviour has attracted the attention of many researchers over the past four decades and an appreciable amount of attention has been given to the numerical study of this problem. These approaches can be classified into three categories. The first approach is the treatment of the problem as a pure bifurcation problem in which both the member and its component plate elements are assumed to be perfectly straight and flat respectively. The interaction strength (i.e incipient buckling strength) is determined using the theory of plasticity applied to thin plates with residual stress accounted for. The second approach focuses on the postbuckling strength of the component plate elements with or without initial out-of-flatness, while the member itself is assumed to be perfectly straight. The interaction strength is computed from linear buckling theory with the decrease in flexural rigidity due to local buckling accounted for. The third approach is supposed to take both initial plate out-of-flatness and the member initial out-of-straightness into account.

Cherry[54] studied the elastic instability of beams and proposed an approxi-

mate method which is applicable to those sections in which the compression flanges alone have buckled. The webs are assumed to be undistorted. The effective width concept was applied in order to account for the post-buckling behaviour of flanges. The theoretical approach was compared with test data on H-sections and T-sections under pure end couples. The 30% overestimation of the test data by the theory was claimed to be the result of excluding geometric initial imperfections. The test results of initially imperfect columns reported by Skaloud and Zornerova[55] demonstrated the significance of the initial imperfection on column behaviour. Goldberg et al [56] reported more sophisticated buckling analysis using the elastic small deflection theory for members of arbitrary cross-section geometry. This approach enables the coupling of membrane and plate bending equations leading to eight first order partial differential equations. The critical load corresponds to the point of vanishing of the determinant of these equations and is obtained by an iteration scheme.

For a column with initial geometric imperfections in the plate elements forming the column section, the bifurcation load for overall buckling may be significantly less than the Euler or local buckling loads. DeWolf et al [57] reported the tests performed at Cornell University on steel I-columns fabricated by connecting cold-formed channels back to back. These columns had plate imperfections and buckled at loads lower than the Euler and local buckling loads when these loads were approximately equal. These test data are useful for the estimation of the effect of the local buckling phenomenon on the overall buckling of columns. An analytical iterative approach for the interactive buckling of rectangular box columns was developed. This method is based on the tangent

modulus and effective width concepts. Kalyanaraman et al[58] also reported the test results on cold-formed inverted hat section and H-columns. Based on these test data an empirical model, using the Winter[59][60] effective width concept, was developed, which approximates the post-buckled stiffness of plate elements. Kalyanaraman[61] also applied the Stowell[62] plasticity index approach to develop an analytical procedure for calculating the local buckling coefficients of the members with stiffened and unstiffened compression elements of cold-formed steel sections. Gale and Pekoz[63] investigated analytically the effect of local buckling on the overall buckling behaviour of singly symmetric thin-walled columns and beam-columns. Tsutomu and Fukumoto [64] investigated the behaviour of welded box compression members experimentally. An effective width approach was developed which proves satisfactory in predicting the behaviour of locally buckled welded box columns with relatively large width-thickness ratio but not those with low width-thickness ratio elements. The reason for this shortfall is attributable to the non-inclusion of the residual stresses induced by welding heat in the model. More recently, Gale and Pekoz[65] reported an experimental investigation conducted on the local buckling interaction in cold-formed steel columns. The interaction between stiffened elements and unstiffened elements and between stiffened and edge-stiffened elements was carefully examined. It was concluded that the effective section that was generally applicable to thin-walled stub columns in which local buckling interaction occurs is not adequate because of the waving exhibited by the unstiffened flanges.

Lee et al[66] applied a moment-curvature-thrust relationship to predict the strength of thin-walled welded steel columns subjected to a combination of

axial load and end moments. Twenty small scale steel box columns were tested. The test results compared favourably with the theory. The theoretical method incorporates the local plate buckling and residual stresses. Longhlan and Howe[67] developed a semi-energy method of analysis for columns. The appropriate differential equation which describes the overall flexural equilibrium behaviour of a locally buckled compression member was included in the method. The method could only be applied to pinned columns.

Many analytical investigations on columns in both the pre-buckling and post-buckling ranges can be found in the literature. Among these are the finite element, finite difference and finite strip methods. The finite strip method has been applied to the study of the behaviour of columns. Yoshida and Maegawa[68] studied the behaviour of H-columns in local, overall and interactive modes. The deformation theory of plasticity based on von Mises yield criterion and small deflection theory was employed. The effect of residual stresses was taken into account. Hancock[69][70] extended the finite strip approach to the post-buckling range and proposed a method for calculating the effective rigidity of locally imperfect box and H-sections. The method estimates satisfactorily the effective rigidity of a box section when compared with the effective width approach. Using the proposed flexural rigidity the interactive buckling loads of H-columns could be obtained. The theoretical results compared very well with Cornell test data. Graves-Smith [71][72][73] developed a numerical method to predict the ultimate strength of locally buckled rectangular hollow cross-sections under concentric compression or pure bending. Strain reversal was not included, thus the column length must be chosen such that elastic local buckling is ensured. Later this method was modified by including an extra

nonlinear transverse in-plane term in the strain expressions. This enables the elastic limit state to be reached and compatibility at the corner is ensured. The theory compared reasonably with test data on silicone rubber columns. He concluded that the ratio of maximum stress to the critical stress is linearly related to the width-thickness ratio. Little[74] applied a moment-curvature-thrust approach to study the ultimate strength of square box columns. The local buckling of the flange was allowed for by applying an appropriate average stress-strain curve to the moment-curvature-thrust relation. Two cases of web behaviour were assumed. The first treatment assumed an unbuckled web (which was treated simply as elastic-perfectly plastic material) and the second a buckled web (which was treated by using an appropriate average stress-strain curve). No attempt was made to allow for strain reversal.

In the past few years effort has been directed towards the study of the interactive buckling analysis of columns. Srinivasan and Ashraf [75] developed a new analytical model for doubly symmetric beam-columns. This model incorporates the interaction of overall buckling and bending with two companion local modes. The concept of amplitude modulation was applied together with the combination of finite strip and finite element methods. Rafeal and Sridharan[76] also reported an approach which combines finite strip with the theory of mode interaction to study the interactive buckling mode of some open cross-sections. Recently, Hancock and David[77] reported tests conducted on thin-walled high strength steel columns. These tests were primarily carried out in order to establish column curves which allow for local and Euler buckling interaction. The test results were compared with various column curves from different sources. Among them are BS5950 Pt1[78], AISI[79] and the

Australian standard[80]. The conservative estimation of I-column strength by BS5950 Pt1 was highlighted.

2.3 Theory Of Plasticity Review

Tresca was the first person to study the plastic behaviour of materials in 1864 by conducting an experiment on the punching and extrusion of metal, which led to conclusion that metal yielded plastically when the shear stress attained a critical value. From then on considerable work was done by many researchers, among them Saint-Venant and Levy. Later, many yield criteria were proposed, but the most significant was the von Mises yield condition in 1913. This yield criterion was deduced purely by mathematical considerations. This was later interpreted by Hencky as implying that yielding occurred when the elastic shear strain energy reached a critical value. Von Mises also independently proposed an equation similar to Levy's equation. It was between 1920 and 1921 that Prandtl showed that the two-dimensional plastic problem is hyperbolic in nature and Hencky supplied the general theory underlying Prandtl's special solution. In 1926 Lode experimentally investigated the Levy-Mises equation by measuring the deformation of tubes of various metals under combined tension and internal pressure. This confirmed the validity of the Levy-Mises stress-strain relation to a first approximation. The generalisation of this theory of plasticity was made by Reuss in 1930 by including the elastic component of strain following the earlier suggestion of Prandtl. Later, the concept of strain hardening was introduced by Schmidt(1932) and Odquist(1933). Experimental confirmations of the Levy-Mises equations have

been undertaken by many researchers. Among them were Hohenemser(1931-1932) and Schmidl. By 1932 a theory had been constructed reproducing the plastic and elastic properties of an isotropic metal at ambient temperature. This theory is known as flow or incremental theory of plasticity.

In 1924 Hencky proposed a rival theory which received attention from scientists for its analytical simplicity in problems where plastic strain is small. Nadai(1931) established this theory firmly and afterward many researchers employed it. This is known as the deformation theory of plasticity. A detailed account of the historical development of the both theories of plasticity can be found in reference [81].

The use of a yield criterion is inevitable in the application of the theory of plasticity to structural analysis. The two prominent yield criteria are Tresca's and von Mises' yield conditions. For a uniaxial state of stress either in tension or compression, the yield condition for most metal is given by:

$$\sigma = \pm\sigma_y \tag{2.1}$$

in which σ_y is the yield strength. In a multiaxial state of stress the yield criterion can be represented by either Tresca's or von Mises' yield condition.

Tresca's yield criterion states that the greatest absolute value of the differences between the principal stresses taken in pairs must be equal to twice the value of the critical shearing stress. Mathematically , this can be expressed as

$$\sigma_1 - \sigma_2 = 2k \tag{2.2}$$

where σ_1, σ_2 and σ_3 are the principal stresses, k is the critical value of the greatest shearing stress and $\sigma_1 > \sigma_2 > \sigma_3$. This relation is a straight line perpendicular to the bisector of the boundaries of the region. Each of the five other possible orders of principal stress magnitude gives a similar line in the appropriate sector of the π -plane (in which the sum of the principal stresses is zero) and the final result is the regular hexagonal prism in principal stress space as shown in Fig. 2.3a

Von Mises' yield criterion is the most mathematically accurate of all yield criteria. To a first approximation it is defined mathematically as

$$J_2 = \left(\frac{1}{2}\right)S_{ij}S_{ij} \quad (2.3)$$

in which S_{ij} is the deviatoric stress tensor which is given by

$$S_{ij} = \sigma_{ij} - \sigma\delta_{ij} \quad (2.4)$$

where σ_{ij} is the stress tensor, σ is the hydrostatic stress and δ_{ij} is the Kronecker delta. The hydrostatic stress is given by

$$\sigma = \left(\frac{1}{3}\right)\sigma_{ii} \quad (2.5)$$

In the stress space the von Mises yield condition defines a circular cylinder as shown in Fig. 2.3b. The constant volume condition is retained, as it should be. In contrast to the Tresca flow rule there is one-to-one correspondence between

the directions of the strain increment vector and the deviatoric stress vector, and in particular there is no ambiguity in the direction of the plastic strain increment vector.

The stress-strain relationship for both deformation and flow theories of plasticity can be established on the basis of J_2 -yield condition to the first approximation. From Hutchinsion[90], the rate-constitutive relation for a three-dimensional solid can be defined as

$$\dot{\sigma}_{kl} = \psi_{ijkl} \dot{\epsilon}_{ij} \quad (2.6)$$

in which

$$\psi_{ijkl} = \psi_{ijkl}^e - q \frac{S_{ij} S_{kl}}{\sigma_e^2} \quad (2.7)$$

and

$$\psi_{ijkl}^e = \frac{E}{1 + \nu} \left(\frac{1}{2} [\delta_{ij} \delta_{jl} + \delta_{il} \delta_{jk}] + \frac{\nu}{1 - 2\nu} \delta_{ij} \delta_{kl} \right) \quad (2.8)$$

in which

S_{ij} is the deviatoric stress tensor

σ_e is the von Mises effective stress

δ_{ij} is the Kronecker delta

E is Young's modulus of elasticity

ν is the Poisson's ratio.

The three-dimensional tensor of moduli ψ_{ijkl} has two branches, one corresponding to plastic loading and the other to elastic unloading. The elastic tensor of moduli is taken to be isotropic.

The J_2 -flow theory stress-strain increment relation for a three-dimensional solid is given by

$$\sigma_{kl} = \left(\psi_{ijkl}^e - \frac{\alpha E h_1 S_{ij} S_{kl}}{(1 + \nu)(1 + \nu + 2h_1 J - 2)} \right) \epsilon_{ij} \quad (2.9)$$

where the material plastic behaviour is determined by parameters α , h_1 and J_2 .

$$J_2 = \frac{1}{3} \sigma_e^2 \quad (2.10)$$

i.e

$$J_2 = \frac{1}{2} S_{ij} S_{ij} \quad (2.11)$$

The parameter α determines when the material loads plastically or unloads elastically. For a plastic case $\alpha = 1$ and for elastic unloading $\alpha = 0$, and h_1 is given by

$$h_1 = 3 \left(\frac{E}{E_T} - 1 \right) \frac{1}{4J_2} \quad (2.12)$$

where E_T is the tangent modulus derived from the uniaxial stress-strain curve.

The J_2 -deformation theory of plasticity applied to a three-dimensional solid follows from Equation (2.6) and the stress-strain increment is given by

$$\begin{aligned} \dot{\sigma}_{kl} = & \frac{E}{(1 + \nu + h_2)} \frac{1}{2} \{ \delta_{ij} \delta_{kl} + \delta_{il} \delta_{jk} \} \dot{\epsilon}_{ij} \\ & + \frac{E}{(1 + \nu + h_2)} \left\{ \frac{3\nu + h_2}{3(1 - 2\nu)} \delta_{ij} \delta_{kl} \right\} \dot{\epsilon}_{ij} \\ & - \frac{E}{(1 + \nu + h_2)} \left\{ \frac{h'_2 S_{ij} S_{kl}}{(1 + \nu + h_2 + 2h'_2 J_2)} \right\} \dot{\epsilon}_{ij} \end{aligned} \quad (2.13)$$

and

$$h'_2(J_2) = 3 \left(\frac{E}{E_s} - 1 \right) \frac{1}{2} \quad (2.14)$$

where $h'_2(J_2)$ is the derivative of h_2 with respect to J_2 . E_s is the secant modulus obtained from the uniaxial stress-strain relation.

The paradox of the flow theory of plasticity has not been completely resolved. Although this theory is physically sound, the buckling loads predicted are always higher than the experimental data. However, the deformation theory of plasticity had been established as an appropriate theory that gives buckling loads in agreement with the experimental data. The inelastic buckling of plates using the concept of bifurcation of equilibrium and the conventional theory of plates neglecting shear deformations have been investigated by Ilyushin[43], Stowell[62] and Bijlaard[82] on the basis of the constitutive relations of the J_2 -deformation theory of plasticity. On the other hand Handleman and Prager[83] employed the constitutive relations of J_2 -flow theory of plasticity. Batdorf[84] showed that a more refined flow theory of plasticity with the vertex on the yield

surface would give better agreement between the two theories. Pearson[85] improved incremental analysis by incorporating Shanley's concept of continuous loading. This improvement did not significantly lower the buckling load. Onat and Drucker[86] and Hutchinson and Budiansky[87] explained the difference between buckling predictions based on incremental plasticity theory and the experimental data as the result of unavoidable geometric initial imperfections. This proposal was demonstrated by analysing a cruciform column using flow theory. Neal[88] also proved that buckling prediction using flow theory could coincide with the experimental data by accepting a certain amount of initial imperfection in the analysis. It has been observed that J_2 -deformation theory can be shown to be equivalent to the refined incremental theory of Sanders[89], taking into account the development of a corner on the yield surface under progressive compression. Thus the bifurcation loads obtained on the basis of J_2 -deformation theory are in fact those obtained from a more complicated and physically acceptable incremental theory of plasticity[90]. Many researchers have established stress-strain relations based on flow theory starting from the Prandtl-Reuss equation. Among them are Yamada et al[91] who established explicitly an incremental stress-strain relationship using the von Mises effective stress as a yield criterion.

Recently, attempts have been made by Damkilde[92] to examine the influence of plasticity on the buckling loads of a finite cruciform column. The two theories of plasticity were considered in his analysis. He concluded that incremental theory predictions would be influenced by plasticity, but not as much as those based on deformation theory. Shrivastara[93] also studied the inelastic buckling of rectangular plates using both theories of plasticity. It

was concluded that the correction for the shear effect is usually larger for the incremental theory than the deformation theory.

The two theories have been used to analyse plate problems by many researchers and the results lead to the notion that deformation theory gives a better estimate of buckling loads.

2.4 Finite Strip Method

In the past seven years considerable effort has been given to the use of the finite strip method in studying the behaviour of plate and plate subassembly. Wittrick[94][95][96],[97][98] laid the foundations of an exact finite strip method(i.e, exact within the limitations of linear theory in the elastic range). In these developments a stiffness matrix for a long flat plate strip subjected to a basic state of membrane stress which varies longitudinally is established. This basic stress state includes uniform longitudinal, transverse and shear stresses. Wittrick's development was based on the assumptions that when buckling occurs in local, overall or coupled modes the three components of displacement vary sinusoidally in the longitudinal direction with a common wavelength. This implies that the buckled half-wavelength is small compared to the length of the plate assembly, or that the component plates are simply supported at their ends so far as transverse displacement is concerned, and are constrained against tangential in-plane displacement but are allowed to move freely in the axial direction. This assumption leads to the problem being governed by ordinary differential equations which can be solved explicitly. The

stiffness matrix relating the amplitudes of the sinusoidally varying edge forces and displacements of the plate strips are obtained. There are four degrees of freedom comprising the three displacements and a rotation component. The inclusion of shear stress leads to the perturbation forces and displacements at the plate longitudinal edges being out of phase. This is accounted for by specifying their magnitudes in terms of complex quantities, and thus the stiffness matrix becomes Hermitian in nature. Plank and Wittrick[99] employed this approach to study the behaviour of plated structures under combined loadings. Generally, the overall stiffness matrix for plate assemblies in the exact finite strip method has components which are complicated transcendental functions of a loading factor and the half wavelength of the buckled mode. The critical loading factor cannot be obtained by a standard eigenvalue method. Wittrick and Williams[96] developed an algorithm which requires the specification of an upper bound for the structure's buckling load when all inter-strip junction lines are fully clamped.

Cheung[100] developed an approximate finite strip method which was applied to obtain the solution of static plate bending problems. This was later extended to solve plate buckling problems. This analysis was limited to the consideration of local buckling. In this method polynomial functions are assumed to describe the variation of the displacements in the transverse direction. The advantage of this approximate finite strip over the exact finite strip is that the coefficients of the overall stiffness matrix are linear functions of the load factor, and thus standard eigenvalue methods can be applied to obtain the buckling loads. Furthermore, the approximate finite strip method is more general than the exact approach. In principle, completely arbitrary geometry

of cross-section can be incorporated together with the anisotropic material behaviour. The restriction to simply supported ends might possibly be removed by considering appropriate longitudinal variation of displacements to account for the distortion. The approximate approach has some disadvantages as well; for example, in order to achieve sufficient accuracy it often requires more than a single strip to model a component plate. This consequently results in increased size and bandwidth of the overall stiffness matrix. The approximate finite strip method is now well established as an economical and efficient method for elastic buckling analysis of plates[101][102][103][104].

The inclusion of curved anisotropic plate in the finite strip method has also received attention. Viswanathan and Tamekumi[105] extended finite strip to include a curved anisotropic plate which has constant transverse curvature and thickness. These basic plates can be subjected to uniform biaxial direct and shear stresses. The formation of the strip stiffness is accomplished numerically and standard eigenvalue routines can not be used; thus a Wittrick algorithm is needed to calculate the buckling loads. Williams[106], and Plank and Williams[107], adopted an idealised flat strip approach for the analysis of curved plates. This requires a large number of flat strips to simulate the curved geometry with the use of substructures, which partly offsets the resulting increase in computational effort.

The behaviour of sandwich panels has been studied by many researchers. Among these are Chan and Cheung[108] who investigated the bending and vibrational behaviour of multi-layered sandwich plates using the finite strip method.

The extension of the finite strip method to simulate plate behaviour in the inelastic range opened up a new dimension in its application. Fukumoto et al[109] applied it to investigate the inelastic behaviour of axially compressed panels stiffened with longitudinal stiffeners. Yoshida and Maegawa[68] studied the inelastic local, overall and interactive buckling of H-columns by applying the deformation theory of plasticity originally developed by Bijlaard[82].

The post-buckling analysis of plates using the finite strip method was first attempted by Graves-Smith and Sridharan[110] by extending the elastic bifurcation range into the post-buckling range. They used new displacement functions different from the linear finite strip type. This enables the in-plane equilibrium equations to be satisfied. The compatibility between out-of-plane and transverse in-plane displacements could not be satisfied at the corners of the structure where component plates meet at an angle. To overcome this problem Sridharan[111] assumed another function for the transverse in-plane displacement which requires a higher number of harmonics. Graves-Smith and Sridharan[112] later included an extra nonlinear term (a transverse in-plane term) into the axial strain expression. This enables the elastic limit state to be reached. Hancock[69] extended the post-buckling finite strip method to include the effect of local initial imperfections. Squared functions are assumed for both the longitudinal and transverse in-plane displacements. Furthermore, the redistribution of Poisson's ratio was accounted for while Graves-Smith kept it constant. Hancock assumed that in-plane displacement functions were divided into two components, the Hookean and geometrically nonlinear displacements of the strip, as shown in Fig. 2.4. The assumed longitudinal in-plane harmonic series eliminates shear straining at the ends of the strip, and permits

compatibility between the out-of-plane and in-plane displacements at the plate junctions to be approximately maintained.

Very recently the finite strip method has been extended to include the theory of mode interaction. Rafeal and Sridharan[76] combined the mode theory with the finite strip method to study the behaviour of T-sections subjected to end moments. The method allows for the inclusion of local and overall initial imperfections. Furthermore, Fau[113][114][115] developed a spline finite strip method in which the longitudinal trigonometric series is replaced by a linear combination of the local B_3 -spline. The usual transverse polynomials are retained. The advantage of this extension is the localised nature of B_3 -spline functions which reduces the computational effort and allows specification of different boundary conditions by slight modification of a few local splines at the boundary. Lau and Hancock[116] later employed this method to study the buckling behaviour of thin flat-walled structures.

The combination of the finite strip method with the finite element method has been attempted by Graves-Smith et al[119] in order to analyse box sections with diaphragms. Bruce et al[117] developed a technique in which the Bogner displacement functions for the rectangular finite element and the displacement functions used with a simply supported finite strip method were combined. This method proves versatile but the increase in degrees of freedom leads to additional computational effort. It is anticipated that this could be taken further in conjunction with the finite element method to yield a more sophisticated method of analysis that would bridge the gap in the numerical analysis.

2.5 Column Buckling At Elevated Temperature

During the course of a building fire structural steelwork undergoes degradation both in material properties and physical consideration. The structural elements lose stiffness as well as yield strength with increasing temperature. In an attempt to safeguard against this the building regulations of many countries grade structural construction materials on the basis of minimum time the element can survive when exposed to the standard fire ISO 834[120]. The design solutions currently in practice normally involve application of fire-proof protecting materials. This fire protection is often designed by consideration of the minimum time protection provided. An investigation into multi-storey building costs by the British Steel Corporation indicates that fire protection is responsible for about 30% of the total cost of steel frame[121].

During fire spread the temperature rise with time in a steel column depends on the following factors:

- the amount of fire load (given as Kg of fuel per square metre of the floor for the test)
- the ventilation factor $\frac{A\sqrt{h}}{A_t}$ where A is the area of the opening in m^2 , h is its height in m and A_t is the area of the surrounding surface in m^2 .
- the thermal properties of the walls

A tremendous amount of work has been done in numerical and regressional

analysis to determine the thermal response of the structural steel[122][123] and thus considerable data on the subject are available in the literature.

The development of a versatile fire engineering system has not been possible up to the present. Law and O'Brien[124] established a comprehensive fire engineering system which is limited to thermal response of structural steel. This method embraces all physical features of fire engineering. The method assumes steady state heat transfer with the collapse temperature set at 550°C in accordance with BS476 Pt8[125]. This target may be conservative, as demonstrated by the series of tests performed by British Steel Corporation and the Fire Research Station at Cardington[166][171]. It is now recognised that unprotected steelwork does not necessarily collapse when its temperature reaches 550°C but can exhibit a range of limiting temperatures higher than 550°C for common design situations, and particularly for those where the load bearing capacity is not fully utilised[126].

The critical temperature of a load bearing steel element, or structural assembly as defined by ECCS[128], is the temperature at which the limit state of failure is expected to be attained. Experimentally, a considerable amount of work has been done to investigate the behaviour of steel columns in fire. Most of the full scale fire tests have followed the standard fire testing procedure because of the difficulty involved in simulating a real fire situation. This makes it impossible to simulate the real situation during fire spread. Knublauch et al[127] tested 23 columns insulated with box-shaped vermiculite insulating plates. The test specimen was not fully immersed in the furnace – only about 80% of its length was actually exposed to fire. The axially applied load was kept constant while

heating progressed and there was no restriction on thermal expansion. It was found that 95% of all the columns tested attained critical temperatures of 500°C or more when subjected to the design load according to DIN 4114. The inclusion of an elastic restraint instead of a hinge by Kertsma et al[129] at the column base resulted in a considerable increase in the critical temperature. Stanke[130] tested steel columns with varying degrees of axial restraint on thermal expansion and found that the load increased rapidly during initial heating because of the axial restraint. At buckling unloading took place, which showed that columns sustained the initial loading much longer than Magnusson et al[131] had predicted theoretically.

Vandamme and Janss[132] and Janss and Minne[133] reported tests conducted on 27 columns, out of which two were uninsulated. In each test the applied load was kept constant without axial restraint while heating progressed. The ends were given rotational restraint with the aid of special device. The critical temperature was accurately predicted by their analytical model based on the ECCS[134] buckling curve C with the modification factor originally proposed by Pettersson and Witteveen[135] taken into account. This factor is used to overcome the deficiencies in reproducibility and repeatability associated with the test data, and thus ensures a better basis for comparing theory with experiment. Olesen's tests[136] were conducted in a horizontal position in a special furnace. In these tests the load was increased with constant loading rate until buckling occurred, while the temperature of the furnace was kept at a prescribed level. Eighteen columns were tested at a constant loading rate while the remaining six columns were tested keeping the axial load constant while heating progressed until buckling. In all the tests the columns were axially

unrestrained. Comprehensive column tests were conducted by Hoffend[137]. Seventy five columns were tested with the following parameters taken into consideration.

- load eccentricity
- column slenderness ratio
- load level
- axis of buckling
- hinged or clamped column ends
- thermal gradient along the column length due to partial protection
- rate of heating
- full axial restraint

The test results were correlated with numerical simulation[138][139]. It was concluded that critical temperature of a slender column is slightly higher than that of a stocky column. The load eccentricity is more detrimental to the critical temperature with increasing column slenderness. Furthermore the longitudinal temperature gradient (shown in Fig. 2.4) has only a minor effect on the load-bearing capacity of the pinned-end columns, in contrast to its effect on the clamped columns.

Quite recently Aasen and Larsen[140] conducted elevated temperature tests on several columns. The test program comprised two phases. The load was

applied in increments at room temperature to a prescribed level and kept constant while the heating progressed. The axial column end displacement could be fixed in order to introduce an axial restraint. The following parameters were taken into consideration during the course of testing.

- slenderness ratio
- load level
- rotational and axial restraint
- end eccentricity
- rate of heating and the temperature gradient

Their observations can be summarised as follows;

For a column without axial restraint:

1. The failure time is significantly affected by the load level.
2. Geometrical imperfections are detrimental to the load carrying capacity of the column(more so than at ambient temperature).
3. The maximum column strength is only slightly influenced by the column slenderness and the heating rate.

For columns with axial restraint:

1. The load level at initial heating, and geometric imperfections, affect the column strength.

2. An imperfect column exhibited a gradual type of failure while perfect columns exhibited a more abrupt reduction in imposed axial load due to the restricted thermal expansion.

The influence of thermal stresses due to non-uniform temperature distribution across the cross-section and residual stress was studied by Alpsten[144]. He showed that the presence of residual stresses has a more adverse effect on column strength than geometric initial imperfections in the range of low to intermediate column slenderness. Culver[145] investigated the effect of thermal gradient along the length of column on its performance. A finite difference scheme was utilised together with a tangent modulus approach. The effect of residual stresses was examined. It was found that the pin-ended column, in which the maximum temperature occurred at the midheight, exhibited the highest loss of buckling strength. This contradicted Hoffend's[137] observations. The reason for this contradiction may be connected with the idealised temperature profile assumed in the Culver formula to predict the critical stress of an axially restrained column at elevated temperature. Ossenbruggen et al[147] studied the effect of thermal gradient across the cross-section using a moment-curvature-thrust-temperature approach. This included both thermal and residual stresses. The thermal bowing induced by the thermal gradient across the cross-section was approximated by a certain amount of initial imperfection. They concluded that thermal gradient is detrimental to the axially loaded column.

Attempts towards the development of an adequate fire engineering system have been made by many researchers. The simplified but practical approach

to strut strength prediction in fire is to assume that the room temperature design curve is valid at elevated temperature, but allowing for the influence of heating on the yield stress and modulus of elasticity. This approach was employed by Vandamme and Janss[132]. The ECCS[128] expressions for yield stress and the modulus of elasticity were used. These expressions are given below:

$$\psi = 1.0 + \frac{\theta}{\left(767 \ln \frac{\theta}{1750}\right)} \quad 0^\circ C < \theta < 600^\circ C \quad (2.15)$$

$$\psi = 108 \frac{\left(1 - \frac{\theta}{1000}\right)}{\theta - 440} \quad 600^\circ C < \theta < 1000^\circ C \quad (2.16)$$

$$\begin{aligned} \gamma = & 1 - 17.2 \times 10^{-12} \theta^4 + 11.8 \times 10^{-9} \theta^3 - 34.5 \times 10^{-7} \theta^2 \\ & + 15.9 \times 10^{-5} \theta \end{aligned} \quad (2.17)$$

$$\psi = \frac{\sigma_{y,\theta}}{\sigma_{y,20}} \quad (2.18)$$

$$\gamma = \frac{E_\theta}{E_{20}} \quad (2.19)$$

$\sigma_{y,20}$ and $\sigma_{y,\theta}$ are the yield stresses at room and elevated temperature respectively, E_{20} and E_θ are the modulus of elasticity at room and elevated temperature respectively. The same approach was adopted by Magnusson et al[131]. The Swedish column design curves were derived from the buckling equations

$$\frac{\sigma_{cr,\theta}}{\sigma_{y,\theta}} = \beta - \sqrt{\beta^2 - \frac{1}{\lambda^2}} \quad (2.20)$$

where

$$\beta = \frac{1 + \bar{\lambda}^2 \times 4.8 \times 10^{-5} + \bar{\lambda}^2}{2\bar{\lambda}^2} \quad (2.21)$$

and

$$\bar{\lambda} = \frac{\lambda}{\pi} \sqrt{\frac{\sigma_{y,20}}{E_{20}}} \quad (2.22)$$

where

$$\lambda = \frac{l}{r} \quad (2.23)$$

The ECCS[134] buckling curve at room temperature may be described by Equation (2.20) provided that

$$\beta = \frac{1 + \alpha(\bar{\lambda} - 0.2) + \bar{\lambda}^2}{2\bar{\lambda}^2} \quad (2.24)$$

with α as the imperfection parameter which ranges from 0.206 to 0.489 for buckling curves a-c. The Swedish buckling curves are related to the proportionality slenderness ratio λ_0 while ECCS buckling curves are related to the relative slenderness ratio $\bar{\lambda}$. At elevated temperature there exists a remarkable deviation between these two design approaches. These disparities are due to the replacement of modulus of elasticity by secant modulus and 0.2% proof stress by 0.5% proof stress in the Swedish buckling equations. Proe et al[148] appraised the CTICM[149] and ECCS[128] fire engineering systems and concluded that the theoretical estimates of buckling stress based on ECCS strength and modulus reduction expressions are considerably more conservative than the estimate based on the CTICM expressions.

The poor repeatability and reproducibility of test results have made it very difficult to compare theory with fire test data. In order to overcome this short-coming Petterson and Witteveen[135] suggested a more unified approach given by the following equation.

$$\sigma_{u,\theta} = f\sigma_{cr,\theta} \quad (2.25)$$

where $\sigma_{cr,\theta}$ is the theoretical buckling load at elevated temperature for a uniform temperature distribution and $\sigma_{u,\theta}$ is the test failure stress. The correction factor f compensates for the difference between the nominal and actual values of the mechanical properties at elevated temperature, the imperfection and non-uniform temperature distribution in the column. This factor is given by

$$f = 1 + \frac{\theta}{1500} \quad 0^\circ C \leq \theta \leq 300^\circ C \quad (2.26)$$

$$f = 1.2 \quad \theta \geq 300^\circ C \quad (2.27)$$

Vandamme and Janss[132] and Janss and Minne [133] have shown that the best correlation between test results and theoretical buckling predictions is obtained by using the actual yield stress instead of nominal values. Hoffend and Kordinal [139] concluded that the value of $f = 1.18$ adopted by the ECCS resulted in a conservative estimate of the buckling load.

The behaviour of pin-ended columns made of HEA200 welded tube and box columns was studied by Setti[150]. Both initial geometric imperfection and residual stresses were taken into account. The Danish[136] and the French[141] tests were simulated using his approach. He concluded that a more favourable

buckling curve than curve C of ECCS can be obtained provided that representative estimates of the structural and geometrical imperfections are taken into account. He also suggested that the ECCS expressions for the mechanical properties are inadequate for theoretical predictions of buckling load.

The influence of creep on column performance becomes more noticeable when the temperature increases beyond 550°C. Aribert and Randrianstara[141] conducted creep buckling tests on 33 HEA100 pinned uninsulated columns. The test specimen was about 2m long with slenderness ratio of 80 about the minor axis. The test program allowed loading at prescribed temperature levels with and without axial restraint. It was noted that creep starts to influence the column strength at about 545°C. This effect depended on the amount of load applied on the column. At high load level the effect of creep was less significant, but at very low load level and temperature of about 600°C, the reduction in the column bearing capacity is about 9%. Fujimoto et al[142] reported on the creep buckling tests conducted on fixed-end H-columns. The test specimen slenderness ratio was 29.1 and the tests were conducted with the following parameters taken into account:

- eccentricity of loading
- different temperature profiles and loads.

The test results were verified numerically. There was an underestimation of the bearing capacity of columns theoretically by about 50% but the modes of creep buckling behaviour of columns are similar for both theory and experiment. Fujimoto et al[143] tested another set of H-columns with slenderness

ratio of 46.9. The theoretical simulation was ammended by using a modified tangent modulus-temperature relationship and creep model. This resulted in reasonable agreement between theory and experiment.

The adoption of a time-independent approach to analysis has been justified by Witteveen et al[151] and Witteveen and Twilt[152]. From the experimental investigation of model structural steel members, it was established that the collapse temperature is time-independent and consequently is not influenced by the heating history. They found that the result for a column calculated at 600°C coincided with a buckling analysis result by Eggwertz[153] for a column with slenderness ratio of 45 subjected to a temperature-time history. Eggwertz's analysis was based on Norton's creep law modified to conform with Dorn-Harmathy theory[154] (only secondary creep is taken into account). Randriantsara[155] derived an interaction formula on the basis of a similar creep model as proposed by Eggwertz. The equilibrium condition is established only at the midheight of a column assuming the deflected shape is a half-sine curve.

Proe et al[156] have given an overall-approach treatment to the behaviour of structural steel members in fire without the inclusion of thermal creep. The method involves both the thermal response based on the regressed temperature equation and the structural response based on the following mechanical property expressions:

$$\frac{\sigma_{y,\theta}}{\sigma_{y,20}} = \frac{895 - \theta}{700} \quad 300^\circ C < \theta < 895^\circ C \quad (2.28)$$

$$\frac{\sigma_{y,\theta}}{\sigma_{y,20}} = 1 - \frac{\theta}{2000} \quad 0^\circ C < \theta < 300^\circ C \quad (2.29)$$

The CTICM expressions for the effective modulus are used.

The application of the finite element method in simulating the structural response at elevated temperature has been undertaken by many researchers. Among them are Muzeau and Lemaire[157] who used a non-linear elasto-plastic model to study the behaviour of beams and external columns. Furumura and Shinoshara[159] applied elasto-plastic analysis, with creep taken into consideration, to study the behaviour of steel columns in high rise frames. The influence of geometrical imperfection was allowed for. Schleich et al[158] also applied an elasto-plastic finite element method to study the behaviour of composite construction and steel structural members. All these models demonstrate the power of the finite element method as a numerical tool, although at the expense of computational efficiency. Until now the finite strip method has not been applied to study the behaviour of steel columns in fire.

The issue of an adequate design philosophy has not been totally resolved. Witteveen[160] concluded that the nonlinearity of the stress-strain relationship of steel at elevated temperature has completely ruled out the application of linear theory of elasticity. Thus the application of plasticity theory is desirable to simulate accurately the steel structural response in the fire environment.

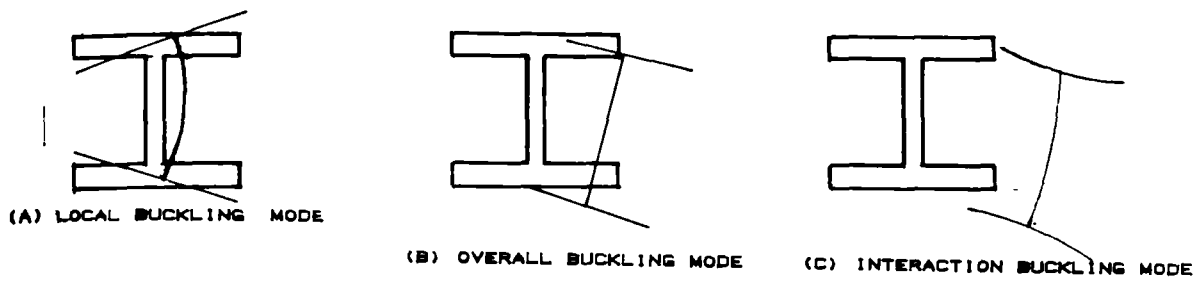


FIG. 2.1 THE BUCKLING MODES OF I - SECTION.

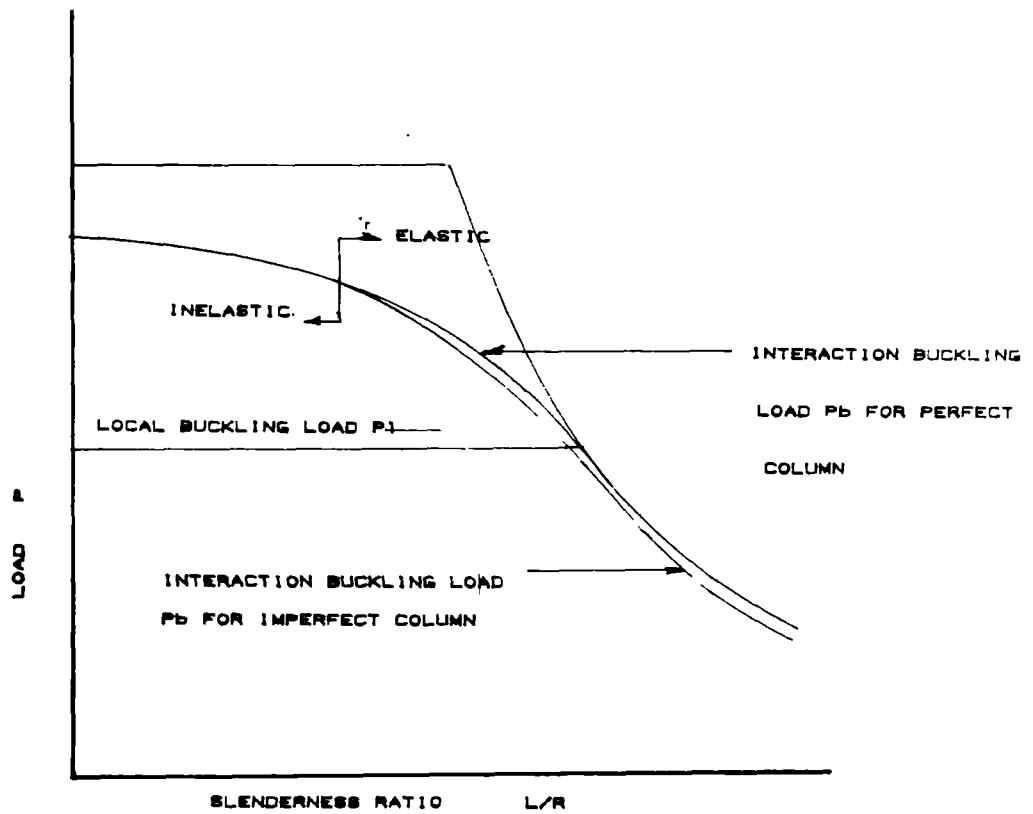


FIG. 2.2 LOAD - SLENDERNESS RATIO CURVE FOR INTERACTION BUCKLING

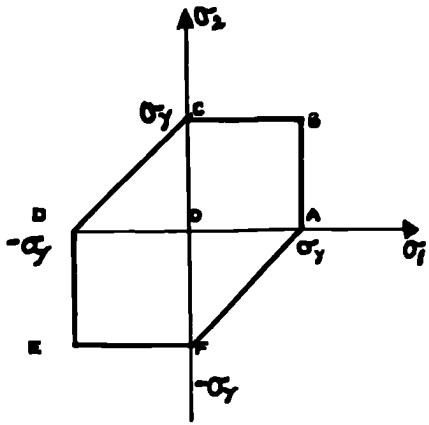


FIG. 2.3A TRESCA YIELD CRITERION

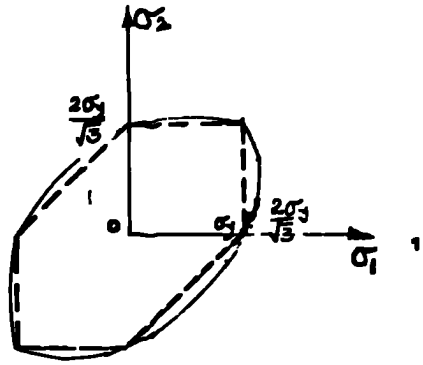
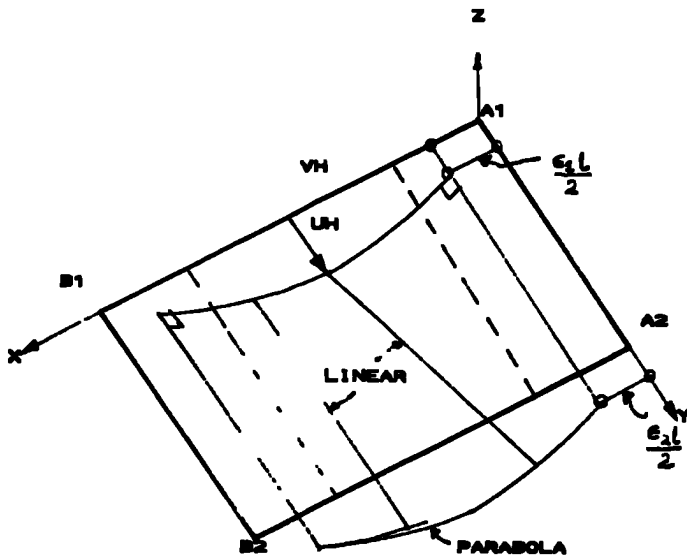
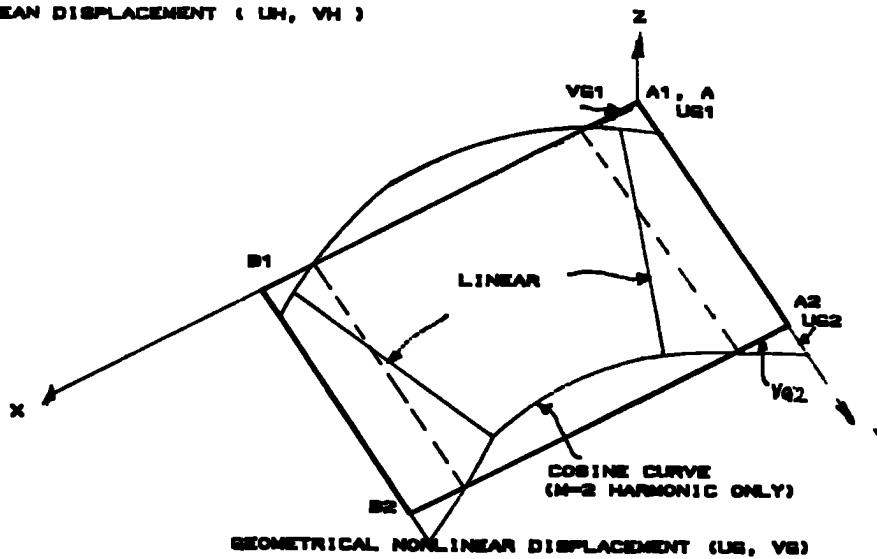


FIG. 2.3B VON MISES YIELD CRITERION



HOOKEAN DISPLACEMENT (LH, VH)



GEOMETRICAL NONLINEAR DISPLACEMENT (U_B, V_B)

FIG. 2.4 MEMBRANE DISPLACEMENT OF A STRIP

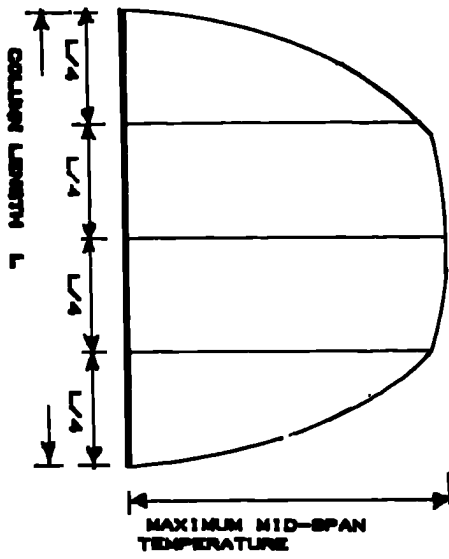


FIG. 2.5 TYPICAL TEMPERATURE DISTRIBUTION ALONG COLUMN LENGTH

Chapter 3

FINITE STRIP METHOD

3.1 Theoretical Basis Of Finite Strip Method

The finite strip method of analysis has been established as an efficient numerical tool for the elastic and inelastic analysis of plate and plate subassemblages [96][99][68]. In the present development the elasto-plastic finite strip originally developed by Mahmoud[161] is extended to include the deformation theory of plasticity applied to thin plates. This method incorporates local, overall and interactive buckling modes. The uniaxial stress-strain relation is represented by a Ramberg-Osgood[168] formula which is continuous. The original Ramberg-Osgood formula is given by:

$$\epsilon = \frac{\sigma}{E_{20}} + 0.002 \left(\frac{\sigma}{\sigma_{0.2}} \right)^n \quad (3.1)$$

where n is the material constant and $\sigma_{0.2}$ is the 0.2% proof stress. This formula is simple and can be easily adjusted to produce the material behaviour of steel by setting n to a high value. The first term of the formula is the elastic component while the second term represents the plastic component. A high value of n represents a sharp knee which tends to idealise elastic-perfectly plastic behaviour. In the present work consideration is given to Galambos' modified version of the formula[172] which gives appropriate representation of the steel properties. This is given by:

$$\epsilon = \frac{\sigma}{E_{20}} + \frac{3}{7} \left(\frac{\sigma_{y,20}}{E_{20}} \right) \left(\frac{\sigma}{\sigma_{y,20}} \right)^n \quad (3.2)$$

in which

E_{20} is the Young modulus of elasticity at ambient temperature

$\sigma_{y,20}$ is the yield strength at ambient temperature

ϵ is the effective strain

σ is the effective stress

n is the material constant set at 30 for the ambient temperature cases.

Since uniaxial compression is considered the effective stress corresponds to the longitudinal stress σ_x .

In the present analysis the structure may be subjected to a combination of longitudinal compression and bending. Thus the state of applied stress in a strip may be longitudinal compression which is uniform or varying linearly across the width of the strip. The inclusion of residual stresses also results in a non-uniform stress state in the strip. The development of the finite strip method is based on small deflection theory of elasticity for initially perfect plates.

At the onset of buckling the strip suffers some deformation and the components of displacement are assumed to vary sinusoidally in the longitudinal direction with half wavelength λ . There are only four independent degrees of freedom corresponding to u, v, w , and Θ at the two edges of the strip as shown in Fig. 3.1.

The extension of the elastic finite strip method to the inelastic range is accomplished by using the deformation theory of plasticity applied to thin plates. This theory was established by Bijlaard[82] and was applied by Yoshida and Meagawa[68] in studying the behaviour of H-columns in the inelastic range. Based on this theory of plasticity the nonlinear material properties are given by the following equations:

$$\{\sigma\} = E_{20} [F] \{\epsilon\} \quad (3.3)$$

where the elasto-plastic modular matrix $[F]$ is given by

$$[F] = \begin{bmatrix} f_{11} & f_{12} & 0 \\ f_{12} & f_{22} & 0 \\ 0 & 0 & f_{33} \end{bmatrix} \quad (3.4)$$

and the coefficients of $[F]$ are given by

$$\begin{aligned} f_{11} &= \frac{(1 + 3\tau)}{\mu} \\ f_{12} &= \frac{2(1 - (1 - 2\nu)\tau)}{\mu} \\ f_{22} &= \frac{4}{\mu} \\ f_{33} &= \frac{1}{2 + 2\nu + 3e} \\ e &= \frac{E_{20}}{E_s} - 1 \\ \tau &= \frac{E_t}{E_{20}} \\ \mu &= 5 - 4\nu + 3e - (1 - 2\nu)^2\tau \end{aligned} \quad (3.5)$$

where

E_t is the tangent modulus

E_s is the secant modulus

E_{20} is Young's modulus of elasticity at ambient temperature.

These moduli are obtained from the uniaxial stress-strain relation.

The moment-curvature relationship is given by

$$\{M\} = \frac{E_{20}t^3}{12} [F] \{\chi\} \quad (3.6)$$

where

$$\{\chi\} = \left\{ -\frac{\partial^2 W}{\partial x^2} \quad -\frac{\partial^2 W}{\partial y^2} \quad 2\frac{\partial^2 W}{\partial x \partial y} \right\} \quad (3.7)$$

and

t is the plate thickness

The elastic material properties can be obtained by setting $\tau = 1$ and $e = 0$ in the stress-strain relation. This results in $[F]$ becoming

$$[F] = \frac{1}{1-\nu^2} \begin{bmatrix} 1 & \nu & 0 \\ \nu & 1 & 0 \\ 0 & 0 & \frac{1}{2}(1-\nu) \end{bmatrix} \quad (3.8)$$

In the derivation of the stiffness matrix the out-of-plane and in-plane effects are considered separately. Both the out-of-plane and in-plane stiffness equations can be combined to enable all buckling modes to be considered. The out-of-plane displacement function is given by

$$f_o = \{W\} \quad (3.9)$$

$$f_o = \{Z\}^T \sin \pi \xi \{\delta_o\} \quad (3.10)$$

where

$$\{Z\}^T = \begin{Bmatrix} C_3 \\ C_4 \\ C_5 \\ C_6 \end{Bmatrix} \quad (3.11)$$

and

$$\begin{aligned} C_3 &= b(\eta - 2\eta^2 + \eta^3) \\ C_4 &= 1 - 3\eta^2 + \eta^3 \\ C_5 &= b(-\eta^2 + \eta^3) \\ C_6 &= 3\eta^2 - 2\eta^3 \\ \xi &= \frac{x}{\lambda} \\ \eta &= \frac{y}{b} \end{aligned} \quad (3.12)$$

$$\{\delta_o\} = \begin{Bmatrix} \Theta_1 \\ w_1 \\ \Theta_2 \\ w_2 \end{Bmatrix} \quad (3.13)$$

The out-of-plane strain vector is related to the curvature as given below

$$\{\epsilon_o\} = z \{\chi\} \quad (3.14)$$

$$\{\epsilon_o\} = [B_o] \{\delta_o\} \quad (3.15)$$

and $[B_o]$ is given by

$$[B_o] = \begin{bmatrix} \frac{\pi^2}{\lambda^2} \{Z\}^T \sin \pi \xi \\ -\frac{\pi}{b^2} \{Z'_{\eta\eta}\}^T \sin \pi \xi \\ \frac{2\pi x}{b\lambda} \{Z'_\eta\}^T \cos \pi \xi \end{bmatrix} \quad (3.16)$$

Applying the principle of virtual work the change in the internal virtual work dW_{i_o} for the out-of-plane behaviour is given by

$$dW_{io} = \int_{vol} \{d\epsilon_o\}^T [F] dvol \quad (3.17)$$

$$dW_{io} = \int_{vol} \{d\delta_o\}^T [B_o]^T [F] [B_o] \{\delta_o\} dvol \quad (3.18)$$

$$dW_{io} = \{d\delta_o\}^T [K_o] \{\delta_o\} \quad (3.19)$$

and the out-of-plane stiffness matrix is given by

$$[K_o] = \int_{vol} [B_o]^T [F] [B_o] dvol \quad (3.20)$$

The in-plane displacement function is given by

$$f_i = \{U \ V\} \quad (3.21)$$

$$f_i = \begin{bmatrix} \{X\}^T \cos \pi\xi \\ \{Y\}^T \sin \pi\xi \end{bmatrix} \{ \delta_i \} \quad (3.22)$$

where

$$\{X\}^T = \{0 \ C_1 \ 0 \ C_2\} \quad (3.23)$$

$$\{Y\}^T = \{C_1 \ 0 \ C_2 \ 0\} \quad (3.24)$$

and

$$C_1 = 1 - \eta$$

$$C_2 = \eta \quad (3.25)$$

$$\{\delta_i\} = \{v_1 \ u_1 \ v_2 \ u_2\} \quad (3.26)$$

The in-plane strain vector is given by

$$\{\epsilon_i\} = \left\{ \begin{array}{c} \frac{\partial U}{\partial x} \\ \frac{\partial V}{\partial y} \\ \frac{\partial U}{\partial y} + \frac{\partial V}{\partial x} \end{array} \right\} \quad (3.27)$$

$$\{\epsilon_i\} = [B_i] \{\delta_i\} \quad (3.28)$$

and

$$[B_i] = \left[\begin{array}{c} -\frac{\pi}{\lambda} \{X\}^T \sin \pi \xi \\ \frac{1}{b} \{Y'_\eta\}^T \sin \pi \xi \\ \left(\frac{1}{b} \{X'_\eta\}^T + \frac{\pi}{\lambda} \{Y\}^T \right) \cos \pi \xi \end{array} \right] \quad (3.29)$$

The change in the internal virtual work for the in-plane behaviour is given by

$$\begin{aligned} dW_{ii} &= \int_{vol} \{d\epsilon_i\}^T [F] \{\epsilon_i\} dvol \\ &= \int_{vol} \{d\delta_i\}^T [B_i]^T [F] [B_i] \{\delta_i\} dvol \\ &= \{\delta_i\}^T [K_i] \{\delta_i\} \end{aligned} \quad (3.30)$$

and the in-plane stiffness matrix is given by

$$[K_i] = \int_{vol} [B_i]^T [F] [B_i] dvol \quad (3.31)$$

In order to account for the membrane stress, the stability matrices for the in-plane and out-of-plane cases are calculated. The out-of-plane virtual work done by the membrane stress system during a virtual out-of-plane displacement is given by

$$dW_{mo} = \int_{vol} \{d\epsilon_{bo}\} \{\sigma\}^T dvol \quad (3.32)$$

By expressing the out-of-plane displacement function as

$$\{f_o\} = [N_o] \{\delta_o\} \quad (3.33)$$

The membrane bending strain vector is given by

$$\{\epsilon_{bo}\} = \frac{1}{2} \left\{ \begin{array}{c} \left(\frac{\partial W}{\partial x} \right)^2 \\ \left(\frac{\partial W}{\partial y} \right)^2 \\ \frac{\partial W}{\partial x} \frac{\partial W}{\partial y} \end{array} \right\} \quad (3.34)$$

$$\{\epsilon_{bo}\} = \frac{1}{2} \begin{bmatrix} \frac{\partial W}{\partial x} & 0 \\ 0 & \frac{\partial W}{\partial y} \\ \frac{\partial W}{\partial y} & \frac{\partial W}{\partial x} \end{bmatrix} \left\{ \begin{array}{c} \frac{\partial W}{\partial x} \\ \frac{\partial W}{\partial y} \end{array} \right\} \quad (3.35)$$

$$\{\epsilon_{bo}\} = \frac{1}{2} \{\delta_o\}^T \left[\begin{array}{c} \frac{1}{\lambda^2} [N'_{o,\xi}]^T [N'_{o,\xi}] \\ \frac{1}{b^2} [N'_{o,\eta}]^T [N'_{o,\eta}] \\ \frac{1}{b\lambda} \{ [N'_{o,\eta}]^T [N'_{o,\xi}] + [N'_{o,\xi}]^T [N'_{o,\eta}] \} \end{array} \right] \{ \delta_o \} \quad (3.36)$$

The bending strain increment is given by

$$\{\epsilon_{bo}\} = \{d\delta_o\}^T [B_{so}] \{\delta_o\} \quad (3.37)$$

Thus the virtual work dW_{mo} is given by

$$\begin{aligned} dW_{mo} &= \int_{vol} \{d\delta_o\}^T [B_{so}] \{\sigma\}^T \{\delta_o\} dvol \\ &= \{d\delta_o\} [S_o] \{\delta_o\} \end{aligned} \quad (3.38)$$

and the out-of-plane stability matrix is given by

$$[S_o] = \int_{vol} [B_{so}] \{\sigma\}^T dvol \quad (3.39)$$

The in-plane stability matrix can be deduced following the above approach.

The in-plane displacement function is given by

$$\begin{aligned} \{f_i\} &= \{U \ V\} \\ &= [N_i] \{\delta_i\} \end{aligned} \quad (3.40)$$

The bending strain is given by

$$\{\epsilon_{bi}\} = \frac{1}{2} \left\{ \begin{array}{c} \left(\frac{\partial U}{\partial x} \right)^2 + \left(\frac{\partial V}{\partial x} \right)^2 \\ \left(\frac{\partial U}{\partial y} \right)^2 + \left(\frac{\partial V}{\partial y} \right)^2 \\ 2 \left(\frac{\partial U}{\partial x} \frac{\partial U}{\partial y} + \frac{\partial V}{\partial x} \frac{\partial V}{\partial y} \right) \end{array} \right\} \quad (3.41)$$

This can be expressed as

$$\{\epsilon_{bi}\} = \frac{1}{2} \begin{bmatrix} \frac{\partial U}{\partial x} & \frac{\partial V}{\partial x} & 0 & 0 \\ 0 & 0 & \frac{\partial U}{\partial y} & \frac{\partial V}{\partial y} \\ \frac{\partial U}{\partial y} & \frac{\partial V}{\partial y} & \frac{\partial U}{\partial x} & \frac{\partial V}{\partial x} \end{bmatrix} \begin{Bmatrix} \frac{\partial U}{\partial x} \\ \frac{\partial V}{\partial x} \\ \frac{\partial U}{\partial y} \\ \frac{\partial V}{\partial y} \end{Bmatrix} \quad (3.42)$$

Following the same procedure for the derivation of the out-of-plane stability matrix the in-plane stability matrix can be established as given below

$$[S_i] = \int_{vol} [B_{si}] \{\sigma\}^T dvol \quad (3.43)$$

Considering equilibrium state, the out-of-plane equilibrium equation is given by

$$dW_{io} = dW_{mo} \quad (3.44)$$

This results in an eigenvalue problem which can be expressed as

$$[[K_o] - [S_o]] \{\delta_o\} = 0 \quad (3.45)$$

Also consideration of the in-plane equilibrium leads to

$$[[K_i] - [S_i]] \{\delta_i\} = 0 \quad (3.46)$$

The expressions for the out-of-plane and in-plane stiffness and stability matrices are documented in appendix A. The stiffness and stability matrix coefficients are numerically integrated over a basic strip width which is subdivided into substrips to ensure accuracy. The equilibrium equations are solved using the Wittrick-Williams[97] algorithm which ensures automatic convergence on the lowest buckling stress σ_{cr} .

3.2 Extension To Elevated Temperature Structural Response

The underlying principle that creep influences the steelwork behaviour at temperatures higher than 550°C has not been totally established. In most reported instances the behaviour of steel columns with the creep phenomenon included coincides with those in which no account is taken of creep effect. If creep is ignored the problem can be considered as time-independent, so that the structural material response can be represented with stress-strain-temperature relationships. A modified form of the finite strip method described in the previous section for ambient temperature behaviour can then be used for the analysis. The collapse can be computed for a given temperature simply by replacing the ambient temperature stress-strain relationship with the a series of stress-strain-temperature relations. The stress-strain-temperature relations are markedly nonlinear and are better represented by the modified form of Ramberg-Osgood formula given by

$$\epsilon = \frac{\sigma}{E_{\theta}} + 0.01 \left(\frac{\sigma_{y\theta}}{E_{\theta}} \right) \left(\frac{\sigma}{\sigma_{y\theta}} \right)^{n_{\theta}} \quad (3.47)$$

where

E_{θ} is the effective modulus of elasticity

$\sigma_{y\theta}$ is the effective yield strength

n_{θ} is the material constant at elevated temperature.

The modulus of elasticity and yield strength expressions are modelled to approximately satisfy the BS5950 Pt8 stress-strain-temperature data. These expressions are given by:

$$\sigma_{y\theta} = \sigma_{y,20}(0.978 - 9.74 \times 10^{-5}\theta) \quad 80^{\circ}C < \theta \leq 400^{\circ}C \quad (3.48)$$

$$\sigma_{y\theta} = \sigma_{y,20}(1.553 - 1.55 \times 10^{-3}\theta) \quad 400^\circ C < \theta \leq 550^\circ C \quad (3.49)$$

$$\sigma_{y\theta} = \sigma_{y,20}(2.34 - 3.143 \times 10^{-2}\theta) \quad 550^\circ C < \theta \leq 600^\circ C \quad (3.50)$$

$$\sigma_{y\theta} = \sigma_{y,20}(1.374 - 1.56 \times 10^{-3}\theta) \quad 600^\circ C < \theta \leq 690^\circ C \quad (3.51)$$

$$\sigma_{y\theta} = \sigma_{y,20}(1.120 - 1.28 \times 10^{-3}\theta) \quad 690^\circ C < \theta \leq 800^\circ C \quad (3.52)$$

$$E_\theta = E_{20}(1 - 1.27 \times 10^{-6}\zeta^2) \quad 80^\circ C < \theta \leq 550^\circ C \quad (3.53)$$

$$E_\theta = E_{20}(1 - 1.402 \times 10^{-6}\zeta^2) \quad 550^\circ C < \theta \leq 800^\circ C \quad (3.54)$$

$$n_\theta = \frac{4600}{\theta} + \Upsilon \quad 80^\circ C < \theta \leq 200^\circ C \text{ and } 690^\circ C < \theta \leq 800^\circ C \quad (3.55)$$

$$n_\theta = \frac{2650}{\theta} + \Upsilon \quad 200^\circ C < \theta \leq 400^\circ C \quad (3.56)$$

$$n_\theta = \frac{2400}{\theta} + \Upsilon \quad 400^\circ C < \theta \leq 550^\circ C \quad (3.57)$$

$$n_\theta = \frac{3900}{\theta} + \Upsilon \quad 550^\circ C < \theta \leq 600^\circ C \quad (3.58)$$

$$n_\theta = \frac{3600}{\theta} + \Upsilon \quad 600^\circ C < \theta \leq 690^\circ C \quad (3.59)$$

$$n_\theta = \frac{4600}{\theta} + \Upsilon \quad 690^\circ C < \theta \leq 800^\circ C \quad (3.60)$$

$$\Upsilon = \frac{\theta}{500 \ln\left(\frac{\theta}{1750}\right)} \quad (3.61)$$

$$\zeta = \theta - 20 \quad (3.62)$$

For clarification the stress-strain models developed are compared with BS5950 Pt8 stress-strain-temperature data, obtained experimentally, as shown in Fig. 3.2.

3.3 Computer Program

In order to solve the simultaneous equations a computer routine was developed. The program is coded in Fortran 77 and the flow chart of this program is shown in Fig. 3.3. The critical stress at different temperatures for the inelastic

analysis is calculated by inputting the temperature. The following stages are incorporated in an analysis:

- The input data is read and printed out.
- The stress at each substrip node is calculated (taking into account the residual stress). The division of the basic strip to a number of substrip is to improve the accuracy of the numerically calculated strip stiffness.
- The inelastic material properties, which are temperature dependent, are generated for each substrip.
- The stiffness matrix for each strip is calculated.
- The stability matrix for each strip is calculated.
- Transformation of the stiffness and stability matrices from cartesian coordinate to the global coordinate system.
- Assembly of the overall stiffness matrix and the imposition of boundary conditions.
- Determination of critical stress using Wittrick-Williams algorithm.
- Printout of results

3.3.1 The Substrip Total Stress

The total stress for each substrip node is the sum of the applied longitudinal stress and the residual stress. This is stored for use in the calculation of the inelastic material properties. The total stress is given by

$$\sigma_T(i) = \sigma_x(i) + \sigma_r(i) \quad (3.63)$$

where

$\sigma_T(i)$ is the resultant stress at the substrip node

$\sigma_x(i)$ is the applied longitudinal stress at the substrip

$\sigma_r(i)$ is the residual stress at the substrip node

3.3.2 The Nonlinear Material Properties

The total stress at every substrip node is used in calculating the tangent modulus $E_t(\theta)$ and secant modulus $E_s(\theta)$ from the temperature-dependent stress-strain relations. These moduli are given by

$$\begin{aligned} \frac{d\epsilon}{d\sigma} &= \frac{1}{E_\theta} + 0.01n_\theta \frac{1}{E_\theta} \left(\frac{\sigma}{\sigma_{y\theta}} \right)^{(n_\theta-1)} \\ E_t(\theta) &= \frac{1}{\frac{d\epsilon}{d\sigma}} \end{aligned} \quad (3.64)$$

$$\begin{aligned} \frac{\epsilon}{\sigma} &= \frac{1}{E_\theta} + \frac{1}{E_\theta} \left(\frac{\sigma}{\sigma_{y\theta}} \right)^{(n_\theta-1)} \\ E_s(\theta) &= \frac{1}{\frac{\epsilon}{\sigma}} \end{aligned} \quad (3.65)$$

The elasto-plastic modular matrix is then generated at every substrip.

3.3.3 The Strip Stiffness Matrix

The stiffness matrix for each strip is generated by numerically integrating the stiffness equations using the Simpson technique. The elasto-plastic matrix

is calculated using the shape functions and the modular matrix. The stiffness matrix is stored for subsequent imposition of boundary conditions and transformation from the cartesian coordinate system to the global coordinate system.

3.3.4 The Strip Stability Matrix

The procedure for calculating the strip stability matrix is similar to the one used for the calculation of the stiffness matrix with the exception of the use of the stress vector instead of the elasto-plastic modular matrix. This is also accomplished by numerical integration.

3.3.5 Impose Boundary Condition

For every strip the two edges are checked to determine whether external boundary conditions need to be applied. If the first edge is free or continuous the routine will check the second edge. If the second edge is free or continuous as well the routine skips that strip and advances to the next strip. The strip stiffness and stability matrices will not be altered. In cases where one edge is hinged, the diagonal element of the stiffness matrix corresponding to the out-of-plane deflection will have a very high value of the order of 1×10^{20} . The corresponding diagonal element in the stability matrix will be set to zero. For a fixed edge both the diagonal elements corresponding to the out-of-plane deflection and the rotation will be modified accordingly.

3.3.6 Transformation and Assembly of the Global Matrix and Solution

The basic strip stiffness and stability matrices are calculated with respect to the cartesian coordinate system. If the strip coordinate system does not coincide with the global coordinates the strip stiffness and stability matrices will be transformed as shown below:

$$[K] = [R]^T [\bar{K}] [R] \quad (3.66)$$

where

$[K]$ is the transformed strip matrix

$[R]$ is the transformation matrix

$[\bar{K}]$ is the strip matrix before transformation.

The transformed stiffness and stability matrices are assembled into the overall global matrix. This overall matrix is triangulated using Gaussian elimination. The resulting eigenvalue problem is solved using the Wittrick-Williams algorithm. The critical stress is determined as the stress at which the determinant of the sum of stiffness and stability matrices is zero.

The adequacy of this approach is established in the succeeding chapter where test data on columns' behaviour at both ambient and elevated temperatures are compared with the results obtained from the finite strip method. Furthermore, a parametric study is undertaken in the subsequent chapter.

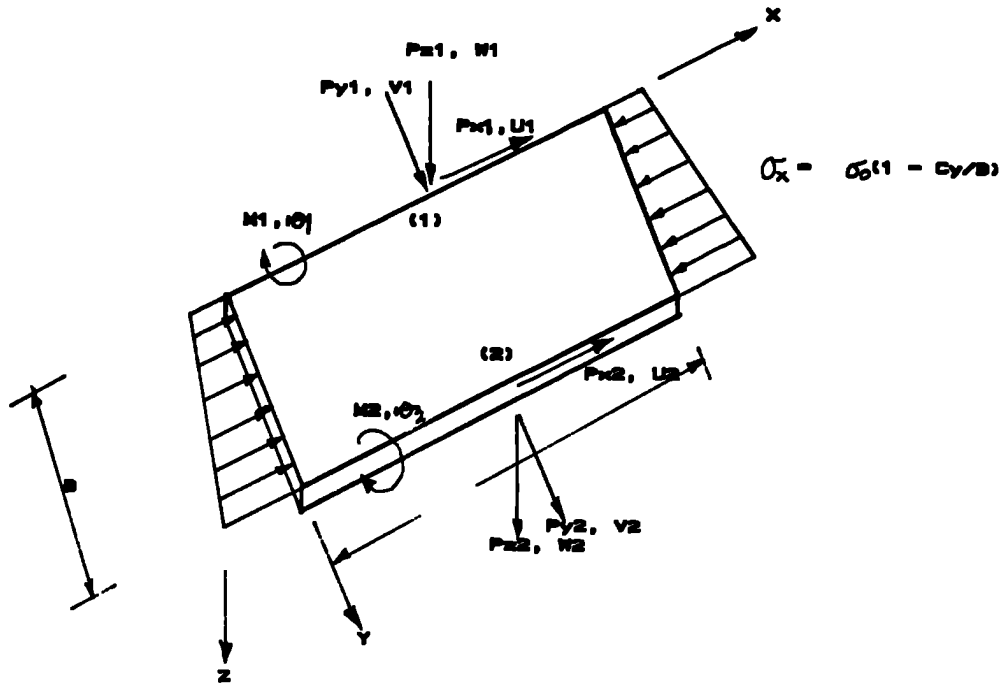


FIG. 3.1 A BASIC PLATE SHOWING COMPRESSIVE STRESS, EDGE FORCES AND DISPLACEMENT SYSTEM

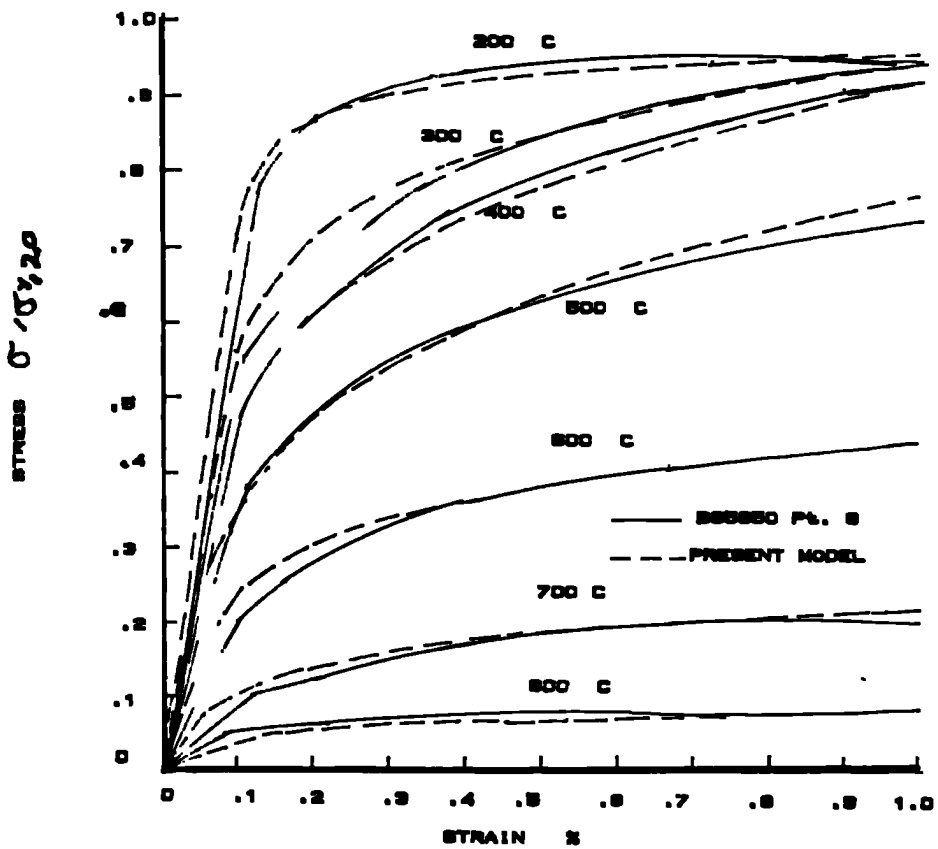
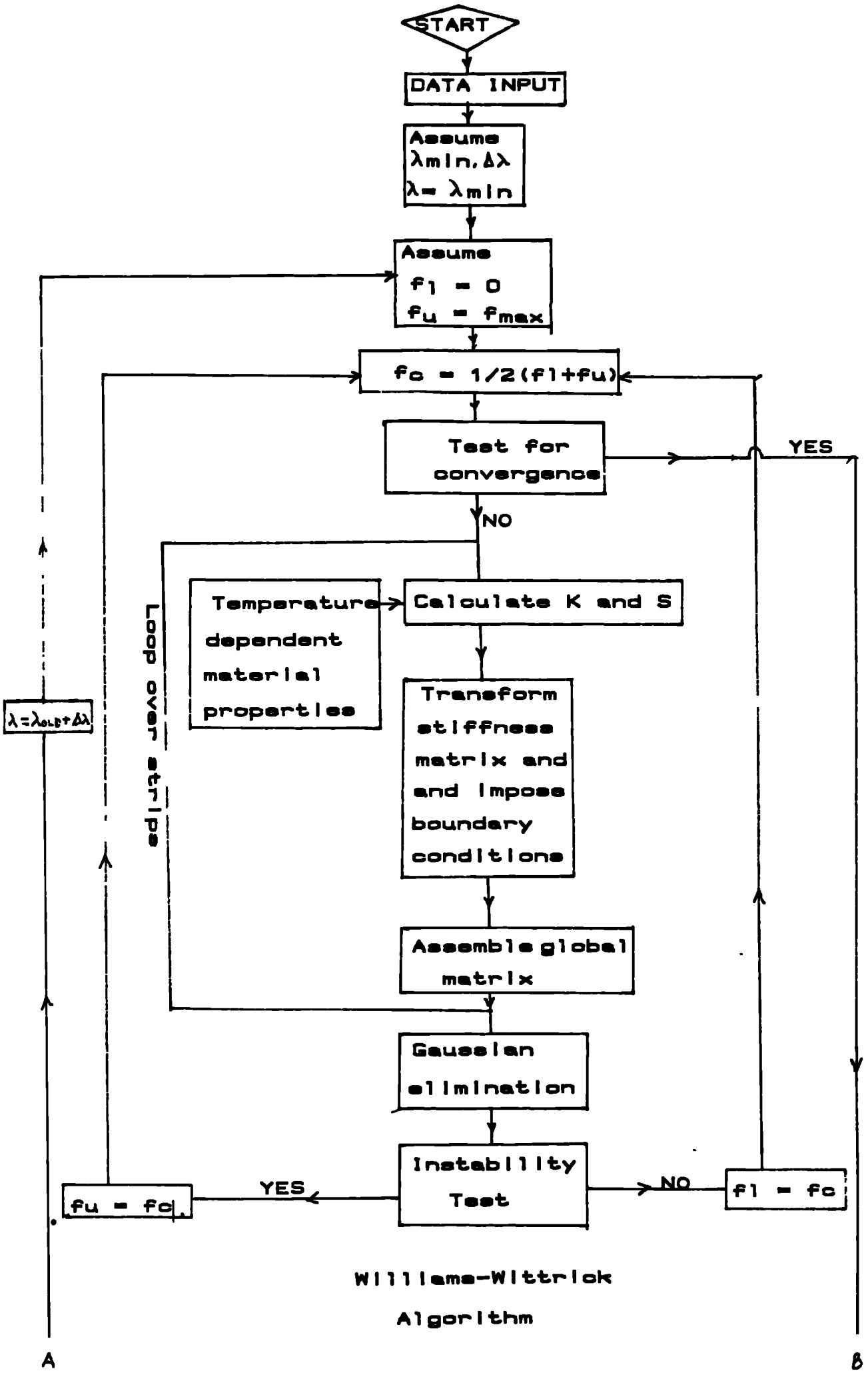
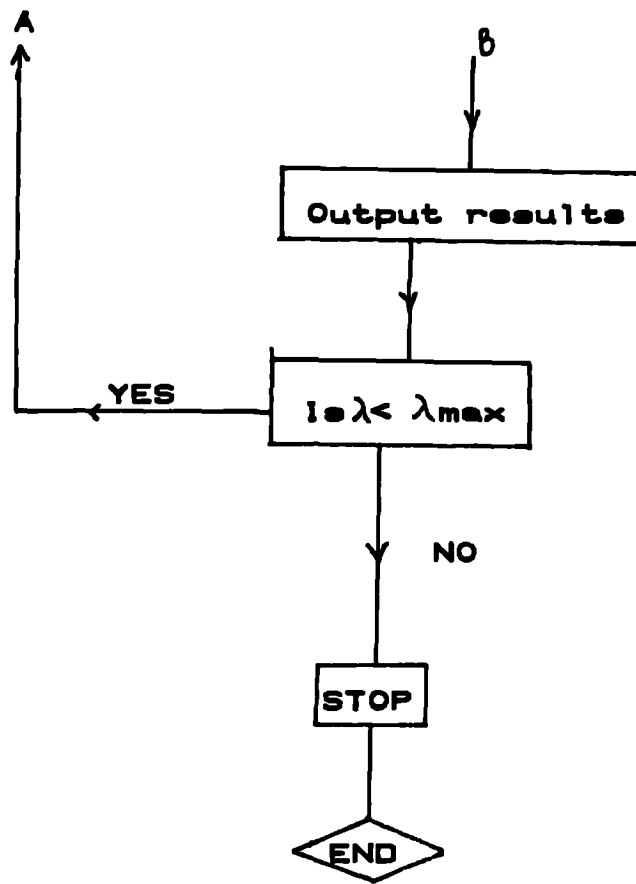


FIG. 3.2 COMPARISON BETWEEN BSSBDO Pt. 8 AND PRESENT METHOD STRESS-STRAIN CURVES





**FIG. 3.3 FLOW CHART FOR ELEVATED TEMPERATURE
BUCKLING ANALYSIS**

Chapter 4

COMPARISON WITH TEST DATA

The finite strip method developed in Chapter 3 has been thoroughly checked by analysing different isolated rectangular plates at ambient temperature. This exercise was undertaken in order to clarify the adequacy of the method at a basic level, and thus this is an auxiliary program validation. For more rigorous validation of the method comparisons were made with available test data on the ambient and elevated temperature buckling behaviour of steel columns.

4.1 Ambient Temperature Comparison

Horsley and Strymowicz[163] carried out tests on 130 columns of high strength steel with ambient temperature yield stress of 447 N/mm^2 . Five sections of dif-

ferent geometries were studied over a range of slenderness ratio. The influence of residual stress was investigated by comparing the behaviour of as-rolled and stress-free stub columns. They found that the residual stress had very little influence on the overall strength of columns tested. This may be connected with the high value of the material yield strength. During the course of testing they found that initial imperfections had very little effect on the final failure load. For comparison purposes a $203 \times 102 \times 25.3$ UC I-section was analysed using the finite strip method. There was no record of residual stresses and thus the finite strip analysis is based on consideration of the perfect member. This is justifiable in as much as the high strength of the material overshadows the effect of residual stresses. It is observed that the finite strip method results are in good agreement with the test data as shown in Fig. 4.1. The finite strip underestimates the buckling load of short columns with slenderness ratio of $l/r \leq 50$ by about 4%. This discrepancy may be attributed to the unavoidable restraint provided by real loading and support systems. Despite this limitation of the test procedure the finite strip method is found to be very efficient and adequate. There is close agreement between theory and experiment.

Tebedge et al[164] performed tests on some European wide flange sections. A total of 16 full-size columns were tested from each of the four source countries (Britain, Belgium, Italy, Germany) with slenderness ratios of 50 and 95. These slenderness ratios were chosen on the basis that they covered the critical range according to theoretical and practical considerations. The support conditions were; pin-ended in the direction of the minor axis and fixed in the direction of the major axis. The geometric characteristics of the columns were measured. These include the initial out-of-straightness. The residual stresses and the yield

strength were measured as well. The measured yield strength for the flanges varied between 198 and 250 N/mm^2 while that of the webs varied between 200 and 253 N/mm^2 . Compressive residual stresses of about $0.28\sigma_{y,20}$ were found at the edges of the columns. For comparison purposes a $W12 \times 161$ section was analysed over a range of slenderness ratio. The average yield strength of about 240 N/mm^2 was used in the analysis together with residual stress of $0.1\sigma_y$. It was found that the finite strip method results compared more closely with the test data than curve $B3 - 27$ of the ECCS. For columns with slenderness ratio $l/r \leq 50$, the finite strip method results and curve $B3 - 27$ are identical but for more slender columns ($l/r > 50$) curve $B3 - 27$ underestimates the test data considerably, as shown in Fig. 4.2. On the whole the finite strip method simulates the test data more accurately than curve $B3 - 27$. This shows the capability of the present method for the analysis of heavy sections.

Dibley[165] carried out a series of tests on beams of I-section under uniform bending moments. Four sections made up of two universal columns and two universal beams were chosen to cover a wide range of sections and slenderness ratios. Both initial imperfections and residual stresses were measured. Only two specimens were found to exhibit measurable values of initial imperfection. The testing was accomplished by a system of loading at four points so that the centre of the unsupported span carried a uniform bending moment. The beams' ends were constrained in guides to move vertically only, with the load applied vertically downwards. The measured values of maximum bending moments were reduced to account for the effect of dead load bending moment of the beam itself, and friction in the loading and support systems. For comparison purposes, both UB and UC sections were analysed with a parabolic

pattern of residual stress, of maximum $0.1\sigma_{y,20}$ accounted for. The plots of critical moment against the effective slenderness ratios are shown in Fig. 4.3a and 4.3b for the universal beam and column respectively. For the universal beam the finite strip method underestimates the critical moments by 4% for beams with effective slenderness ratio of $l/r \leq 60$, but the correlation between theory and experiment is good for more slender beams. The observations for the universal columns are similar to those for universal beams. In the two cases the finite strip method is found to compare very well with the test data.

The agreement between the theory and experiment demonstrated by these comparisons validates the finite strip method as an accurate numerical tool for the analysis of the collapse behaviour of structural elements under uniaxial compression or uniform bending moment.

4.2 Elevated Temperature Comparison

The above comparisons cover ambient temperature structural response. In this section the elevated temperature structural response is given consideration. It is apparent that previous theoretical predictions of elevated temperature fire resistance of steel columns is markedly lower than the experimental data. In an attempt to bridge this gap modification factors were used to buffer the theoretical predictions[135]. In the present consideration the unfactored results are compared with test data.

Vandamme and Janss[132] carried out high temperature tests on 29 columns.

The tests covered a wide range of parameters such as different cross-sections and slenderness ratios. During the course of experimentation both the geometrical and structural imperfections were measured. These imperfections were found to be within the acceptable tolerance adopted by the ECCS for study of the buckling characteristics of columns at ambient temperature. Material yield stresses were measured as well. Most of the specimens were protected, which ensured fairly uniform temperature distribution in the columns. The test specimens were placed in the furnace vertically and clamped in a special end device intended to provide rotational restraint at both ends. Each column was loaded axially and exposed to fire in accordance with the ISO 834 standard. The load applied to the column at ambient temperature was kept constant for the whole duration of the fire test. The longitudinal expansion of the loaded column was not restrained and the failure time was considered to be the time at which the thermal elongation due to temperature is balanced by the deflection due to softening. For comparison purposes, a buckling length of 50% of the test specimen length was used. As shown in Fig. 4.4 the finite strip results compared favourably with the test data. Although there is some scatter in the correlated results, the theory shows significant agreement with experiment.

Olesen[136] carried out tests on 30 columns covering a range of slenderness ratios. The columns were mounted horizontally in a special furnace and the furnace temperature was kept at a prescribed level for different tests. The loading on the column was increased at a constant rate until buckling developed. It was observed that the loading rate did not significantly affect the buckling load at temperatures lower than 500°C but its influence became no-

ticeable when the temperature was higher than 550°C due to creep effect. No information was reported on the extent of the creep effect on the behaviour of columns. The finite strip calculations were carried out assuming effective length of 50% of the test specimen. The theoretical and experimental data are compared in Fig. 4.5. There is remarkable agreement between the two although it should be noted that, due to lack of information reported for the tests, a nominal yield strength of $250N/mm^2$ was used in the calculations.

Aasen and Larsen[140] performed tests on 15 pin-ended and 5 end-restrained columns. All the test specimens were milled from IPE160 section. The average measured yield strength was $448N/mm^2$. Residual stresses were not measured i.e assumed zero residual stress due to milling. The tests covered a wide spread of parameters such as slenderness ratio, load level, rotational and axial restraints, end eccentricity, rate of loading, heating rate and temperature gradient. The test columns were mounted vertically and bolted to end fixtures which acted as hinged bearings. The heating was accomplished by low voltage elements attached to the outside of each flange. The test specimens were insulated with blankets of ceramic fibres which were made from a synthetic mixture of alumina and silica. The testing procedure comprised two phases. First, the load was applied in increments at room temperature. Second, at a prescribed level the load was kept constant while heating progressed. In order to introduce axial restraint the axial end displacement was fixed. For comparison purposes, the columns were analysed with 100% of the test specimen length used in the calculations. The results are compared in Fig. 4.6, which shows very good correlation between theory and experiment although there is some scatter of test results.

Knublauch et al[127] carried out comprehensive elevated temperature tests on steel columns in BAM-Berlin. The test specimen length was 3.6m with the ends outside the furnace. The lower end was placed on a hydraulic jack (supposed to function as a hinged end) which pressed the upper end against a beam connected to the loading frame (supposed to function as a built-in end). The ISO 834 heating path was followed. Due to the test specimen arrangement there was a thermal gradient along the length of the column. The temperature difference between the hottest and coldest parts of the column was in excess of 200°C. The temperature distribution in the embedded length(80% of test specimen) is fairly uniform. During testing the axial loading was kept constant while heating progressed and the thermal elongation was not restrained. The critical temperature was taken to be the average of the centre point temperatures. In the finite strip calculation, the uniform temperature assumed is taken over a buckling length corresponding to 70% of the specimen length. The theory is found to agree with the experiment to an appreciable extent as shown in Fig. 4.7.

Hoffend[137] carried out elevated temperature tests on steel columns with deliberate eccentricity of loading. The columns were tested vertically with an eccentrically applied axial load. No detailed information on the support conditions, residual stresses and initial out-of-straightness was reported. For comparison purposes, the finite strip analysis is based on the 70% of the specimen length without consideration given to the structural imperfections. The correlation between the finite strip method and test data is good as shown in Fig. 4.8. The scatter exhibited by the compared data is reasonably low.

British Steel Corporation[?] carried out fire tests on three 203 × 203 × 52UC columns to BS 476 Pt8 requirements. Two of these columns were partially protected with lightweight bricks built between the flanges using an ordinary strength mortar. This left the webs protected against thermal exposure. The third column was tested unprotected. The yield stress was measured and found to range between 276 and 349 N/mm^2 . The base of each column was embedded in concrete and a concrete cap was cast at the top to leave a 3m length of steel exposed. No information was available on base fixity and the residual stresses. For comparison purposes, the finite strip method analysis was based on 50% of the column length. It is found that the blocked-in-web columns tests were accurately simulated by the finite strip method while the bare column failure load was overestimated by 8% as shown in Table 4.1.

* blocked-in-web column

Table 4.1: Comparison between BSC test data and FSM

Column I.D	Temperature(°C)		Test Failure Stress	Computed Stress
	Flanges	Web		
1*	626	302	138	139
1*	701	395	83	80
1**	685	692	83	76

** bare column.

In all cases of elevated temperature comparisons the failure stress is the mean stress obtained by dividing the failure load by the member cross-sectional area.

From the above comparisons it is apparent that the finite strip approach is an efficient numerical method for analysing the collapse behaviour of steel columns

at elevated temperature. This method is subsequently used for parametric studies presented in the following chapter.

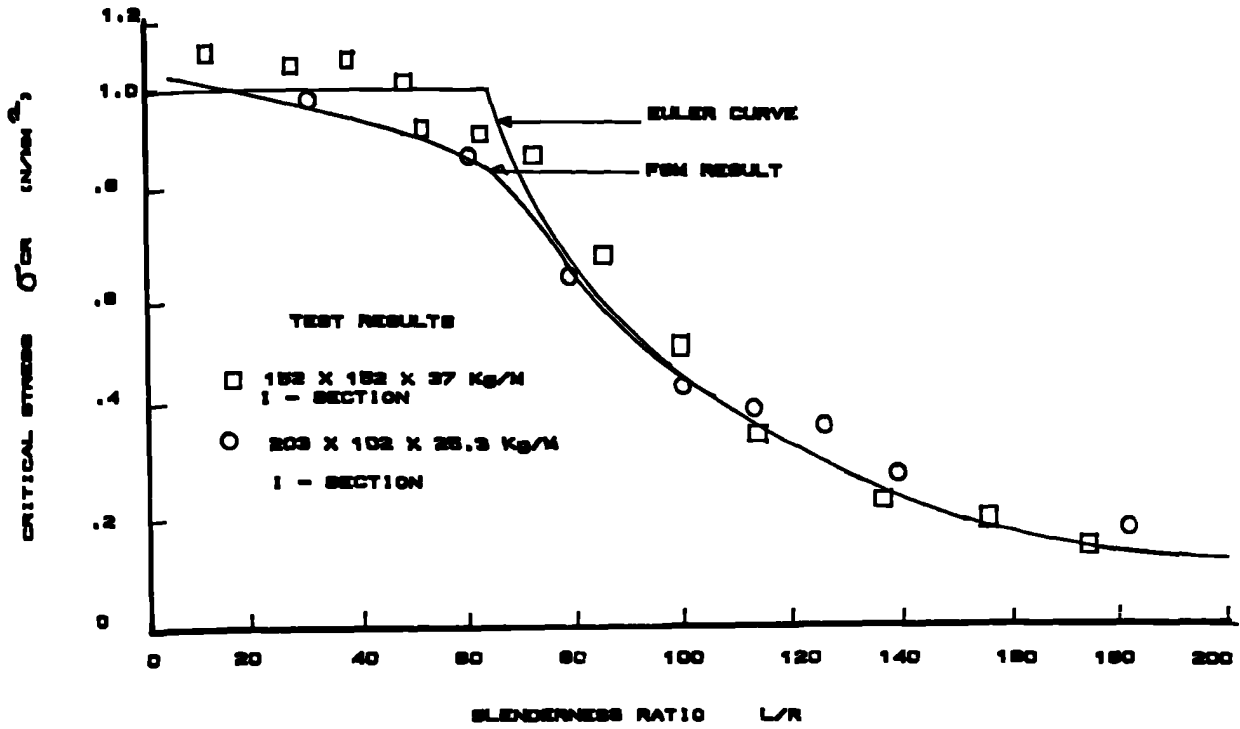


FIG. 4.1 COMPARISON OF FEM WITH HORSLEY AND STRYNOWICZ TEST RESULTS

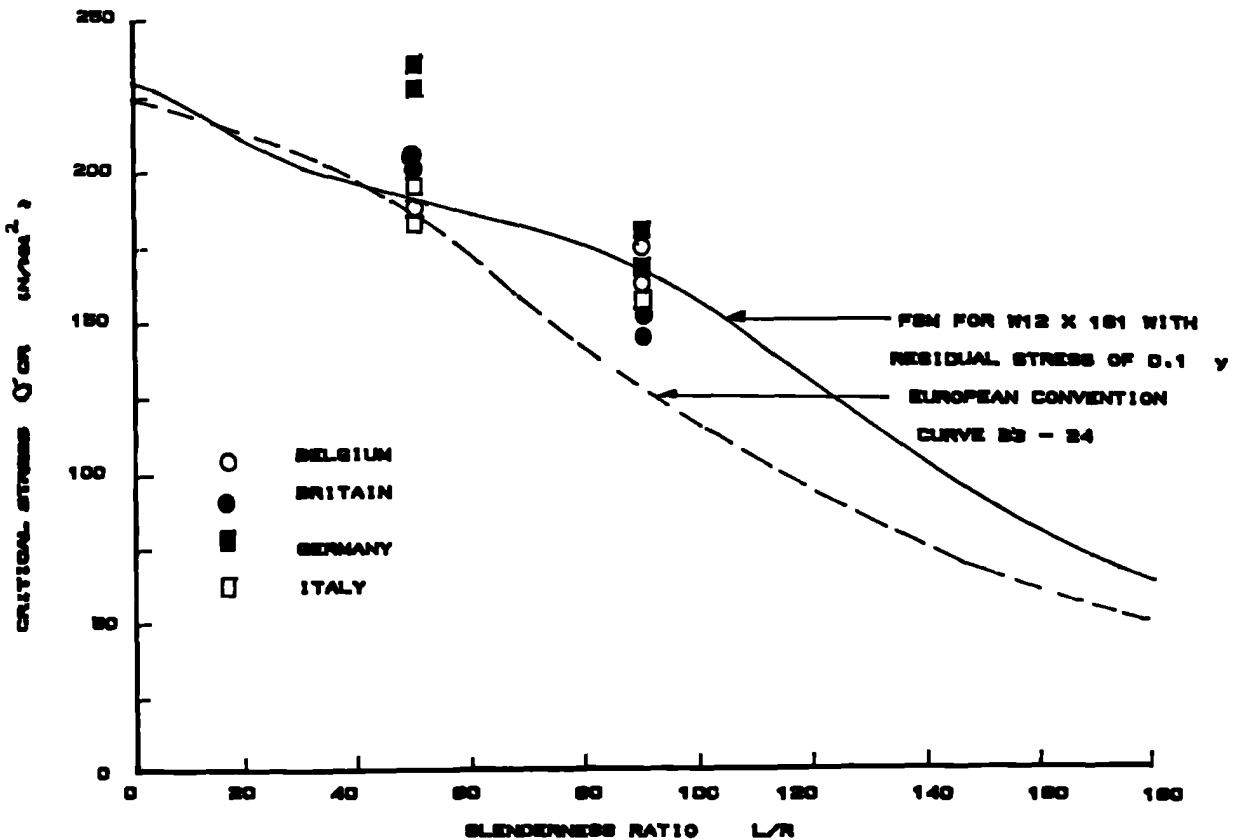


FIG. 4.2 COMPARISON OF FEM WITH COLUMN TEST RESULTS OF EUROPEAN WIDE FLANGE SHAPE

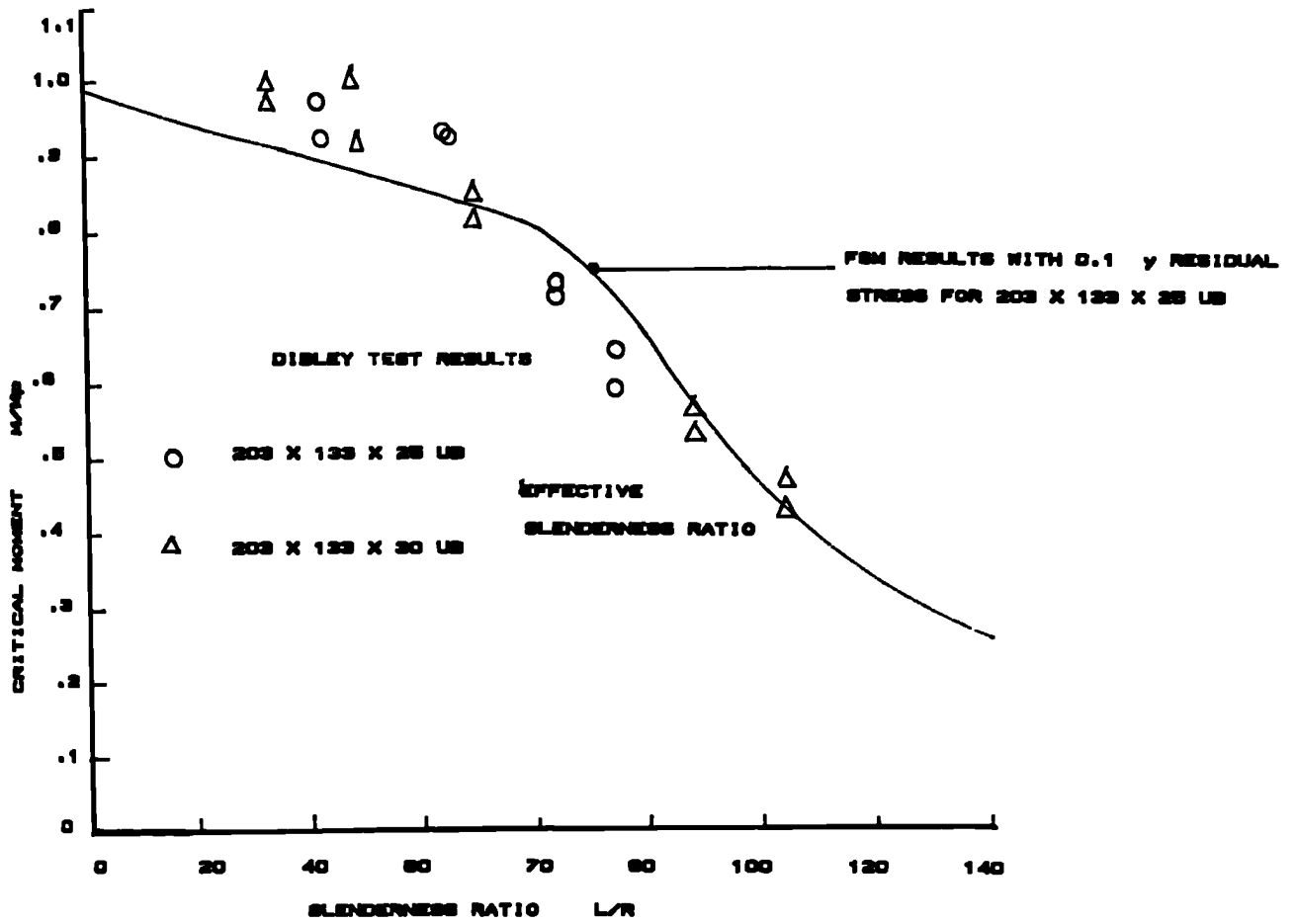


FIG. 4.3A UB - SECTIONS

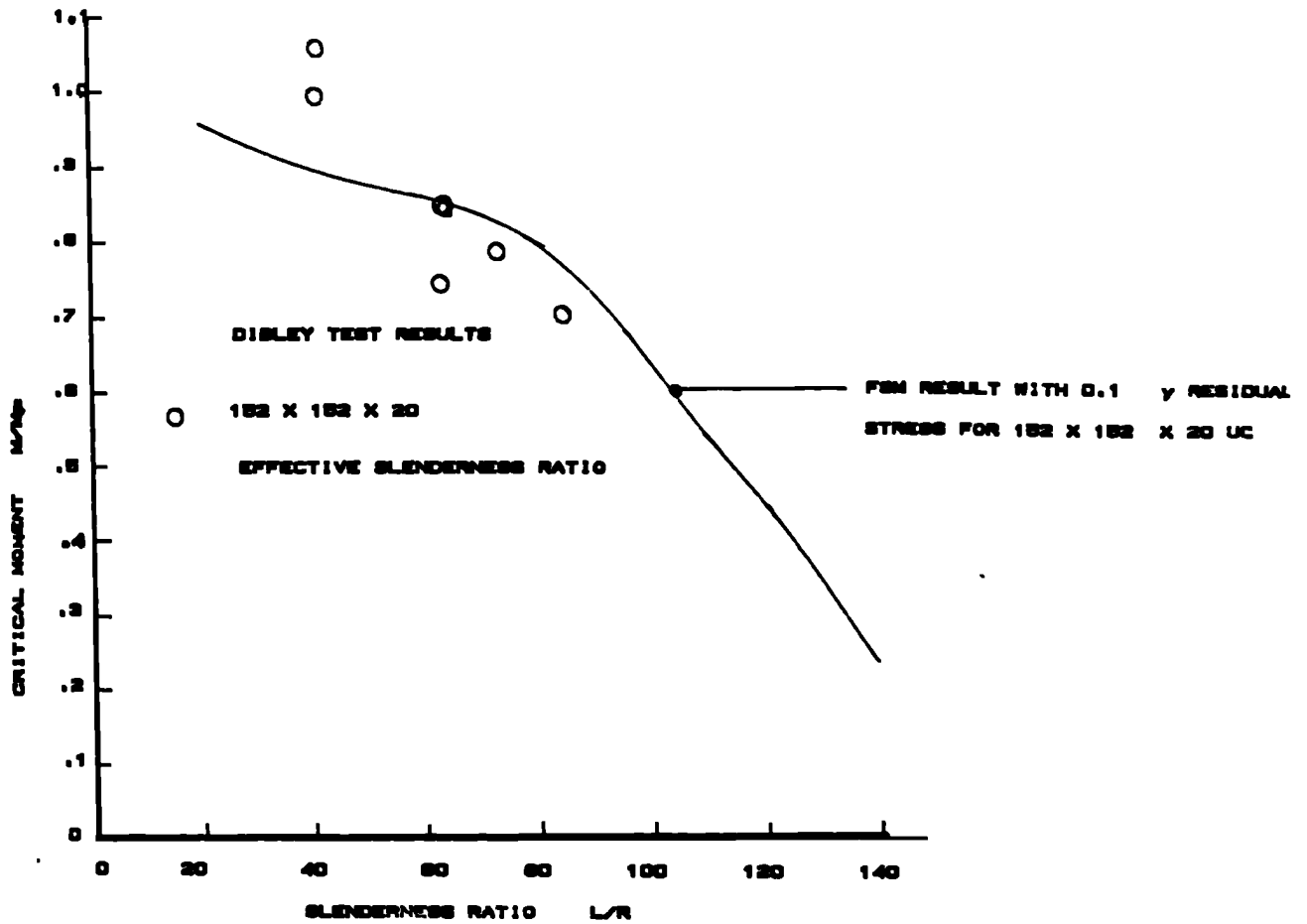


FIG. 4.3B COMPARISON OF FEM WITH DISLEY TEST RESULTS UC - SECTION

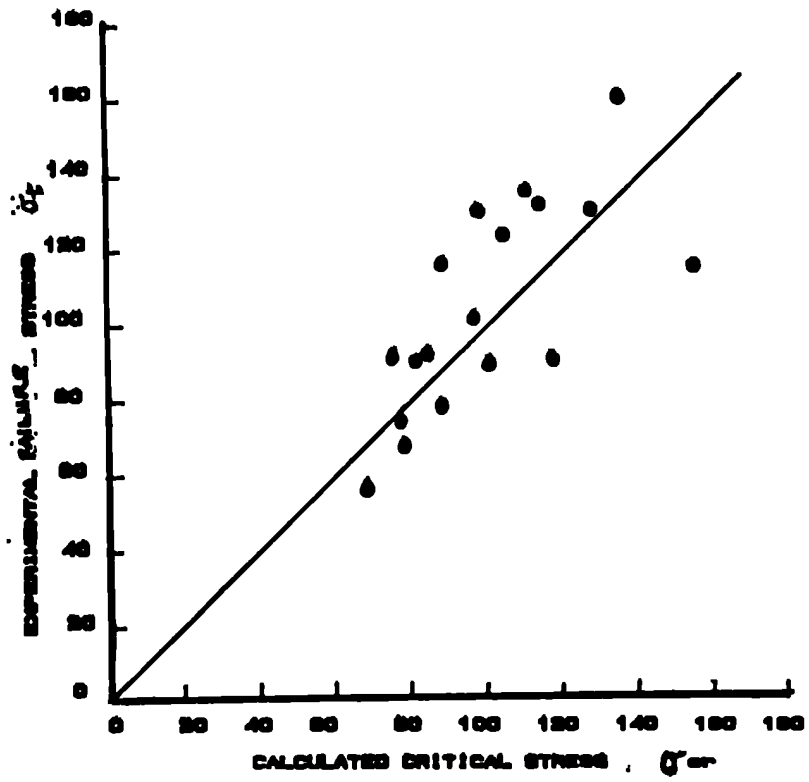


FIG. 4.4 COMPARISON OF FEM WITH VANDAMME AND JANSSE TEST RESULTS

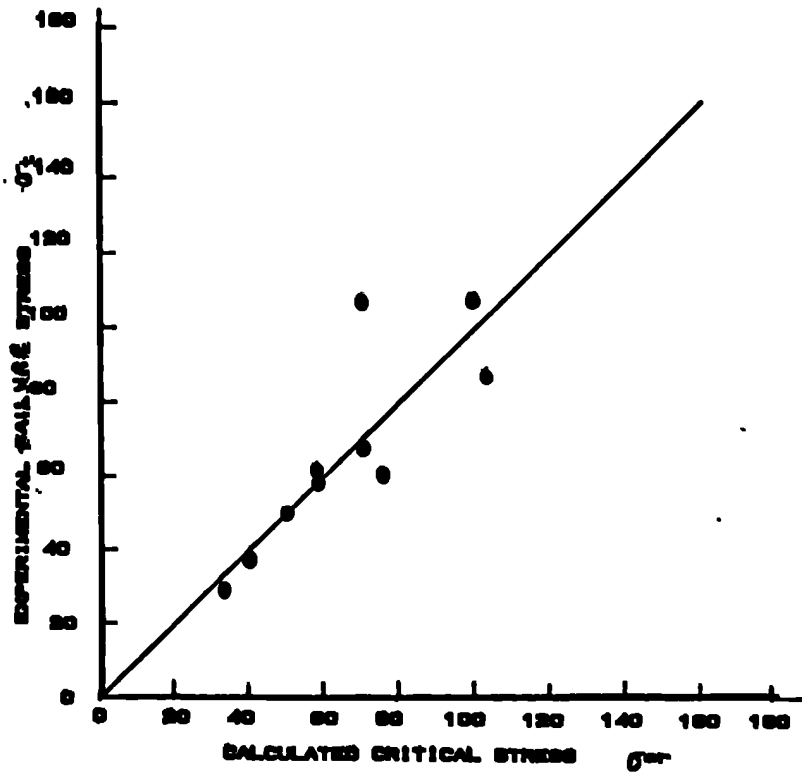


FIG. 4.8 COMPARISON OF FEM WITH DANISH TEST RESULTS

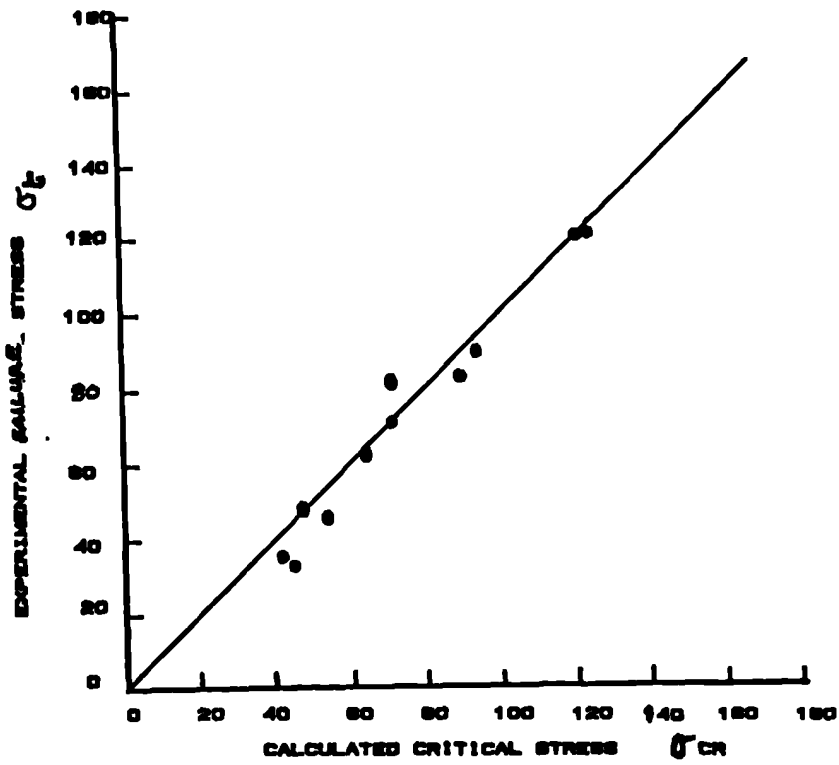


FIG. 4.6 COMPARISON OF FEM WITH ASEN TEST RESULTS

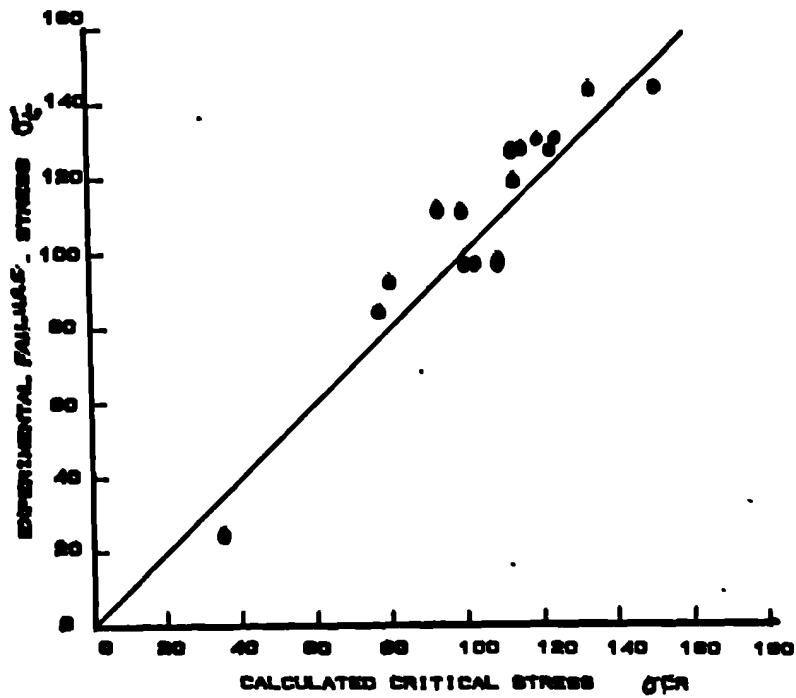


FIG. 4.7 COMPARISON OF FEM WITH BAM (WEST GERMANY) TEST RESULTS

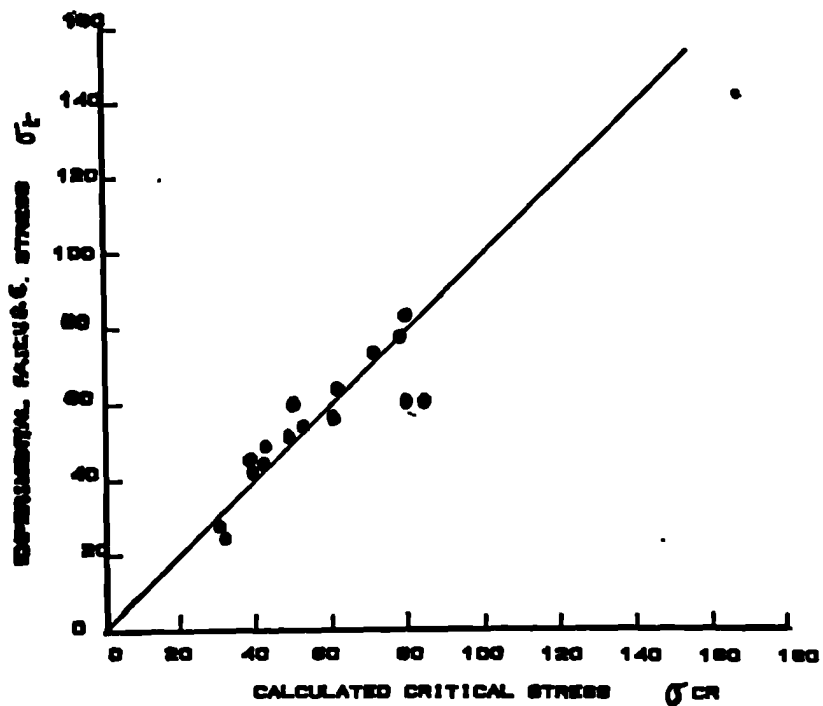


FIG. 4.8 COMPARISON OF FEM WITH HOFFEND TEST RESULTS.

Chapter 5

PARAMETRIC STUDIES

The finite strip method described in the previous chapter has been used to study the inelastic buckling of structural members at elevated temperature. Both columns and beams have been analysed with pin-ended conditions. This means that restriction is placed on the lateral deflection and twist at the ends but lateral bending is not restricted. The analysis excludes geometric initial imperfections and axial load-deformation behaviour. Only uniform temperature distributions are considered. These are the limitations of the present finite strip method. In practice, depending on the position of a member in a building, the temperature distribution in a member, both along its length and across the cross-section, may not be uniform. However, for internal columns exposed to fire from all sides the heating will be approximately uniform and the majority of investigations by others have been for such conditions. Hence the problems considered in this chapter, although restricted to uniform temperature distribution, have practical application. Non-uniform temperature

distribution across the cross-section is covered in Chapter 6.

The possible modes of failure are local and overall buckling, and material yielding. In general these will not occur in isolation but will interact, although in many cases one mode may be dominant. This will depend on many factors such as

- the slenderness ratio
- the stress-strain relationships and the material property expressions
- the magnitude and distribution of residual stress
- the eccentricity of loading
- the local buckling phenomenon

Many of the investigations carried out to date have been experimental. Because of the high cost involved only a limited number of parameters have been considered. The use of the present analysis offers an opportunity for extensive parametric study without the costs associated with a large experimental programme.

The effects of slenderness ratio of the member, the stress-strain-temperature relationships, residual stresses and load eccentricity are investigated. In addition a section is analysed under uniform bending to estimate the effect of fire on beams. The influence of local buckling on the behaviour of columns at elevated temperature is also investigated. The behaviour of blocked-in web columns is studied as well.

5.1 Effect of slenderness ratio

The inelastic behaviour of columns at ambient temperature depends on the slenderness ratio of the member. Elastic buckling can be divided into three main regions namely local, interaction and overall. The influence of each of these buckling modes depends on the magnitude of slenderness ratio. In some cases failure by material yielding may occur depending on the material stress-strain relationship. By applying the finite strip method to analyse columns at increasing temperature over a range of slenderness ratio, the effect of fire on each of these failure modes can be studied.

For the purpose of this study a $203 \times 203 \times 52$ UC section is analysed for a range of slenderness ratios from 20 to 180. The ambient temperature yield strength and modulus of elasticity are assumed to be 250 N/mm^2 and 205 kN/mm^2 respectively.

Fig. 5.1 shows the relationship between critical stress, σ_{cr} , and slenderness ratio for increasing temperature. The critical stress is non-dimensionalised with respect to ambient temperature yield stress, $\sigma_{y,20}$. At ambient temperature the familiar pattern of material yielding dominates for low slenderness ratio and elastic overall buckling at high slenderness ratios is evident. At 200°C a similar curve is obtained but the critical stress is clearly reduced compared with the ambient temperature condition. This reduction is approximately 12% for slenderness ratios up to 100 but becomes negligible for slenderness ratios greater than about 120.

At higher temperatures ($\theta > 200^\circ\text{C}$) the curves have the same form but again

the critical stress decreases with increasing temperature due to softening of the material. Also shown are the Euler overall buckling curves and the yield stress for various temperatures. For high slenderness ratios there exists a good approximation to the critical stress where loss of stiffness is evident while in the low slenderness ratios region the loss of strength dominates the behaviour. It is evident that for all slenderness ratios the influence of buckling is important.

The same information in Fig. 5.1 is presented in Fig. 5.2 as non-dimensionalised critical stress ($\sigma_{cr}/\sigma_{y,20}$) against temperature. It is noted that very stocky columns ($l/r \leq 20$) lose strength gradually as the temperature increases up to 500°C. The decrease in the buckling stress becomes rapid as the temperature increases further. This behaviour is similar to the variation of yield stress with temperature also shown in Fig. 5.2. This shows that the failure of very stocky columns is dominated by yielding.

The response of intermediate columns, $40 \leq l/r \leq 80$, is similar to that of stocky columns but at reduced buckling stress. However, in this range of slenderness ratios the reduction in buckling stress with increasing temperature is more uniform and shows no sudden drop, due to the interaction between buckling and yielding.

The slender columns, $100 \leq l/r \leq 140$, respond differently by exhibiting a much reduced rate of loss of capacity within the temperature range $20^\circ\text{C} \leq \theta \leq 250^\circ\text{C}$. This rate decreases further with increasing slenderness ratio. For such slender columns Euler buckling is of course more important, and the influence of material stiffness is therefore more pronounced. At temperatures higher than 250°C the bearing capacity begins to decrease more rapidly.

Fig. 5.3 shows the same information as Fig. 5.2 but as a plot of critical stress, non-dimensionalised with respect to ambient temperature critical stress, $\sigma_{cr,20}$, rather than yield stress, $\sigma_{y,20}$. The curves show a wide spread depending on slenderness ratio. It becomes clear that columns with different slenderness ratios lose strength at different rates as temperature increases. The critical temperature can be considered as the temperature at which the critical stress is reduced to, say, 60% of the ambient temperature bearing capacity. The wide range of critical temperatures exhibited by these columns is quite evident. For example, stocky columns ($l/r = 20$) exhibit critical temperatures of about 520°C while the corresponding value for a slender column ($l/r = 100$) is about 300°C. This suggests that the general notion that columns become unstable at 550°C is not applicable to all columns.

It may seem surprising that failure of some columns occurs at temperature as low as about 300°C. However this was also shown to be the case by Witteveen and Twilt[152] whose experimental data are also shown on Fig. 5.4 where critical temperature is plotted against slenderness ratio. It is quite clear that experimental data are somewhat lower than predicted values but the general form of critical temperature variation with slenderness ratio is similar. The difference in the predicted and experimental critical temperatures may be connected with the fact that the finite strip calculations are based on perfect column conditions. The inclusion of structural imperfections such as residual stresses may reduce the predicted critical temperature. It is clear that both the stocky and very slender columns exhibit a better performance than columns of intermediate slenderness ratios which are perhaps more typical of those used in buildings. It seems reasonable to conclude that the behaviour of stocky

columns is dependent on the yield strength while slender columns are greatly influenced by the elastic modulus. The interaction between the yield strength and reduction of stiffness may be dominant in the behaviour of intermediate columns. This appears to result in the reduced performance of such columns.

Clearly this should be reflected in any quantitative design approach for columns in fire because of different conditions prevailing in their behaviours. For example, the behaviour of stocky columns is dominated by material yielding while slender columns show an elastic overall buckling. The response of intermediate columns is controlled by the interaction between material yielding and elastic overall buckling. These features must be reflected in any fire engineering system for column design.

5.2 Effect of stress-strain relationships

In fire steel strength properties degrade with increasing temperature. At a temperature in excess of 300°C these properties become markedly non-linear. This clearly indicates a continuous form of material constitutive equation. This brings into question the validity of a bilinear stress-strain-temperature relationship. However, because of its simplicity such a bilinear form is attractive, with the stress-strain-temperature relationship represented in terms of yield stress and elastic modulus. Many proposals for expressions relating yield stress and modulus of elasticity to temperature have been reported in the literature but only the ECCS[128], CTICM[149] and those derived on the basis of BS5950 Pt.8[162] test data (Equation (3.48) to (3.62)) are considered. The

expressions for strength properties recommended by ECCS for fire resistance analysis and design of structural steel members are

$$\sigma_{y,\theta} = \sigma_{y,20} \left(1 + \frac{\theta}{767 \ln \left(\frac{\theta}{1750} \right)} \right) \quad 0^\circ\text{C} \leq \theta \leq 600^\circ\text{C}$$

$$\sigma_{y,\theta} = \sigma_{y,20} \left(\frac{108 \left(1 - \frac{\theta}{1000} \right)}{\theta - 440} \right) \quad 600^\circ\text{C} \leq \theta \leq 1000^\circ\text{C} \quad (5.1)$$

$$E_\theta = E_{20} \left(-17.2 \times 10^{-12} \theta^4 + 11.8 \times 10^{-9} \theta^3 - 34.5 \times 10^{-7} \theta^2 + 15.9 \times 10^{-5} \theta + 1 \right) \quad 0^\circ\text{C} \leq \theta \leq 600^\circ\text{C} \quad (5.2)$$

$\theta > 600^\circ\text{C}$, E_θ is not defined.

The CTICM expressions are given by:

$$\sigma_{y,\theta} = \sigma_{y,20} \left(1 + \frac{\theta}{900 \ln \left(\frac{\theta}{1750} \right)} \right) \quad 0^\circ\text{C} \leq \theta \leq 600^\circ\text{C}$$

$$\sigma_{y,\theta} = \sigma_{y,20} \left(\frac{340 - 0.34\theta}{\theta - 240} \right) \quad 600^\circ\text{C} \leq \theta \leq 1000^\circ \quad (5.3)$$

$$E_\theta = E_{20} \left(1 + \frac{\theta}{2000 \ln \left(\frac{\theta}{1100} \right)} \right) \quad 0^\circ\text{C} \leq \theta \leq 750^\circ \quad (5.4)$$

$\theta > 750^\circ\text{C}$, E_θ is not defined.

where

$\sigma_{y,\theta}$ is the yield stress at elevated temperature

$\sigma_{y,20}$ is the ambient temperature yield stress

E_θ is the modulus of elasticity at elevated temperature

θ is the temperature in $^\circ\text{C}$

The continuous stress-strain-temperature relationship is modelled on the Ramberg-Osgood formula (Equation (3.47)) as shown in Fig. 3.2 and the elastic-perfectly plastic stress-strain-temperature relationship is given by:

$$\sigma = E_\theta (\epsilon_{y,\theta} + \delta (\epsilon - \epsilon_{y,\theta})) \quad (5.5)$$

$$\delta = 1 \quad \sigma < \sigma_{y,\theta}$$

$$\delta = 0 \quad \sigma \leq \sigma_{y,\theta}$$

where σ is the stress and $\epsilon_{y,\theta}$ is the effective yield strain corresponding to $\sigma_{y,\theta}$ at elevated temperature.

For the purpose of this study a $203 \times 203 \times 52$ UC section was analysed. The assumed ambient temperature yield stress and modulus of elasticity are 250N/mm^2 and 205kN/mm^2 respectively. The results are presented as critical stress-slenderness ratio and critical stress-temperature relationships. The critical stress is non-dimensionalised with respect to ambient temperature yield strength.

5.2.1 Comparison between bilinear and continuous stress-strain-temperature representation(BS5950)

The curves shown in Figs. 5.1 and 5.2 in section 5.1 were obtained using the BS5950 data represented as a continuous stress-strain-temperature relationship. The characteristics of the predicted column behaviour based on this representation have been discussed in the previous section.

Similar calculations for the same stress-strain-temperature relationships but using an assumed bilinear representation are presented in Fig. 5.5 and 5.6. The relationship between critical stress and slenderness ratio is plotted in Fig. 5.5. The critical stress is non-dimensionalised with respect to the ambient temperature yield stress, $\sigma_{y,20}$. There are two distinct features associated with

these curves. The stocky and intermediate columns, $l/r \leq 80$, buckle at effective squash loads while slender columns, $l/r > 80$, fail in an elastic overall buckling mode. It is observed that the tendency for columns to buckle at effective squash loads increases with temperature. For example at ambient temperature the maximum slenderness ratio for column buckling at effective squash is 80 while at 700°C this value has increased to 105. This is in sharp contrast to the observation made on the column curves generated using a continuous stress-strain relationship with the same material property expressions (Fig. 5.1), where a sharp decline in the buckling stress was noted at a slenderness ratio of about 25 for temperatures beyond 200°C . It is interesting to note that there is no difference in the behaviour of columns with slenderness ratios of $l/r \leq 80$ under bilinear stress-strain representation.

In Fig. 5.6 the same information as in Fig. 5.5 is presented as a non-dimensionalised critical stress ($\sigma_{cr}/\sigma_{y,20}$)-temperature relationship. It is clear that the buckling stress decreases gradually within the temperature range of $20^\circ\text{C} \leq \theta \leq 450^\circ\text{C}$ for the whole range of slenderness ratios, $l/r \leq 180$, considered. As temperature increases further the decrease in buckling stress becomes rapid. Comparing these characteristics with Fig. 5.2 shows that bilinear form of representation of material properties leads to the behaviour of stocky and intermediate columns, $l/r \leq 80$, being identical. This is in marked contrast to the response of such columns under continuous form of representation in which a clear distinction in behaviour is observed.

5.2.2 Comparison between bilinear and continuous stress-strain-temperature representation(ECCS)

The results presented in Figs. 5.7 to 5.10 represent the same analysis in which the ECCS[134] expressions were used with both bilinear and continuous stress-strain-temperature representations. The range of data generated using the ECCS expressions is limited to a maximum temperature of 600°C, due to the fact that E_{θ} is not defined at temperatures greater than this.

In Figs. 5.7 and 5.8 the curves show the results of calculations using continuous stress-strain-temperature relationships. In Fig. 5.7 the critical stress(non-dimensionalised with respect to ambient temperature yield stress)-slenderness ratio relationship is plotted at increasing temperature. The familiar response of columns under continuous stress-strain-temperature representation is evident, although at a different buckling stress level depending on the yield stress and elastic modulus expressions. Generally the buckling stress decreases with increasing temperature.

The same information in Fig. 5.7 is presented in Fig. 5.8 as a non-dimensionalised critical stress-temperature relationship. This shows a steady decline in buckling stress for stocky columns ($20 \leq l/r \leq 40$) throughout the range of temperatures considered. The behaviour of intermediate columns, $40 < l/r \leq 80$, does not differ significantly from this. However slender columns, $100 \leq l/r \leq 140$, exhibit a gradual decline in buckling stress within the temperature range of $20^{\circ}\text{C} \leq \theta \leq 200^{\circ}\text{C}$ but as temperature increases beyond 200°C there exists a rapid decrease.

The results of the same analysis using a bilinear stress-strain-temperature relationship are presented in Figs. 5.9 and 5.10. In Fig. 5.9 the curves show a non-dimensionalised critical stress($\sigma_{cr}/\sigma_{y,20}$)-slenderness ratio relationship at increasing temperature. It is clear that both the stocky and intermediate columns, $l/r \leq 80$, buckle at effective squash loads within the temperature range of $20^\circ\text{C} \leq \theta \leq 500^\circ\text{C}$. This range of columns buckling at effective squash loads decreases slightly as the temperature increases beyond 500°C .

Fig. 5.10 shows the same information as in Fig. 5.9 as a non-dimensionalised critical stress($\sigma_{cr}/\sigma_{y,20}$)-temperature relationship. There is consistent depreciation in buckling stress with temperature for a range of columns with slenderness ratios $l/r \leq 80$. For other columns there exists a more gradual decline in the buckling stress up to a certain temperature before rapid decrease in buckling stress is experienced. For example, a column with slenderness ratio of 100 exhibits a gradual decline in bearing capacity up to a temperature of about 200°C while a column with a slenderness ratio of 140 exhibits the same behaviour up to 400°C . This shows that as the slenderness ratio increases the influence of temperature reduces. It is quite evident that the bilinear stress-strain-temperature representation results in an identical behaviour for stocky and intermediate columns, $l/r \leq 80$ unlike the continuous stress-strain-temperature representation.

5.2.3 Comparison between bilinear and continuous stress-strain-temperature representations(CTICM)

The same calculations described above were performed using CTICM[149] expressions using both the continuous and bilinear stress-strain-temperature representations. The results of these are presented in Figs. 5.11 to 5.14.

In Figs. 5.11 and 5.12 the results of the analysis using a continuous stress-strain-temperature representation are presented as curves of non-dimensionalised critical stress($\sigma_{cr}/\sigma_{y,20}$)-slenderness ratio. The familiar response of columns under continuous stress-strain-temperature representation is evident again but at a different buckling stress level depending on the yield stress and modulus of elasticity expressions. It is noted that buckling strength decreases with increasing temperature.

In Fig. 5.12 the same information as in Fig. 5.11 is plotted as a non-dimensionalised critical stress-temperature relationship. The linear relationship between critical stress and temperature for stocky columns($l/r \leq 40$) is quite evident. For intermediate columns, $60 \leq l/r \leq 80$, the characteristics of these curves do not differ significantly from the behaviour of stocky columns except that the buckling stress shows an increasingly marked decline at a temperature of about 200°C. For more slender columns the initial loss of strength within the low temperature range, $\theta \leq 200^\circ\text{C}$, is less.

The characteristics of the column behaviour using a bilinear stress-strain-temperature representation are shown in Figs. 5.13 and 5.14. The curves in Fig. 5.13 show the non-dimensionalised critical stress ($\sigma_{cr}/\sigma_{y,20}$)-slenderness

ratio relationship at increasing temperature. It is clear that the columns with slenderness ratios of $l/r \leq 90$ buckle at an effective squash load.

In Fig. 5.14 the same information as in Fig. 5.13 is plotted as the relationship between non-dimensionalised critical stress and temperature. It is clear that both stocky and intermediate columns, $l/r \leq 90$, exhibit a steady decline in buckling stress throughout the range of temperature considered. It is noted that this group of columns exhibit identical characteristics.

5.2.4 Comparison between different continuous stress-strain-temperature representations

In order to draw comparisons between different strength expressions using continuous stress-strain-temperature representations the relationship between non-dimensionalised critical stress ($\sigma_{cr}/\sigma_{y,20}$) and slenderness ratio for the three proposals (BS5950, ECCS and CTICM) is plotted in Fig. 5.15. It is clear that the predictions of buckling behaviour of columns based on the ECCS expressions are the most conservative of the three. The BS5950 expressions result in the highest buckling stress predictions. This difference increases with increasing temperature. The difference in the column response using these expressions increases with temperature. For example, for low slenderness ratios, $l/r \leq 80$, at 200°C the difference between critical stress calculated using BS5950 and ECCS expressions is about 10% but at about 400°C this increases to about 31%. However, for high slenderness ratios, $l/r > 120$, at 200°C the CTICM expressions result in the highest buckling stress, albeit marginally different. It

is noted that with further increase in temperature this discrepancy decreases even further. Generally, the CTICM expressions result in a column response intermediate between the other two. The column responses using these expressions become identical as slenderness ratio increases beyond the region where interactive buckling is effective (i.e. for slender column). For example the difference in the behaviour of slender columns, $l/r > 120$, using these expressions is insignificant within the temperature range of $\theta \leq 200^\circ\text{C}$. It is noted that both ECCS and CTICM expressions result in almost identical predictions at 200°C .

5.2.5 Comparison between different bilinear stress-strain-temperature representations

In order to draw comparisons between different strength expressions using the bilinear stress-strain-temperature representation the relationship between non-dimensionalised critical stress ($\sigma_{cr}/\sigma_{y,20}$) and slenderness ratio for the three proposals (BS5950, ECCS and CTICM) is plotted in Fig. 5.16. It is noted that BS5950 expressions always yield the highest buckling predictions, especially in the region of stocky and intermediate columns, $l/r \leq 80$. This difference increases with temperature. For example, at 200°C the difference between buckling stress calculated using both the BS5950 and ECCS expressions is about 6% while at 400°C the difference is about 31%. For more slender columns, $l/r > 100$, their behaviour becomes identical under the three sets of expressions within the temperature range of $20^\circ\text{C} \leq \theta \leq 400^\circ\text{C}$. Both the BS5950 and CTICM expressions result in the same buckling predictions for such columns

throughout the range of temperature considered.

5.2.6 Summary of comparisons

For more comparisons the critical stress-temperature relationships using both bilinear and continuous stress-strain-temperature representations for each of the three proposals (BS5950, ECCS and CTICM) are plotted in Fig. 5.17(a to d) for different slenderness ratios. It is noted that for stocky and intermediate columns the bilinear stress-strain-temperature representation results in higher buckling strength prediction than the continuous form of representation, although the discrepancy diminishes as slenderness ratio increases. For example at 300°C the difference in the buckling stress corresponding to an intermediate column, $l/r = 80$, under both bilinear and continuous stress-strain-temperature relationships is about 24% while for a slender column, $l/r = 140$, the difference is about 8%. For a very slender column, $l/r > 140$, all the three sets of expressions result to the same buckling strength within the temperature range of $20^{\circ}\text{C} \leq \theta \leq 200^{\circ}$. It is observed that the ECCS expressions result in the same curves under the two stress-strain representations.

From the discussion above it is clear that the non-linear representation of the steel material properties exhibits a considerable influence compared to the bilinear stress-strain-temperature representation. This is evident in the region of stocky and intermediate columns in which the bilinear form fails to show any distinction in such columns' behaviour under all cases of strength property expressions. Furthermore the buckling strength predictions under the bilinear stress-strain-temperature representation result in higher values compared

with the continuous form. It is noted that the discrepancy between columns' response under both bilinear and continuous representations diminishes with increasing slenderness ratio.

5.3 Effect of residual stress

Residual stresses are known to influence the early failure of hot-rolled and welded structural members at ambient temperature. These stresses result from differential cooling taking place during fabrication or manufacture. The differential cooling leads to variation in the temperature, and the parts which cool first contain residual compressive stress while the parts that cool later contain residual tension. The residual stresses depend on the shape of the cross-section (i.e the heavier the section the larger the magnitude of the residual stresses). Up to the present no experimental work has been reported on the measurement of the effect of residual stresses on steel columns in fire. This leaves a gap in understanding the extent of their influence on the behaviour of steel columns in fire.

In order to study the influence of residual stresses on steel columns in fire a parabolic residual stress pattern is assumed, as shown in Fig. 5.18a. No attempt is made to redistribute these stresses in fire. Since the heating encountered by a member in a building fire differs substantially from the heating and cooling cycles in the annealing processes the residual stress magnitude at elevated temperature is assumed to be the same as its ambient temperature magnitude. A $203 \times 203 \times 52$ UC section was analysed over a range of slender-

ness ratios at various levels of residual stress magnitude ($0.1\sigma_{y,20} - 0.5\sigma_{y,20}$). The ambient temperature yield stress and modulus of elasticity are assumed to be $250N/mm^2$ and $205kN/mm^2$ respectively.

In Fig. 5.18a to 5.18d the non-dimensionalised critical stress ($\sigma_{cr}/\sigma_{y,20}$)-temperature relationships at various levels of residual stress are plotted for different slenderness ratios. It is clear that buckling strength decreases as residual stress increases but the effect is approximately even for stocky and intermediate columns, $l/r \leq 60$. For example in Fig. 5.18a the curves for a stocky column, $l/r = 20$, are evenly distributed throughout the range of temperature considered. The general trend of buckling stress decreasing as temperature increases is still evident. The decrease is steady until a temperature of about $500^\circ C$ is reached, beyond which a rapid decline in the buckling strength is evident. The behaviour of intermediate columns, $l/r = 60$, differs significantly from that of stocky columns as shown in Fig. 5.18b. The buckling strength varies approximately linearly with temperature at low levels of residual stress ($0.1\sigma_{y,20} - 0.2\sigma_{y,20}$), but at high residual stress levels there is a sudden drop in the buckling strength within the temperature range of $200^\circ C \leq \theta \leq 400^\circ C$. These characteristics are identical to the behaviour of slender columns, $l/r = 100$, as shown in Fig. 5.18c but at a reduced buckling stress level. The behaviour of a very slender column, $l/r = 140$, differs significantly from that of stocky and intermediate columns(Fig. 5.18d). It is noted that only high values of residual stress, $\sigma_r \geq 0.5\sigma_{y,20}$, influence the behaviour of such columns at relatively low temperature.

It becomes apparent that only a very high value of residual stress influences

the behaviour of very slender columns at temperatures lower than 200°C. Generally, the influence of residual stress diminishes as slenderness ratio increases at elevated temperature.

In Fig. 5.19a to 5.19e the non-dimensionalised critical stress ($\sigma_{cr}/\sigma_{cr,20}$) with respect to ambient temperature critical stress is plotted against temperature. For columns with slenderness ratio of $l/r > 60$ it is obvious that as the level of residual stress increases these curves become more tightly grouped. In the region where the critical stress is reduced to, say, 60% of the ambient temperature bearing capacity there exists a wide range of critical temperature depending on slenderness ratios. These are plotted as critical temperature-slenderness ratio relationships at different residual stress levels as shown in Fig. 5.20. It is interesting to note that at low levels of residual stress ($\sigma_r = 0.1\sigma_{y,20}$) the pattern of these curves does not differ significantly from the curve corresponding to an initially stress-free condition. The critical temperature decreases as the residual stress level increases. The behaviour of a stocky column, $l/r = 20$, is not significantly influenced by the residual stress, as reflected in the limited range of critical temperature exhibited (512°C to 526°C). It is noted that at the maximum level of residual stress considered, $\sigma_r = 0.5\sigma_{y,20}$, the critical temperature for columns with a slenderness ratio of $l/r \geq 80$ remains fairly constant (i.e about 260°C).

The very slender columns, $l/r \geq 160$, show a considerable variation in critical temperature with increasing level of residual stress. For example, the range of critical temperature exhibited by columns with a slenderness ratio of 160 is between 272°C and 413°C at maximum and minimum levels of residual

stress respectively. This shows that this class of columns is more susceptible to the influence of residual stress in terms of performance in fire relative to the ambient temperature condition.

It can be concluded that residual stress is detrimental to the performance of steel columns in fire but the magnitude of the effect of these stresses varies from column to column. The behaviour of very stocky columns, $l/r \leq 20$, is not influenced by the presence of residual stress. It can be concluded that the bigger the magnitude of residual stress the more is the possibility for slender columns to exhibit identical behaviour (the same critical temperature).

5.4 Effect of eccentricity of loading

The difficulty in achieving a properly aligned structure implies that eccentricity of loading will often occur in columns. The direction of eccentricity of loading may be along both axes of buckling in the plane of the sections. It is understood that when this tends to induce bending about the strong axis its effect is very small and thus can be neglected. The maximum effect occurs when it acts to induce bending about the weak axis. Thus at elevated temperature only the applied eccentricity inducing bending about the weak axis is considered with uniform temperature distribution.

For the purpose of this study a normal $203 \times 203 \times 52$ UC section was analysed at different levels of applied eccentricity (0.01, 0.05, 0.1, 0.3 and 1.0 of the half flange width) for a range of slenderness ratios. The ambient temperature

yield strength and modulus of elasticity are assumed to be $250N/mm^2$ and $205kN/mm^2$ respectively.

In Fig. 5.21a to 5.21e the relationship between critical stress, σ_{cr} , and temperature is plotted at increasing levels of eccentricity. The critical stress is non-dimensionalised with respect to ambient temperature yield strength. The influence of eccentricity on the behaviour of stocky columns with slenderness ratio of $l/r = 20$ is evident (Fig. 5.21a) with the buckling strength decreasing as the level of eccentricity increases. Between 20°C and 400°C the buckling strength decreases fairly steadily at low eccentricity level, $e \leq 0.3b_f$, but as temperature increases beyond 400°C there is a rapid decrease in the buckling stress. With increasing level of eccentricity the temperature at which this sudden drop in capacity occurs increases. For example, at an eccentricity level of $0.01b_f$ this temperature is about 450°C while at the maximum eccentricity considered, $e = 1.0b_f$, it is about 500°C .

The behaviour of more slender columns, $l/r \geq 60$, is different from that of stocky columns as shown in Fig. 5.21b to 5.21e. It is noted that there is a fairly steady decline in the buckling strength throughout the range of temperature and eccentricity considered. It is evident from Fig. 5.21e that low levels of eccentricity do not influence significantly the behaviour of very slender columns, $l/r \geq 140$, but the influence of high levels of eccentricity is significant.

In Fig. 5.22a to 5.22e the curves show the plot of non-dimensionalised critical stress with respect to ambient temperature critical stress ($\sigma_{cr}/\sigma_{cr,20}$) against temperature. By inspecting these curves it is clear that they become more evenly distributed with increasing level of eccentricity. This is an indication

that the critical temperature-slenderness ratio relationship becomes more linearly related as the level of eccentricity increases.

In the region where the critical stress reduced to, say, 60% of the ambient temperature bearing capacity the wide range of critical temperatures is apparent. These are plotted in Fig. 5.23 as a critical temperature-slenderness ratio relationship. It is noted that there are two distinct features associated with the behaviour of columns when the level of eccentricity is low, $e \leq 0.3b_f$. For columns with slenderness ratio $l/r \leq 100$ the critical temperature increases with the level of eccentricity, while the reverse is the case for more slender columns, $l/r > 100$.

At the maximum level of eccentricity considered, $e = 1.0b_f$, the critical temperature decreases approximately linearly throughout the range of slenderness ratio considered ($l/r \leq 160$).

Generally, the influence of eccentricity decreases with increasing temperature. The effect of this imperfection on the behaviour of columns differs from column to column. It is noted that there is improved performance in fire condition relative to ambient temperature for both the stocky and intermediate columns, $l/r \leq 80$, with increasing level of eccentricity, while slender columns, $l/r \geq 100$, exhibit decreasing critical temperatures with increasing level of eccentricity.

5.5 Effect of local buckling phenomenon

Local buckling is often responsible for the early failure of stocky columns with slender component plates. The local buckling of any component of the structural element depends largely on the width-to-thickness ratio of that component. For a low ratio the ultimate strength of the member may be reached before buckling occurs while for a large ratio local buckling will be evident. The extent of this phenomenon in fire has not been established.

To study the effect of local buckling on the behaviour of steel columns in fire different sections, with flange width-to-web width ratios of $b_f/b_w = 0.25, 0.45, 0.50, 0.60$ and width-thickness ratio of flange outstands of $b_f/t_f = 10, 18, 20, 24$ were analysed. In all the analyses the ambient temperature yield strength and modulus of elasticity are assumed to be $250N/mm^2$ and $205kN/mm^2$ respectively.

In Fig. 5.24a to 5.24g the relationship between critical stress and half wavelength, λ , is plotted for the different cross-sections. The critical stress, σ_{cr} , and half wavelength are non-dimensionalised with respect to ambient temperature yield strength and web width respectively.

Generally there are three categories of half wavelength λ/b_w -large, intermediate and low, which characterise these buckling curves. It is noted that at ambient temperature (Fig. 5.24a) the point on the curves where elastic overall buckling starts to be prominent depends on the dimension of cross-section. As expected, for slender cross-section the range of slenderness ratios for which local buckling is predominant increases. There is an increase in the range of

half wavelength over which local buckling occurs as the cross-section dimension increases.

The buckling curves start to deviate from elastic overall buckling as the half wavelength decreases. The deviation from the elastic buckling as half wavelength decreases may be as a result of inelastic material behaviour, elastic local buckling or a combination of the two.

In order to establish the extent of the influence of local buckling on the behaviour of columns the elastic analysis of columns with $b_f/b_w = 0.6$ was undertaken at increasing temperature. It is noted from the superimposed elastic curves in Fig. 5.24a to 5.24e that the influence of local buckling is evident only at ambient temperature. For example, at ambient temperature the reduction in capacity as a result of local buckling interaction is about 12.5% but at 200°C its influence is completely eliminated. This shows that, in design situations in which local buckling has been safeguarded against at ambient temperature, its influence on the the structural behaviour at elevated temperature is remote. It can be concluded that local buckling does not influence the behaviour of steel columns in fire. The influence of degradation of the material properties in fire overshadows the effect of this phenomenon on the behaviour of steel column in fire.

In Fig. 5.25a to 5.25e the plots of non-dimensionalised critical stress with respect to ambient temperature critical stress ($\sigma_{cr}/\sigma_{cr,20}$) against temperature are shown for different half wavelengths. These curves exhibit a fairly linear pattern. In the region where the critical stress reduces to, say, 60% of the ambient temperature capacity a very limited range of critical temperatures is

evident.

These temperatures are plotted in Fig. 5.26 as critical temperature-slenderness ratio relationships. The most compact section, $b_f/b_w = 0.25$, exhibits a fairly wide range of critical temperatures (360°C to 440°C) compared to the most slender section, $b_f/b_w = 0.6$, with critical temperature range of 315°C to 350°C. The compact section, $b_f/b_w = 0.25$, shows an increasing critical temperature in contrast to the more slender section, $b_f/b_w > 0.25$.

5.6 Sections under uniform bending

It is well known that beams buckle laterally when subjected to loading. The capability of a beam to carry its full plastic moment depends on its slenderness ratio. A very short beam can sustain a full plastic moment while a very slender beam may buckle at a moment which is significantly less than the plastic moment at ambient temperature. Local buckling can also be an important factor if the member is made up of very slender component plates. At elevated temperature the behaviour of beams depends on the material properties and the temperature distribution. In the present study only uniform temperature distribution is considered.

For the purpose of this study a 203 × 203 × 52UC section was analysed over a range of slenderness ratios. The ambient temperature yield strength and modulus of elasticity are assumed to be 250N/mm² and 205kN/mm² respectively.

The curves in Fig. 5.27 show the non-dimensionalised critical bending stress

$(\sigma_{b,cr}/\sigma_{y,20})$ -slenderness ratio relationship at increasing temperature. At ambient temperature beams with low slenderness ratios fail by material yielding while those with high slenderness ratios fail in an elastic overall buckling mode. At 200°C their behaviour is similar to that at ambient temperature, but at a reduced critical bending stress. This reduction in the critical bending stress becomes marginal at slenderness ratios greater than 140.

At higher temperatures the pattern of these curves is similar but at reducing critical bending stress with increasing temperature.

Fig. 5.28 shows the same information as in Fig. 5.27. The non-dimensionalised critical bending stress $(\sigma_{b,cr}/\sigma_{y,20})$ is plotted against temperature. The variation of critical bending stress with temperature clearly depends on the slenderness ratio. Stocky beams, $l/r \leq 40$, exhibit a gradual decrease in critical bending stress up to a temperature of 450°C before a rapid decline. Intermediate beams, $40 < l/r \leq 80$, show a steady decrease in critical bending stress throughout the range of temperature considered while slender beams, $l/r \geq 100$ show a gradual decline in the strength between 20°C and 200°C before a rapid decrease is evident.

Fig. 5.29 shows the relationship between critical bending stress non-dimensionalised with respect to the ambient temperature critical bending stress and temperature. It is noted that these curves are widely distributed, especially in the region where the critical bending stress reduces to say, 60% of the ambient temperature critical bending stress. This shows a wide range of critical temperature. This temperature is plotted against the slenderness ratio in Fig. 5.30. It is evident that stocky and intermediate beams, $l/r < 60$, exhibit

critical temperatures higher than those of the more slender beams, $l/r > 60$. It is noted that stocky and intermediate beams perform better than the slender beams in fire relative to ambient temperature. This is in contrast to the behaviour of sections under compressive load, in which stocky and slender columns perform better than intermediate columns.

5.7 Behaviour of blocked in web columns

A blocked in web column can be described as a column with blocks laid between the inner faces of the flanges as shown in Fig. 5.31. This is intended to protect the web from radiant and convected heat resulting in a reduced rate of temperature increase, thus improving the fire resistance in term of the time taken for collapse to occur. There is limited information on the behaviour of blocked in web columns in fire. The only published works are concerned with the tests conducted by British Steel Corporation[171]. The results of these tests have been used as the basis for a grading of such columns by the Building Research Establishment[175]. This implies that the performance of blocked in web columns in term of fire resistance is independent of slenderness ratio. In view of the results described earlier for bare columns suggesting that slenderness ratio is an important factor in this respect, further studies have been conducted on blocked in web columns to investigate the influence of slenderness ratio on this form of construction. To this end a range of columns with slenderness ratios in the range $l/r \leq 160$, are analysed. The section considered is a $203 \times 203 \times 52$ UC and the temperature profile is assumed to be that measured in the British Steel Corporation tests[171] for a stocky column

of the same section with slenderness ratio of 40.7.

Fig. 5.32(a) shows the plot of non-dimensionalised critical stress, $\sigma_{cr}/\sigma_{y,20}$, against slenderness ratio at increasing temperature for both bare and blocked in web columns. It is noted that both columns show an identical behaviour implying that blocking in of a column results in no increase in failure temperatures. However, the same information is plotted with respect to time as shown in Fig. 5.32(b). The influence of the blocking in of the web is now clearly evident at any time the blocked in web columns fail at consistently higher buckling capacities compared to bare columns. This means that blocked in web columns will survive for longer period in a fire than the equivalent bare columns.

The behaviour of the blocked in web columns is clearly dependent on slenderness ratio like bare columns.

The relationship between non-dimensionalised critical stress, $\sigma_{cr}/\sigma_{cr,20}$ and temperature for a range of slenderness ratio, $l/r \leq 140$, is shown in Fig. 5.33. It is noted that at the region where the buckling stress is reduced to say, 60% of the ambient temperature bearing capacity there is a wide range of critical temperatures exhibited by these columns. These temperatures are plotted in Fig. 5.34 as critical temperature - slenderness ratio relationship. It is interesting to note that only stocky columns, $l/r \leq 20$, show critical temperatures of about 530°C which corresponds to a failure time of about 30 minutes. For other slenderness ratios the failure time is dependent on the slenderness ratio but is always lower than 30 minutes. For example, a column with a slenderness ratio of 60 shows a failure time of about 15 minutes while

a column with a slenderness ratio of 120 shows a failure time of about 24 minutes. This contradicts the published information in the Building Research Establishment Digest[175] which implies that all blocked in web columns have the same fire resistance time of 30 minutes.

It can be concluded that the performance of blocked in web columns is not influenced by the blocking in of the web in term of failure temperature but there is significant improvement in their performance in term of failure time. It is noted that in any circumstances, the behaviour of blocked in web columns is dependent on the slenderness ratio and that in view of the published guidance further research in this area would be valuable.

Concluding Remarks:

From the inelastic buckling analysis of H-sections under axial compression and pure bending it is clear that many parameters influence the behaviour of steel columns in fire. Such parameters include the slenderness ratio, residual stresses, eccentricity of loading, different stress-strain relationships and cross-section dimensions. The following conclusions may be drawn:

1. The behaviour of stocky and intermediate columns is controlled largely by yield strength while the behaviour of slender columns is controlled by modulus of elasticity. The behaviour of intermediate columns is controlled by the interaction between material yielding and elastic overall buckling.
2. The range of critical temperature exhibited by different columns shows that columns with different slenderness ratios behave differently in fire.

Stocky and slender columns perform better than those with intermediate slenderness ratios, which are perhaps more typical of those used in building. The lowest critical temperatures of about 300°C are for columns within the range of slenderness ratio of $80 \leq l/r \leq 100$.

3. The non-linear form of the material properties of steel at elevated temperature is better represented by a continuous stress-strain-temperature representation instead of bilinear form. A bilinear form of representation results in a higher buckling strength prediction than the continuous stress-strain-temperature representation with any of the three sets of expressions considered. A continuous representation has a considerable influence on any column's behaviour in fire whereas a bilinear representation results in identical behaviour for stocky and intermediate columns. However, for more slender columns the discrepancy in buckling predictions using these representations decreases.
4. The ECCS expressions for yield strength and modulus of elasticity have been found to be the most conservative of the three sets of expressions considered. This shows that there is a likelihood of underestimating the buckling strength of columns when designed to the ECCS recommendations. The BS5950 expressions consistently result in the highest buckling strength prediction, while the prediction based on the CTICM expressions falls in between the predictions based on BS5950 and ECCS expressions irrespective of the stress-strain relationships.
5. Generally residual stress has a detrimental influence on the behaviour of columns in fire. This varies from column to column depending on slenderness ratio. The critical temperature decreases with increasing

level of residual stress for the whole range of columns considered with the exception of a very stocky column, $l/r = 20$, which shows minor variation in its critical temperature with increasing level of residual stress. The bigger the magnitude of residual stress the more the tendency for slender columns, $l/r \geq 80$, to exhibit identical critical temperature.

6. The maximum effect of load eccentricity occurs when it acts so as to induce bending about the weak axis. The effect of load eccentricity depends on its magnitude. For a very low level of eccentricity its effect on the behaviour of slender columns is insignificant at relatively low temperature. It is noted that there is improved performance in fire relative to ambient temperature for both the stocky and intermediate columns, $l/r \leq 80$, with increasing level of eccentricity, while for more slender columns the exhibited critical temperatures decrease with increasing level of eccentricity.
7. It is noted that the influence of local buckling on the behaviour of columns diminishes with increasing temperature. It can be concluded that if local buckling is not a problem at ambient temperature then it is less of a problem at elevated temperature.
8. The behaviour of a section under uniform bending is similar to that under compressive load, but the range of beams with low values of critical temperature is higher than that of columns.
9. The performance of blocked in web columns is not influenced by the blocking in of the web in term of failure temperature but there is significant improvement in their performance in term of failure time. It is noted

that in any circumstances, the behaviour of blocked in web columns is dependent on the slenderness ratio.

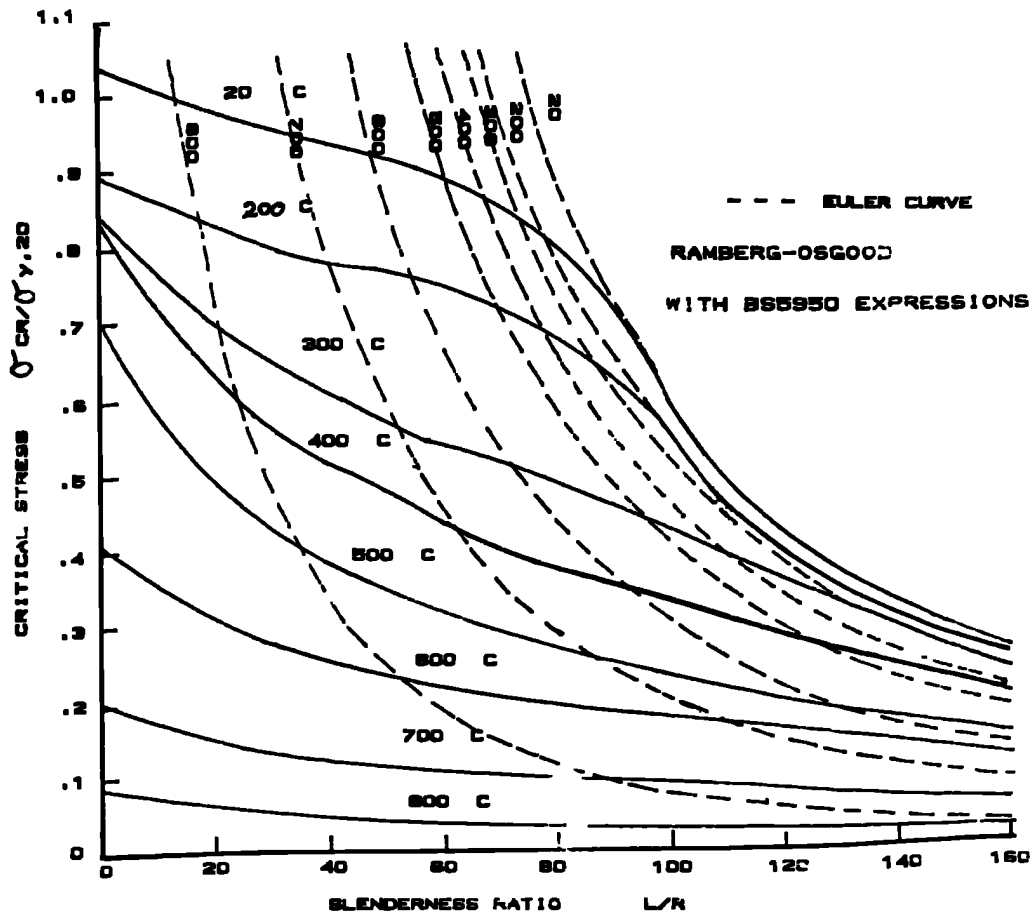


FIG. 5.1 VARIATION OF CRITICAL STRESS WITH SLENDERNESS RATIO AT INCREASING TEMPERATURE

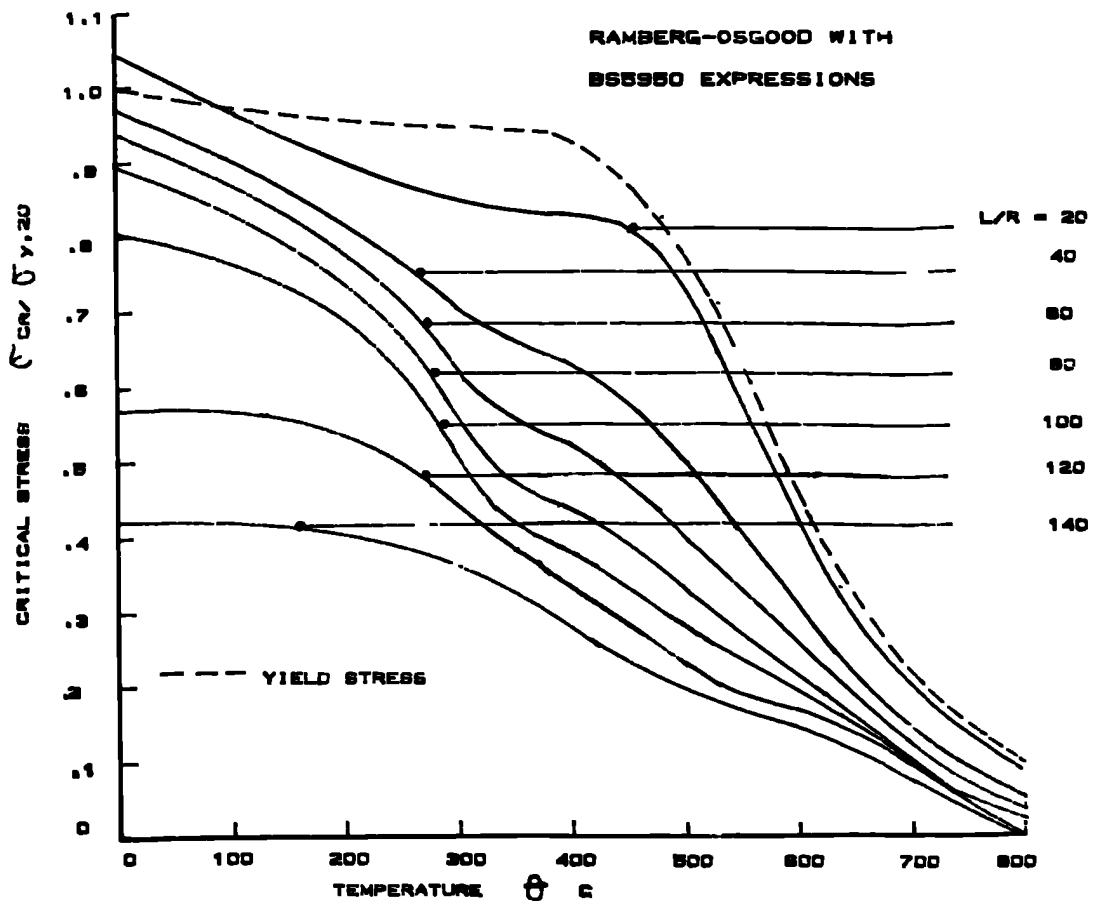


FIG. 5.2 VARIATION OF CRITICAL STRESS WITH TEMPERATURE

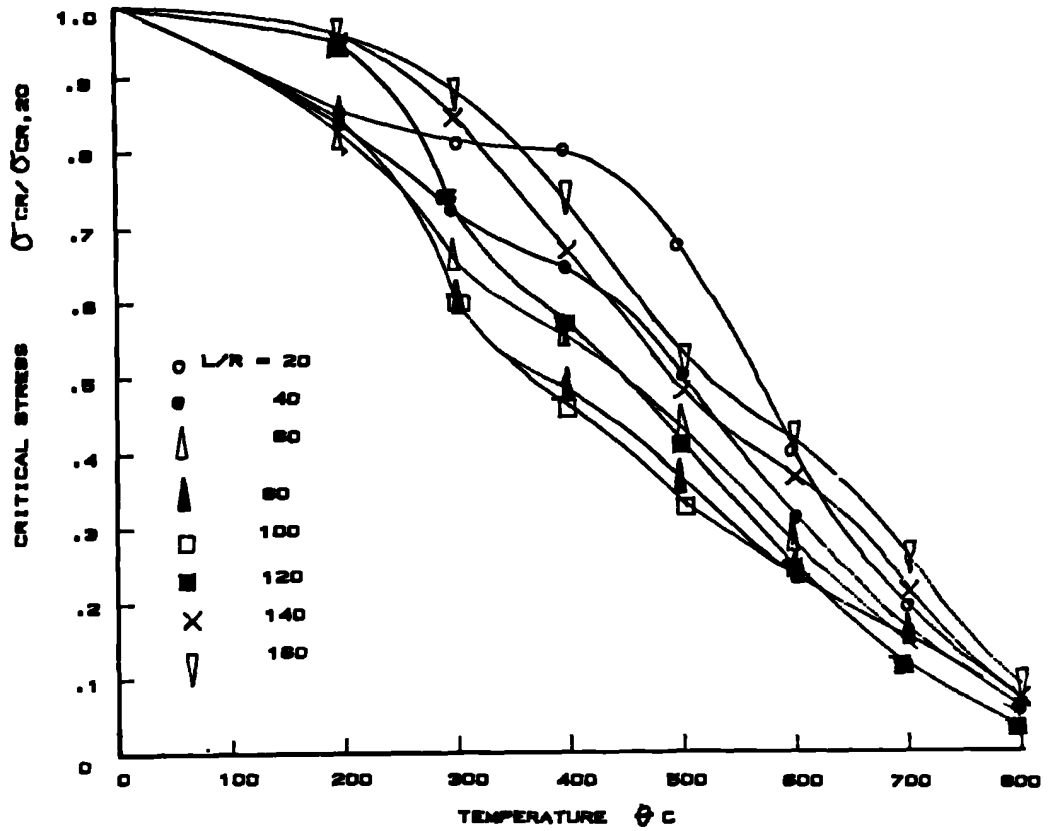


FIG. 5.3 VARIATION OF CRITICAL STRESS (RELATIVE TO AMBIENT TEMPERATURE CRITICAL STRESS) WITH TEMPERATURE

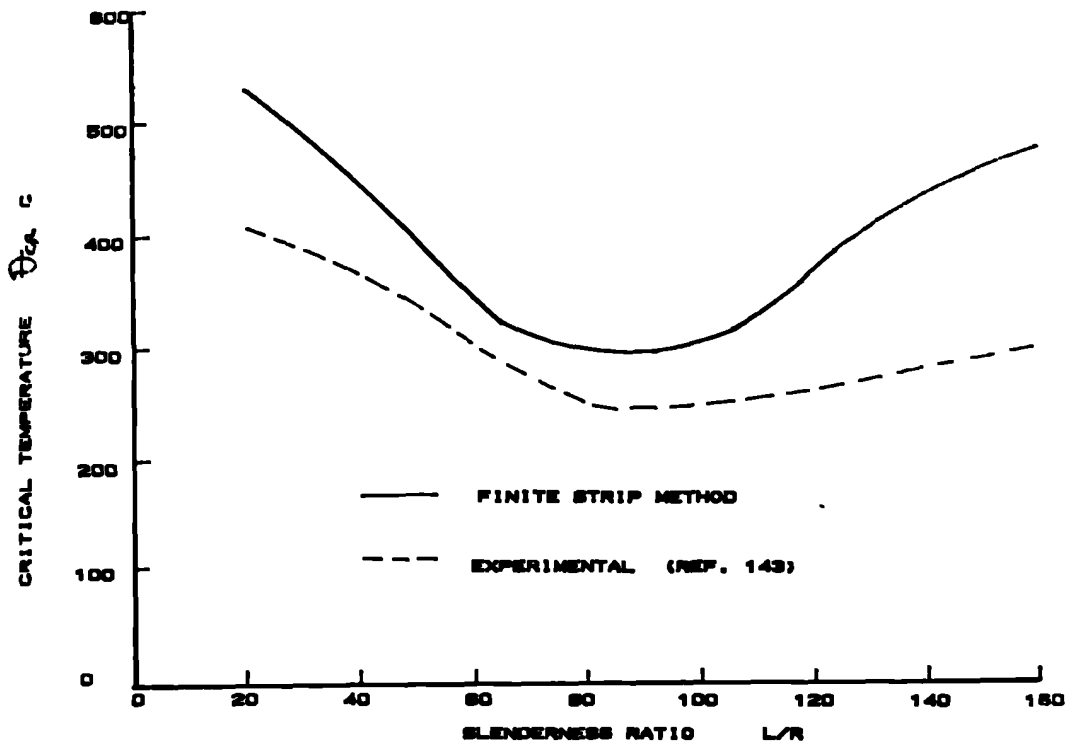


FIG. 5.4 VARIATION OF CRITICAL TEMPERATURE WITH SLENDERNESS RATIO

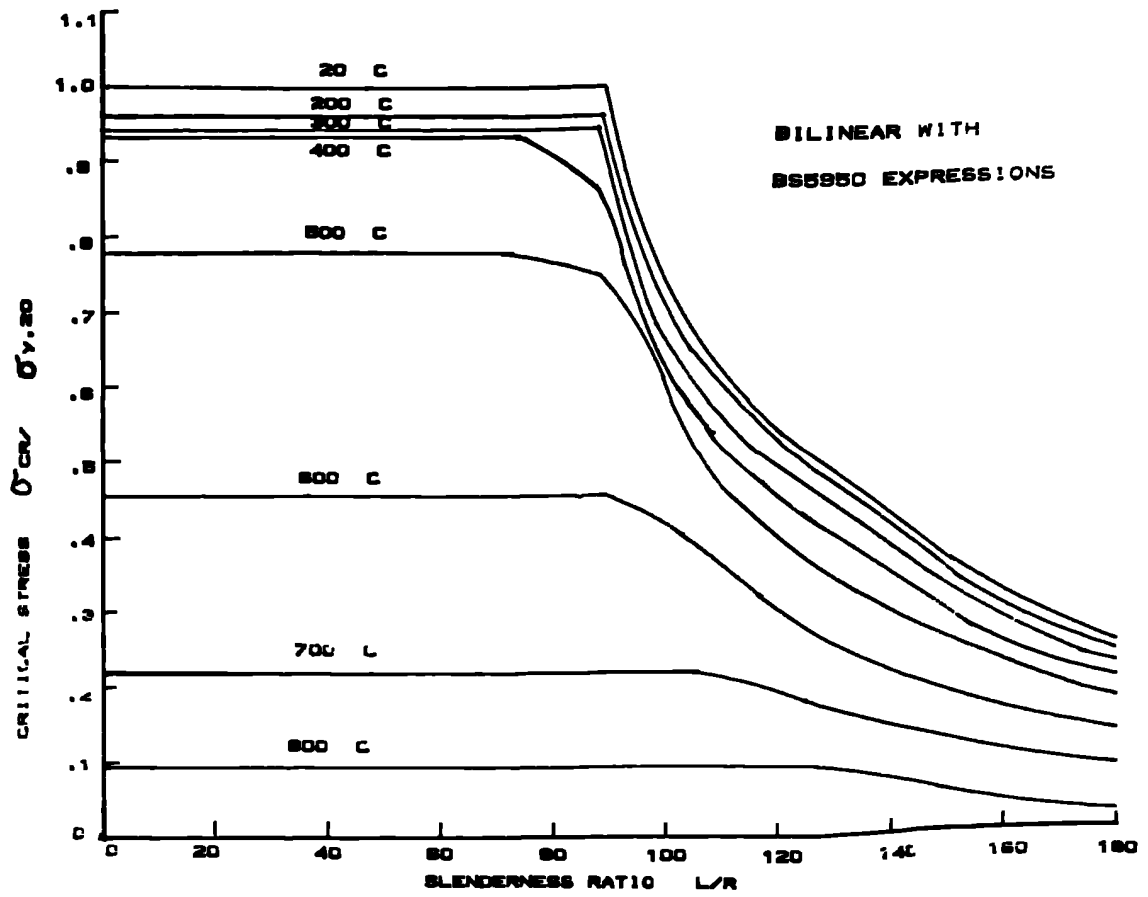


FIG. 5.5 VARIATION OF CRITICAL STRESS WITH SLENDERNESS RATIO AT INCREASING TEMPERATURE

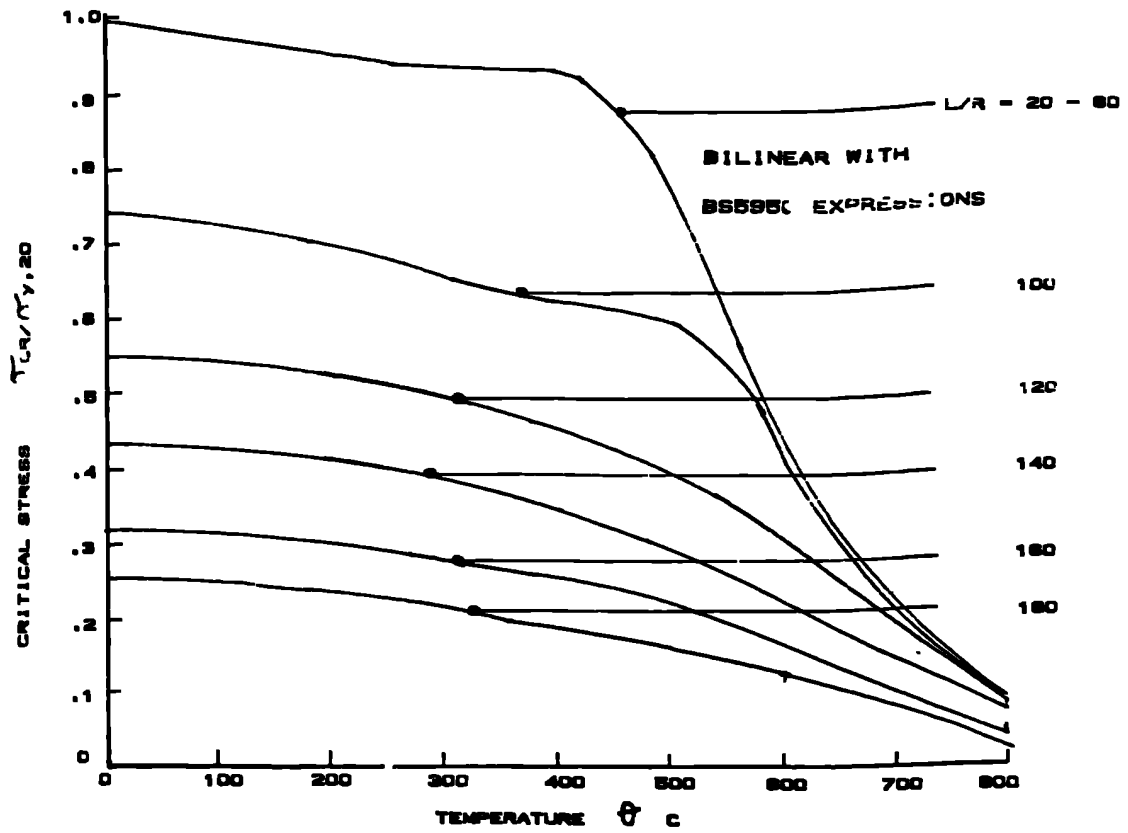


FIG. 5.6 VARIATION OF CRITICAL STRESS WITH TEMPERATURE

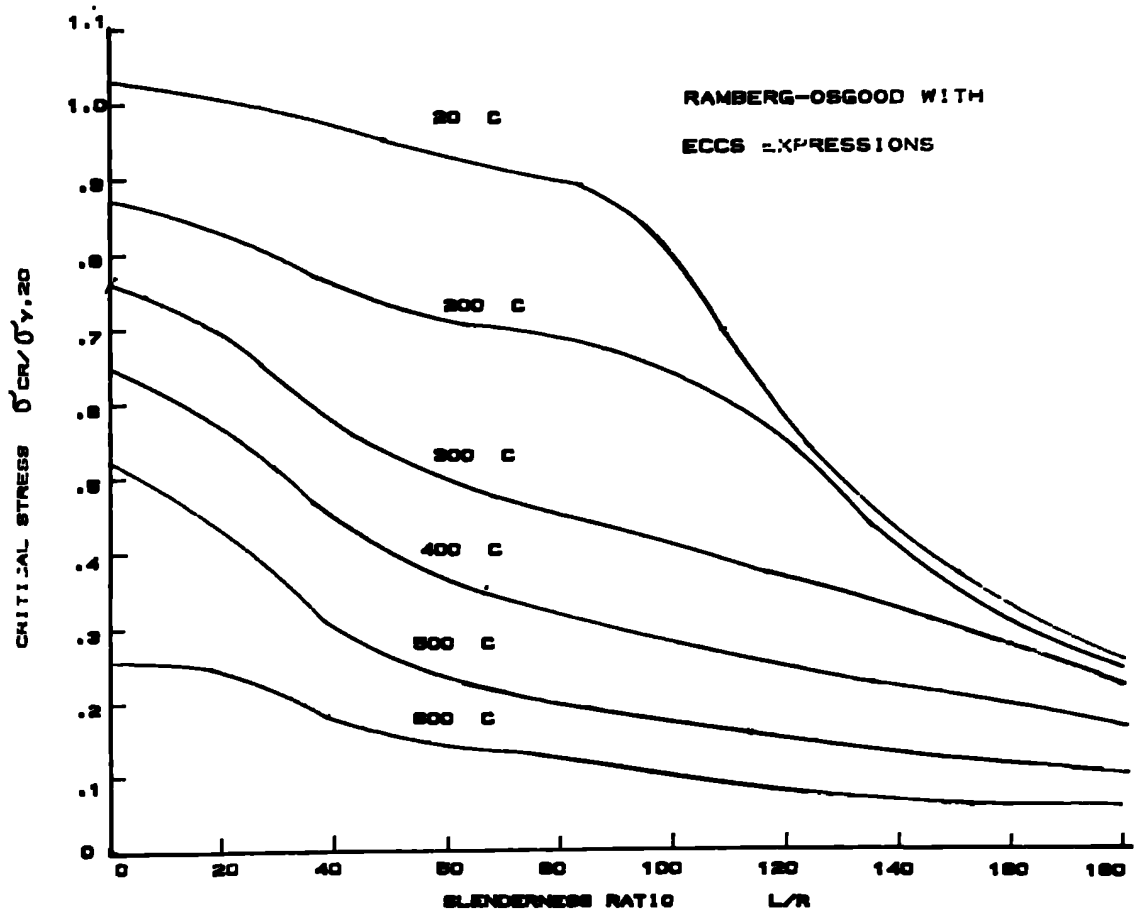


FIG. 5.7 VARIATION OF CRITICAL STRESS WITH SLENDERNESS RATIO AT INCREASING TEMPERATURE

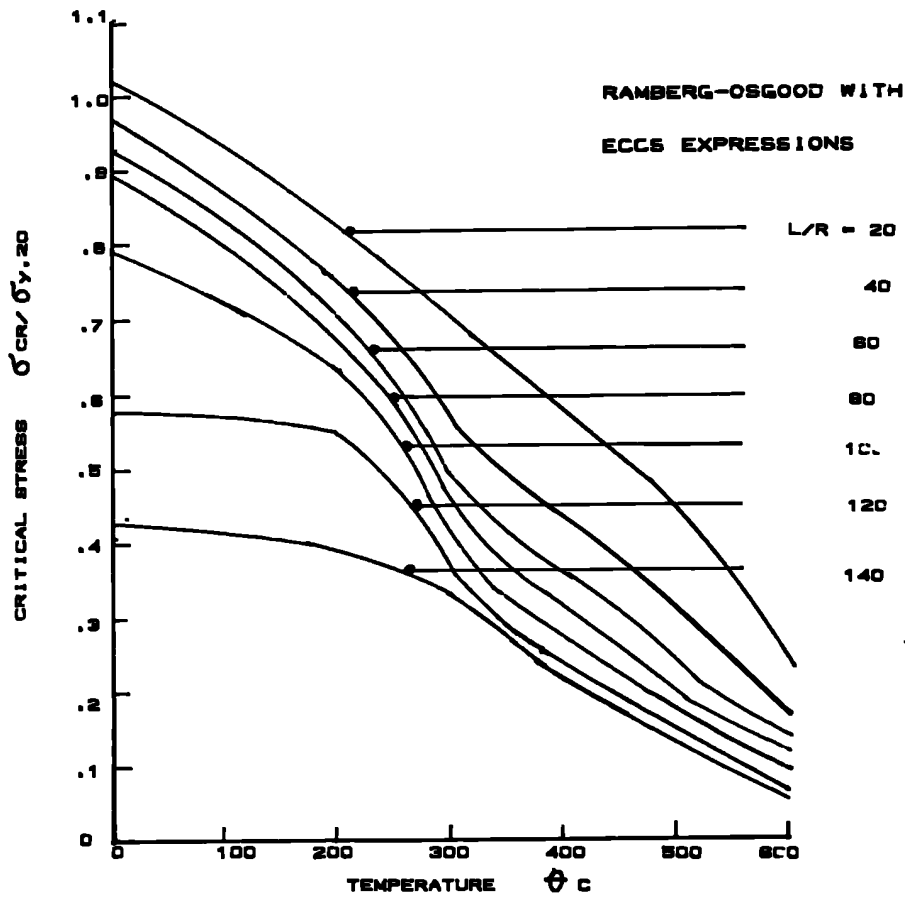


FIG. 5.8 VARIATION OF CRITICAL STRESS WITH TEMPERATURE

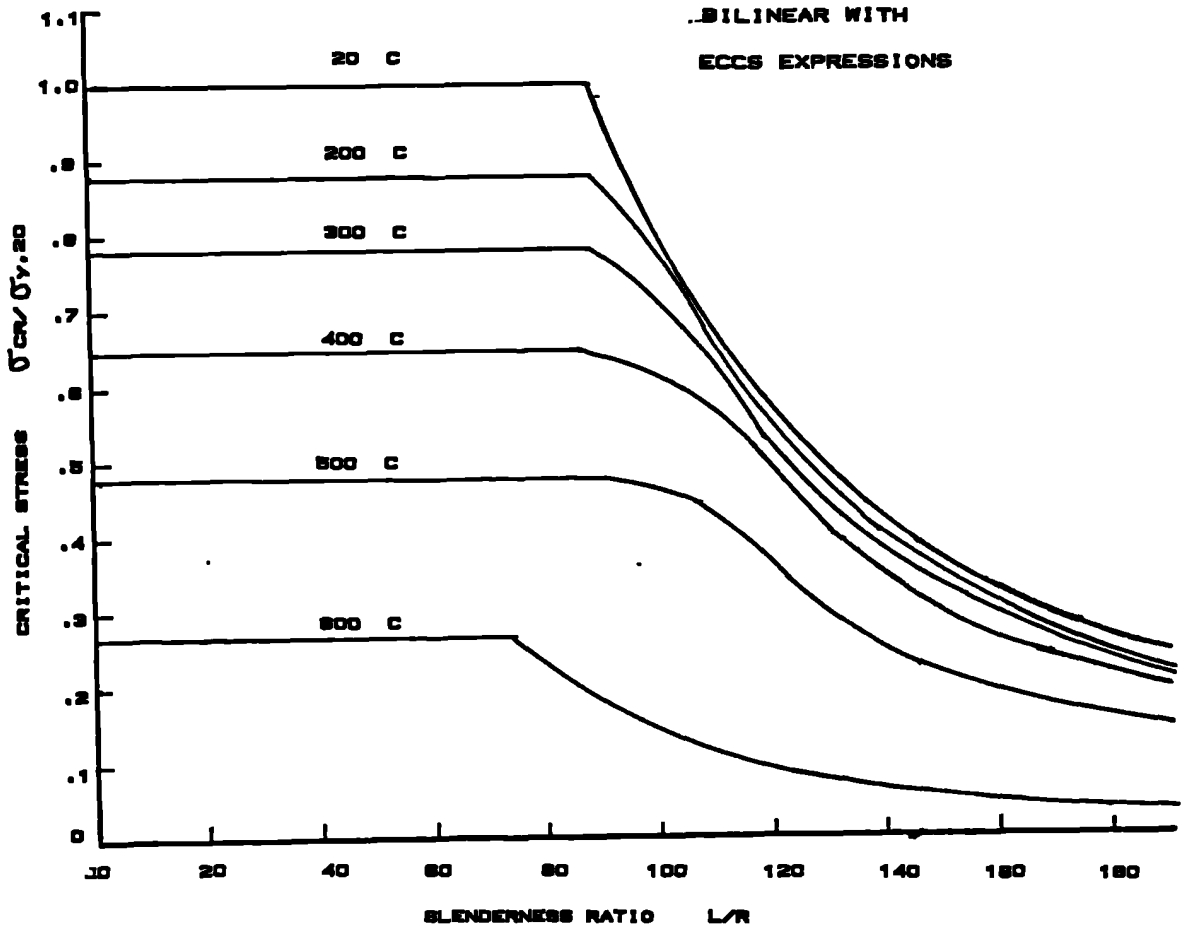


FIG. 5.9 VARIATION OF CRITICAL STRESS WITH SLENDERNESS RATIO AT INCREASING TEMPERATURE

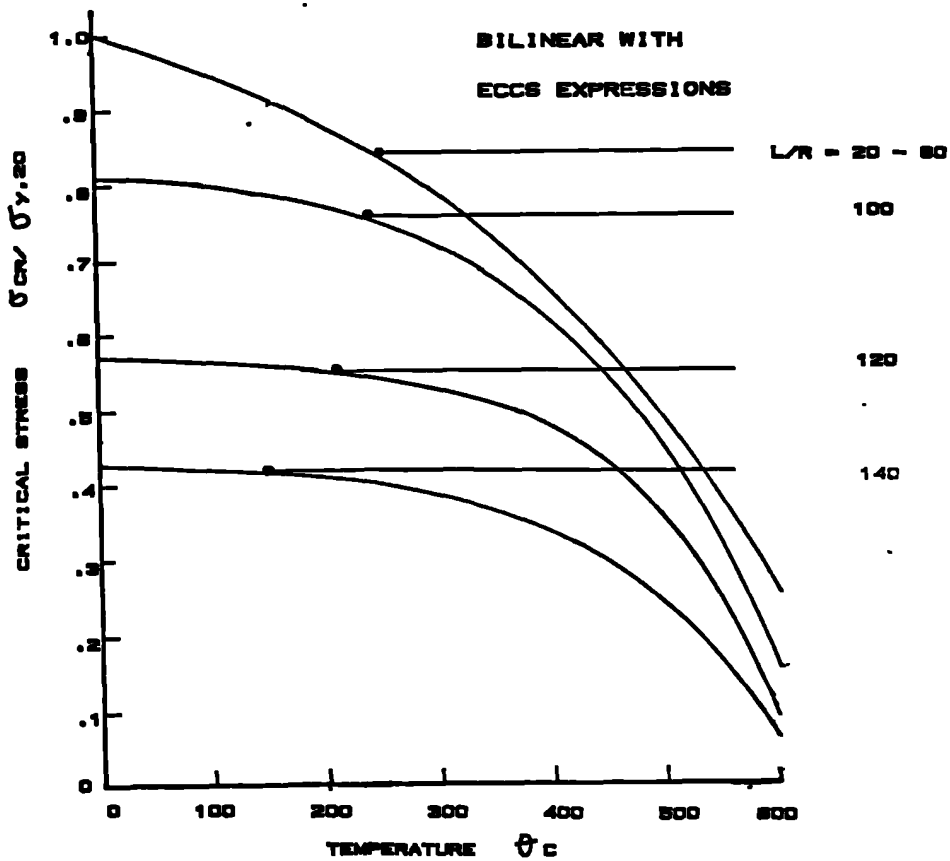


FIG. 5.10 VARIATION OF CRITICAL STRESS WITH TEMPERATURE

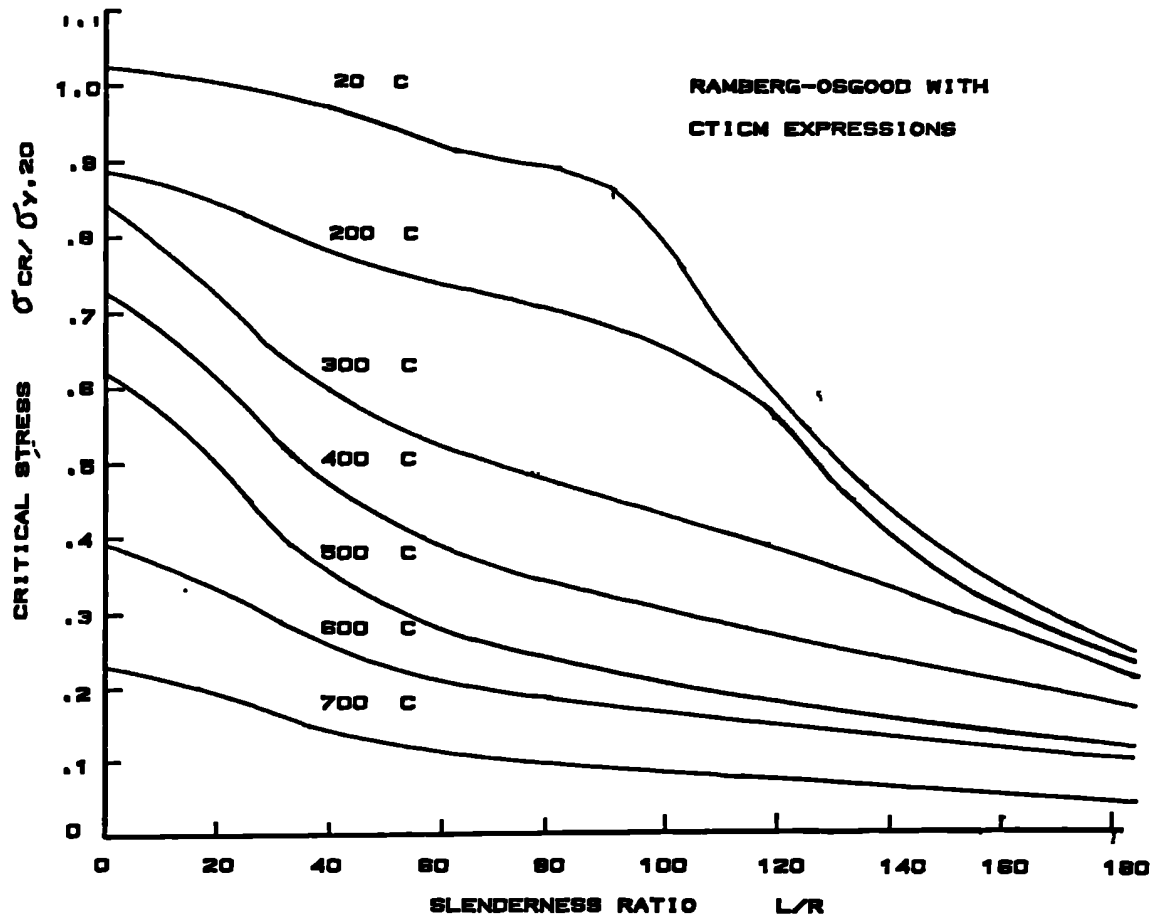


FIG. B.11 VARIATION OF CRITICAL STRESS WITH SLENDERNESS RATIO AT INCREASING TEMPERATURE

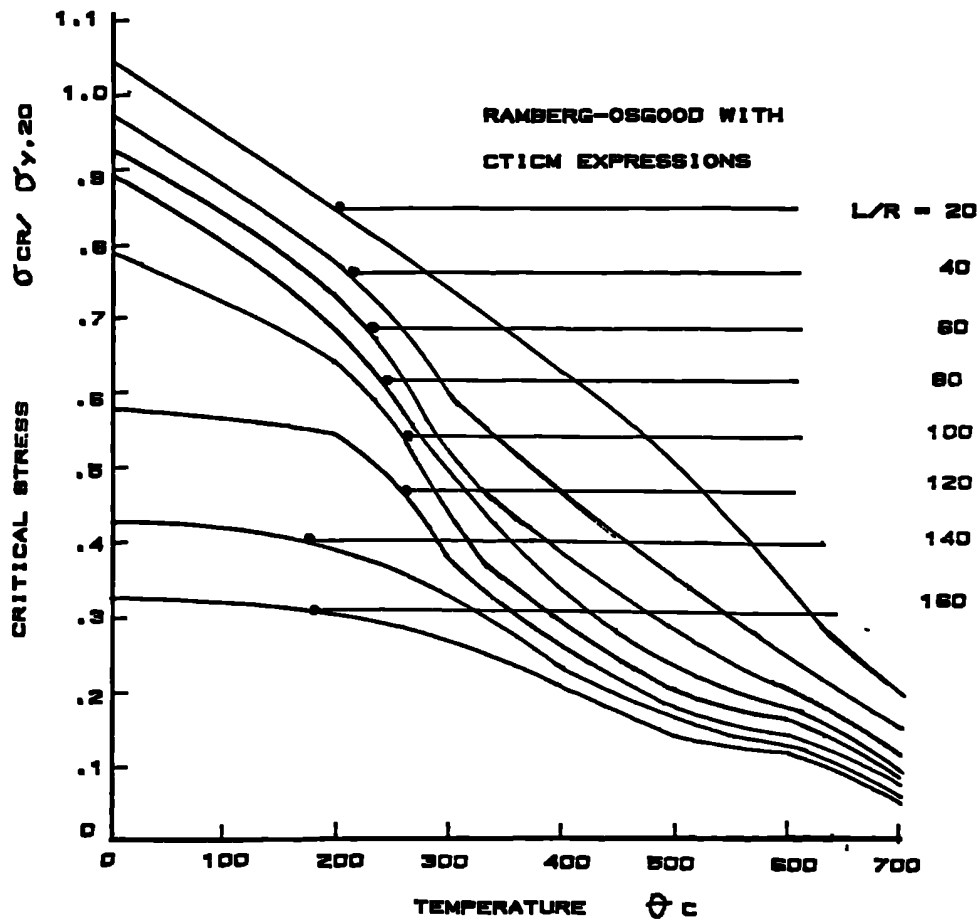


FIG. B.12 VARIATION OF CRITICAL STRESS WITH TEMPERATURE

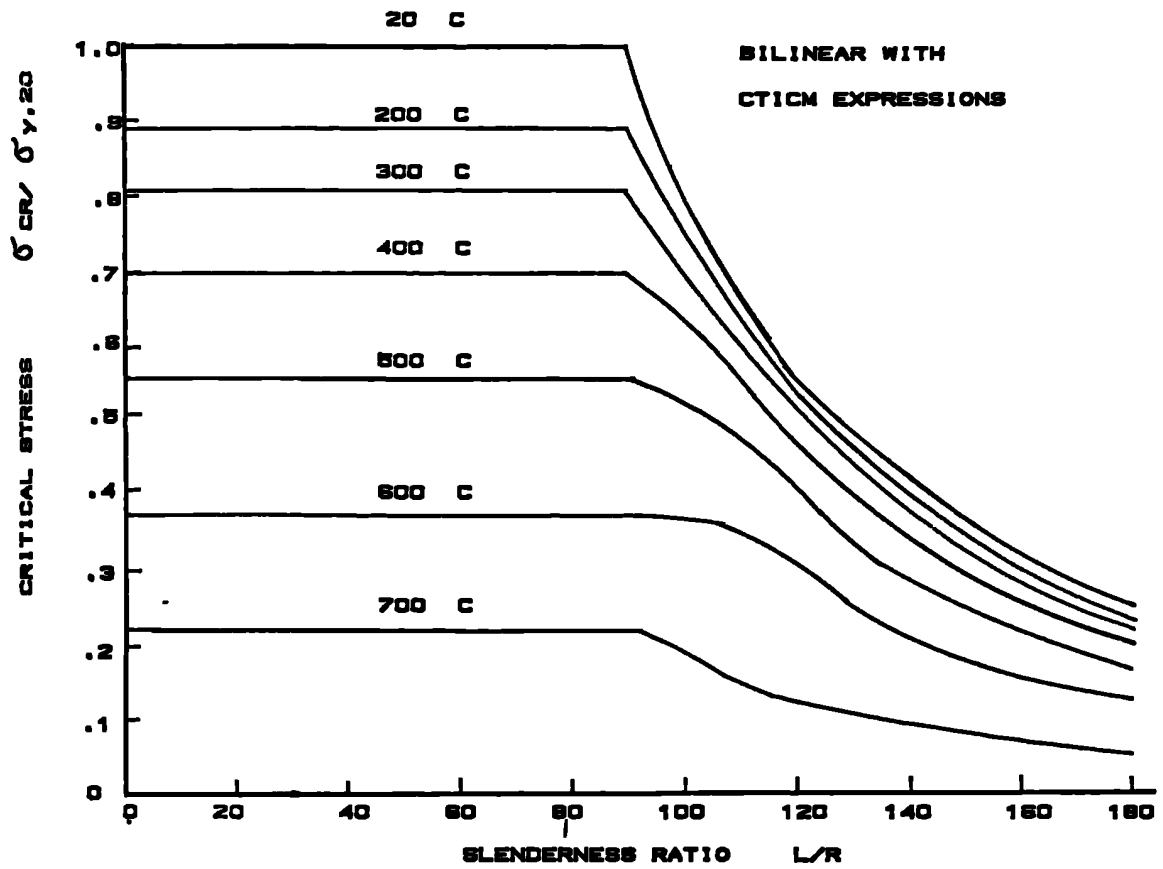


FIG. 5.13 VARIATION OF CRITICAL STRESS WITH SLENDERNESS RATIO AT INCREASING TEMPERATURE

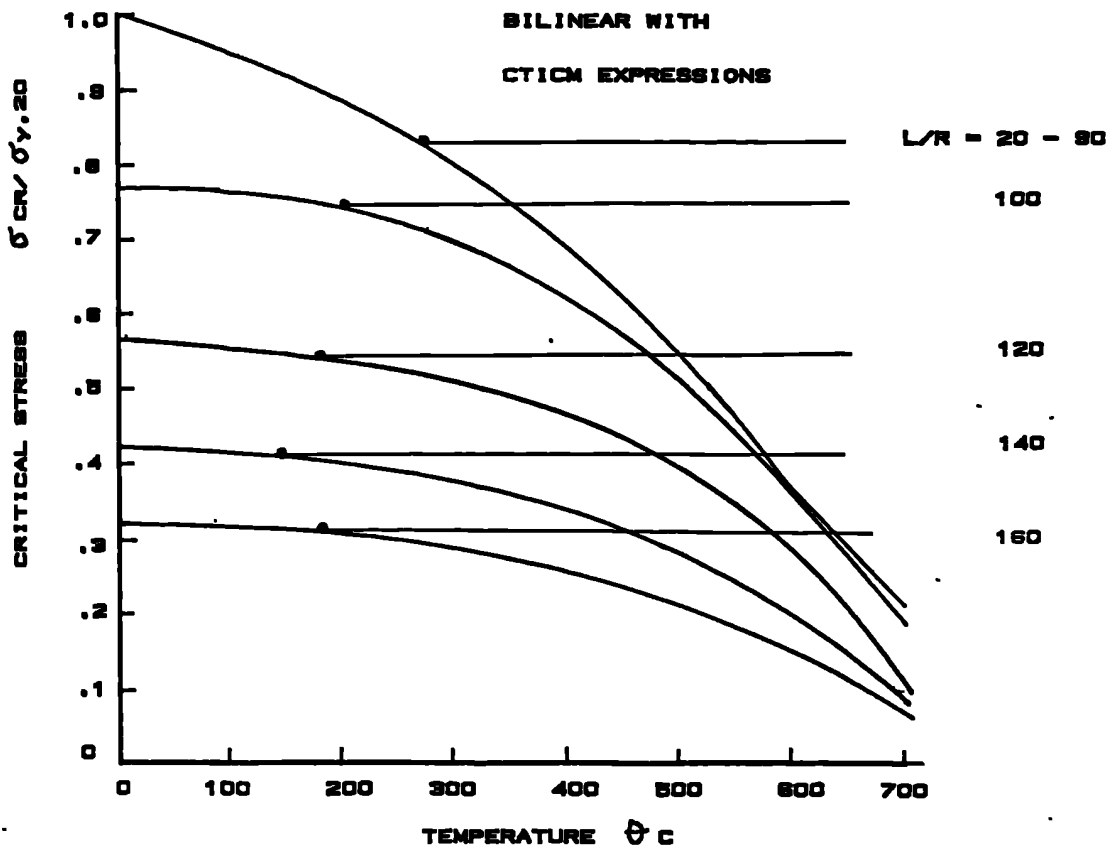


FIG. 5.14 VARIATION OF CRITICAL STRESS WITH TEMPERATURE

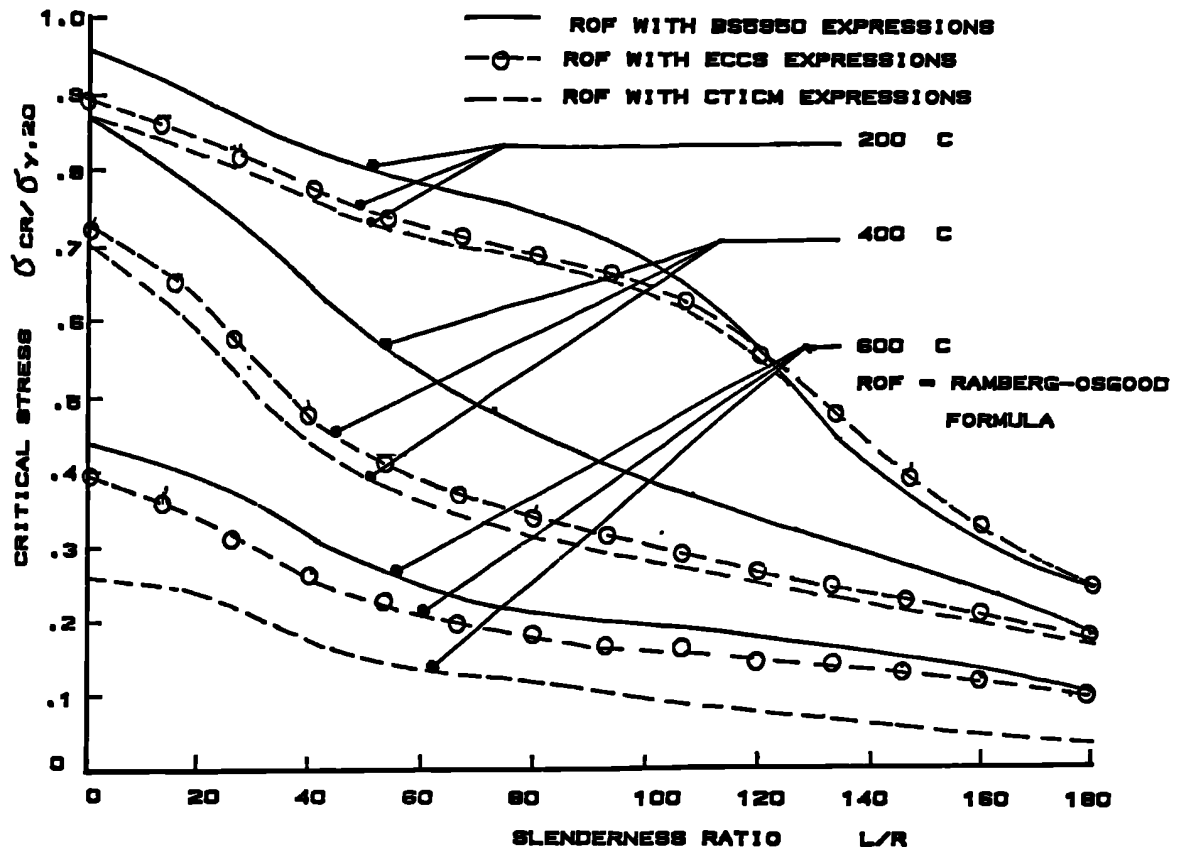


FIG. 5.15 COMPARISON OF COLUMN RESPONSE USING DIFFERENT STRENGTH EXPRESSIONS WITH RAMBERG-OSGOOD REPRESENTATION

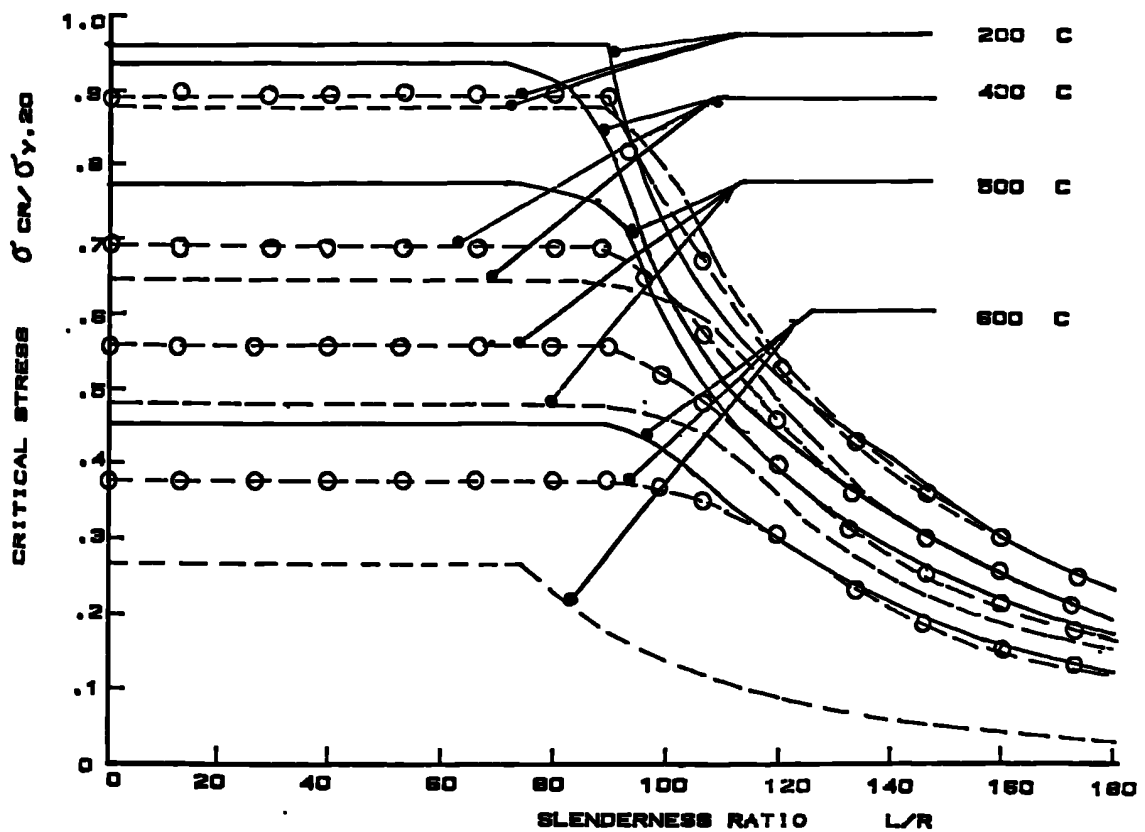


FIG. 5.16 COMPARISON OF COLUMN RESPONSE USING DIFFERENT STRENGTH EXPRESSIONS WITH BI-LINEAR REPRESENTATION

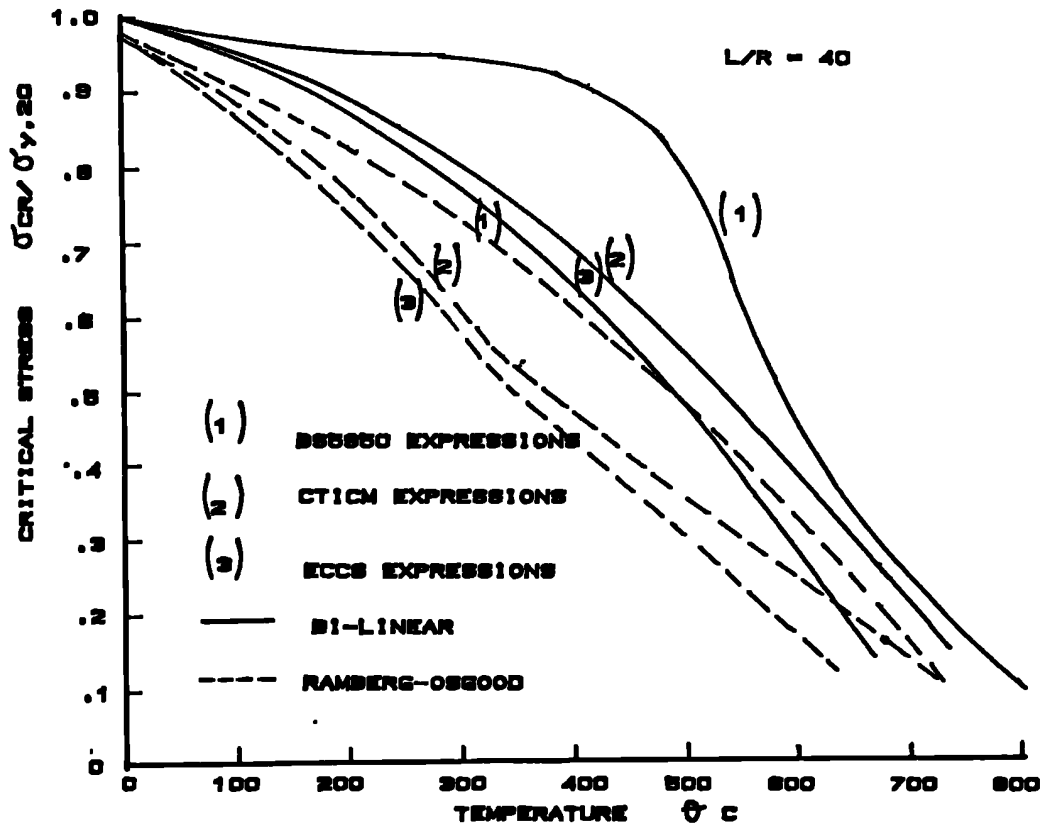


FIG. B.17a. COMPARISON OF COLUMN RESPONSE USING RAMBERG-OSGOOD AND BI-LINEAR REPRESENTATIONS WITH DIFFERENT STRENGTH EXPRESSIONS (BSSSBO, ECCS AND CTICM)

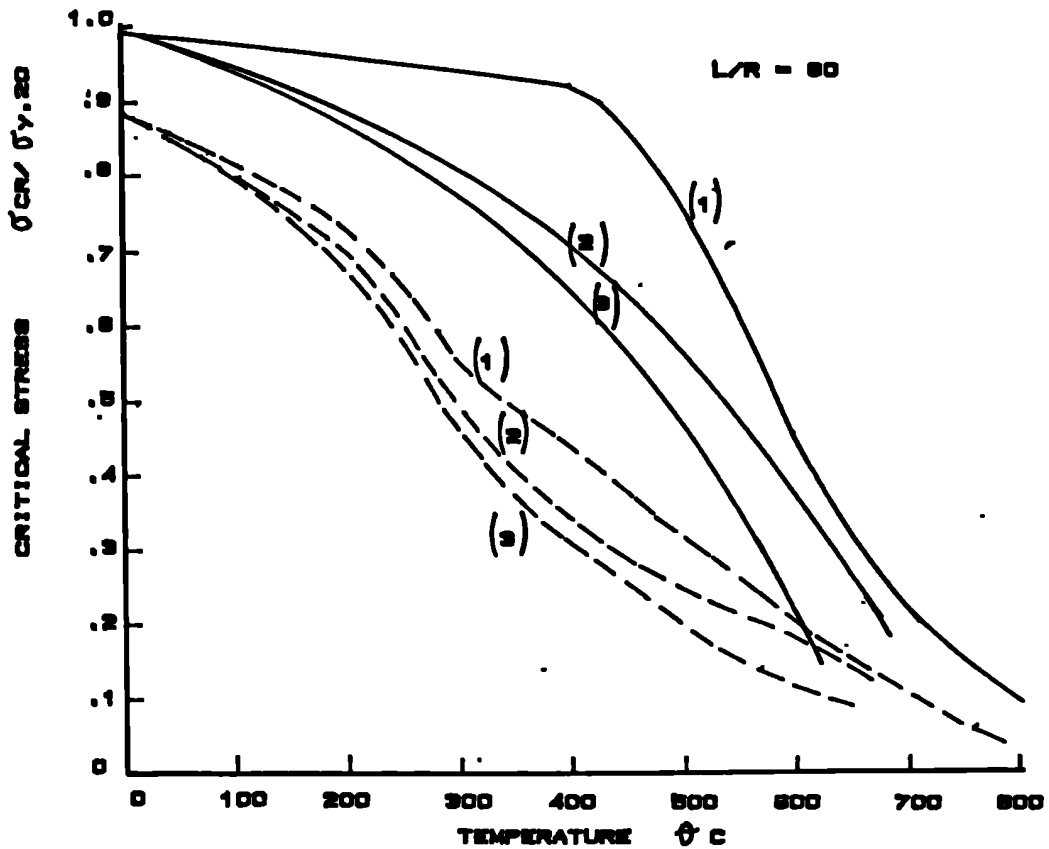


FIG. B.17b

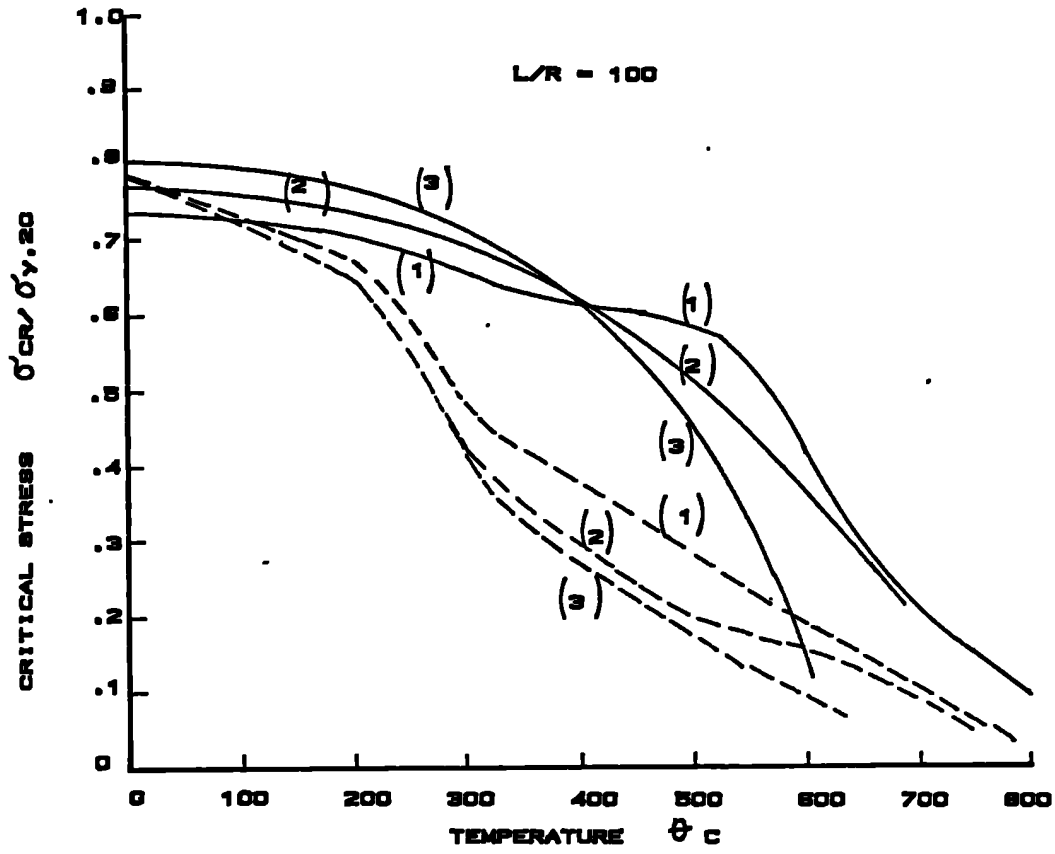


FIG. B.17c

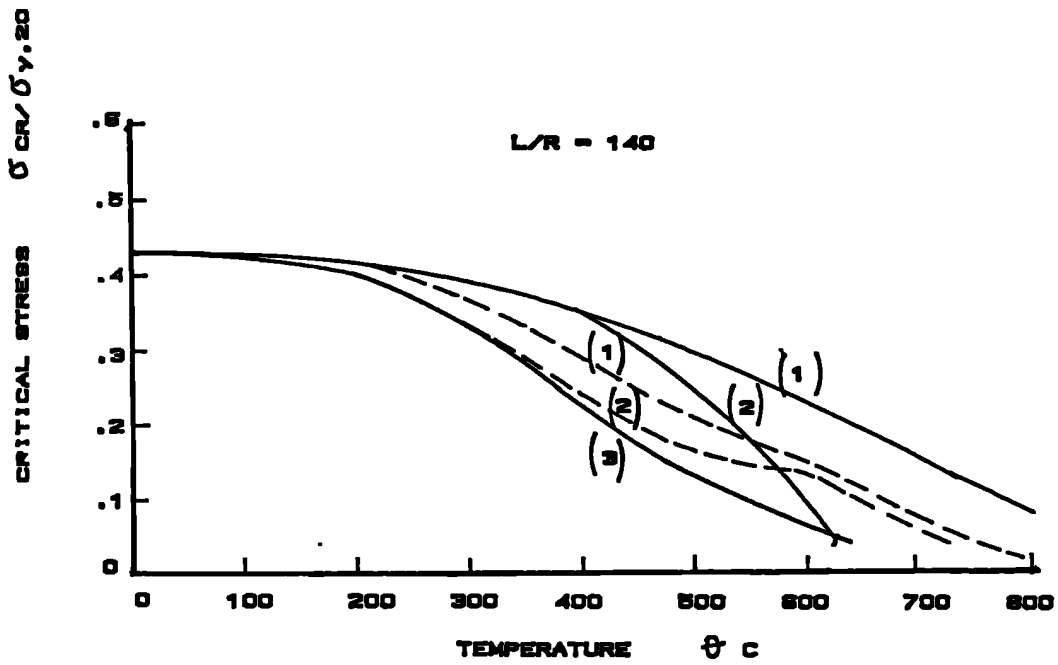


FIG. B.17d

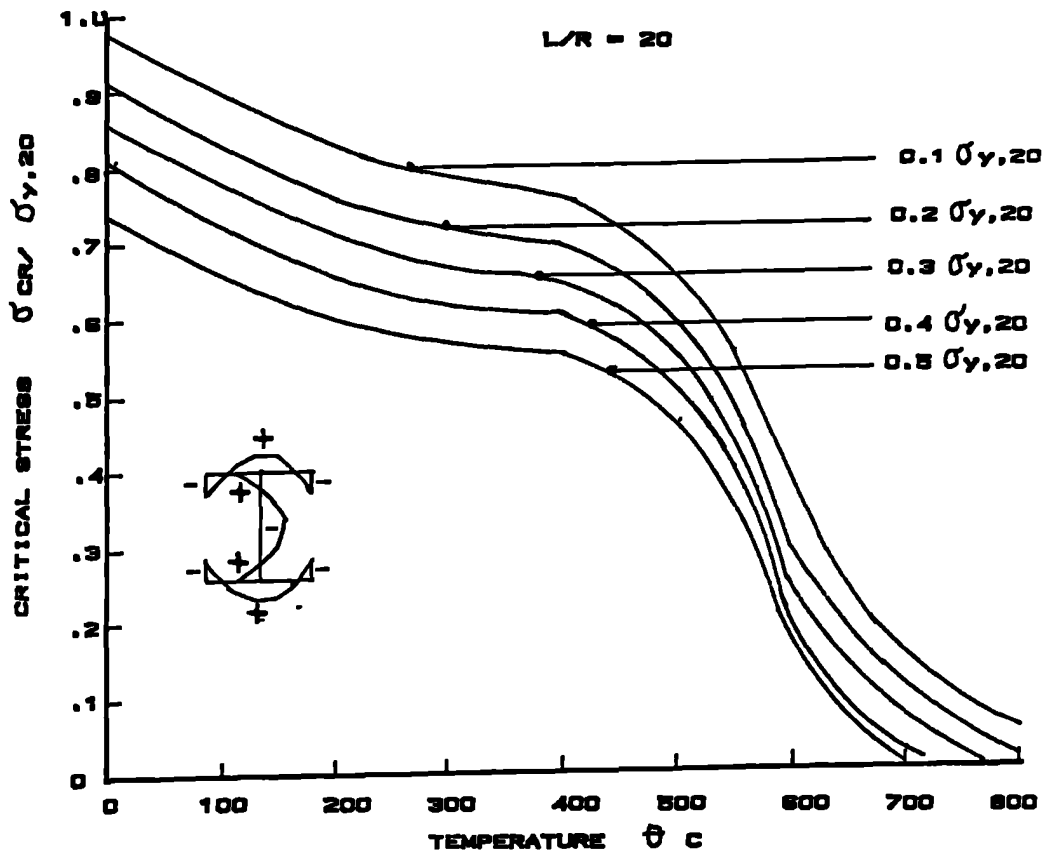


FIG. 5.16a VARIATION OF CRITICAL STRESS WITH TEMPERATURE AT INCREASING RESIDUAL STRESS

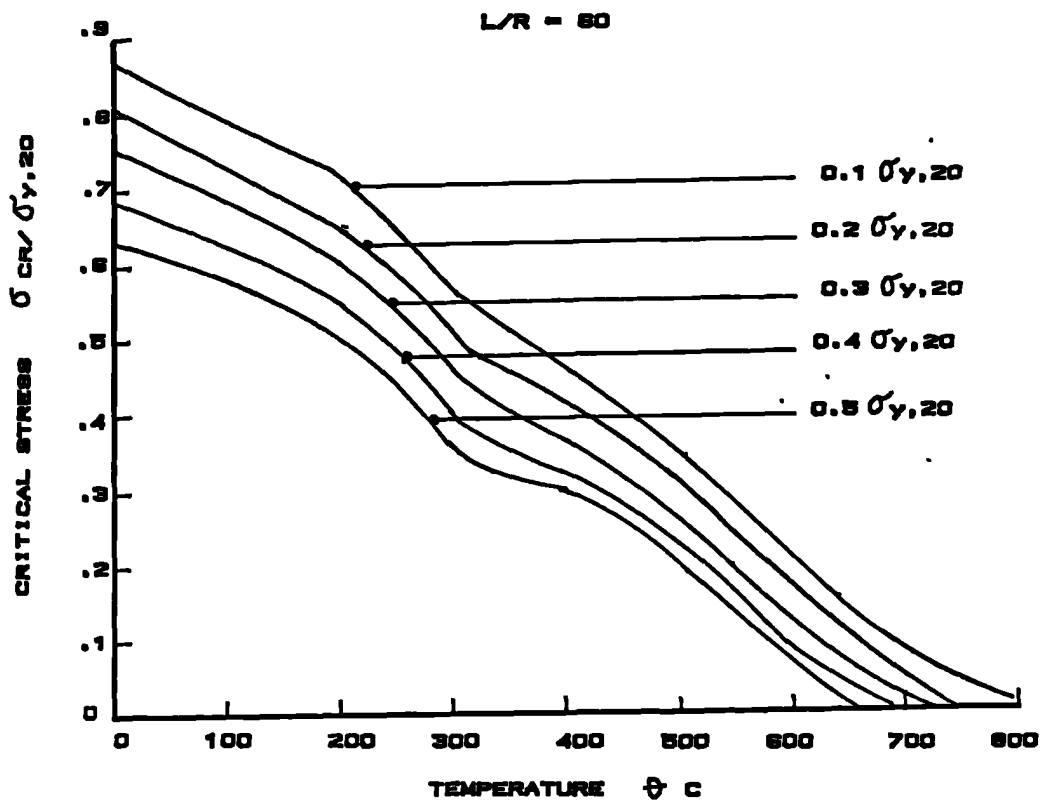


FIG. 5.16b

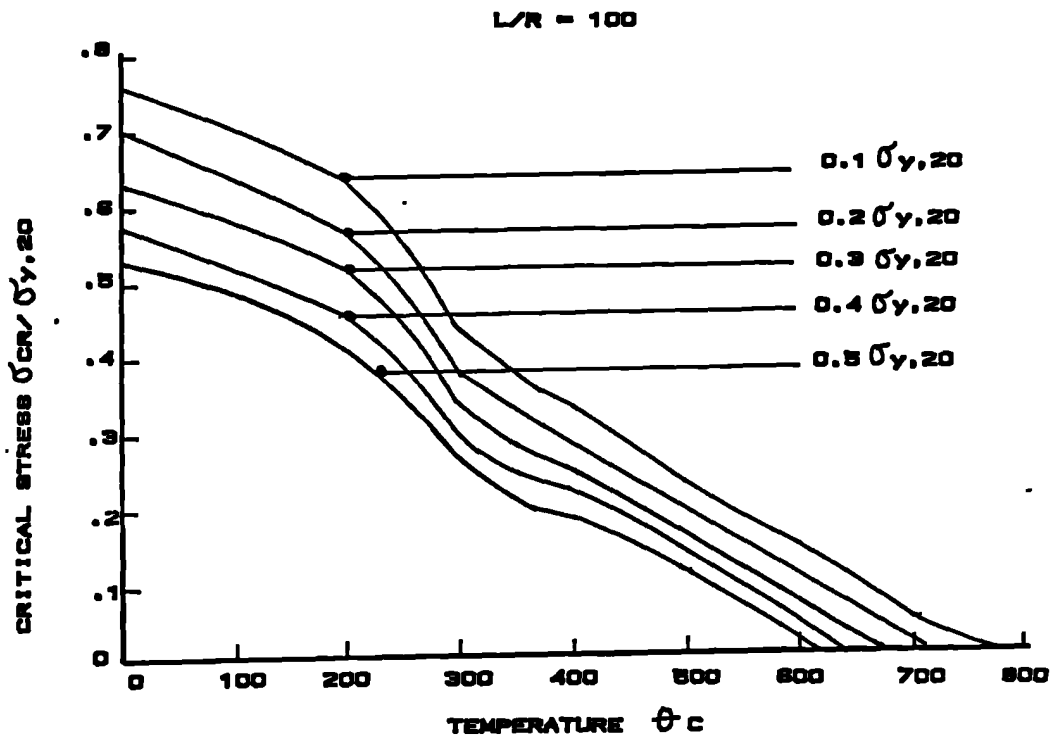


FIG. B.18c

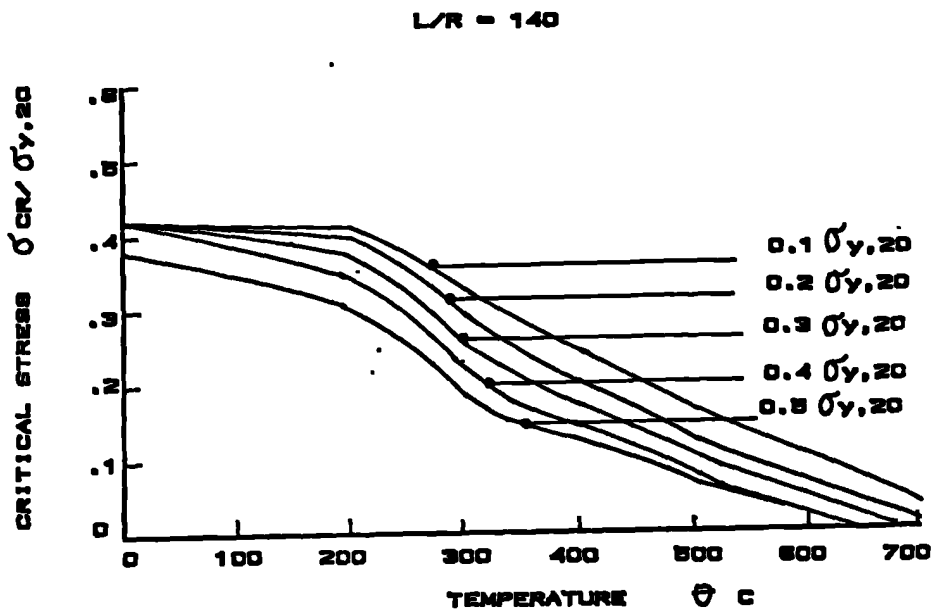


FIG. B.18d

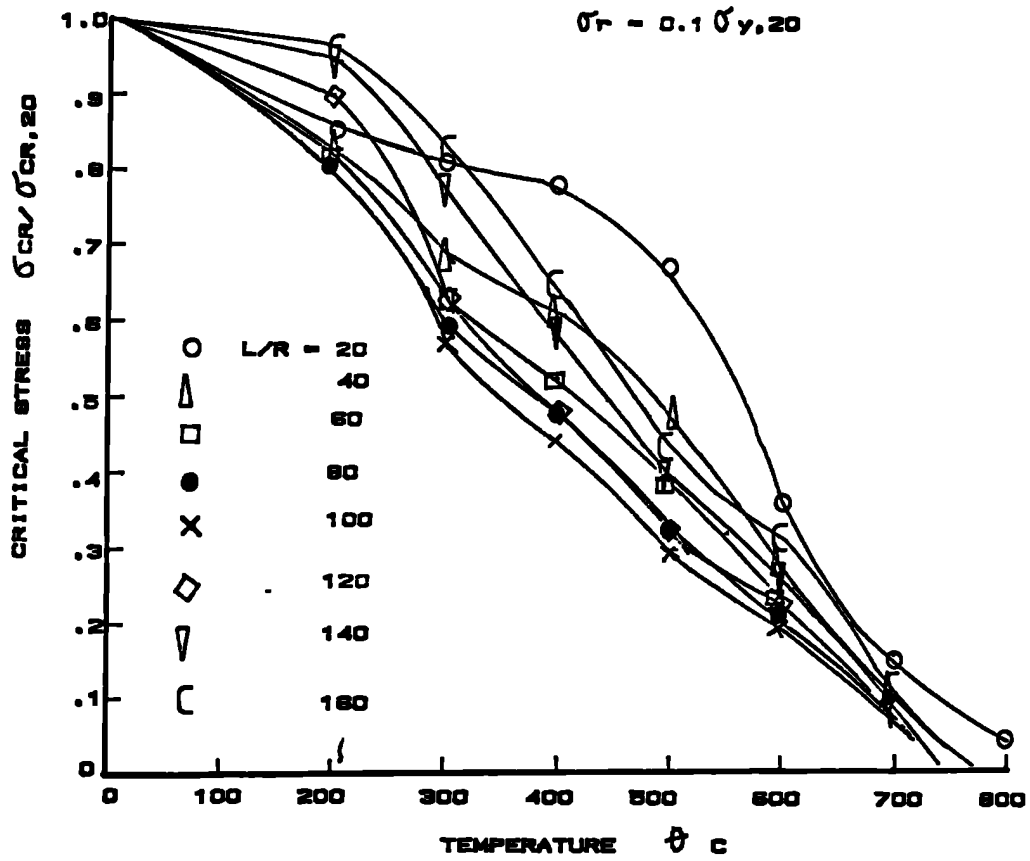


FIG. B.19a VARIATION OF CRITICAL STRESS (RELATIVE TO AMBIENT TEMPERATURE CRITICAL STRESS) WITH TEMPERATURE AT DIFFERENT RESIDUAL STRESS LEVEL

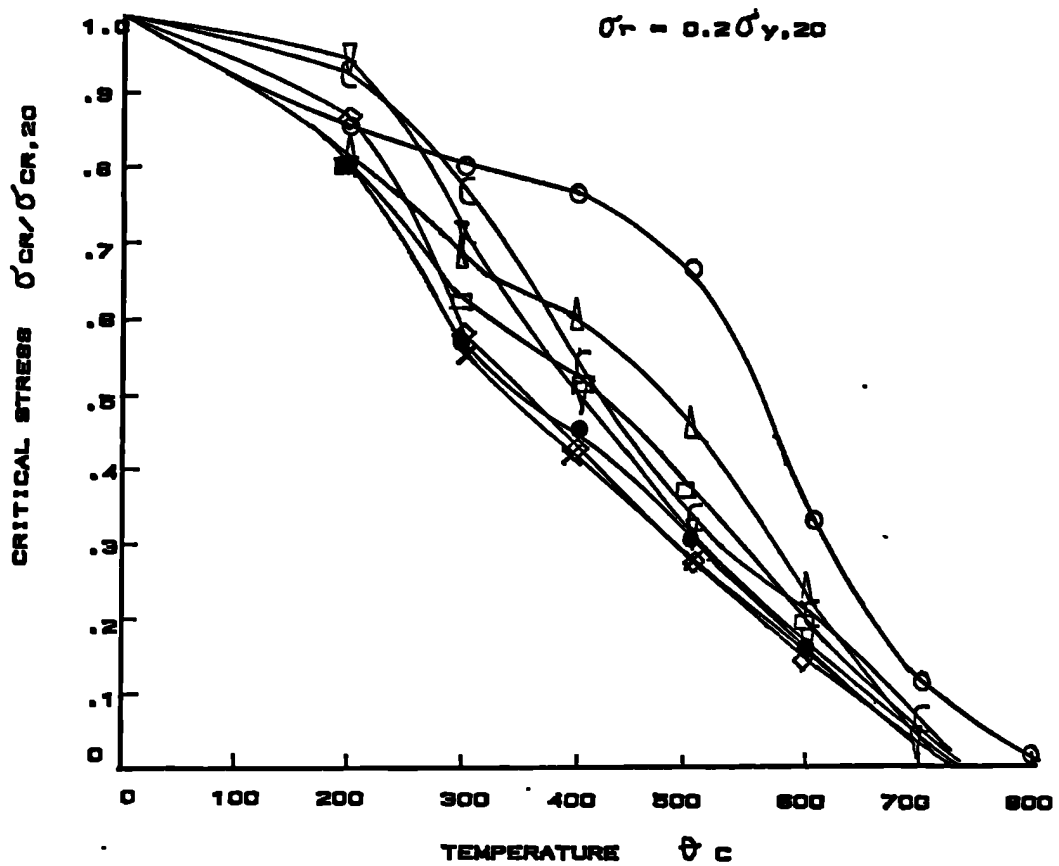
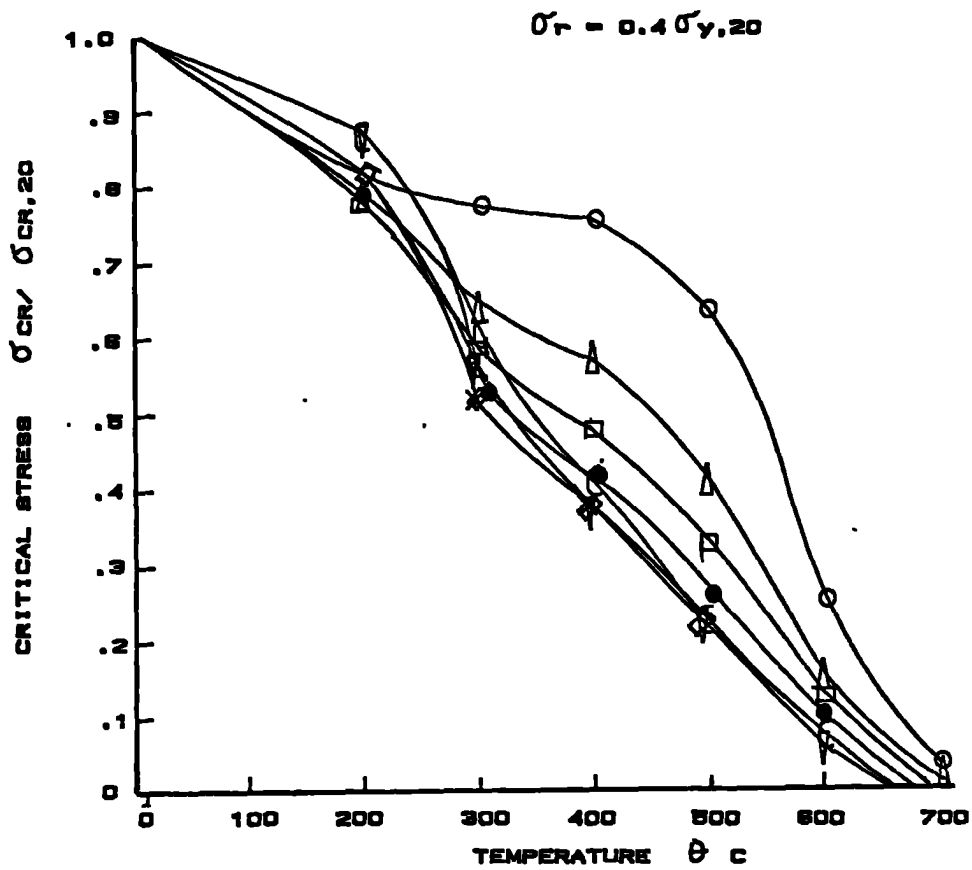
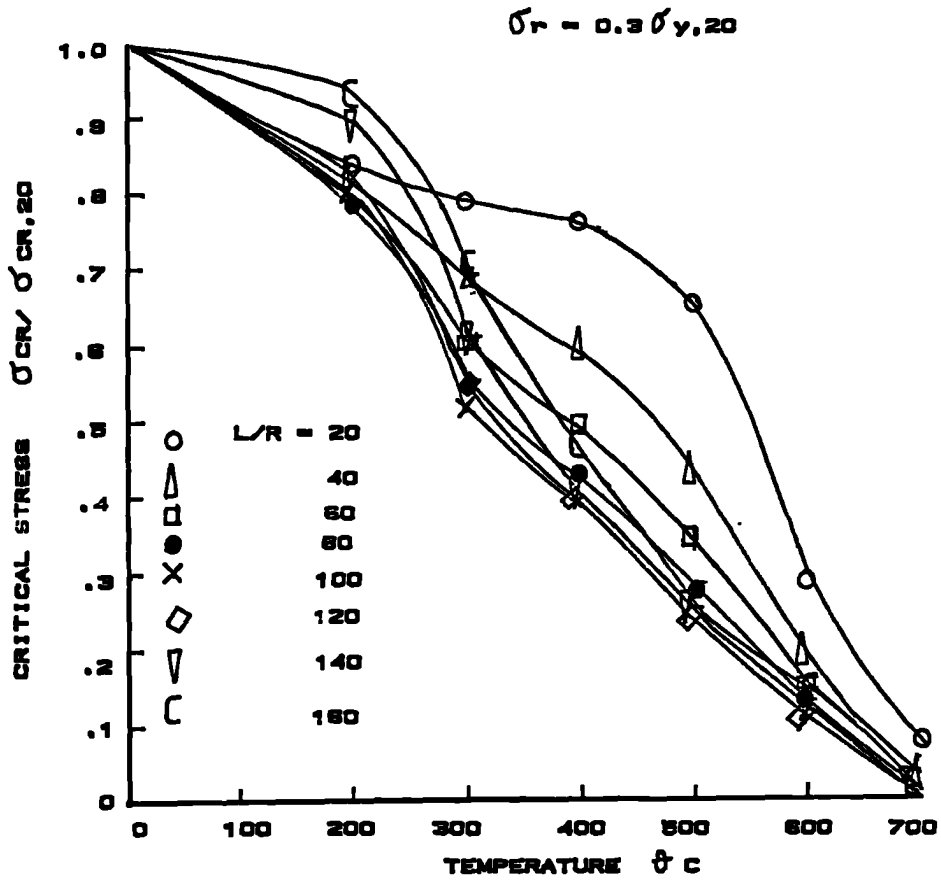


FIG. B.19b



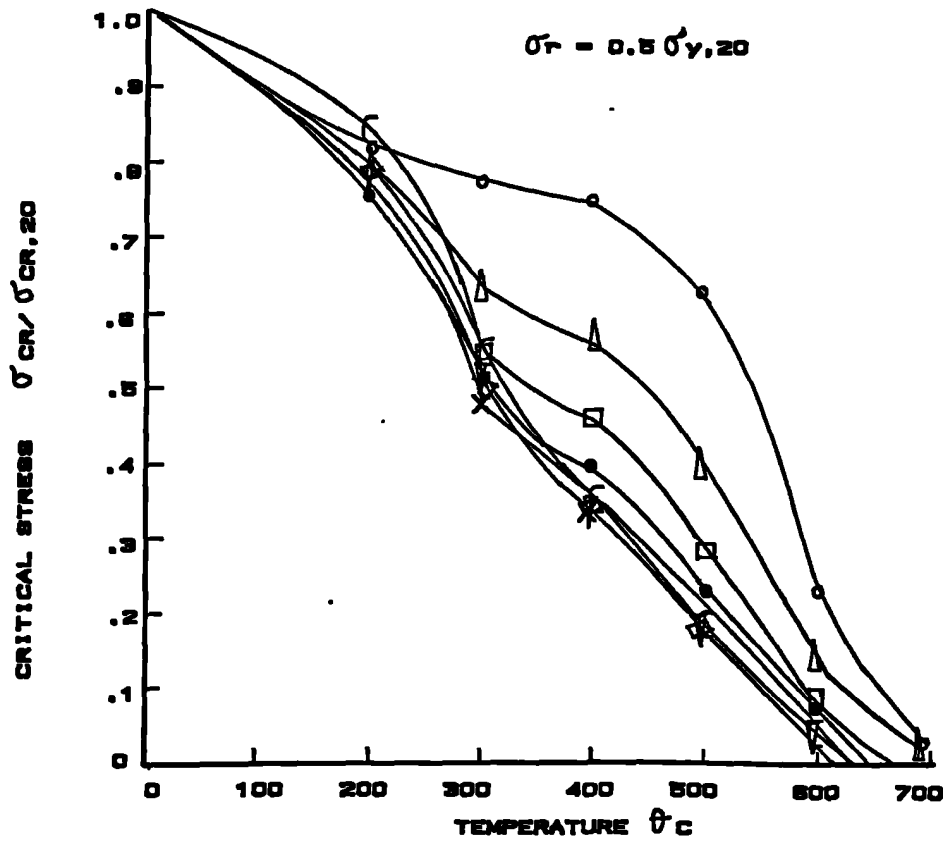


FIG. 5.19a

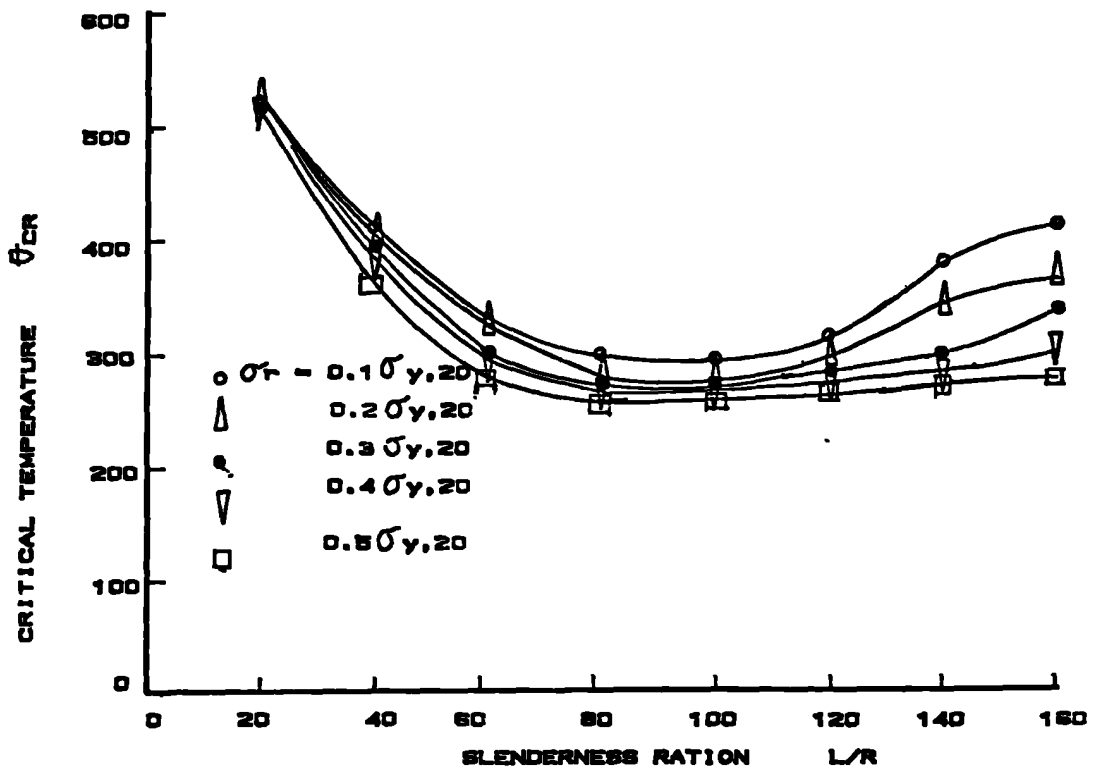


FIG. 5.20 VARIATION OF CRITICAL TEMPERATURE WITH SLENDERNESS RATIO AT INCREASING RESIDUAL STRESS

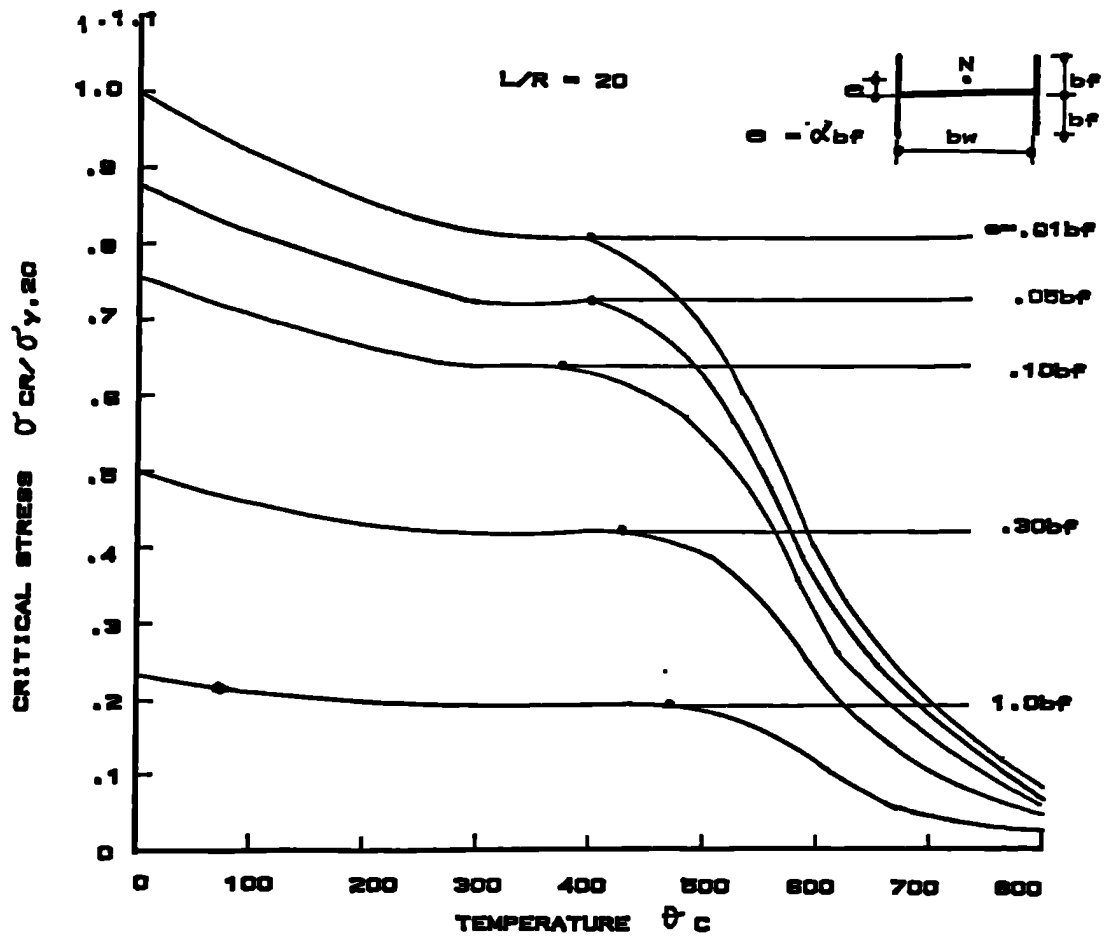


FIG. 5.21a VARIATION OF CRITICAL STRESS WITH TEMPERATURE AT INCREASING ECCENTRICITY OF LOADING

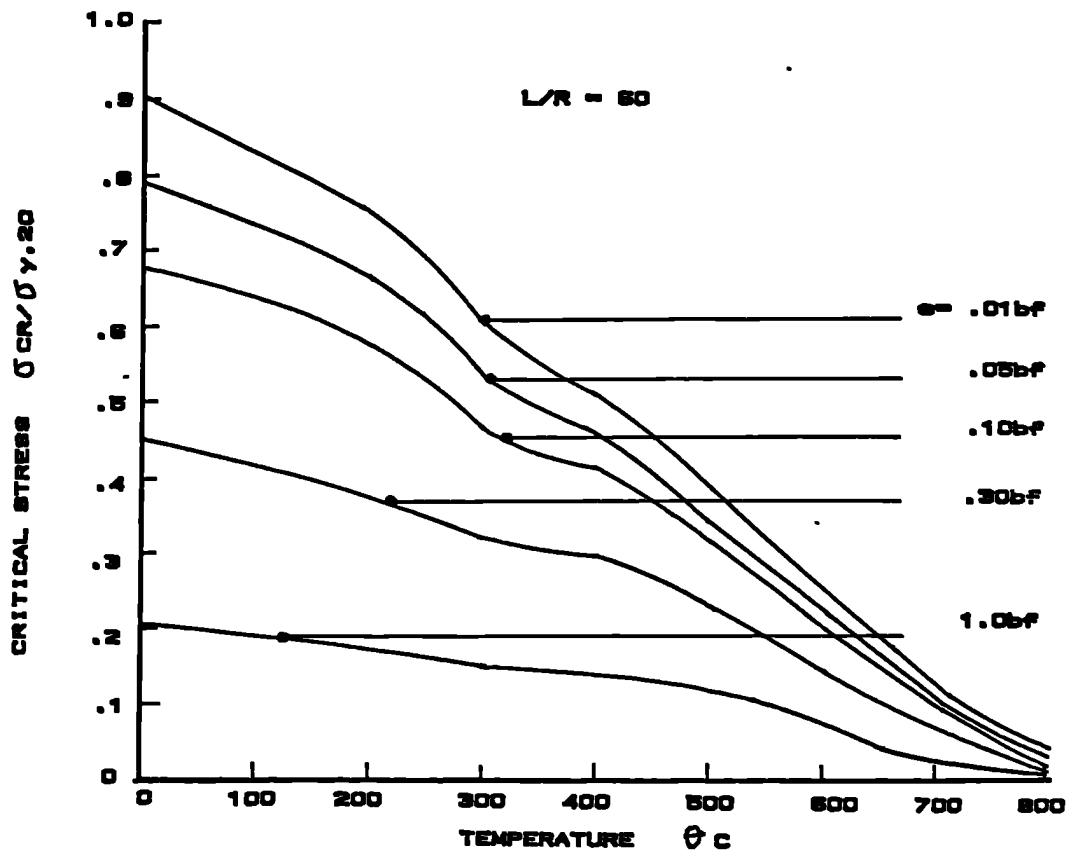


FIG. 5.21b

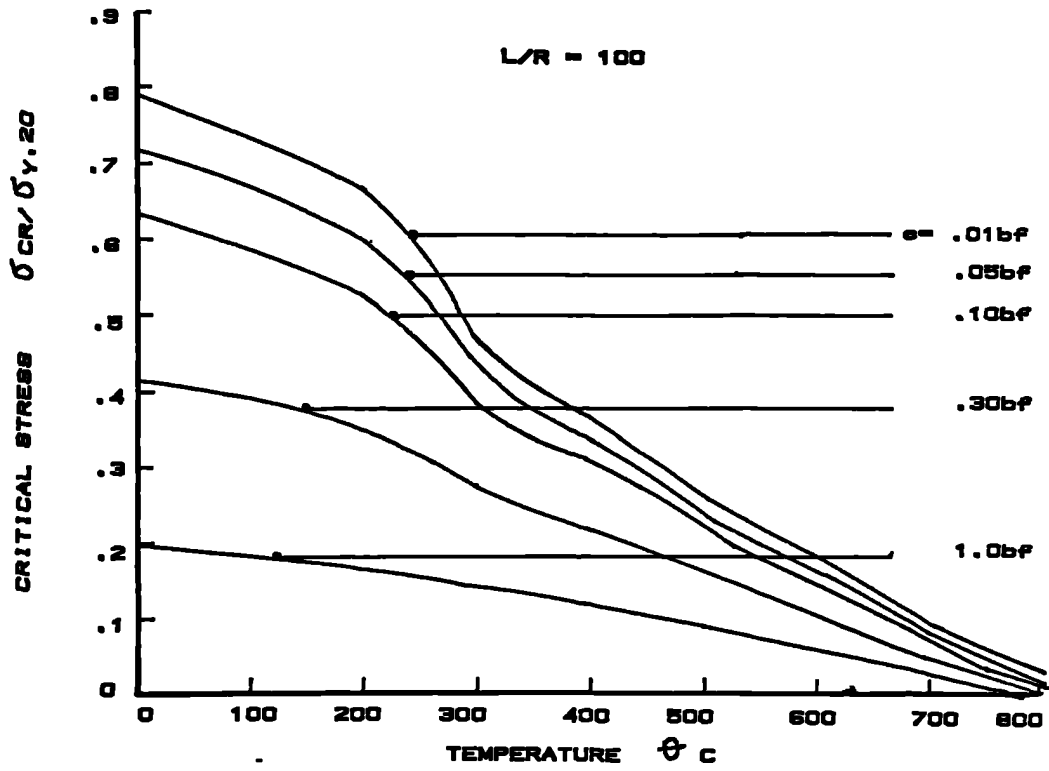


FIG. 5.21c

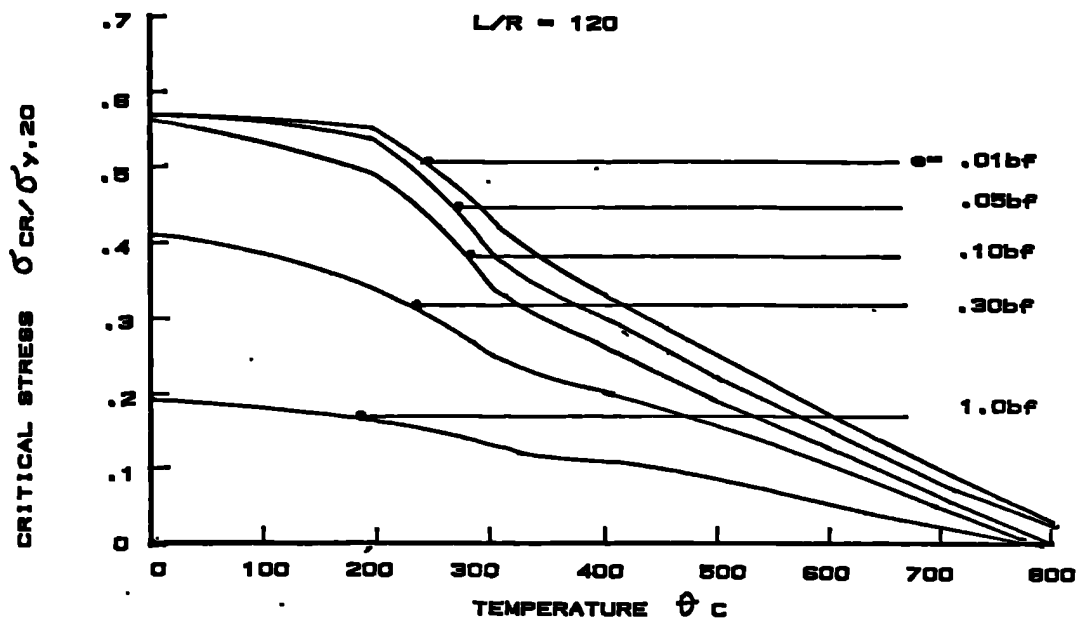


FIG. 5.21d

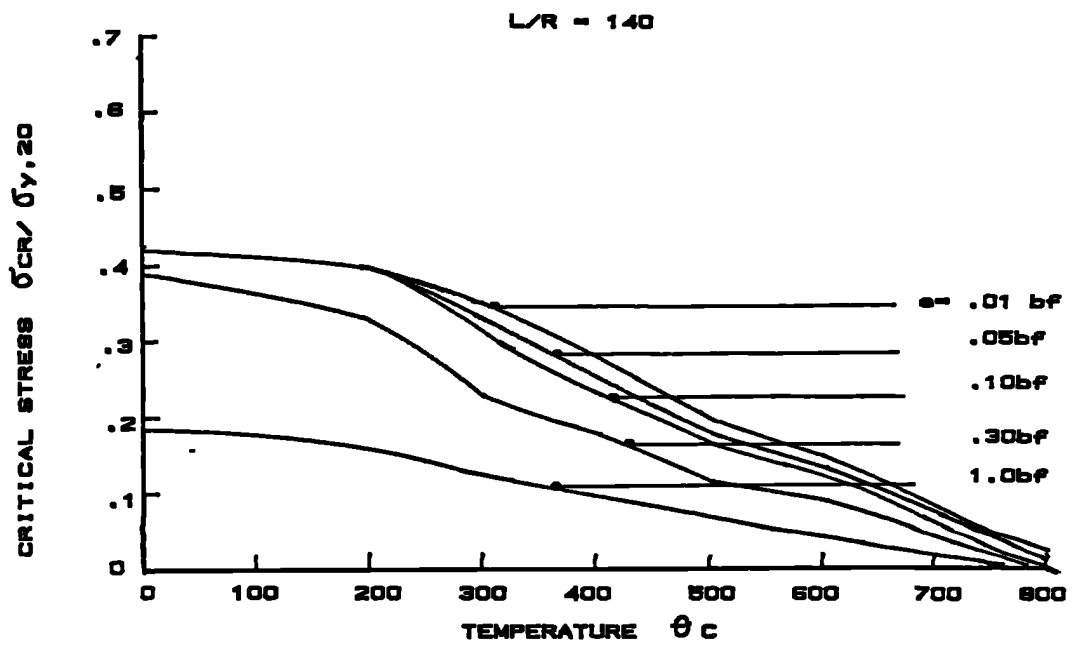


FIG. 5.21e

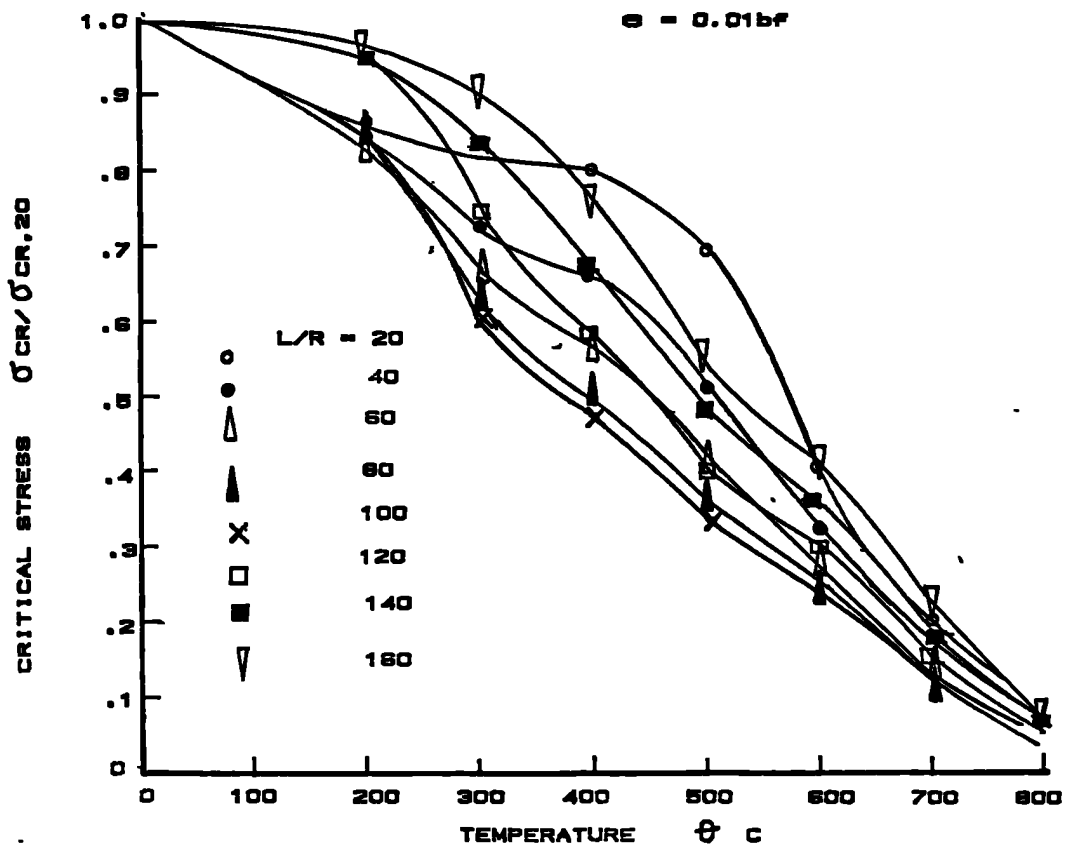


FIG. 5.22a VARIATION OF CRITICAL STRESS (RELATIVE TO AMBIENT TEMPERATURE CRITICAL STRESS) WITH TEMPERATURE AT DIFFERENT ECCENTRICITY LEVEL

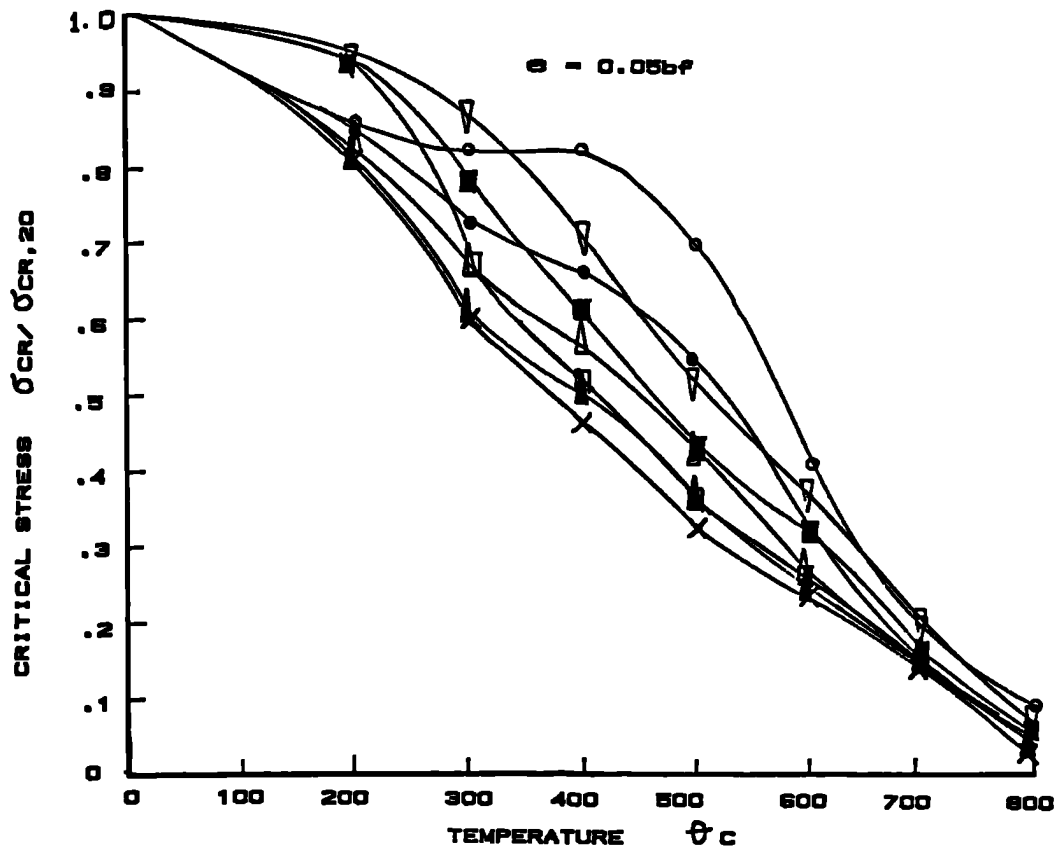


FIG. 5.22b

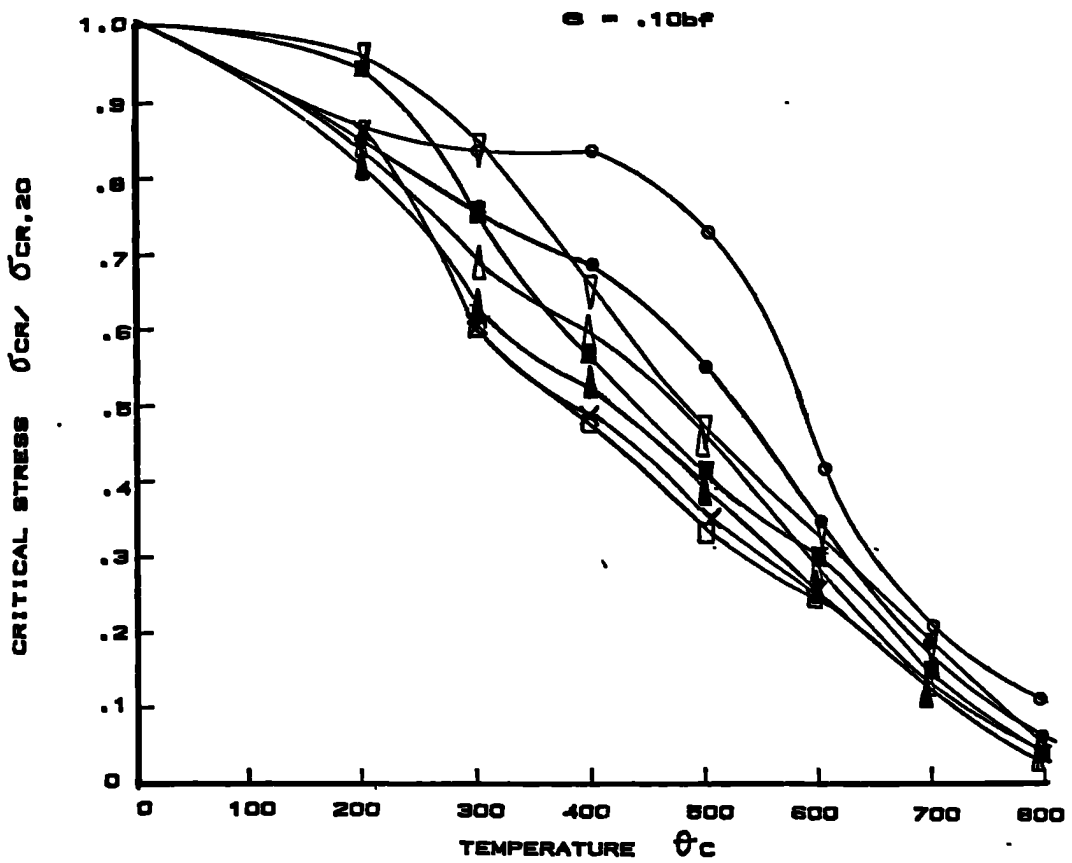


FIG. 5.22c

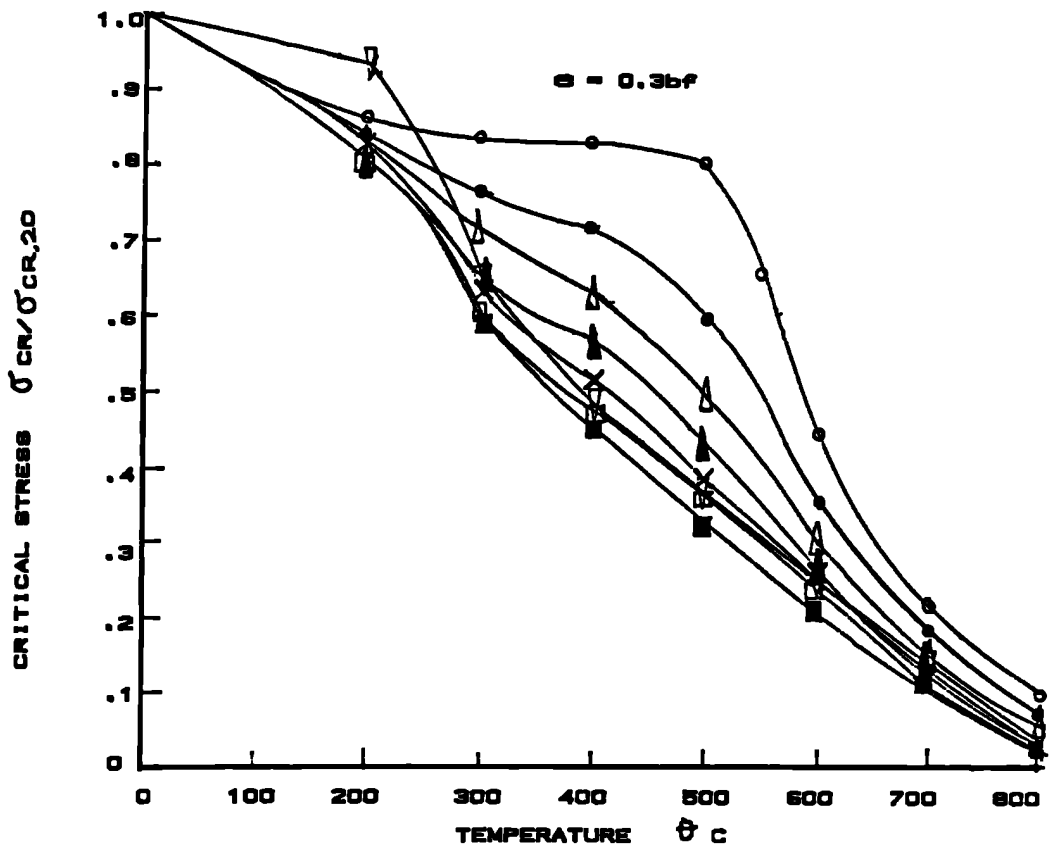


FIG. 5.22d

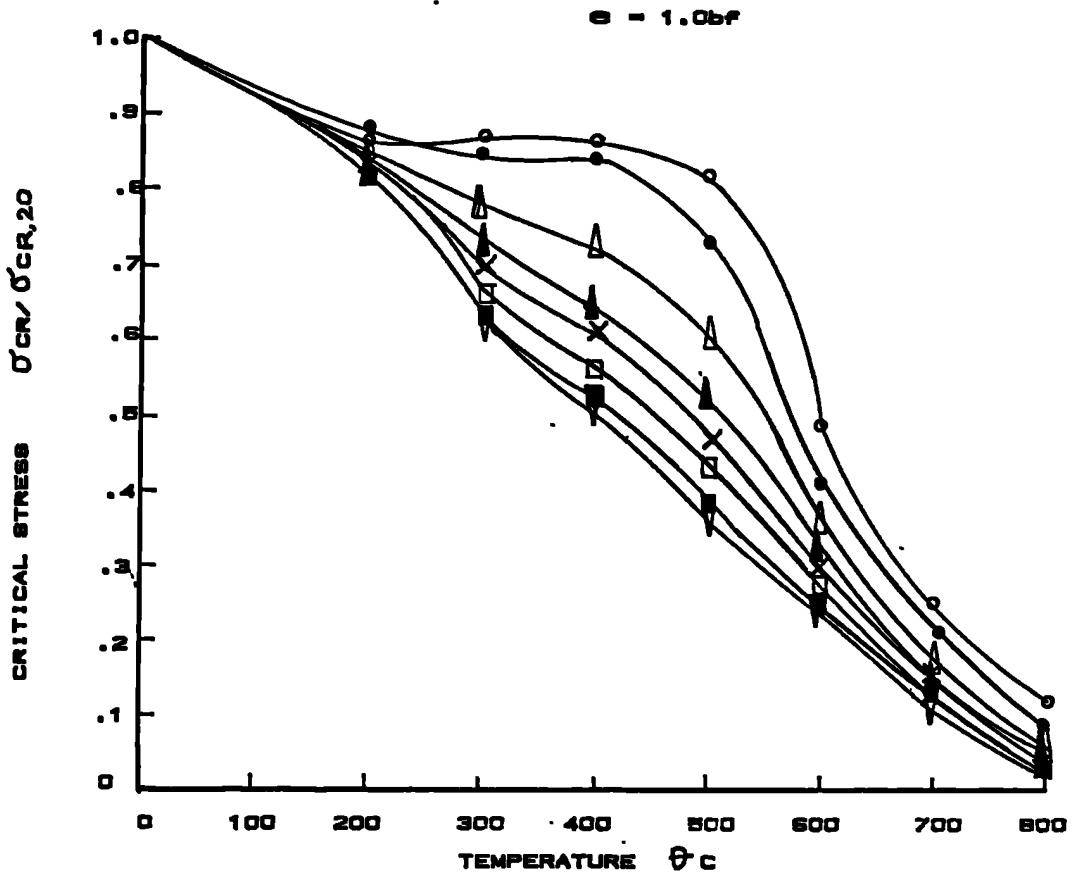


FIG. 5.22e

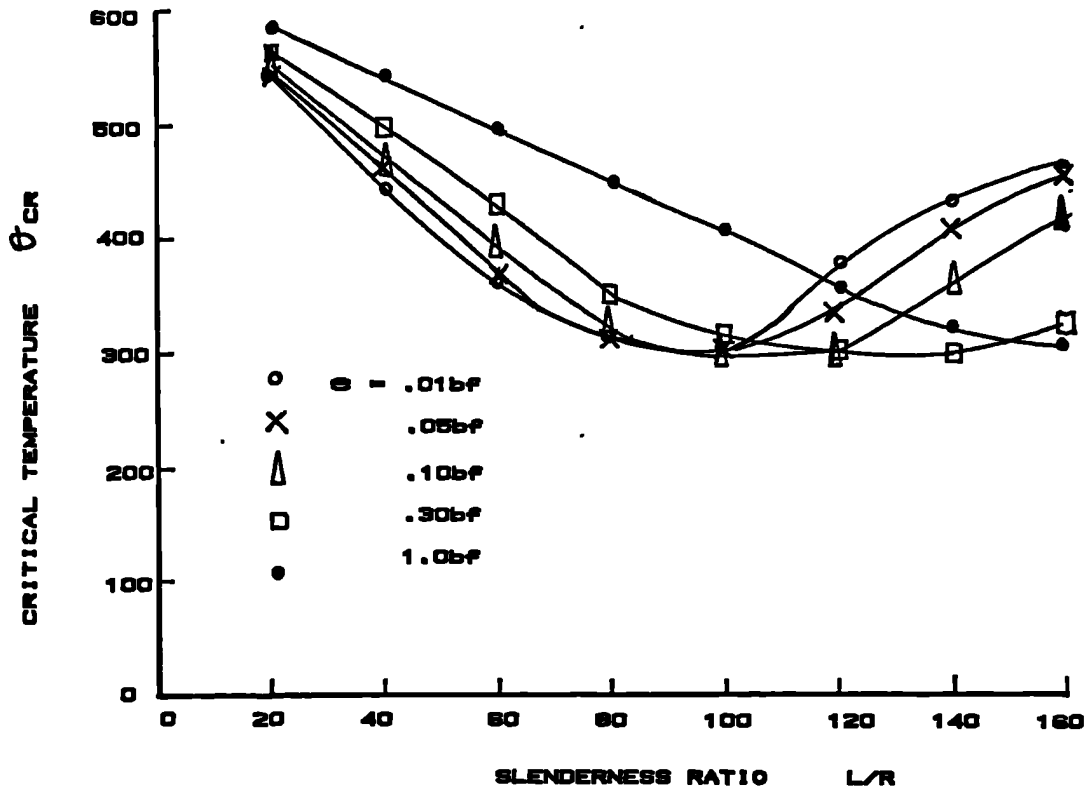


FIG. 5.23 VARIATION OF CRITICAL TEMPERATURE WITH SLENDERNESS RATIO AT INCREASING ECCENTRICITY OF LOADING

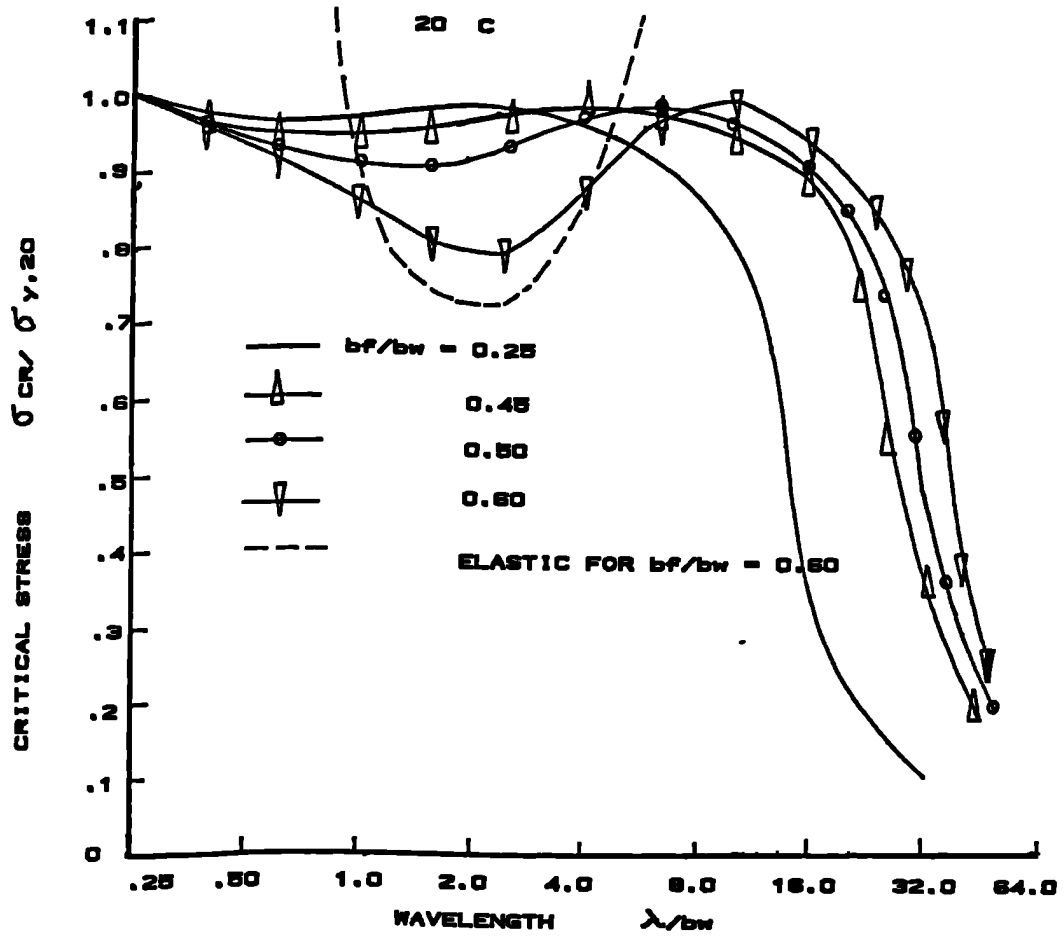


FIG. 5.24a VARIATION OF CRITICAL STRESS WITH WAVELENGTH

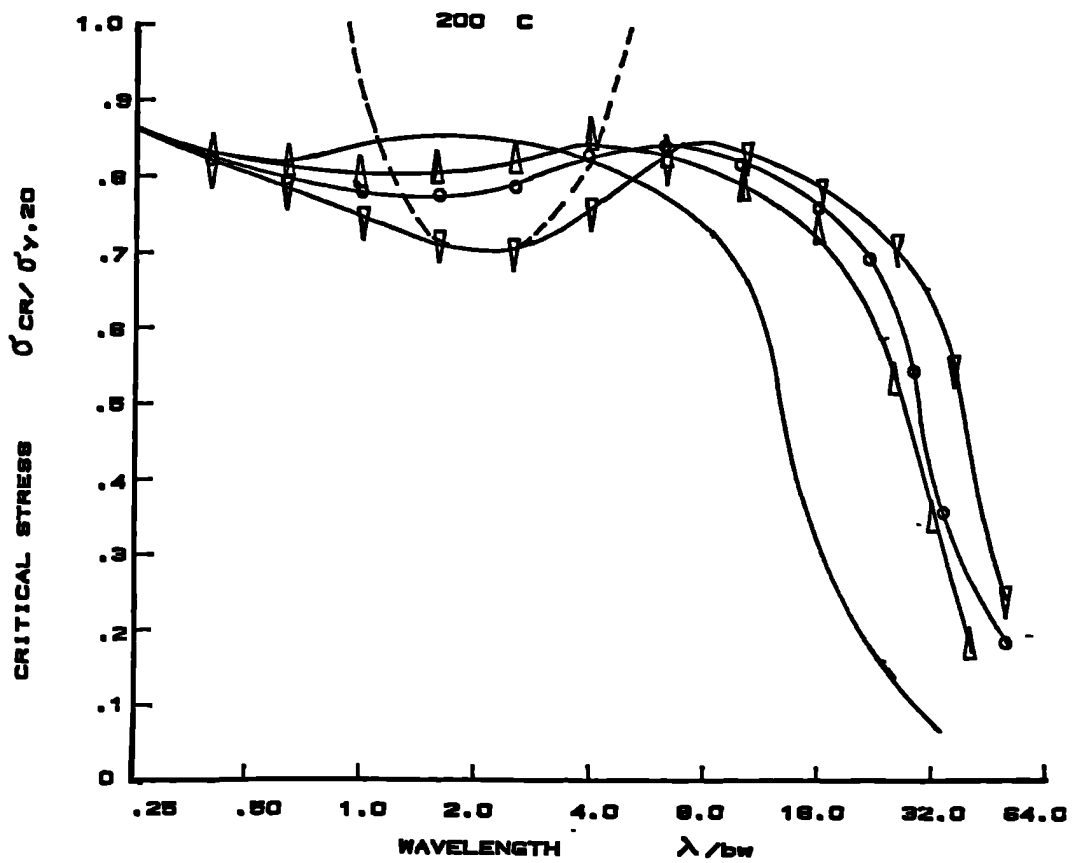


FIG. 5.24b

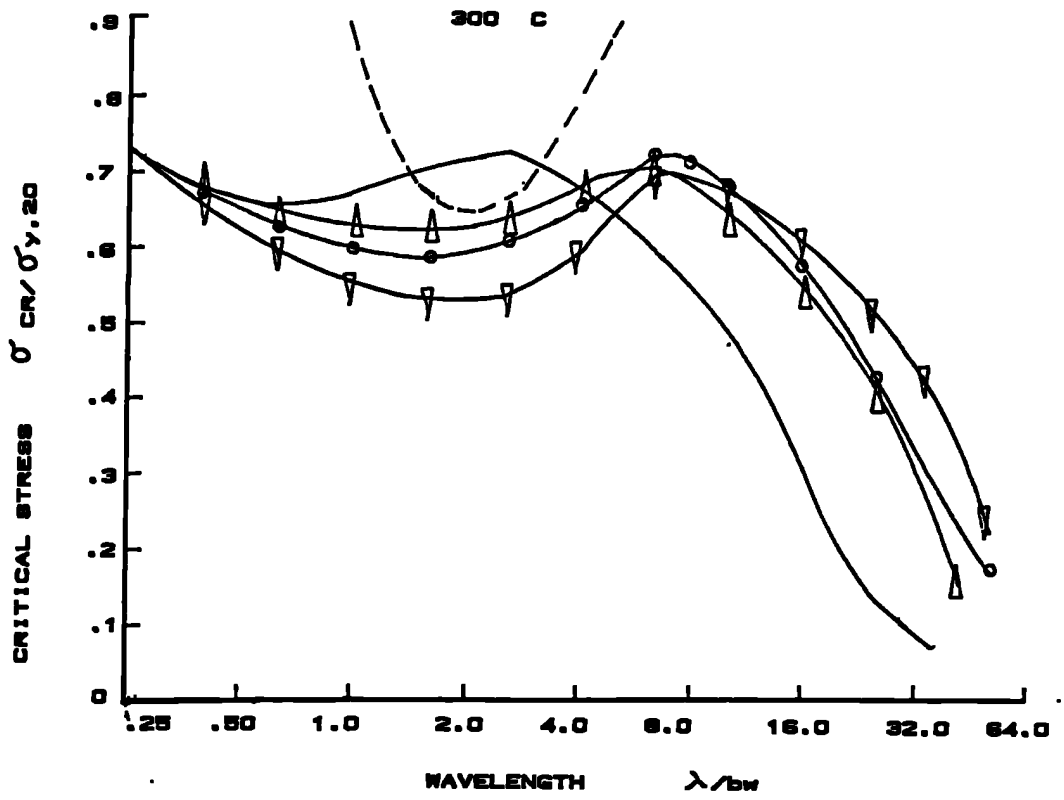


FIG. B.24c

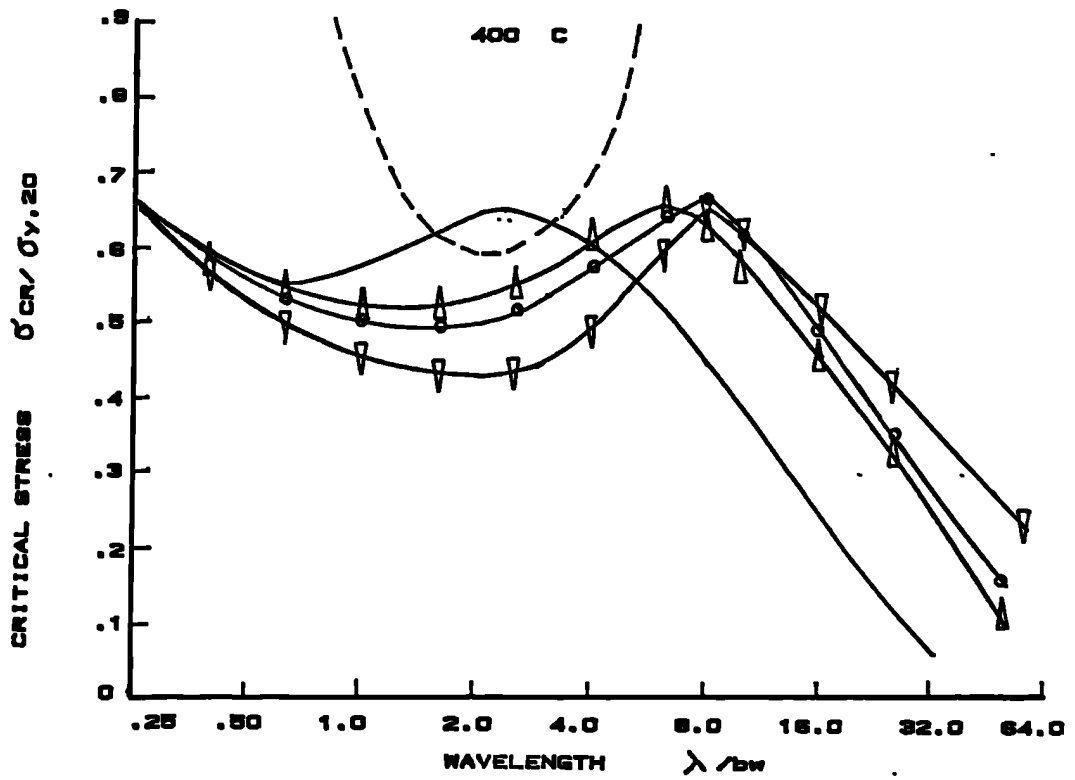


FIG. B.24d

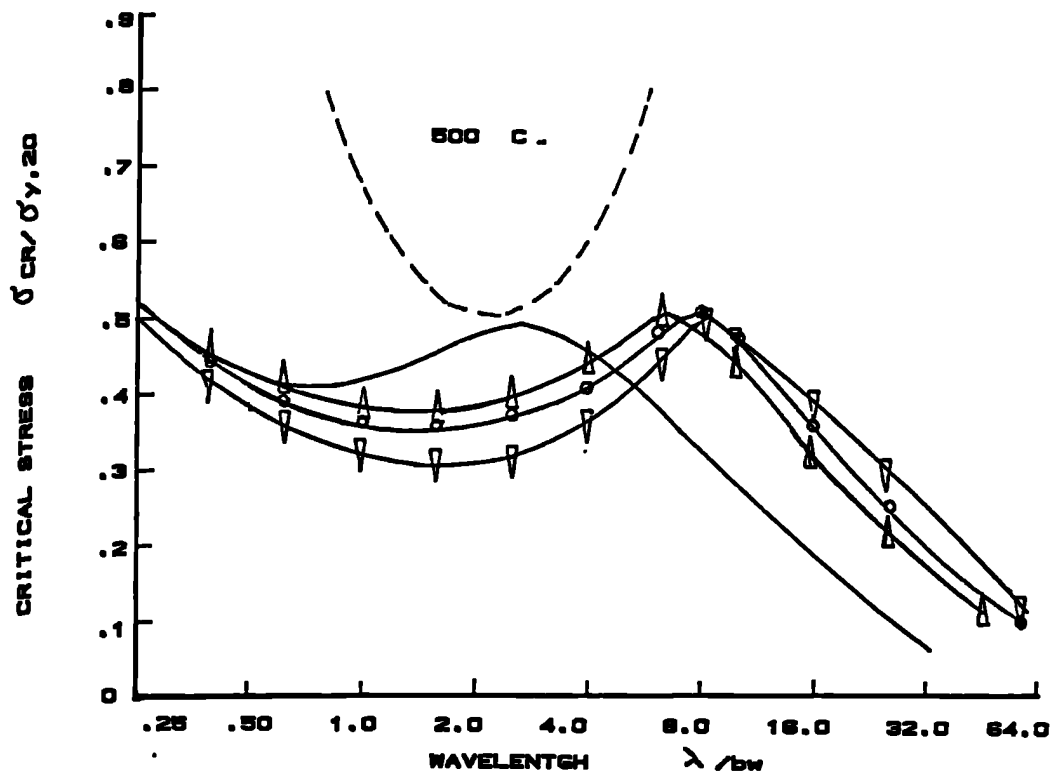


FIG. B.24e

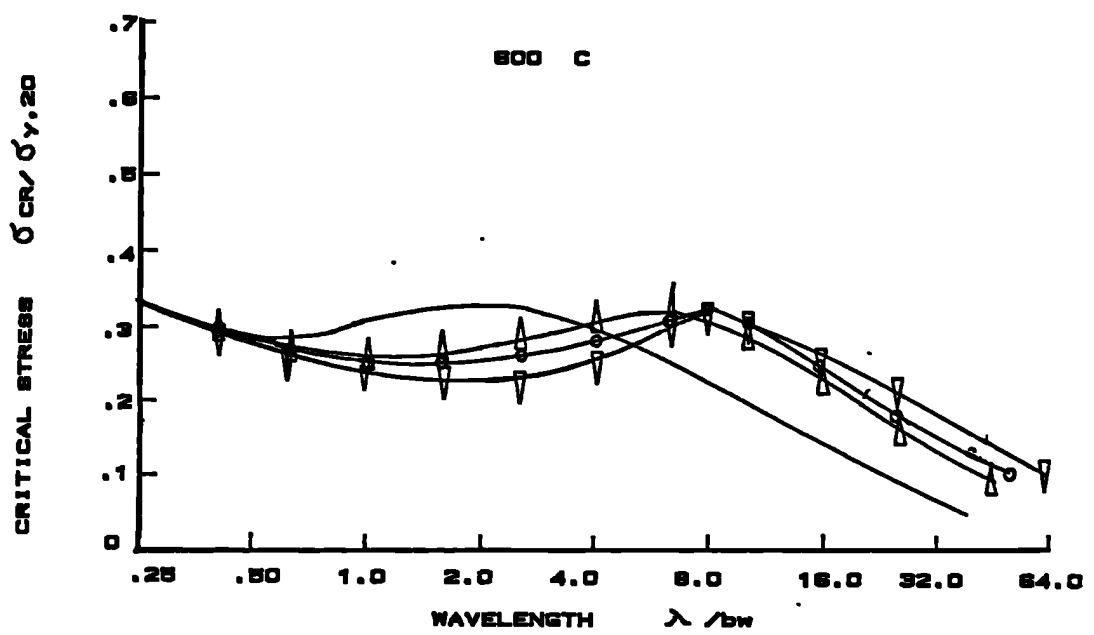


FIG. B.24f

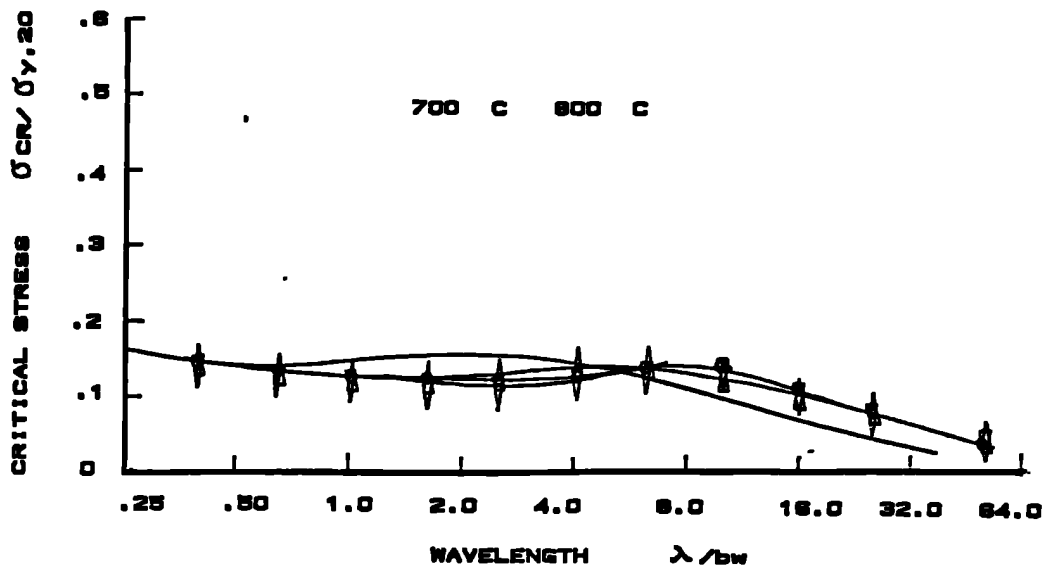


FIG. 5.24g

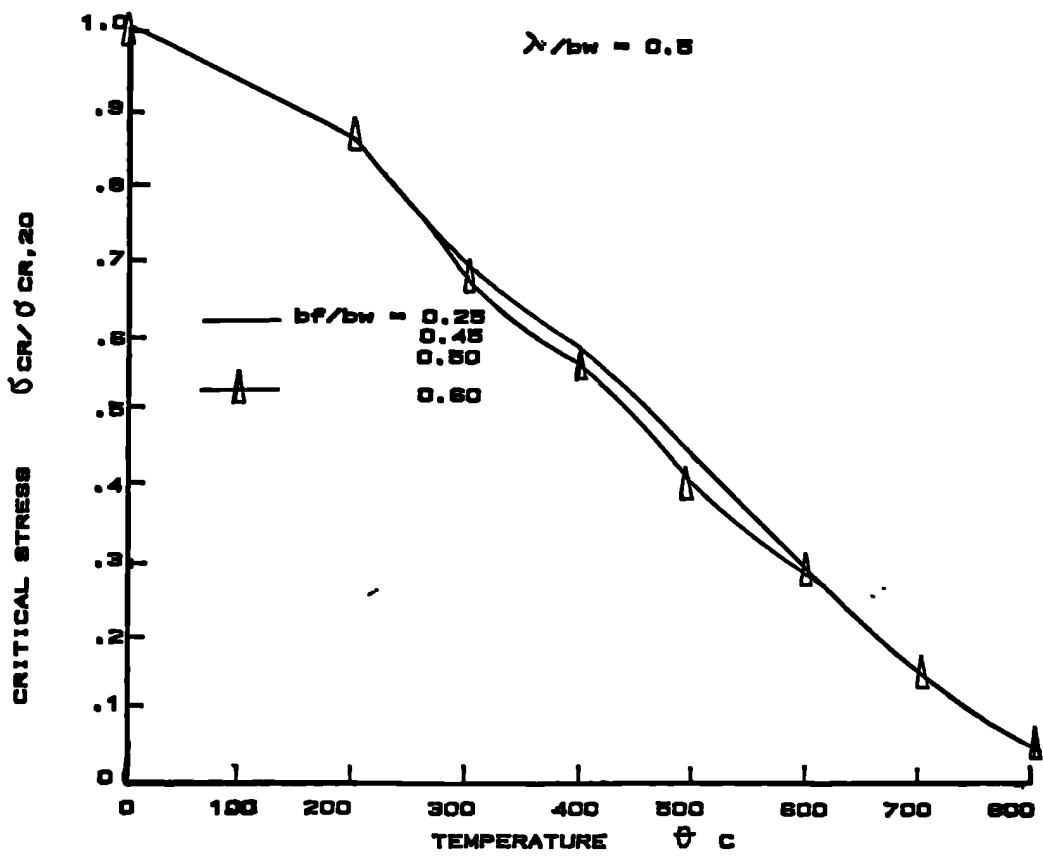


FIG. 5.25g VARIATION OF CRITICAL STRESS WITH TEMPERATURE FOR DIFFERENT HALF WAVELENGTH

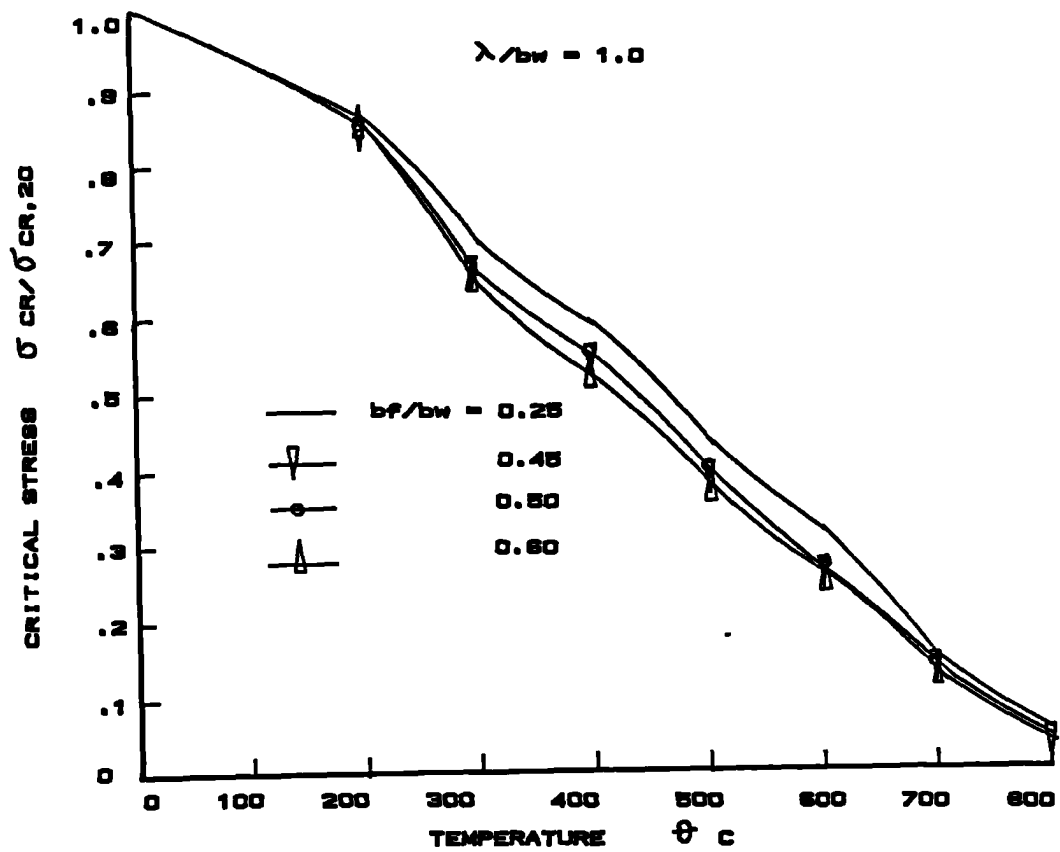


FIG. 5.25b

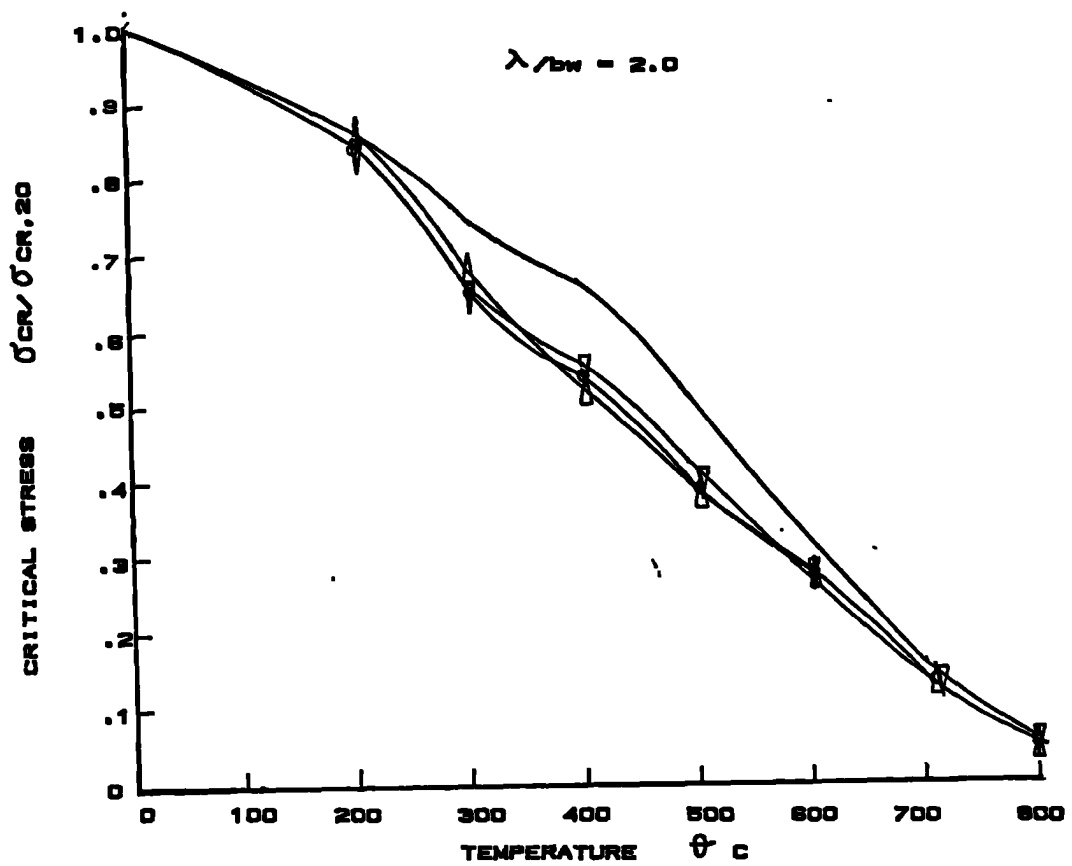


FIG. 2.25c

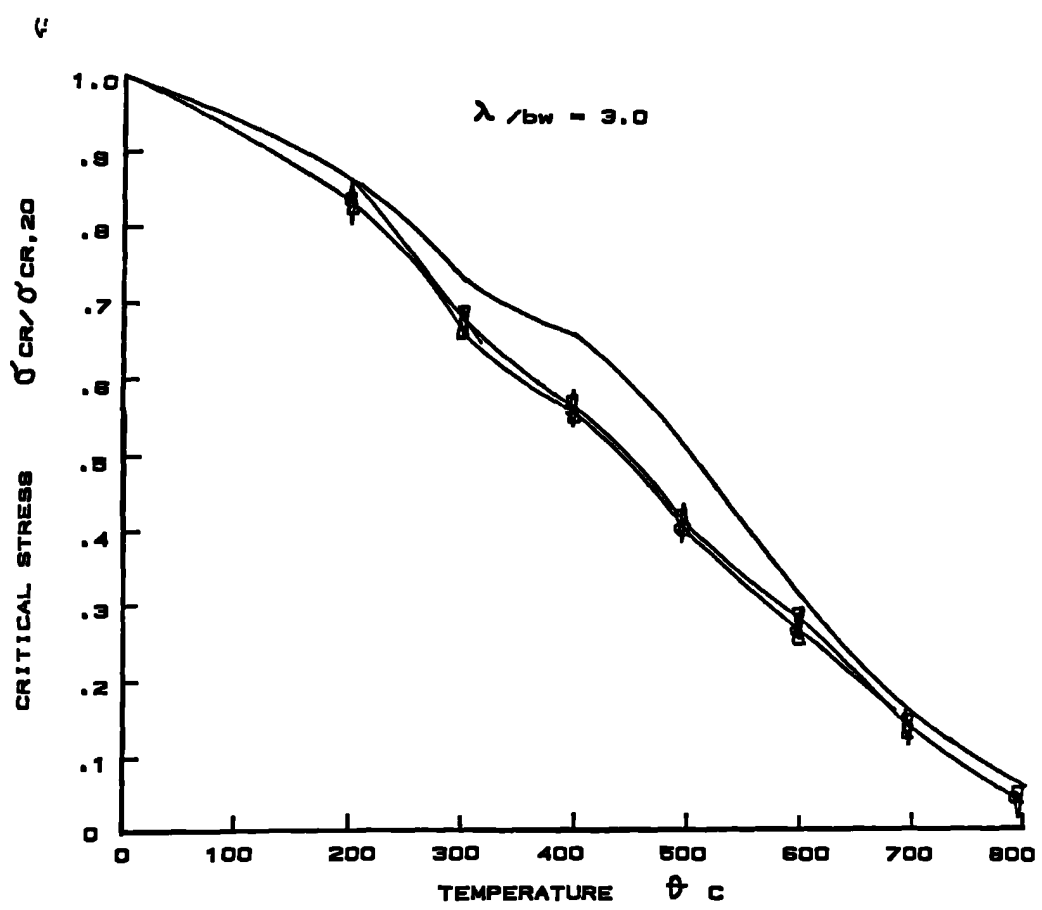


FIG. 5.25d

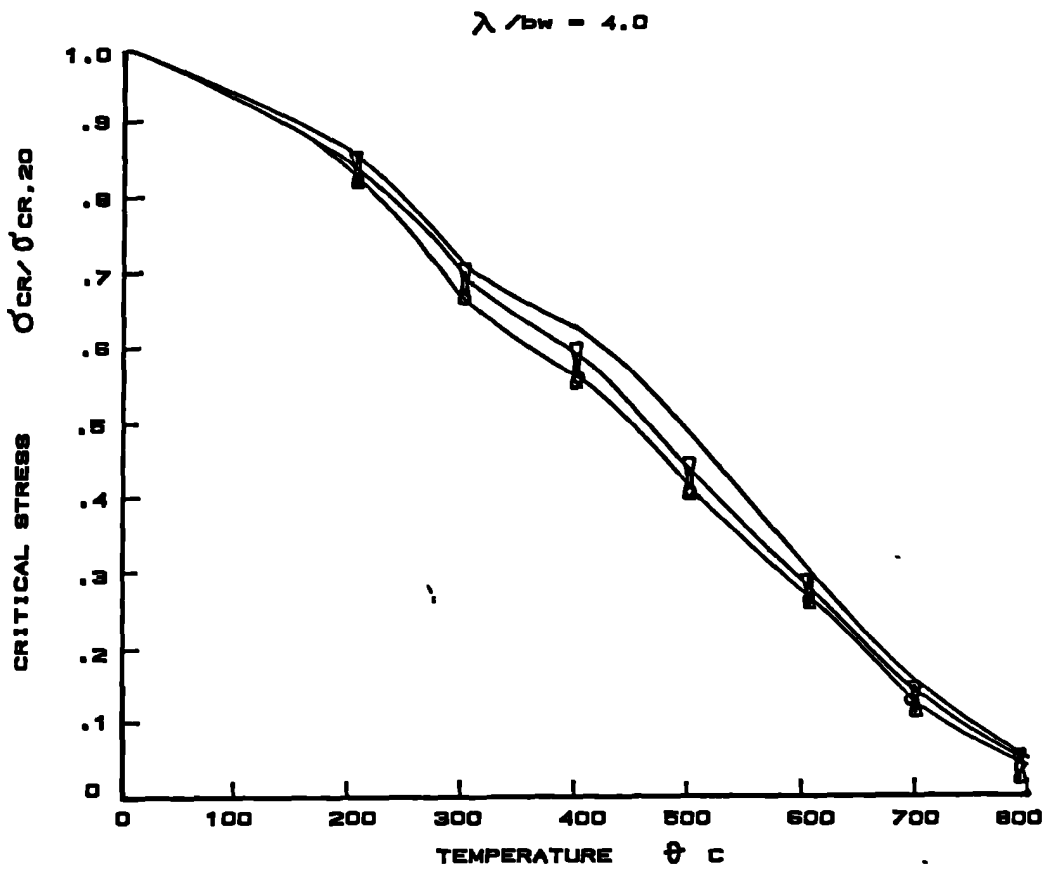


FIG. 5.25e

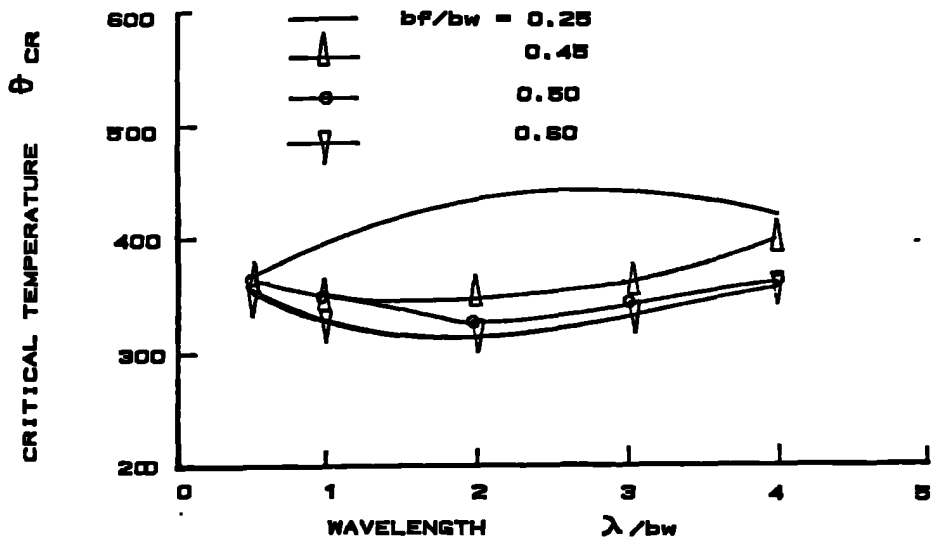


FIG. 5.26 VARIATION OF CRITICAL TEMPERATURE WITH WAVELENGTH

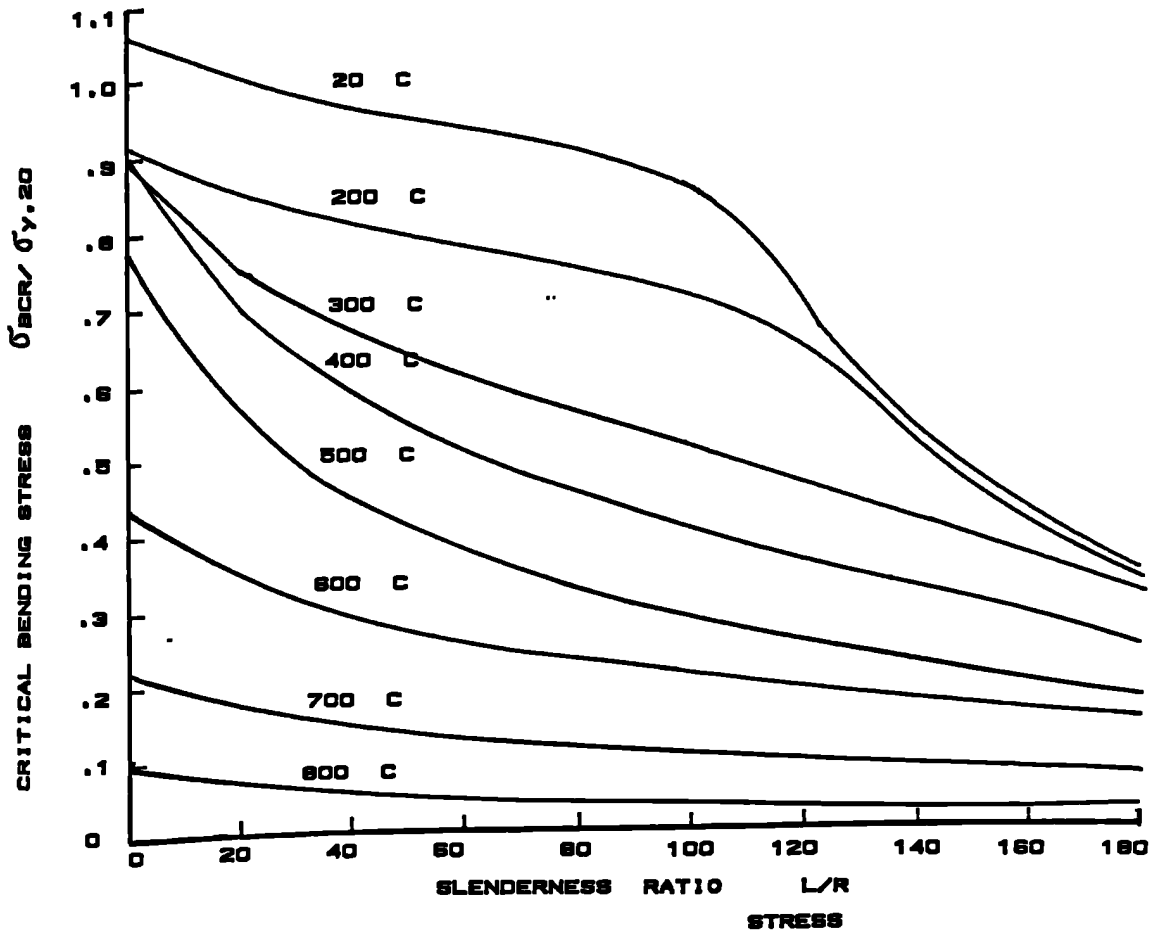


FIG. 5.27 VARIATION OF CRITICAL BENDING STRESS WITH SLENDERNESS RATIO AT INCREASING TEMPERATURE

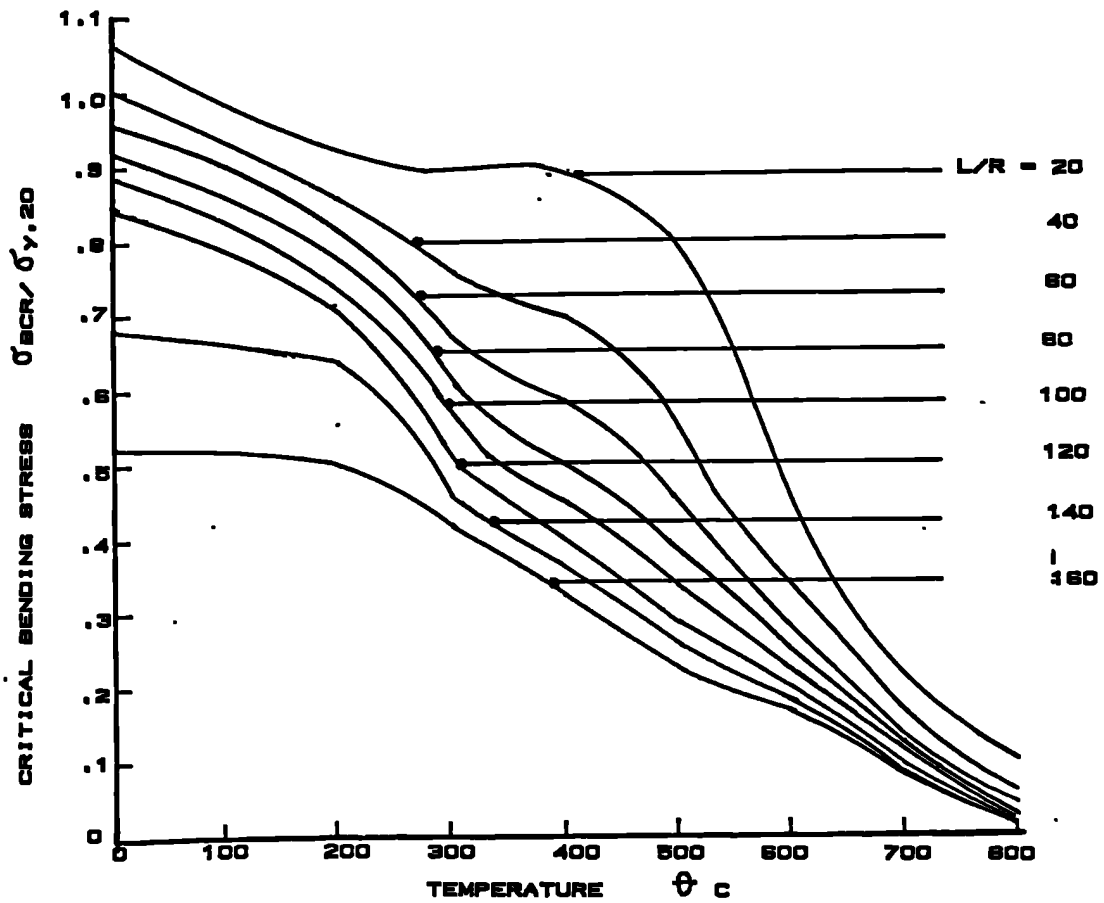


FIG. 5.28 VARIATION OF CRITICAL BENDING STRESS WITH TEMPERATURE

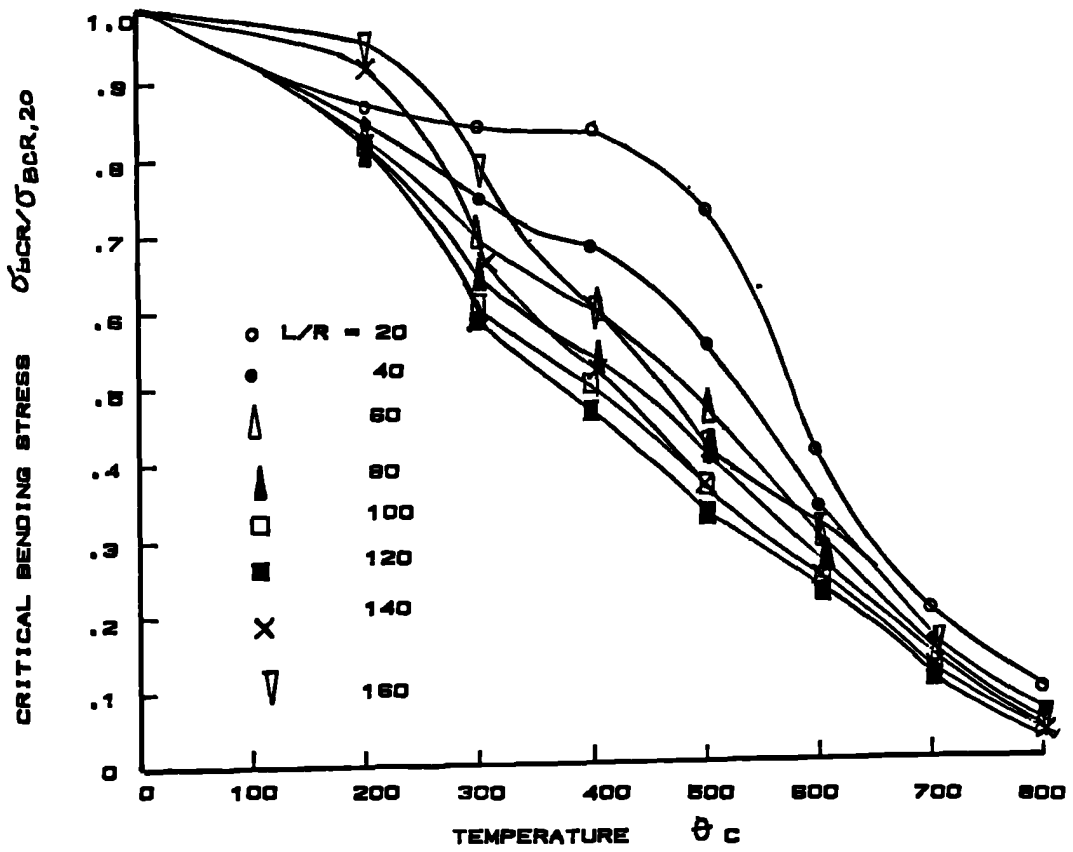


FIG. 5.29 VARIATION OF CRITICAL BENDING STRESS (RELATIVE TO AMBIENT TEMPERATURE CRITICAL BENDING STRESS) WITH TEMPERATURE

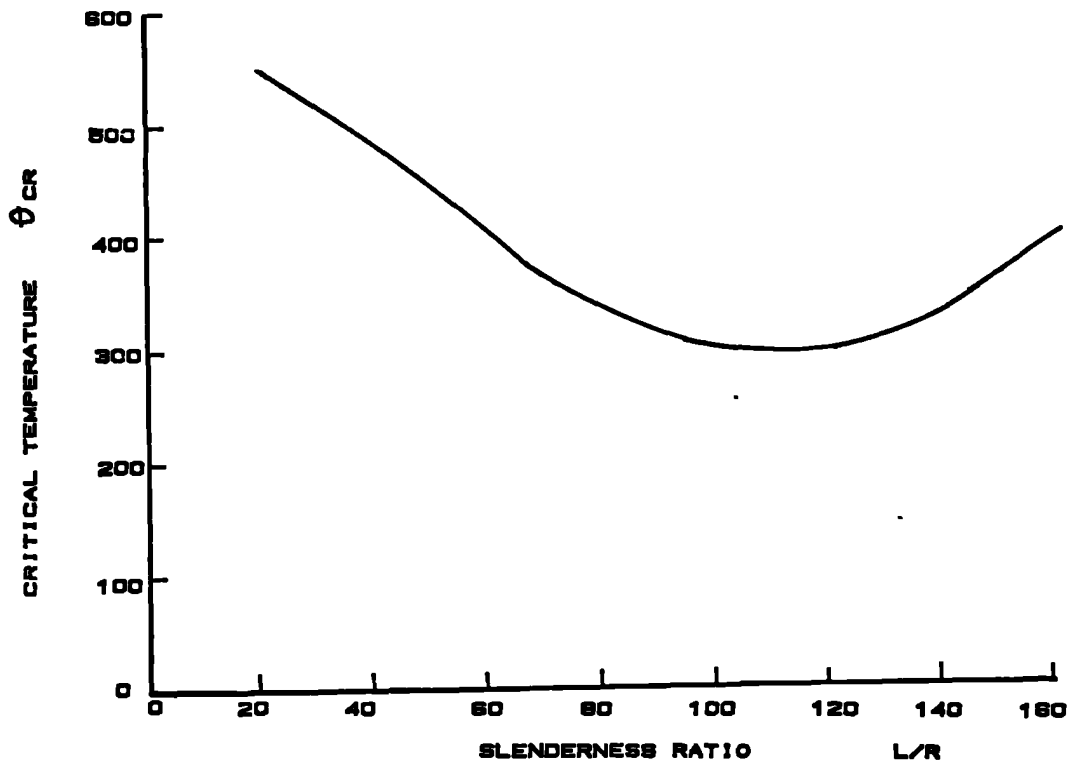


FIG. 5.30 VARIATION OF CRITICAL TEMPERATURE WITH SLENDERNESS RATIO

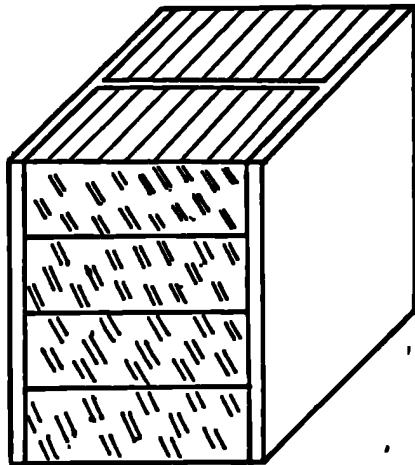


FIG. 5.31 Blocked in web column

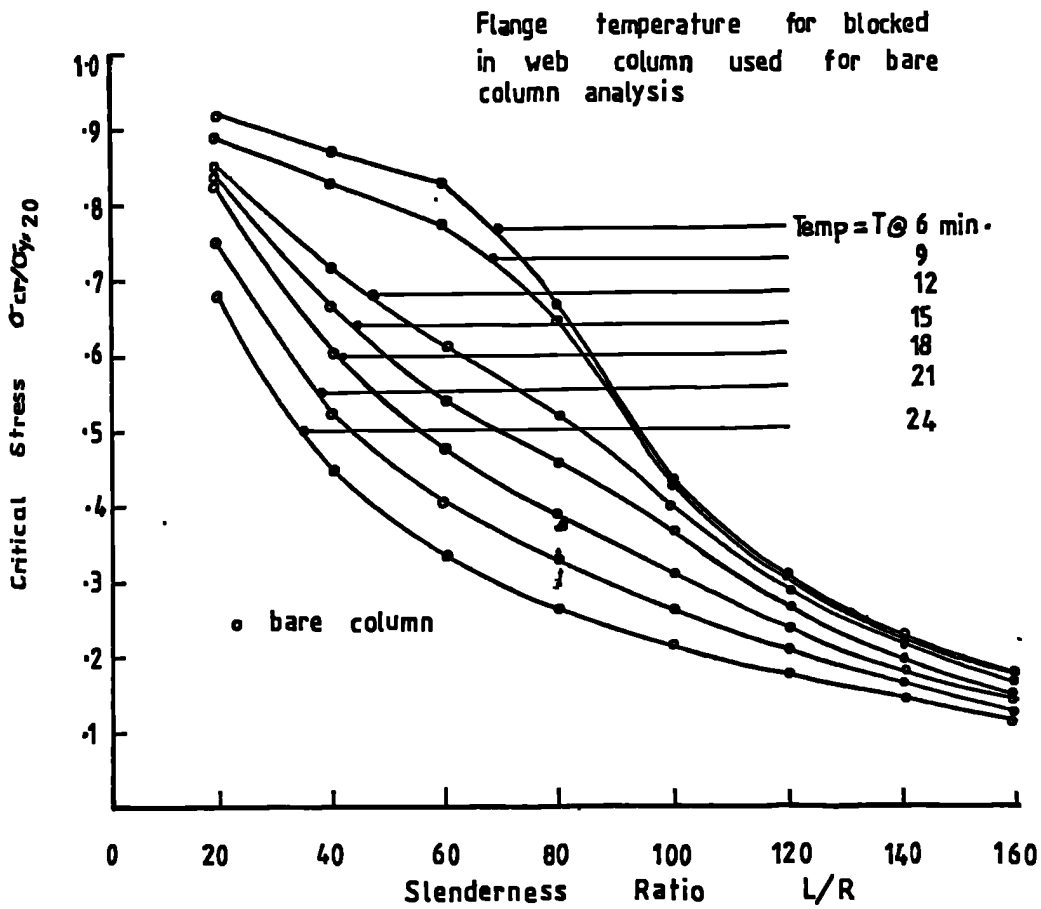


FIG. 5.32(a) Variation of critical stress with slenderness ratio for bare and blocked in web columns at increasing temperature

T REPRESENTS TEMPERATURE
INTO TESTING TIME

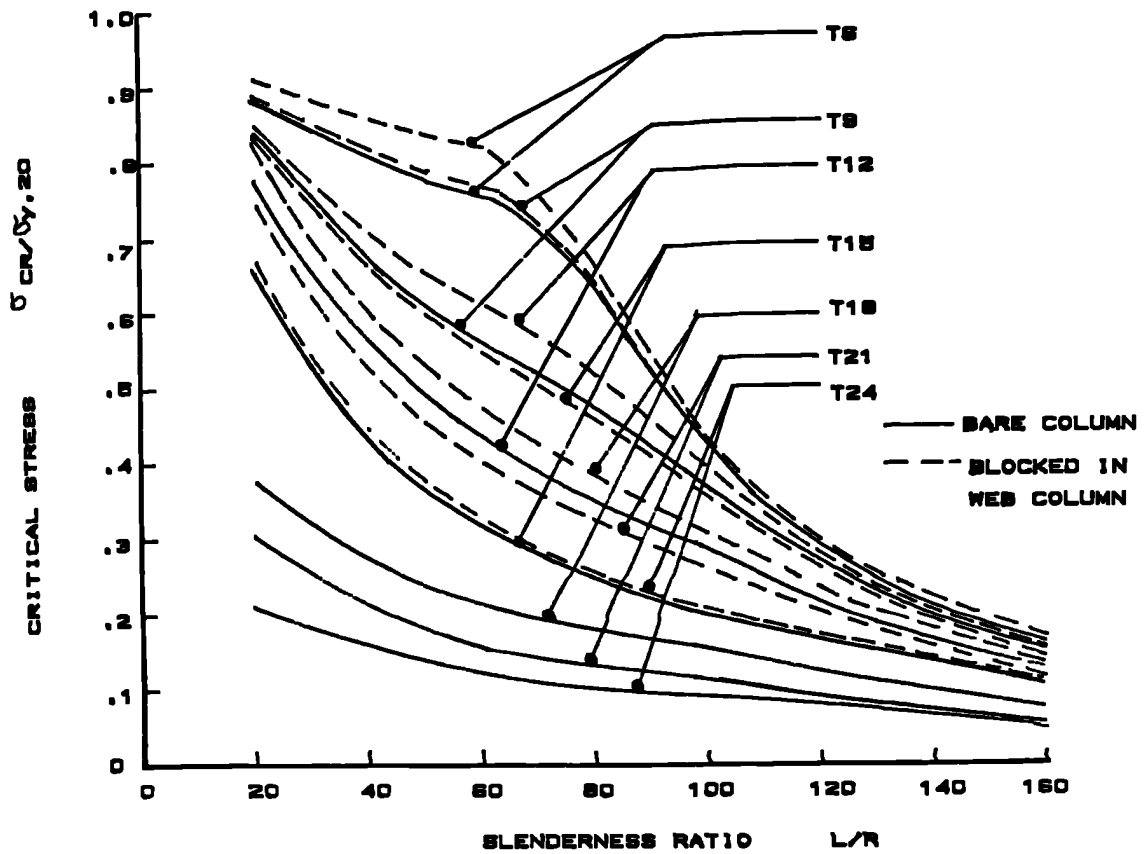


FIG. 5.32 VARIATION OF CRITICAL STRESS WITH SLENDERNESS RATIO FOR BARE AND BLOCKED IN WEB COLUMNS

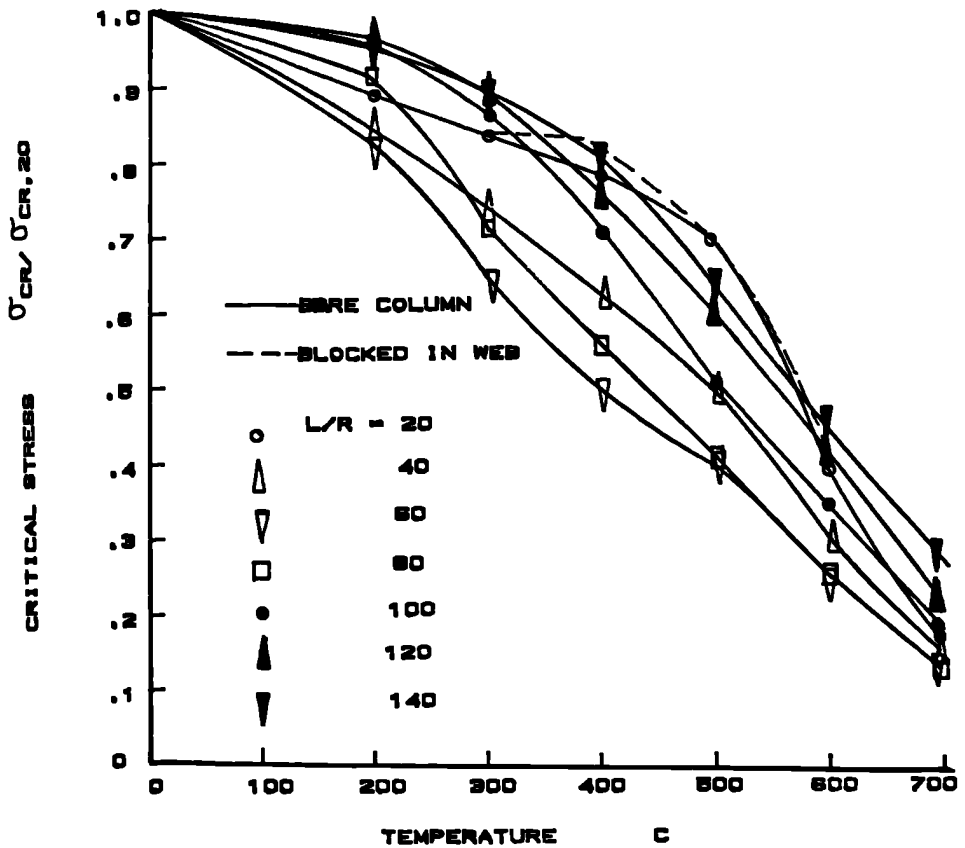


FIG. 5.33 CRITICAL STRESS (RELATIVE TO AMBIENT TEMPERATURE CRITICAL STRESS) - TEMPERATURE RELATIONSHIP FOR BARE AND BLOCKED IN WEB COLUMNS

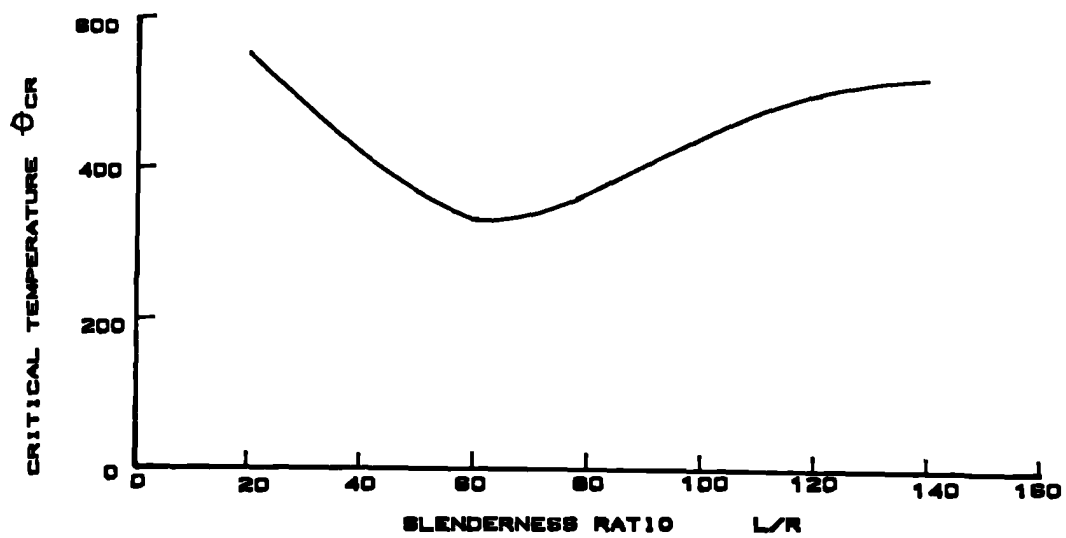


FIG. 5.34 VARIATION OF CRITICAL TEMPERATURE WITH SLENDERNESS RATIO FOR BARE AND BLOCKED IN WEB COLUMNS

Chapter 6

THE EFFECT OF THERMAL GRADIENT ON STEEL COLUMNS

6.1 Theoretical Development Of The Finite Element Method

During the course of a fire temperature distribution in the steel, both along and across the cross-section, may not be uniform. This may be due to the heating pattern or partial protection of the member offered by walls or floors. The exposure of a steel member to a heat source from one side results in thermal bowing towards the fire. This is due to the expansion of the hot material on the fire side.

The distribution pattern of temperature in a structural member depends on its position in the building. An external or partially protected column may be exposed to the building fire from one side. The partial protection arises if columns are built into walls or have webs completely blocked-in with bricks or brickwork. The protected part of the steel maintains its strength properties at a value close to those of ambient temperature. This is clearly a beneficial effect. However, the thermal gradient which results from the partial heating leaves the column with an induced thermal bowing if the element is not restrained or an induced bending moment if the element is rotationally restrained at its ends. This can be described as the bowing of a beam or column due solely to the internal strains caused by the temperature gradient over the *cross-section* of the member.

The magnitude of the thermal bowing depends on the pattern of the temperature distribution across the cross-section. At present there is no proper understanding of this phenomenon.

The reversed bowing often experienced in fire tests might be as a result of the early bowing towards the heat source (thermal bowing) but as heating progresses this is overshadowed by the degradation of stiffness towards the hotter parts. This phenomenon is often observed in the fire resistance tests of steel columns. Cooke[170] reported the occurrence of reversed bowing in the elevated temperature tests conducted on model columns in which thermal gradient was intentionally simulated. This phenomenon makes the understanding of the thermal gradient more difficult and thus exhaustive analytical studies are required to explicitly establish the thermal gradient theory.

Culver et al[147] studied (analytically) the behaviour of steel columns under thermal gradient by assuming the induced thermal bowing as initial out-of-straightness. They concluded that thermal gradient is detrimental to the steel column behaviour. The extent of the effect of thermal gradient is not yet quantifiable. The induced bowing depends on the type of support condition provided in the fire tests. For a pinned-end column the bowing can be considered as equivalent to an arc of a circle. This is Cooke's[170] approach in modelling the effect of thermal gradient on beams(Fig. 6.1).

In an attempt to study this phenomenon an existing finite element program, INSTAF[169], which is concerned with the ultimate strength analysis of braced and unbraced multi-storey frames, has been extended and modified. The program was originally developed at the University of Alberta. The necessity to adapt this method to study the thermal gradient effect on steel columns is born out of the deficiency of the finite strip method previously developed to cater for the overall geometrical imperfection of the member and interaction between axial load and thermal bowing. The analysis is based on a stiffness formulation which accounts for geometric and material nonlinearity. The basic assumption of the finite element development is that the element is treated as a beam-column which corresponds to a line element approach. The basic degrees of freedom are shown in Fig. 6.2. Generally, this approach helps with the inclusion of many parameters such as residual stresses and eccentricity of loading. The load-deformation characteristics of the structure can be traced by solving the finite element equations using the Newton-Raphson iteration technique.

In order to include the effect of thermal gradient within the INSTAF development the displacement functions have been modified by superposing the induced bowing on the original displacement functions. This results in a complete remodelling of the problem parallel to the original development, with other original assumptions retained. At the same time the tri-linear stress-strain relationship has been replaced with a series of the stress-strain-temperature relations modelled by Ramberg-Osgood formulae as earlier used in the finite strip method.

The thermal bowing displacement component comprises the thermal bowing amplification factor K which varies sinusoidally along the member length with a half-sine wavelength. Thus the in-plane displacement functions are as shown in Fig. 6.3 and are given by:

$$\begin{aligned} U &= U_o - y \sin \beta - K S_z \tan \beta \\ V &= V_o - y(1 - \cos \beta) + K S_z \end{aligned} \quad (6.1)$$

in which U_o and V_o are the displacement functions corresponding to the reference axes. These are basically functions of assumed interpolating polynomials.

In the original development of INSTAF it was assumed that the slope at any point along the reference axis is given by Equation (6.2)

$$V'_o = \frac{\Delta V_o}{\Delta z} = \sin \beta \quad (6.2)$$

where β is the rotation. Differentiating Equation (6.2) with respect to z yields Equation (6.3)

$$V_o'' = \cos \beta \frac{d\beta}{dz} \quad (6.3)$$

From Equation (6.3)

$$\frac{d\beta}{dz} = \frac{V_o'}{\cos \beta} \quad (6.4)$$

The thermal bowing amplification factor K is given by

$$K = \frac{\alpha \Delta \theta l^2}{8d}$$

where

α is the coefficient of thermal expansion

$\Delta \theta$ is the difference between coldest and hottest flange

l is the length of the element

d is the depth of the section.

The method of deriving the thermal bowing amplification factor is documented in ref [170].

The derivatives of the displacement functions with respect to z are given by

$$\begin{aligned} U' &= U_o' - yV_o'' - \frac{K\pi C_z}{l} \frac{V_o'}{\sqrt{1-(V_o')^2}} - KS_z \frac{V_o''}{(1-(V_o')^2)^{\frac{3}{2}}} \\ V' &= V_o' - y \frac{V_o'V_o''}{\sqrt{1-(V_o')^2}} + \frac{K\pi}{l} C_z \end{aligned} \quad (6.5)$$

where

$$\begin{aligned} S_z &= \sin \frac{\pi z}{l} \\ C_z &= \cos \frac{\pi z}{l} \end{aligned} \quad (6.6)$$

The axial strain is related to the displacements as given below, to second order

$$\epsilon_z = U' + \frac{1}{2} \{(U')^2 + (V')^2\} \quad (6.7)$$

By substituting Equation (6.5) into Equation (6.7) the resulting strain equation is

$$\begin{aligned} \epsilon_z = & U'_o + \frac{1}{2} [(U'_o)^2 + (V'_o)^2] - yV''_o \left[1 + U'_o + \frac{(V'_o)^2}{\sqrt{1 - (V'_o)^2}} \right] \\ & + \frac{1}{2} y^2 (V''_o)^2 \left[1 + \frac{(V'_o)^2}{1 - (V'_o)^2} \right] - \frac{K\pi C_z}{l} \frac{V'_o}{\sqrt{1 - (V'_o)^2}} [1 + U'_o] \\ & - KS_z \frac{V''_o}{(1 - (V'_o)^2)^{\frac{3}{2}}} [1 + U'_o + yV''_o] + \frac{K\pi C_z}{l} V'_o \\ & + \frac{K^2 \pi^2 C_z^2}{2l^2} \left[\frac{(V'_o)^2}{1 - (V'_o)^2} + 1 \right] + \frac{K^2 \pi C_z S_z}{2l} \frac{V'_o V''_o}{(1 - (V'_o)^2)^2} \\ & + \frac{K^2 S_z^2}{2} \frac{(V''_o)^2}{(1 - (V'_o)^2)^3} \end{aligned} \quad (6.8)$$

The strain increment $\delta\epsilon_z$ is

$$\begin{aligned} \delta\epsilon_z = & [1 + U'_o - yV''_o] \delta U'_o + \left[V'_o - 2y \frac{V'_o V''_o}{\sqrt{1 - (V'_o)^2}} \right. \\ & \left. - y \frac{(V'_o)^3 V''_o}{(1 - (V'_o)^2)^{\frac{3}{2}}} + y^2 \frac{V'_o (V''_o)^2}{1 - (V'_o)^2} + y^2 \frac{(V'_o)^3 (V''_o)^2}{(1 - (V'_o)^2)^2} \right] \delta V'_o \\ & + \left[y^2 V''_o - y(1 + U'_o) - y \frac{(V'_o)^2}{\sqrt{1 - (V'_o)^2}} \right] \delta V''_o \\ & - \left[\frac{K\pi C_z}{l} \frac{V'_o}{\sqrt{1 - (V'_o)^2}} + KS_z \frac{V''_o}{(1 - (V'_o)^2)^{\frac{3}{2}}} \right] \delta U'_o \\ & - \left[\frac{K\pi C_z}{l} (1 + U'_o) \left(\frac{1}{\sqrt{1 - (V'_o)^2}} + \frac{(V'_o)^2}{(1 - (V'_o)^2)^{\frac{3}{2}}} \right) \right. \\ & \left. + KS_z (1 + U'_o + yV''_o) \left(\frac{3V'_o V''_o}{(1 - (V'_o)^2)^{\frac{3}{2}}} \right) \right. \\ & \left. - \frac{K^2 \pi^2 C_z^2}{l^2} \left(\frac{V'_o}{1 - (V'_o)^2} + \frac{(V'_o)^3}{(1 - (V'_o)^2)^2} \right) \right] \delta V'_o \end{aligned}$$

$$\begin{aligned}
& - \frac{K^2 \pi C_z S_z}{2l} \left(\frac{V_o''}{(1 - (V_o')^2)^2} + \frac{4(V_o')^2 V_o''}{(1 - (V_o')^2)^3} \right) \\
& - \left[3K^2 S_z^2 \frac{(V_o'')^2 V_o'}{(1 - (V_o')^2)^4} - \frac{K \pi C_z}{l} \right] \delta V_o' \\
& - \left[y K S_z \frac{V_o''}{(1 - (V_o')^2)^{\frac{3}{2}}} + K^2 S_z^2 \frac{V_o''}{(1 - (V_o')^2)^3} \right] \delta V_o''
\end{aligned} \tag{6.9}$$

The displacement function components U_o and V_o are

$$\begin{aligned}
U_o &= [\{\phi\} : \{0\}] \{q\} \\
V_o &= [\{0\} : \{\phi\}] \{q\}
\end{aligned} \tag{6.10}$$

where the displacement parameter vector is

$$\{q\} = \begin{Bmatrix} U_1 \\ \left(\frac{\partial U}{\partial z}\right)_1 \\ U_2 \\ \left(\frac{\partial U}{\partial z}\right)_2 \\ V_1 \\ \Theta_1 \\ V_2 \\ \Theta_2 \end{Bmatrix} \tag{6.11}$$

The shape function polynomials are

$$\{\phi\}^T = \begin{Bmatrix} \frac{1}{4}(\xi + 2)(\xi - 1)^2 \\ \frac{1}{8}(\xi + 1)(\xi - 1)^2 \\ \frac{1}{4}(2 - \xi)(\xi + 1)^2 \\ \frac{1}{8}(\xi - 1)(\xi + 1)^2 \end{Bmatrix} \tag{6.12}$$

where

$$\xi = \frac{z}{l} \tag{6.13}$$

The change in stress, $\Delta\sigma$, is

$$\Delta\sigma = \Delta\epsilon_x - \Delta\epsilon^\theta$$

where

$$\Delta \epsilon^\theta = \alpha \Delta \theta$$

Application of the principle of virtual work results in the following energy equation.

$$\delta W = \int_v \sigma_z \delta \epsilon_z dv - \{Q\}^T \{\delta q\} = 0 \quad (6.14)$$

in which

σ_z is the stress

$\{Q\}^T$ is the external load vector

$\{\delta q\}^T$ is the incremental displacement parameter vector

The energy equation can be rewritten as

$$\psi_i = 0 \quad (6.15)$$

where

$$\psi_i = \int_v \sigma_z \frac{\partial \epsilon_z}{\partial q_i} dv - Q_i \quad (6.16)$$

for $i = 1$ to 4

By substituting the strain increment expression into Equation (6.15), the resulting equation is

$$\left[\int_v \int_A \sigma_z \right] \left([1 + U'_o - yV''_o] \delta U'_o \right) + \left[V'_o - 2y \frac{V'_o V''_o}{\sqrt{1 - (V'_o)^2}} - y \frac{V''_o (V'_o)^3}{(1 - (V'_o)^2)^{\frac{3}{2}}} \right]$$

$$\begin{aligned}
& - y \frac{V'_0 (V''_0)^2}{1 - (V'_0)^2} + y^2 \frac{(V''_0)^2 (V'_0)^3}{(1 - (V'_0)^2)^2} \delta V'_0 \\
& + \left[y^2 V''_0 - y(1 + U'_0) + y^2 \frac{V''_0 (V'_0)^2}{1 - (V'_0)^2} \right. \\
& - y \frac{(V'_0)^2}{\sqrt{1 - (V'_0)^2}} \delta V''_0 - \left[\frac{K \pi C_z}{l} \frac{V'_0}{\sqrt{1 - (V'_0)^2}} \right. \\
& + \left. K S_z \frac{V''_0}{(1 - (V'_0)^2)^{\frac{3}{2}}} \right] \delta U'_0 - \left[\frac{K \pi C_z}{l} (1 + U'_0) \right. \\
& \quad \left. \left(\frac{1}{\sqrt{1 - (V'_0)^2}} + \frac{(V'_0)^2}{(1 - (V'_0)^2)^{\frac{3}{2}}} \right) \right. \\
& + \left. K S_z (1 + U'_0 + y V''_0) \left(\frac{3 V'_0 V''_0}{(1 - (V'_0)^2)^{\frac{3}{2}}} \right) \right. \\
& - \frac{K^2 \pi^2 C_z^2}{l^2} \left(\frac{V'_0}{1 - (V'_0)^2} + \frac{(V'_0)^3}{(1 - (V'_0)^2)^2} \right) \\
& - \frac{K^2 \pi C_z S_z}{2l} \left(\frac{V''_0}{(1 - (V'_0)^2)^2} + \frac{4 (V'_0)^2 V''_0}{(1 - (V'_0)^2)^3} \right) \\
& - \left. 3 K^2 S_z^2 \frac{(V''_0)^2 V'_0}{(1 - (V'_0)^2)^4} - \frac{K \pi}{l} C_z S_z \right] \delta V'_0 \\
& - \left[y K S_z \frac{V''_0}{(1 - (V'_0)^2)^{\frac{3}{2}}} + K S_z (1 + U'_0 + y V''_0) \right. \\
& \quad \left. \left(\frac{V''_0}{(1 - (V'_0)^2)^{\frac{3}{2}}} \right) - \frac{K^2 \pi C_z S_z}{2l} \frac{V'_0}{(1 - (V'_0)^2)^2} \right. \\
& - \left. \left. K^2 S_z^2 \frac{V''_0}{(1 - (V'_0)^2)^3} \right] \delta V''_0 \right] dA \cdot dz \\
& - \{Q\}^T \{\delta q\} = 0
\end{aligned} \tag{6.17}$$

By defining the stress resultants as

$$\begin{aligned}
N &= \int_A \sigma_z dA \\
M &= \int_A \sigma_z y dA \\
M^* &= \int_A \sigma_z y^2 dA
\end{aligned} \tag{6.18}$$

the energy equation can be written as

$$\left[\int_l (A_1 \delta U'_o + A_2 \delta V'_o + A_3 \delta V''_o) dz \right] - \{Q\}^T \{\delta q\} = 0 \quad (6.19)$$

where

$$A_1 = N(1 + U'_o) - M V''_o - N \left[\frac{K \pi C_z}{l} \frac{V'_o}{\sqrt{1 - (V'_o)^2}} + K S_z \frac{V''_o}{(1 - (V'_o)^2)^{\frac{3}{2}}} \right] \quad (6.20)$$

$$\begin{aligned} A_2 = & N V'_o - M \frac{V'_o V''_o}{\sqrt{1 - (V'_o)^2}} \left[2 + \frac{(V'_o)^2}{1 - (V'_o)^2} \right] \\ & + M^* \frac{V'_o (V''_o)^2}{1 - (V'_o)^2} \left[1 + \frac{(V'_o)^2}{1 - (V'_o)^2} \right] \\ & + N \left[3 K S_z (1 + U'_o) \frac{V'_o V''_o}{(1 - (V'_o)^2)^{\frac{3}{2}}} \right. \\ & - \frac{K \pi C_z}{l} (1 + U'_o) \left(\frac{1}{\sqrt{1 - (V'_o)^2}} + \frac{V'_o}{(1 - (V'_o)^2)^{\frac{3}{2}}} \right) \\ & - \frac{K^2 \pi^2 C_z^2}{l^2} \left(\frac{V'_o}{1 - (V'_o)^2} + \frac{(V'_o)^3}{(1 - (V'_o)^2)^2} \right) \\ & \left. - 3 K^2 S_z^2 \frac{(V''_o)^2 V'_o}{(1 - (V'_o)^2)^4} - \frac{K \pi C_z}{l} \right] + 3 M K S_z \frac{V'_o (V''_o)^2}{(1 - (V'_o)^2)^{\frac{3}{2}}} \end{aligned} \quad (6.21)$$

$$\begin{aligned} A_3 = & -M \left[1 + U'_o + \frac{(V'_o)^2}{\sqrt{1 - (V'_o)^2}} \right] \\ & + M^* V'_o \left[1 + \frac{(V'_o)^2}{1 - (V'_o)^2} \right] + N \left[\frac{K^2 \pi C_z S_z}{2l} \frac{V'_o}{(1 - (V'_o)^2)^2} \right. \\ & \left. + K^2 S_z^2 \frac{V''_o}{(1 - (V'_o)^2)^3} - K S_z (1 + U'_o) \frac{V''_o}{(1 - (V'_o)^2)^{\frac{3}{2}}} \right] \\ & - M \left[K S_z \frac{V''_o}{(1 - (V'_o)^2)^{\frac{3}{2}}} + K S_z \frac{(V''_o)^2}{(1 - (V'_o)^2)^{\frac{3}{2}}} \right] \end{aligned} \quad (6.22)$$

From Equation (6.16) the expression for ψ_i can be deduced as follows

$$\psi_i = \int_l \left[A_1 \frac{\partial U'_o}{\partial q_i} + A_2 \frac{\partial V'_o}{\partial q_i} + A_3 \frac{\partial V''_o}{\partial q_i} \right] dz - Q_i = 0 \quad (6.23)$$

in which i has a range of 1 to n (i.e $n = 4$). If Equations (6.23) are not satisfied, corrections to the q_i may be obtained by the Newton-Raphson iteration method as follows;

$$\Delta\psi_i = \frac{\partial\psi_i}{\partial q_j} \Delta q_j = -\psi_i \quad (6.24)$$

in which a repeated suffix summation convention is used and j also has a range of 1 to n . By substituting the expression for ψ_i into Equation (6.24), the resulting equation is

$$\begin{aligned} & \left[\int_l \left[\frac{\partial A_1}{\partial q_j} \frac{\partial U'_o}{\partial q_i} + \frac{\partial A_2}{\partial q_j} \frac{\partial V'_o}{\partial q_i} + \frac{\partial A_3}{\partial q_j} \frac{\partial V''_o}{\partial q_i} \right] dz \right] \Delta q_j \\ & = Q_i - \int_l \left[A_1 \frac{\partial U'_o}{\partial q_i} + A_2 \frac{\partial V'_o}{\partial q_i} + A_3 \frac{\partial V''_o}{\partial q_i} \right] dz \end{aligned} \quad (6.25)$$

Equation (6.25) is the basic Newton-Raphson equation which leads to the extraction of the tangent stiffness $[K_T]$ and the out-of-balance load vector $\{\Delta Q\}$. Thus Equation (6.25) can be written as

$$[K_T] \{\Delta q\} = \{\Delta Q\} \quad (6.26)$$

in which

$$K_{T,i,j} = \int_l \left[\frac{\partial A_1}{\partial q_j} \frac{\partial U'_o}{\partial q_i} + \frac{\partial A_2}{\partial q_j} \frac{\partial V'_o}{\partial q_i} + \frac{\partial A_3}{\partial q_j} \frac{\partial V''_o}{\partial q_i} \right] dz \quad (6.27)$$

and the unbalanced load vector ΔQ_i is given by

$$\Delta Q_i = Q_i - \int_l \left[A_1 \frac{\partial U'_o}{\partial q_i} + A_2 \frac{\partial V'_o}{\partial q_i} + A_3 \frac{\partial V''_o}{\partial q_i} \right] dz \quad (6.28)$$

The incremental equilibrium equation for an element is given by Equation (6.26). The element stiffness matrix for any given temperature profile can be evaluated with respect to nodal displacements within the framework of the cartesian coordinate system shown in Fig. 6.2 . The global nodal displacements for the structure are given by

$$\{q\}_G = [T]^{-1} \{q\} \quad (6.29)$$

and the transformation matrix $[T]$ is given by

$$[T] = \begin{bmatrix} C & S & 0 & 0 & 0 & 0 & 0 & 0 & 0 & 0 \\ 0 & 0 & 0 & C^2 & S^2 & 0 & 0 & 0 & 0 & 0 \\ 0 & 0 & 0 & 0 & 0 & C & S & 0 & 0 & 0 \\ 0 & 0 & 0 & 0 & 0 & 0 & 0 & 0 & C^2 & S^2 \\ S & -C & 0 & 0 & 0 & 0 & 0 & 0 & 0 & 0 \\ 0 & 0 & -1 & CS & -CS & 0 & 0 & 0 & 0 & 0 \\ 0 & 0 & 0 & 0 & 0 & S & -C & 0 & 0 & 0 \\ 0 & 0 & 0 & 0 & 0 & 0 & 0 & -1 & CS & -CS \end{bmatrix} \quad (6.30)$$

where

$$\begin{aligned} C &= \cos \gamma \\ S &= \sin \gamma \end{aligned} \quad (6.31)$$

and γ is the orientation of cartesian coordinate system relative to the global reference axes. The derivation of the transformation matrix is documented by Zanaty et al [169]. The global displacement vector is given by

$$\{q^I\}_G^T = \left\{ U^I \quad V^I \quad \Theta^I \quad \left(\frac{\partial U}{\partial Z}\right)^I \quad \left(\frac{\partial V}{\partial Y}\right)^I \right\} \quad (6.32)$$

where the superscript I denotes the node I .

The transformed incremental equations can be expressed as

$$[K_T]_G \{\Delta q_e\}_G = \{\Delta R_e\}_G \quad (6.33)$$

where

$[K_T]_G$ is the transformed stiffness matrix for an element

$\{\Delta q_e\}_G$ is the transformed incremental displacement vector for an element

$\{\Delta R_e\}_G$ is the transformed unbalanced force vector for an element.

Assembly of the element stiffness matrix leads to a structural tangential stiffness matrix, and the structural incremental equilibrium equation is obtained as follows:

$$[K_T] \{\Delta r\} = \{\Delta R\} \quad (6.34)$$

in which

$[K_T]$ is the structural tangent stiffness matrix

$\{\Delta r\}$ is the assembled vector of incremental nodal displacements

$\{\Delta R\}$ is the assembled vector of incremental nodal forces called out-of-balance forces.

The load-deformation characteristics of the structure can be traced at any specified temperature profile by solving Equation (6.34) for the incremental nodal displacements, which are added to the total nodal displacements to ensure equilibrium.

6.1.1 Evaluation Of Tangential Stiffness $(K_T)_{ij}$

The tangential stiffness is given by

$$(K_T)_{ij} = \int_l \left(e_{1j} \frac{\partial U'_o}{\partial q_i} + e_{2j} \frac{\partial V'_o}{\partial q_i} + e_{3j} \frac{\partial V''_o}{\partial q_i} \right) dz \quad (6.35)$$

in which

$$\begin{aligned} e_{1j} &= \frac{\partial A_1}{\partial q_j} \\ e_{2j} &= \frac{\partial A_2}{\partial q_j} \\ e_{3j} &= \frac{\partial A_3}{\partial q_j} \end{aligned} \quad (6.36)$$

The expressions for e_{1j} , e_{2j} and e_{3j} are given in appendix B.

To evaluate the stiffness coefficients $(K_T)_{ij}$ and the incremental unbalanced forces ΔQ_i , the stress resultants N, M and M^* with their derivatives $\frac{\partial N}{\partial q_j}$, $\frac{\partial M}{\partial q_j}$ and $\frac{\partial M^*}{\partial q_j}$ must be evaluated first.

For inelastic behaviour the stress resultants are evaluated when the strain distribution is known and the stress-strain-temperature relation is defined. The stress resultants may then be calculated numerically in the x-y reference plane. To accomplish this the plate is divided into 5 regions and the summation of the stress resultants over the plate length is effected as reported by Zanaty et al[169]. This leads to the following equations;

$$N = \int_A \sigma_x dA$$

$$= \sum_{k=1}^n \sum_{r=1}^5 \frac{1}{2} l_r t_k (\sigma_{ir} + \sigma_{jr}) \quad (6.37)$$

$$\begin{aligned} M &= \int_A \sigma_x y dA \\ &= \sum_{k=1}^n \sum_{r=1}^5 \frac{l_r t_k}{6} [\sigma_{ir} (y_{jr} + 2y_{ir}) + \sigma_{jr} (y_{ir} + 2y_{jr})] \end{aligned} \quad (6.38)$$

$$\begin{aligned} M^* &= \int_A \sigma_x y^2 dA \\ &= \sum_{k=1}^n \sum_{r=1}^5 \frac{l_r t_k}{12} [\sigma_{ir} (4y_{ir}^2 + 2y_{jr}^2 - l_r^2) \\ &\quad + \sigma_{jr} (4y_{jr}^2 + 2y_{ir}^2 - l_r^2)] \end{aligned} \quad (6.39)$$

in which

r is the plate region

n is the number of the plate segments

k is the plate segment index

t_k is the plate segment thickness

l_r is the plate region length

i and j refer to the two ends of each region.

Full details of this approach can be found in Zanaty et al[169].

The evaluation of cross-section properties is based on the transformed area approach which allows for nonlinearity in the material properties. The method of evaluation of transformed area of the cross section is extensively covered in Zanaty et al [169] but for completeness a brief review of the method is presented herein.

If each element area is transformed such that the product of the current tangent modulus at any temperature, $E_t(\theta)$, times the element area A , is equal to the original effective modulus, E_θ , and the element of transformed area, A^t , then

$$E_t(\theta)A = E_\theta A^t \quad (6.40)$$

and also

$$b_r^t = \frac{E_t(\theta)b_r}{E_\theta} \quad (6.41)$$

in which b_r^t is the transformed thickness of a particular region r and b_r is the original thickness of this region. The tangent modulus is obtained from the stress-strain-temperature relation. This is given by the following equation:

$$\begin{aligned} E_t(\theta) &= \frac{1}{\frac{d\epsilon}{d\sigma}} \\ \frac{d\epsilon}{d\sigma} &= \frac{1}{E_\theta} + 0.01n_\theta \left(\frac{1}{E_\theta}\right) \left(\frac{\sigma}{\sigma_{y\theta}}\right)^{(n_\theta-1)} \end{aligned} \quad (6.42)$$

The value of E_θ is obtained from the reduction equations given in the previous finite strip development (Equations (3.48) to (3.62)). Thus the section is transformed and the cross-section properties are evaluated as given below;

$$\begin{aligned} A^t &= \int_{A^t} dA^t \\ &= \sum_{k=1}^n A_k \\ I_1^t &= \int_{A^t} y dA^t \\ &= \sum_{k=1}^n A_k Y_k \\ I_2^t &= \int_{A^t} y^2 dA^t \\ &= \sum_{k=1}^n (I_{xx})_k + \sum_{k=1}^n A_k Y_k^2 \\ I_3^t &= \int_{A^t} y^3 dA^t \\ &= 3 \sum_{k=1}^n (I_{xx})_k Y_k + \sum_{k=1}^n A_k Y_k^3 \end{aligned}$$

$$\begin{aligned}
I_4^t &= \int_{A^t} y^4 dA^t \\
&= \sum_{k=1}^n (I_{4xx})_k Y_k^2 + \sum_{k=1}^n A_k Y_k^4
\end{aligned} \tag{6.43}$$

in which $(I_{xx})_k$ is the moment of inertia of the segment k about the centroidal axis x-x of the segment and $(I_{4xx})_k$ is defined as

$$I_{4xx} = \int_A y^4 dA \tag{6.44}$$

6.1.2 Evaluation of the incremental stress resultant vector for the inelastic element

The incremental stress resultants $\frac{\partial N}{\partial q_j}$, $\frac{\partial M}{\partial q_j}$ and $\frac{\partial M^*}{\partial q_j}$ are evaluated by considering the variation in the stress resultants N , M and M^* at any stage of loading for a given temperature profile:

$$\begin{aligned}
\delta N &= \int_A E_t(\theta) \delta \epsilon dA \\
\delta M &= \int_A E_t(\theta) \delta \epsilon y dA \\
\delta M^* &= \int_A E_t(\theta) \delta \epsilon y^2 dA
\end{aligned} \tag{6.45}$$

where $E_t(\theta)$ is the tangent modulus at elevated temperature. The elemental area dA is given by

$$dA = \frac{E_\theta dA^t}{E_t(\theta)} \tag{6.46}$$

Thus the transformed section properties are completely defined. The substitution of these properties together with the strain increment into Equation

(6.48) followed by differentiation with respect to q_j results in the following stress resultants upon integration of Equation (6.48).

$$\begin{aligned}
 \frac{\partial N}{\partial q_j} &= E_\theta A^t b_{1j} - E_\theta I_1^t b_{2j} + E_\theta I_2^t b_{3j} \\
 \frac{\partial M}{\partial q_j} &= E_\theta I_1^t b_{1j} - E_\theta I_2^t b_{2j} + E_\theta I_3^t b_{3j} \\
 \frac{\partial M^*}{\partial q_j} &= E_\theta I_2^t b_{1j} - E_\theta I_3^t b_{2j} + E_\theta I_4^t b_{3j}
 \end{aligned} \tag{6.47}$$

expressions for b_{1j} , b_{2j} and b_{3j} are given in appendix B.

The evaluation of the stress resultants is achieved by using a continuous stress-strain-temperature relationship of a Ramberg-Osgood type as used in Chapter 3. For elevated temperature, a set of stress-strain curves, Equations (3.48) to (3.62), are substituted to replace the ambient temperature stress-strain relationship. For any defined temperature profile the stiffness matrix, stress resultant and their derivatives are evaluated. The load-deformation characteristics of the structure can be traced at any defined temperature profile by solving the Newton-Raphson equations. The accuracy of the present development is established in the following section.

6.2 Validation Of The Finite Element Method

The finite element program INSTAF has been modified as described in the previous section to incorporate continuous stress-strain relationships at both ambient and elevated temperatures. In order to establish the adequacy of the method comparison was made with the finite strip method developed in Chapter 3 together with appropriate test data on steel columns. These data

include thermal gradient tests reported in the literature although it should be appreciated that this evidence is limited.

First, a $152 \times 152 \times 23$ UC column was analysed using the methods at ambient temperature for a range of slenderness ratios. The finite strip analysis is based on an initially perfect column without inclusion of structural imperfections while the finite element calculation is carried out with a small initial imperfection of magnitude $l/10000$. The need to prescribe a small initial imperfection arises from the inability of finite element method to handle perfect members. The results from the two calculations are shown in Fig. 6.4. It can be seen that the two theories are in close agreement.

Second, some fire tests on steel columns were simulated using the two methods. Both Olesen's[136] and Vandamme and Janss's[132] test data were used. From experimental details these tests can be classified as uniform temperature fire tests. The finite element analysis is carried out with a small initial imperfection of the magnitude stated above. As shown in Fig. 6.5 the two theories agree with each other significantly. It has been shown earlier that the finite strip approach is in close agreement with the test data. On this basis the good correlation between the two signifies the accuracy of the finite element approach. Furthermore, the finite element method is compared with both test data as shown in Fig. 6.6(a & b). In both cases the theory and experiment are in good agreement with minimal scatter. Based on these comparisons the method has been proved accurate for the analysis of uniformly heated columns.

Cooke[170] carried out fire tests on model steel columns fabricated by milling to size hot rolled mild steel bars. The columns were pin ended and are 1360mm

long. The variation in the member cross-sections provides a range of slenderness ratios to be tested. The actual yield stress and elastic modulus at ambient temperature were measured prior to testing. The fabrication processes were carefully controlled to ensure a minimum level of residual stress in the specimens. The applied load on each column was calculated according to BS449[167]. Heating of the member was accomplished by attaching the electric heating element to one flange. This resulted in a non-uniform temperature distribution across the cross-section. Temperature over the cross-section and both horizontal and vertical displacements were measured at various times into the tests. For comparison purposes, the finite element analysis was based on an initially deflected column. This is of the order of $l/1000$, and is assumed to vary with a half sine wavelength along the member. The temperature-deformation history is plotted in Fig. 6.7, which shows good agreement between theory and experiment.

British Steel Corporation[171] carried out fire tests on steel columns built into a fire resistant wall to assess the effect of such partial protection on steel column behaviour. The columns used in these tests were $203 \times 203 \times 52$ UC's. The actual yield stress of the specimens was measured at ambient temperature, but no information was provided on initial out-of-straightness. The end conditions were not known and but the base details indicate a support condition close to full restraint. For comparison purposes the finite element calculations are undertaken by admitting a fully fixed-ended condition. As shown in Fig. 6.8 the temperature-deformation plot shows considerable agreement between theory and experiment.

From the above validation this approach can be expected to provide a reliable basis to analyse steel columns under fire conditions. The influence of thermal gradient across the member cross-section is investigated as reported in the next chapter.

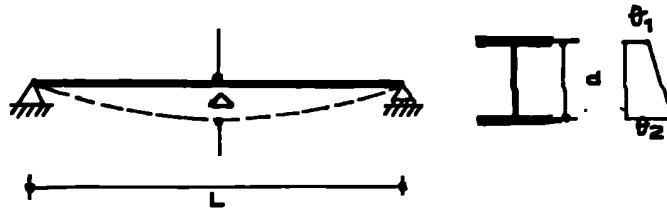


FIG. 6.1 THERMAL BOWING DEFLECTION FOR SIMPLY SUPPORTED BEAM

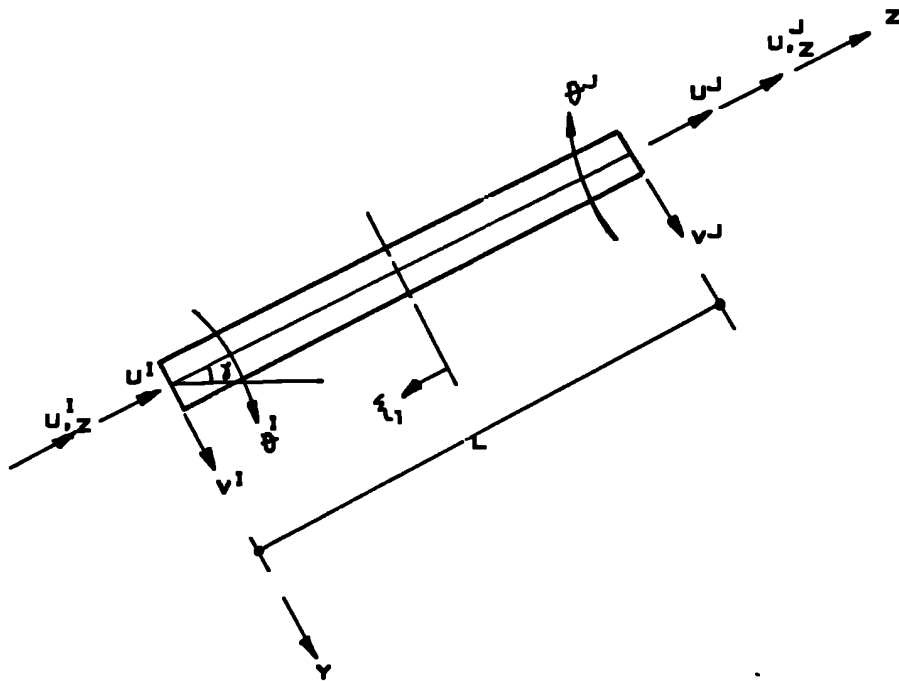


FIG. 6.2 LOCAL NODAL DISPLACEMENT SYSTEM

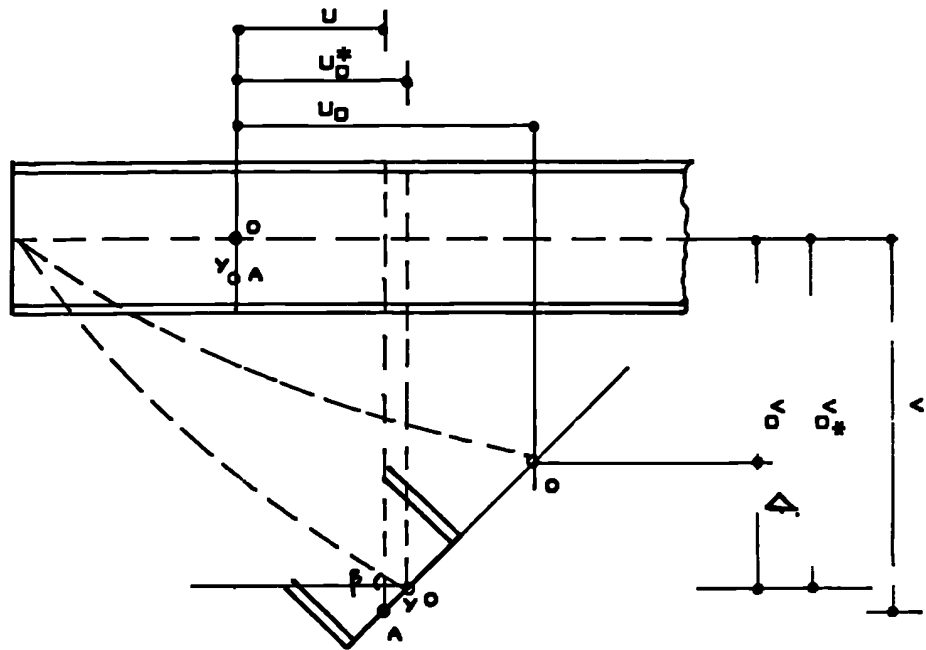


FIG. 6.- DISPLACEMENT CONFIGURATION OF THE FINITE ELEMENT MODEL WITH THERMAL BOWING SUPERIMPOSED

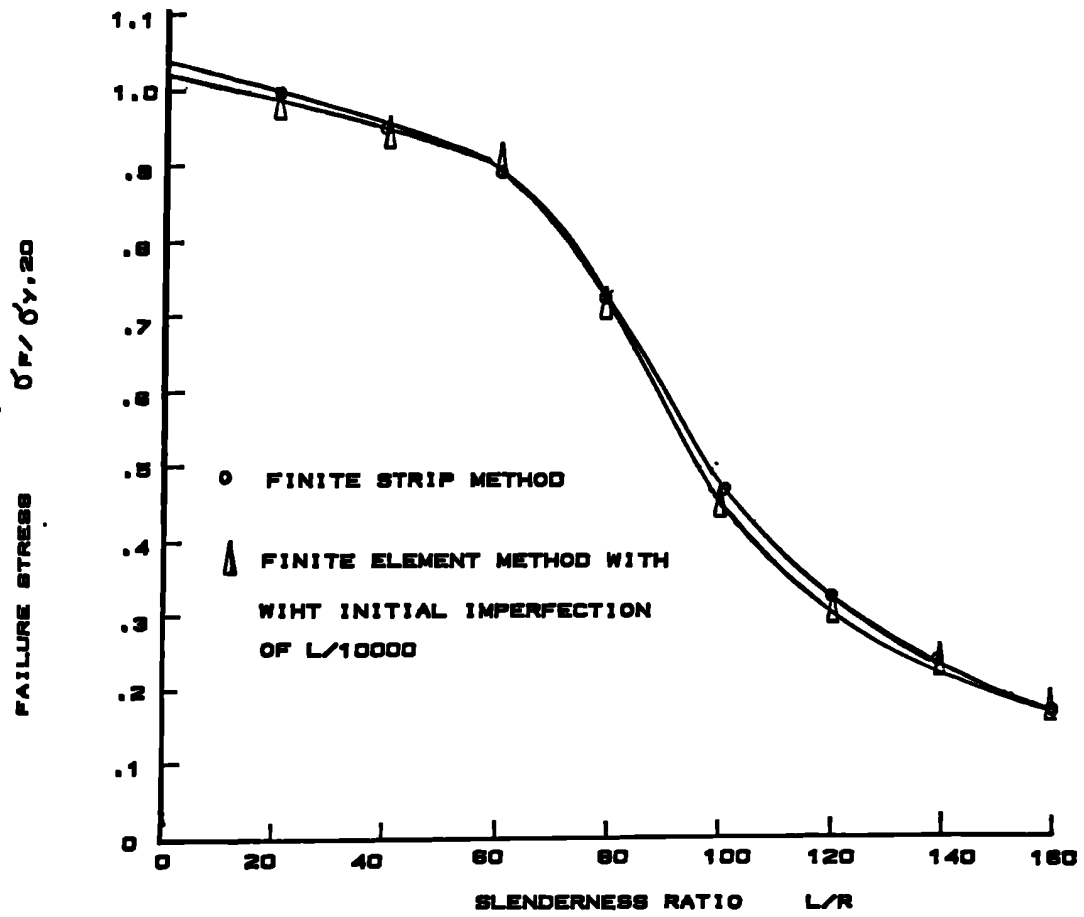


FIG. 6.4 COMPARISON BETWEEN FINITE STRIP AND FINITE ELEMENT METHODS AT AMBIENT TEMPERATURE

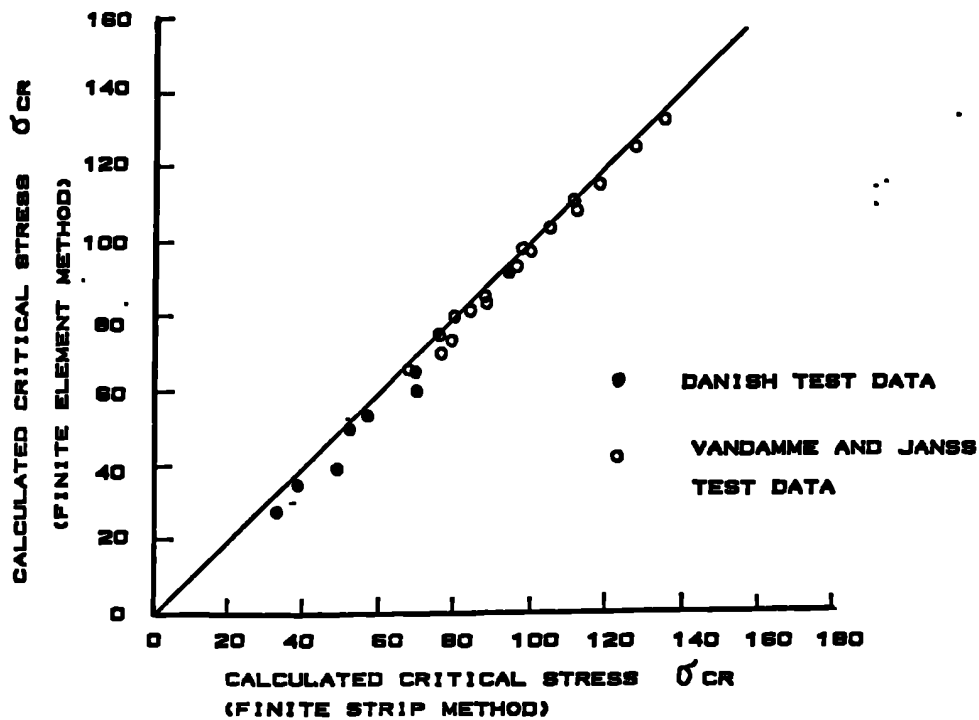


FIG. 6.5 COMPARISON BETWEEN FINITE STRIP AND FINITE ELMENT METHODS AT ELEVATED TEMPERATURE

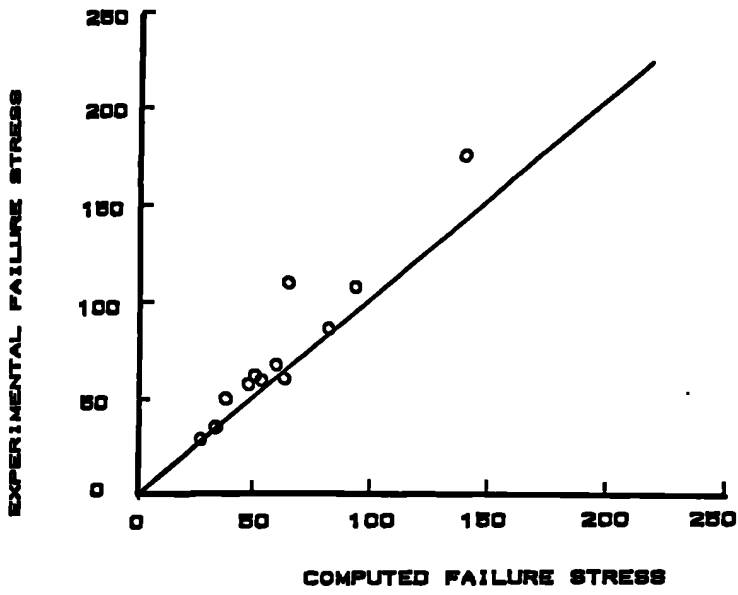


FIG. 8.8(A) COMPARISON OF FEM WITH DANISH TEST RESULTS

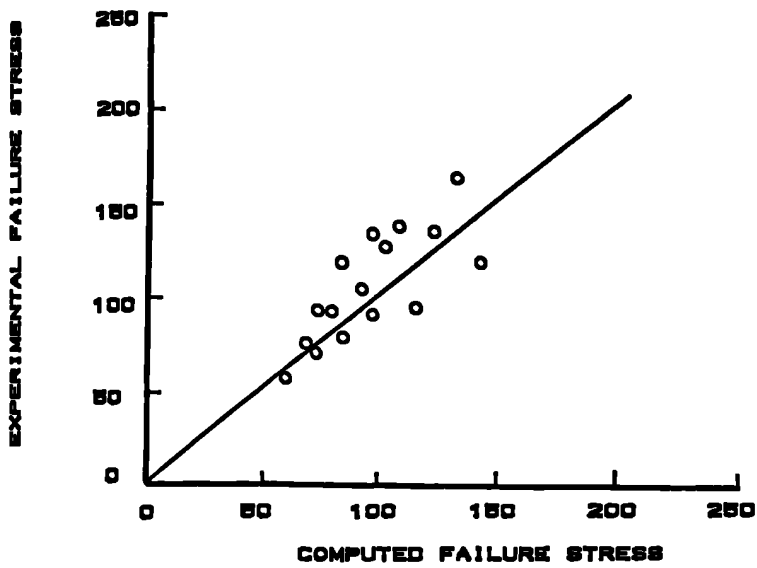


FIG. 8.8(B) COMPARISON OF FEM WITH BELGIAN TEST RESULTS

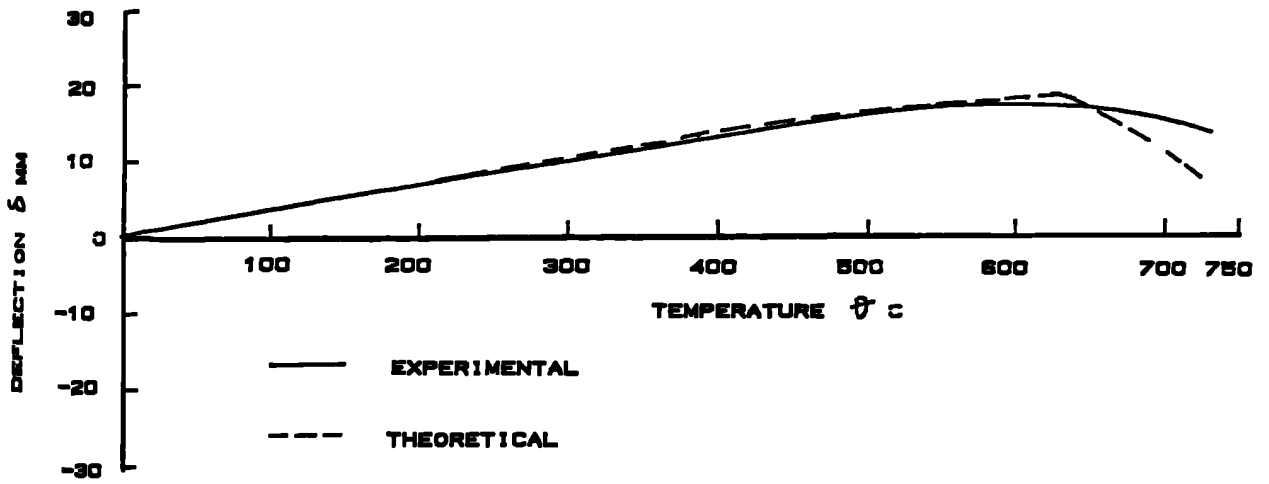


FIG. 8.7 COMPARISON OF THE TEMPERATURE-DEFLECTION CHARACTERISTICS OF FINITE ELEMENT WITH TEST 3 OF FIRE RESEARCH STATION

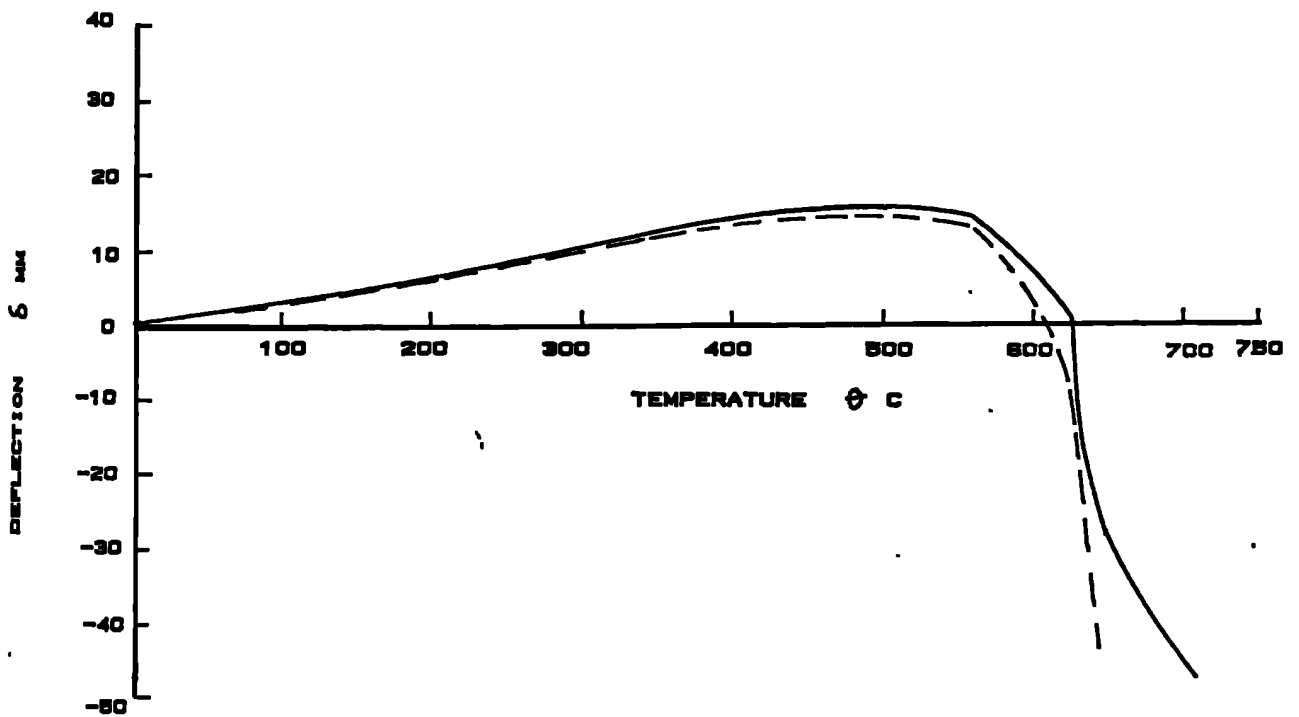


FIG. 8.8 COMPARISON OF THE TEMPERATURE-DEFLECTION CHARACTERISTICS OF FINITE ELEMENT WITH BRITISH STEEL TEST SH/RS/3664/3/83/B

Chapter 7

PARAMETRIC STUDIES

The finite element method described in Chapter 6 has been used to study the influence of various parameters on the behaviour of columns in fire. The parameters considered are the initial out-of-straightness, thermal gradient, different end conditions and eccentricity of loading which until now have received only very limited attention in the context of column behaviour in fire.

The occurrence of thermal gradient is common in building fires. This may be as a result of partial protection of steel columns or, in case of an external column, being exposed to fire from one side only. The early bowing towards the heat source is caused by differential heating across the cross-section. It is possible to assess the interaction of this phenomenon with the variation of material properties that arises from the non-uniform temperature distribution across the cross-section.

Furthermore, a simple column model based on Shanley's theory was developed

to demonstrate the influence of interaction of thermal gradient with eccentricity of loading on the behaviour of columns in fire.

7.1 Effect of initial out-of-straightness

In practice no perfectly straight members exist and there is some measure of initial out-of-straightness associated with any structural member. The initial out-of-straightness can be local when component plates are initially deformed or overall in case of a member bowing longitudinally, and the combination of both. This may cause some loss of stiffness prior to loading. For uniformly heated columns the presence of initial out-of-straightness may result in early buckling. No experimental work has been reported in which the influence of this imperfection on column behaviour has been properly assessed.

The effect of initial out-of-straightness on columns in fire is studied by analysing an H-section over a range of slenderness ratios at various levels of initial out-of-straightness ($l/10000$ $l/1000$ $l/500$ $l/250$). The deflected shape for this study was assumed to be a half sine wave over the length of the member. This is achieved with the program by entering the values of the initial deflections at the nodes. For this study only uniform temperature distribution throughout the member is considered.

In Fig. 7.1(a to e) the failure stress-temperature relationship at various levels of initial out-of-straightness is plotted for a stocky column with a slenderness ratio of 20. The failure stress is non-dimensionalised with respect to ambient

temperature yield strength. It is clear from Fig. 7.1a that the influence of this imperfection is not significant on stocky columns. The reduction in failure stress is very low within the temperature range of $20^{\circ}\text{C} \leq \theta \leq 400^{\circ}\text{C}$. With further increase in temperature the failure stress decreases rapidly at all levels of the initial out of straightness. Generally the failure stress decreases with increasing level of initial out-of-straightness.

As slenderness ratio increases the influence of the initial out-of-straightness increases. In Fig. 7.1b the intermediate column, $l/r = 60$, shows a significant response to the presence of initial out-of-straightness at relatively low temperature ($\theta \leq 400^{\circ}\text{C}$). However as the temperature increases further the influence of this imperfection diminishes. For example at ambient temperature the difference between the column capacity at zero and $l/1000$ out-of-straightness levels is about 13% while at 500°C this decreases to about 8%.

From Fig. 7.1c to 7.1e it is clear that the response of slender columns, $l/r \geq 100$, does not differ significantly from that of the intermediate columns. It is noted that columns with a slenderness ratio of 100(Fig. 7.1c) show the greatest response to the presence of initial out-of-straightness. As the slenderness ratio increases beyond 100 initial out-of-straightness has a diminishing effect as shown in Fig. 7.1d and 7.1e. Thus both the stocky and very slender columns do not respond significantly to the presence of initial out-of-straightness.

Fig. 7.2a to 7.2d shows plot of a failure stress non-dimensionalised with respect to the ambient temperature failure stress against temperature for a range of slenderness ratios and initial imperfections. It is evident that these curves be-

come tightly grouped as the level of initial out-of-straightness increases. Thus the range of critical temperature corresponding to the point where failure stress reduces to, say, 60% of the ambient temperature bearing capacity decreases with increasing level of initial out-of-straightness. The critical temperature-slenderness ratio relationship is plotted in Fig. 7.3. It is noted that the behaviour of both the stocky columns, $l/r \leq 40$, and slender columns, $l/r \geq 125$, is not influenced significantly by the presence of initial out-of-straightness. These columns exhibit a very short range of critical temperature variation with initial out-of-straightness. For example a stocky column, $l/r = 20$, has a critical temperature varying between 530°C under perfect conditions and 500°C at maximum level of initial out-of-straightness. It is apparent that columns with slenderness ratios of 40 and 130 show no response to the presence of initial out-of-straightness in terms of critical temperatures. For intermediate slenderness ratios, $40 < l/r < 125$, the critical temperature increases with the level of initial out-of-straightness. For example a column with slenderness ratio of 80 exhibits an increase of about 113°C at maximum level of initial out-of-straightness compared with the perfect condition.

It is clear that initial out-of-straightness has variable influence on different columns depending on their slenderness ratio. In term of critical temperature, it is evident that both stocky and slender columns are detrimentally influenced by this imperfection but only marginally while the remaining columns show an improved performance with increasing level of initial out-of-straightness, when comparing high temperature with ambient temperature performance.

7.2 Effect of different end conditions

In practice columns are rarely pin-ended but are connected to other components of the structure by a variety of connection types. Although the basic pin-ended column has traditionally been used as a reference point on which real columns are designed the influence of different end restraint is significant and the increase in strength associated with rigid supports is well established. The concept of effective length is often used to model this influence. This length decreases as the degree of end restraint provided increases, allowing the member to buckle at a load higher than the pin-ended condition.

In this study only two types of end restraint are considered, namely hinged and fully fixed end conditions. A $203 \times 203 \times 52$ UC section was analysed under uniform temperature distribution over a range of slenderness ratios. The ambient temperature yield strength and modulus of elasticity are assumed to be 250N/mm^2 and 205kN/mm^2 respectively.

In Fig. 7.4 the curves show the failure stress-slenderness ratio relationships. The failure stress is non-dimensionalised with respect to ambient temperature yield strength. It is clear that at ambient temperature a significant difference exists between the column response for the two different end conditions when the slenderness ratio is greater than 80. For stockier columns, $l/r \leq 80$ there is no response to the variation in the end restraints at ambient temperature. This is not the case as temperature rises. Between 200°C and 600°C full fixity at the ends results in higher failure stress for the whole range of slenderness ratios considered. For example at 600°C for a column with slenderness ratio

of 80 there is about 20% difference in its response. However this difference in column response as a result of different end conditions decreases as temperature increases beyond 600°C. For example at 700°C the two end conditions result in almost the same column curves.

The same information is replotted in Fig. 7.5 as non-dimensionalised failure stress-temperature relationships for different slenderness ratios. It is apparent that at relatively low temperature, $\theta \leq 300^\circ\text{C}$, the stocky and intermediate columns, $l/r \leq 60$, are not significantly influenced by the variation in the end conditions. Between 300°C and 500°C there is a noticeable difference in the column behaviour under the two end conditions, with the fully fixed end condition resulting in a higher failure stress. For example, at 400°C for an intermediate column, $l/r = 60$, the difference in its response is about 17%. This difference increases with slenderness ratio.

Fig. 7.6 shows the relationship between non-dimensionalised failure stress with respect to ambient temperature failure stress and temperature for the fixed-end condition. Similar curves for the pinned-end condition are plotted in Fig. 7.2a. In the region where the failure stress reduces to, say, 60% of the ambient temperature failure stress the corresponding critical temperature shows a wide range under both conditions.

This variation becomes clearer with the plot of the critical temperature-slenderness ratio relationship shown in Fig. 7.7. It is apparent that the fixed-end condition improves the performance of columns with slenderness ratios of $20 < l/r < 100$ while for more slender columns, $l/r > 100$, there is a significant reduction in the critical temperature compared with the pinned-end condition. For a col-

umn with slenderness ratio of $l/r = 100$ the two end conditions result in identical critical temperature. The same is true for stocky columns, $l/r = 20$. It is clear that both stocky and intermediate columns show an improvement in their performance when fully fixed at both ends while very slender columns, $l/r > 100$, show an improved performance under the pinned-end condition in term of critical temperature.

It can be concluded that the influence of end conditions depends on the slenderness ratio of the columns and in a fire resistance test the the influence of end conditions must be carefully assessed. It is clear that different columns respond differently to end condition variation.

7.3 Effect of thermal gradient

In order to investigate the effect of thermal bowing on steel columns a $203 \times 203 \times 52$ UC section was analysed over a range of slenderness ratios. Different temperature distribution patterns were assumed.

In Fig. 7.8 the curves show the plot of non-dimensionalised failure stress with respect to the ambient temperature yield strength against the ratio of the minimum to maximum temperature. The distribution was assumed in such a way that maximum temperature is fixed and the minimum temperature is increased gradually to ensure a linearly decreasing thermal gradient across the cross-section. It is noted that the effect of thermal gradient is not significant with this type of temperature distribution although there is slight improvement

in the behaviour of columns as thermal gradient increases.

The curves presented in Fig. 7.9 show the failure stress-slenderness ratio relationship. It is shown that thermal gradient enhances the performance of columns generally. The reason for this may be connected with the variation in the material properties throughout the member which compensates for the induced bowing that arises from thermal gradient. Furthermore, the shift in the neutral axis of the section towards the coldest flanges induces a bending moment as a result of the eccentricity of loading that arises. This moment counteracts the applied load to such an extent that the columns appear to sustain applied load longer.

In Fig. 7.10 the results of the calculations using linear temperature distributions with three thermal gradients considered ($0, -1, -1.52^\circ\text{C}/\text{mm}$) are presented. The failure stress-centre line temperature relationship is plotted for various thermal gradients. This is to examine the possibility of thermal gradient having a detrimental influence on column behaviour in fire. However, for this case of temperature distribution the thermal gradient is shown to be detrimental to the performance of columns in fire. It should be born in mind that the calculations for the zero thermal gradient is based on the centre line temperature which was assumed to be uniformly distributed throughout the member. This observation agrees with Culver et al[147] who concluded that thermal gradient is detrimental to the behaviour of steel columns in fire. The reverse of this behaviour may be experienced when maximum temperature is used as the parameter for comparison with uniform temperature. This is demonstrated in Fig. 7.11 in which stepwise temperature distribution is as-

sumed across the cross-section. It is interesting to note that thermal gradient tends to improve the performance of columns in fire. It becomes apparent that the influence of thermal gradient depends very much on the temperature profile across the cross-section. The variation of strength over the cross-section overshadows the detrimental effect of thermal bowing to the extent that columns tend to sustain applied load longer compared to uniform temperature condition. It is very difficult to assess the influence of this phenomenon properly because of the interaction of the variation of strength with the thermal bowing. The cutoff line of the influence of thermal bowing cannot be defined and thus the influence of thermal bowing on its own on the behaviour of columns in fire remains a subject for further studies. From all indications thermal bowing on its own will not considerably influence the behaviour of steel columns in fire. Its effect can be equated to that of initial out-of-straightness which depends very much on the slenderness ratio of the column.

7.4 Effect of eccentricity of loading with thermal gradient

The interaction of thermal gradient with applied eccentricity of loading is investigated in this section. Thermal gradient causes induced eccentricity as a result of the shift in neutral axis towards the cold flange. This, coupled with applied eccentricity of loading may have some significant effect on the behaviour of a column in fire. Thus the point of application of the applied eccentricity influences its effect on the response of the columns. For a uniform

temperature distribution the possibility of a shift in the neutral axis does not occur. and thus the likelihood of induced eccentricity is less significant. For the purpose of this study temperature distributions measured by the British Steel Corporation(SH/RS/3664/6/84/B) test on $203 \times 203 \times 52$ UC columns are used in the calculations. These temperatures are shown in Fig. 7.12.

Fig. 7.12 shows the response of two columns, one with an intermediate slenderness ratio, $l/r_x = 60$, and a slender column, $l/r_x = 120$. The temperature profile designated as T_3 was used in the calculation. The load-eccentricity, $e = \alpha b_w/2$, relationship is plotted.

For the intermediate column, $l/r = 60$, the maximum load capacity occurs at an eccentricity of about -72mm away from the centre line of the strong axis. As the hottest flange softens the neutral axis shifts towards the coldest flange. The point of maximum load capacity may correspond to the location where the point of the applied eccentricity coincides with the shifted neutral axis.

For a more slender column, $l/r = 120$, the maximum load capacity occurs at an eccentricity of about -54mm away from the centre line of the strong axis. This shows a decreasing influence of applied eccentricity of loading with increasing slenderness ratio. This may be as a result of more induced thermal bowing which is directly proportional to the member length.

In Fig. 7.13 the load-eccentricity characteristics of the same intermediate column, $l/r = 60$, is plotted at increasing thermal gradient. It is interesting to note that the eccentricity of the point of occurrence of maximum load capacity increases with thermal gradient. This shows that the increasing induced

eccentricity results in more counteracting induced moment which enables the column to sustain applied load longer than usual.

It is clear that eccentricity of loading can either deteriorate or improve the columns' performance depending on the level of thermal gradient and the amount of eccentricity. If this point coincides with the shifted neutral axis then an improvement in the performance of a column in fire may be achieved.

7.5 The Shanley column model

The thermal gradient effect can be demonstrated using the simple Shanley column model. This model was originally used to demonstrate the fact that inelastic buckling will begin as soon as the tangent-modulus load is exceeded (the lower bound of the column buckling load) and that the maximum column load will be reached somewhere between the loads predicted by the tangent modulus and reduced modulus theories respectively. The reduced modulus load corresponds to the upper bound of the column buckling load.

The Shanley model has been modified in order to incorporate the thermal gradient that will arise as a result of differential heating of the column. As shown in Fig. 7.14 the two elements of the column cell are assumed to have deflected in opposite directions through the distances e_1 and e_2 respectively which may be regarded as the strains that occur after the column starts to bend. The lateral deflection d is made up of the thermal bowing plus the deflection induced by the applied loading system P on the column. Thus the

total deflection is given by:

$$\begin{aligned} d &= \beta \frac{l}{2} + \alpha \frac{\Delta\theta}{8} \\ &= \frac{l}{4}(e_1 + e_2) + a \end{aligned} \quad (7.1)$$

where

$a = \alpha \frac{\Delta\theta}{8}$ is the thermal bowing
and β is the rotation.

The external bending moment at the hinge is given by:

$$\begin{aligned} M_e &= Pd + Px \\ &= \frac{Pl}{4}(e_1 + e_2) + P(x + a) \end{aligned} \quad (7.2)$$

$$\Delta\theta = \theta_2 - \theta_1 \quad (7.3)$$

in which

θ_2 is the hottest flange temperature

θ_1 is the coldest flange temperature

x is the eccentricity of loading

α is the coefficient of thermal expansion(constant).

The axial force in each flange due to bending is given by:

$$\begin{aligned} P_1 &= e_1 E_1 (A/2) \\ P_2 &= e_2 E_2 (A/2) \end{aligned} \quad (7.4)$$

where E_1 and E_2 are the effective values of E_θ for each flange element respectively. E_θ is given by Equations (3.53) and (3.54).

The internal bending moment(about the hinge point) may be expressed as

$$M_i = \frac{1}{2}P_1 + \frac{1}{2}P_2$$

$$= \frac{A}{4}(e_1 E_1 + e_2 E_2) \quad (7.5)$$

Equating internal and external bending moments gives

$$M_e = M_i$$

$$P = \frac{A}{l(e_1 + e_2) + 4(x + a)\{e_1 E_1 + e_2 E_2\}} \quad (7.6)$$

By equating $E_1 = E_2 = E_t(\theta)$ then the tangent-modulus load P_t is given by:

$$P_t = \frac{AE_t(\theta)(d - a)}{l(d + x)} \quad (7.7)$$

i.e on substitution of the value of e_1 given by

$$e_1 = 4 \frac{d - a}{l} \quad (7.8)$$

and using $E_1 = E_t(\theta_1)$

and $E_2 = E(\theta_2) = kE_t(\theta_1)$

and

$$k = \frac{E(\theta_2)}{E_t(\theta_1)} \quad (7.9)$$

Then

$$P = \frac{AE_t(\theta_1)d}{l(d + x)} \left\{ 1 - \frac{a}{d} + \frac{l}{4d}(k - 1)e_2 \right\} \quad (7.10)$$

Another expression for P may be obtained by assuming that after the tangent modulus load is reached, the column load continues to increase. This increase

is given by the difference between the element loads P_1 and P_2 which is given by:

$$\begin{aligned}\Delta P &= P_1 - P_2 \\ &= \frac{AE_t(\theta_1)}{2} \left\{ \frac{4}{l}(d-a) - (k+1)e_2 \right\}\end{aligned}\quad (7.11)$$

This value should be added to the tangent-modulus load to obtain the total load P .

$$\begin{aligned}P &= P_t + \Delta P \\ &= \frac{AE_t(\theta_1)d}{l(d+x)} \left\{ 1 - \frac{a}{d} + 2(d-a)\frac{d+x}{d} - 2(k+1)\frac{d+x}{d}le_2 \right\}\end{aligned}\quad (7.12)$$

From Equations (7.10) and (7.12) the value of e_2 can be evaluated as given by:

$$e_2 = \frac{8(d-a)(d+x)}{l\{(k-1) + 2(k+1)(d+x)\}}\quad (7.13)$$

Substituting the value of e_2 into Equation (7.10) results in the buckling axial load P given by:

$$P = \frac{AE_t(\theta_1)d}{l(d+x)} \left\{ 1 - \frac{a}{d} + \frac{2(d-a)(d+x)}{d\{1 + 2(d+x)(k+1)/(k-1)\}} \right\}\quad (7.14)$$

By letting $\tau = E_t(\theta_1)/E(\theta_2)$ then P is given by:

$$P = \frac{AE_t(\theta_1)d}{l(d+x)} \left\{ 1 - \frac{a}{d} + \Gamma \right\}\quad (7.15)$$

where

$$\Gamma = \frac{2(d-a)(d+x)}{d\{1 + 2(d+x)(\tau+1)/(1-\tau)\}}\quad (7.16)$$

The average stress σ_{ave} is given by:

$$\sigma_{ave} = \frac{E_t(\theta_1)d}{l(d+x)} \left\{ 1 - \frac{a}{d} + \Gamma \right\} \quad (7.17)$$

The average stress-deflection relationships for eccentricities of ± 0.2 and zero-eccentricity are plotted in Fig. 7.15. To simulate thermal gradient the cold and hot flange temperature are set at 150°C and 450°C respectively. It is interesting to note that negative eccentricity improves the performance of the column while positive eccentricity is detrimental to its behaviour. The influence of thermal gradient on the behaviour of the column was investigated by tracing the average stress-deflection characteristics at a uniform temperature of 450°C . This situation corresponds to zero thermal gradient and it was found that the influence of thermal gradient is quite minimal. The shift in the curves is mainly as a result of the degradation of the strength properties with temperature. This observation conforms with the earlier experience reported in section 7.3. Although this is not an exhaustive investigation of the effect of thermal gradient on columns some insight is provided to justify the observed behaviour reported earlier in the previous sections.

Concluding Remarks:

From the analytical studies reported in the preceding sections the influence of some parameters on the column behaviour in fire has been assessed. These parameters include the initial out-of-straightness, different end conditions (pinned-end and fixed-end conditions), thermal gradient and the interaction of eccentricity of loading with thermal gradient. A simple Shanley model was used to assess the influence of thermal gradient and applied eccentricity of loading on

the column behaviour in fire. The following conclusions may be drawn:

1. The influence of initial out-of-straightness on columns depends on slenderness ratio. Stocky and very slender columns are detrimentally influenced in terms of critical temperatures while the intermediate columns show an improved behaviour with the presence of initial out-of-straightness.
2. In terms of failure temperature the fixed-end stocky and intermediate columns show an improved performance over the pinned-end condition while slender columns, $l/r > 100$, respond favourably to the pinned-end condition. For a column with slenderness ratio of 100 the variation in the end conditions does not influence its performance in terms of failure temperature. Thus the type of end condition to be imposed during a fire test must be assessed with respect to the slenderness ratio of the test specimen.
3. The occurrence of a significant temperature gradient across the cross-section results in variation of the strength properties and induced thermal bowing. Because of the variation of these properties the loss of stiffness resulting from the induced bowing can be compensated for. This overshadowing influence of the strength properties enables the columns to perform better than in the uniform temperature condition. It can be concluded that partially protected columns will sustain applied load longer than expected. Thus designers could allow for this benefit in designing columns either built into fire resistant walls or with partial protections that ensures thermal gradient.
4. The point of application of the loading influences a column's response

under thermal gradient. If the eccentricity is applied along the positive direction of the shifted neutral axis the influence of thermal bowing will be reduced. Furthermore, the variation of the material properties across the cross-section ensures reduced influence that thermal bowing will have.

5. The modified Shanley column model shows that thermal bowing may not constitute a menace to the behaviour of columns in fire compared to uniformly heated columns(i.e assuming maximum temperature for the uniform distribution). The influence of eccentricity of loading depends on the point of application of loading.

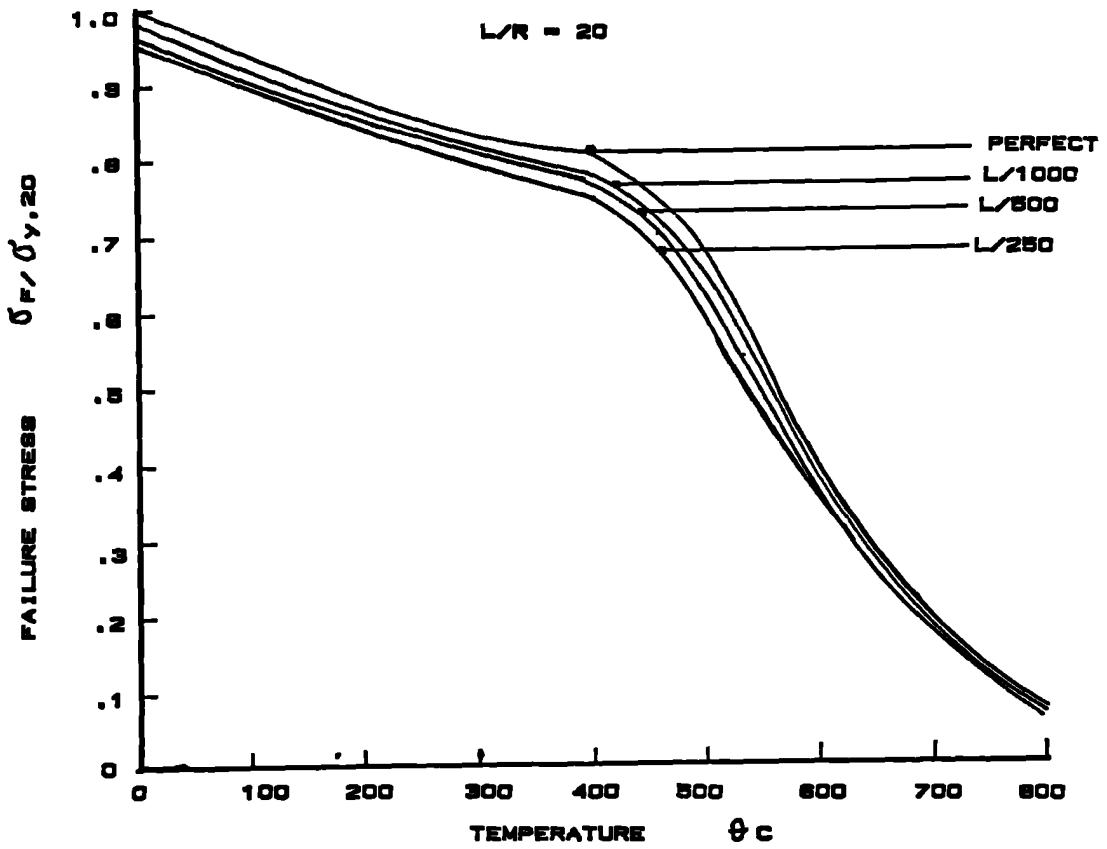


**FIG. 7.1a VARIATION OF FAILURE STRESS WITH TEMPERATURE
AT INCREASING LEVEL OF INITIAL IMPERFECTION**

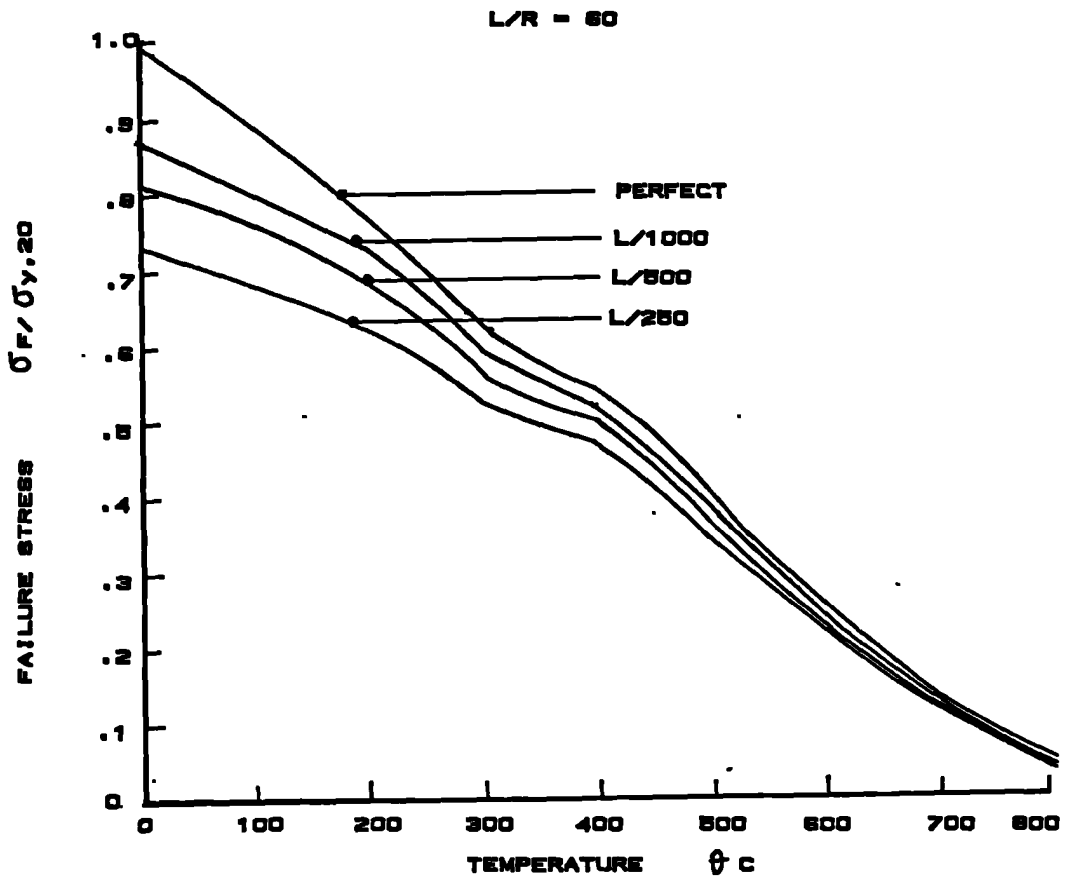


FIG. 7.1b

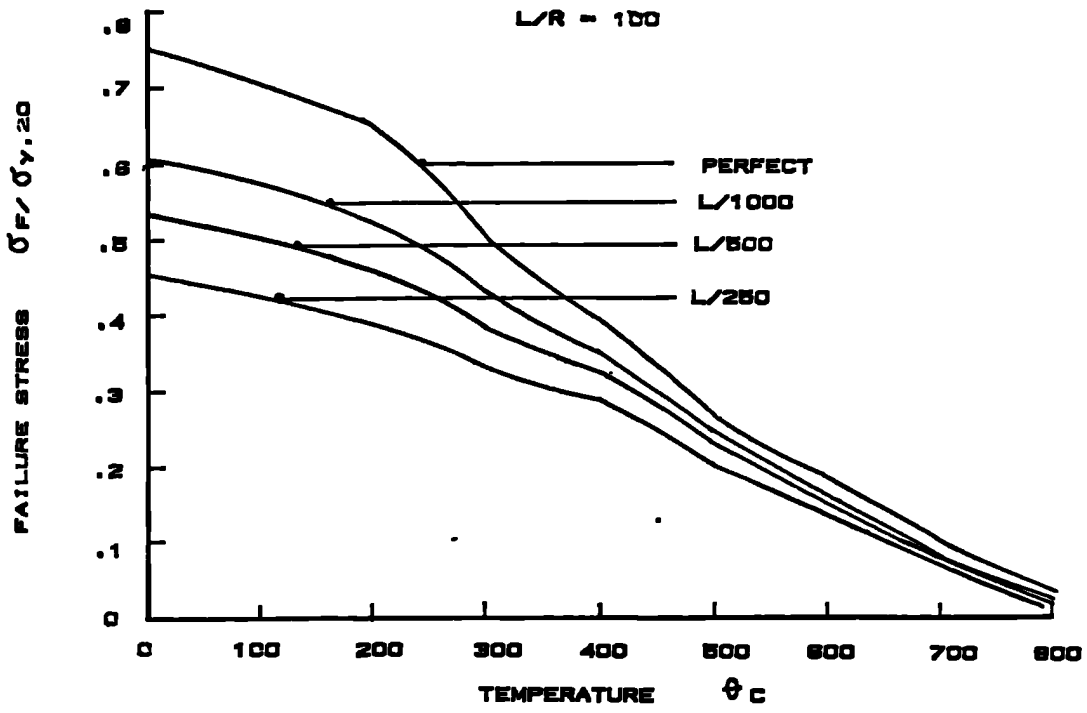


FIG. 7.1a

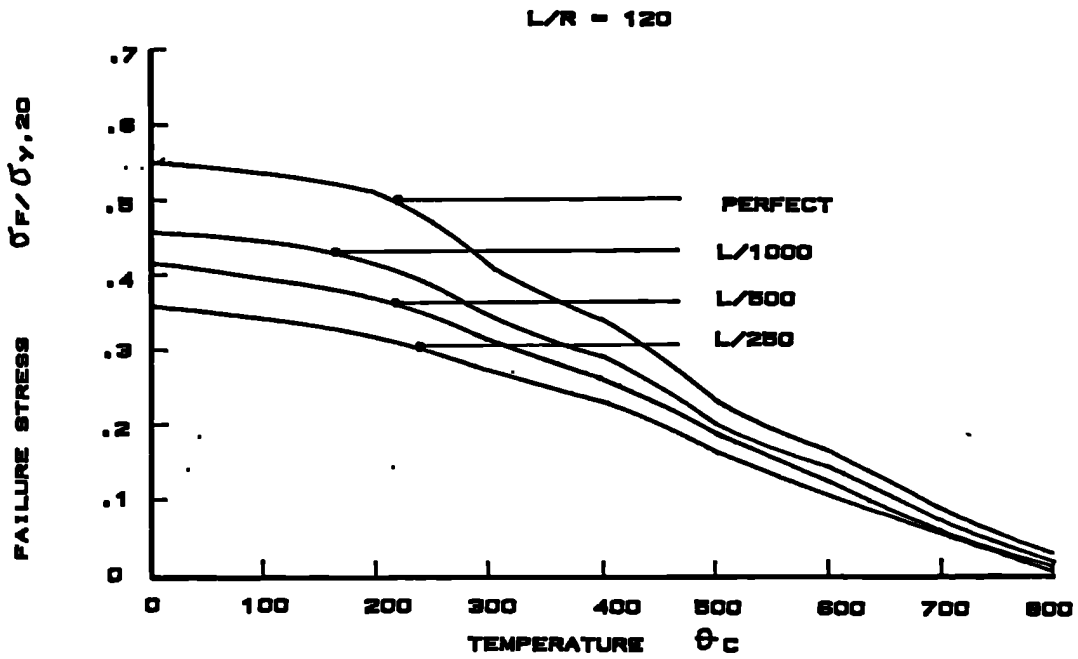


FIG. 7.1d

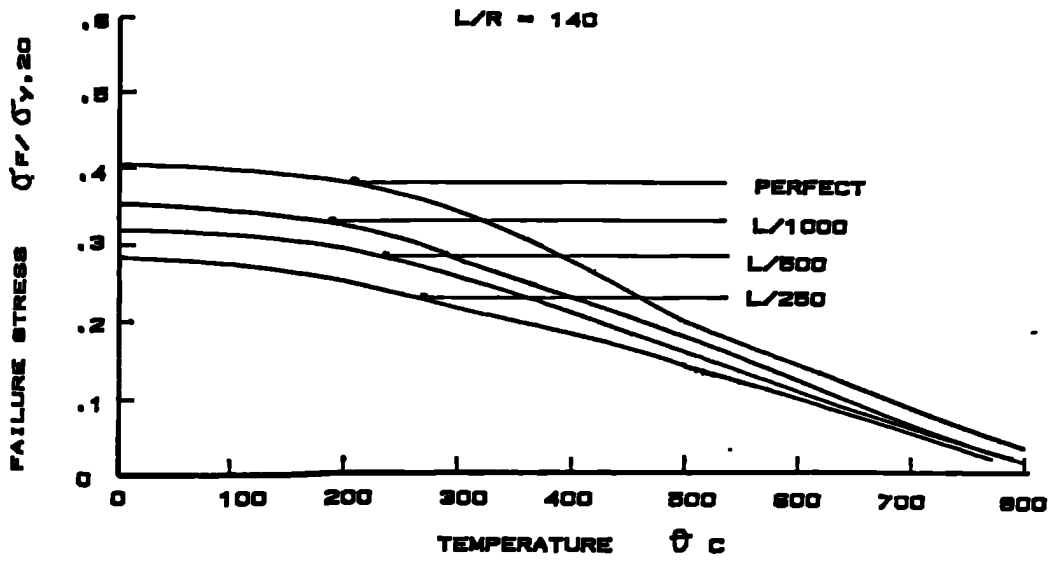


FIG. 7.18

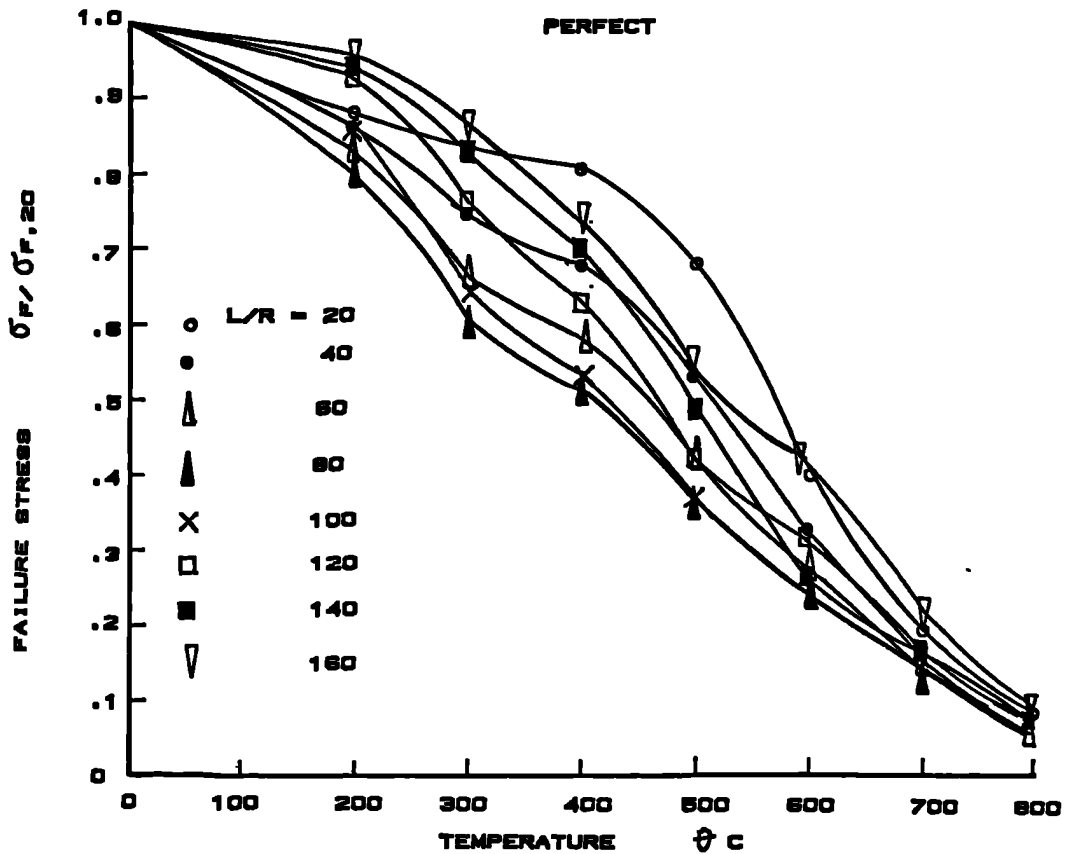


FIG. 7.26 VARIATION OF FAILURE STRESS (RELATIVE TO AMBIENT TEMPERATURE FAILURE STRESS) WITH TEMPERATURE AT DIFFERENT INITIAL IMPERFECTION LEVEL

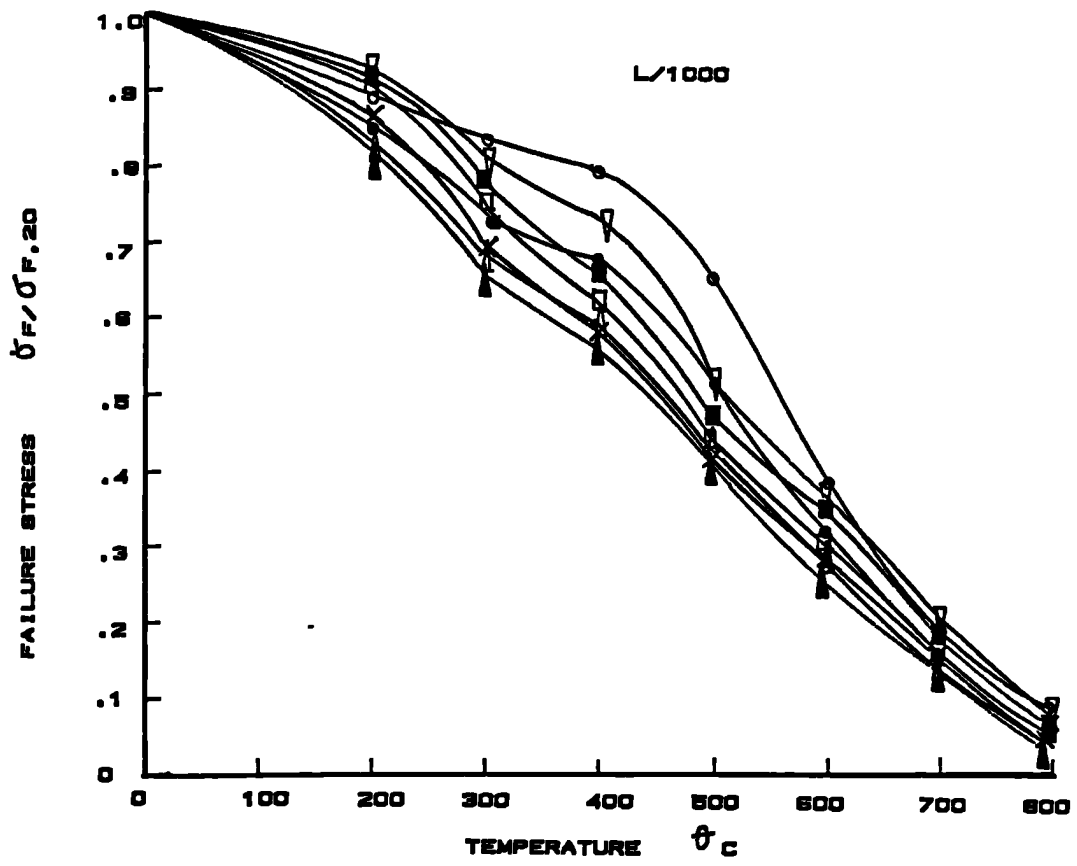


FIG. 7.2b

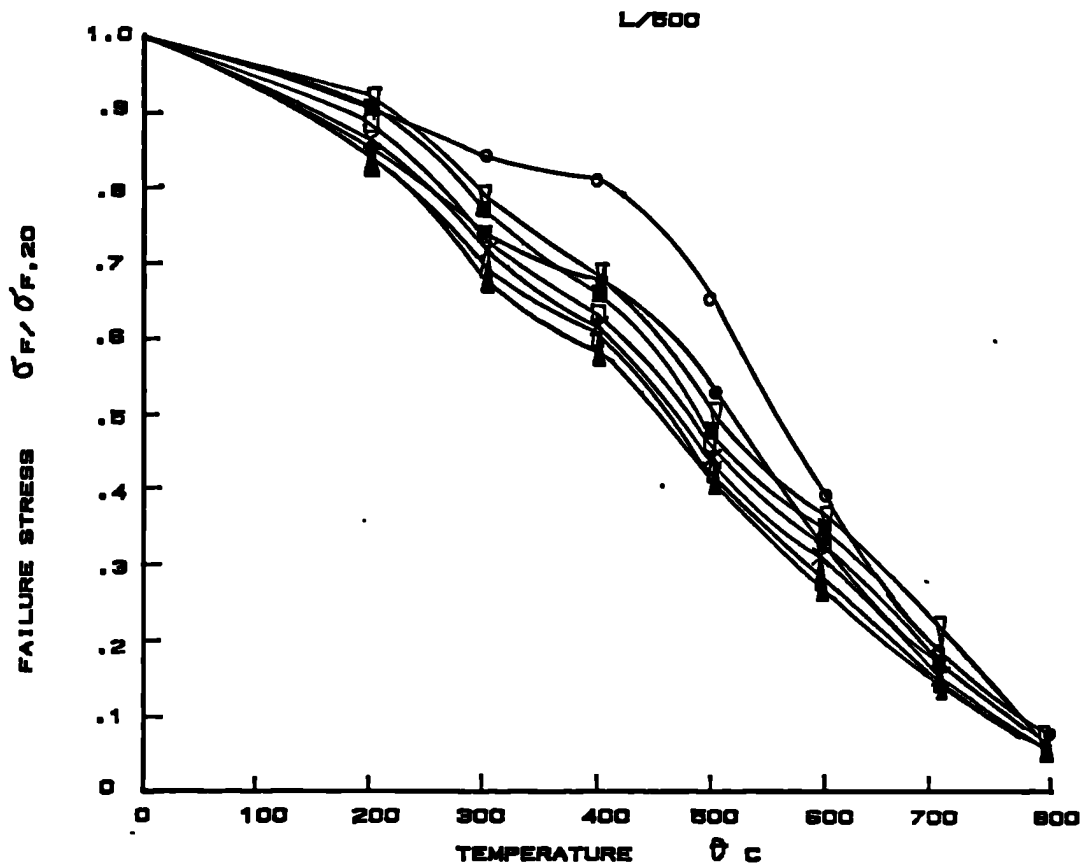


FIG. 7.2c

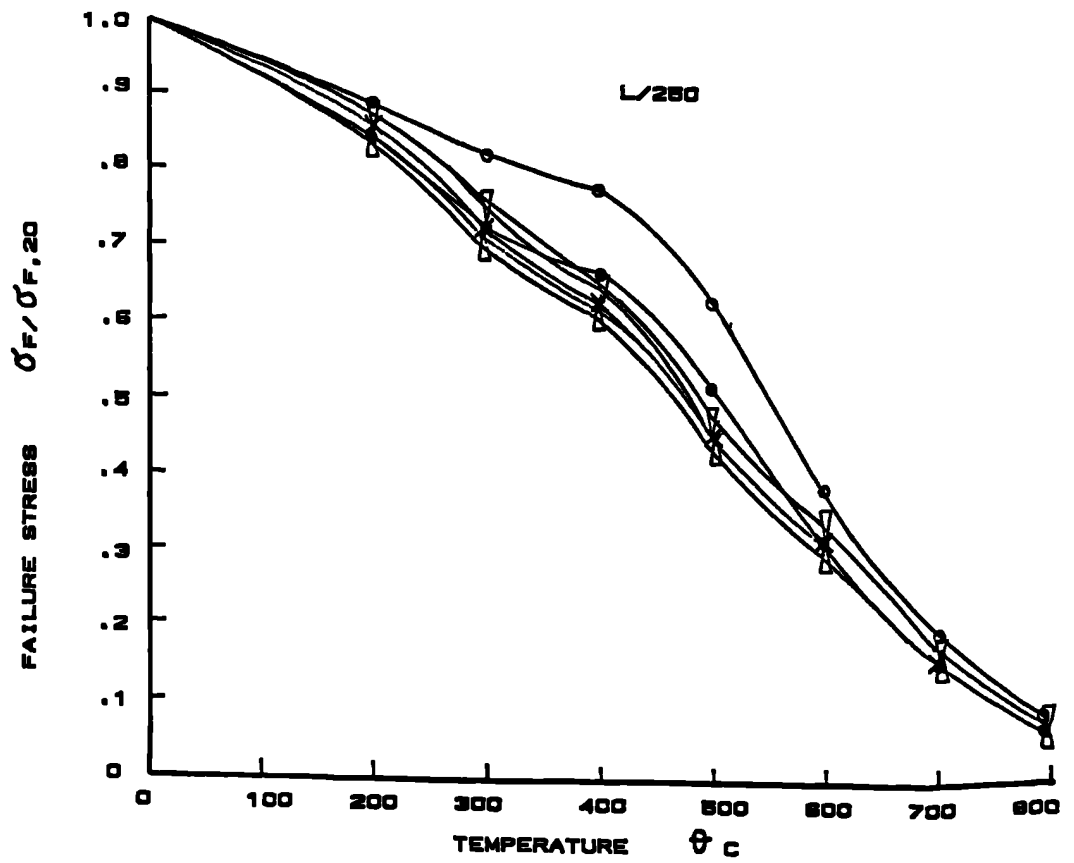


FIG. 7.2d

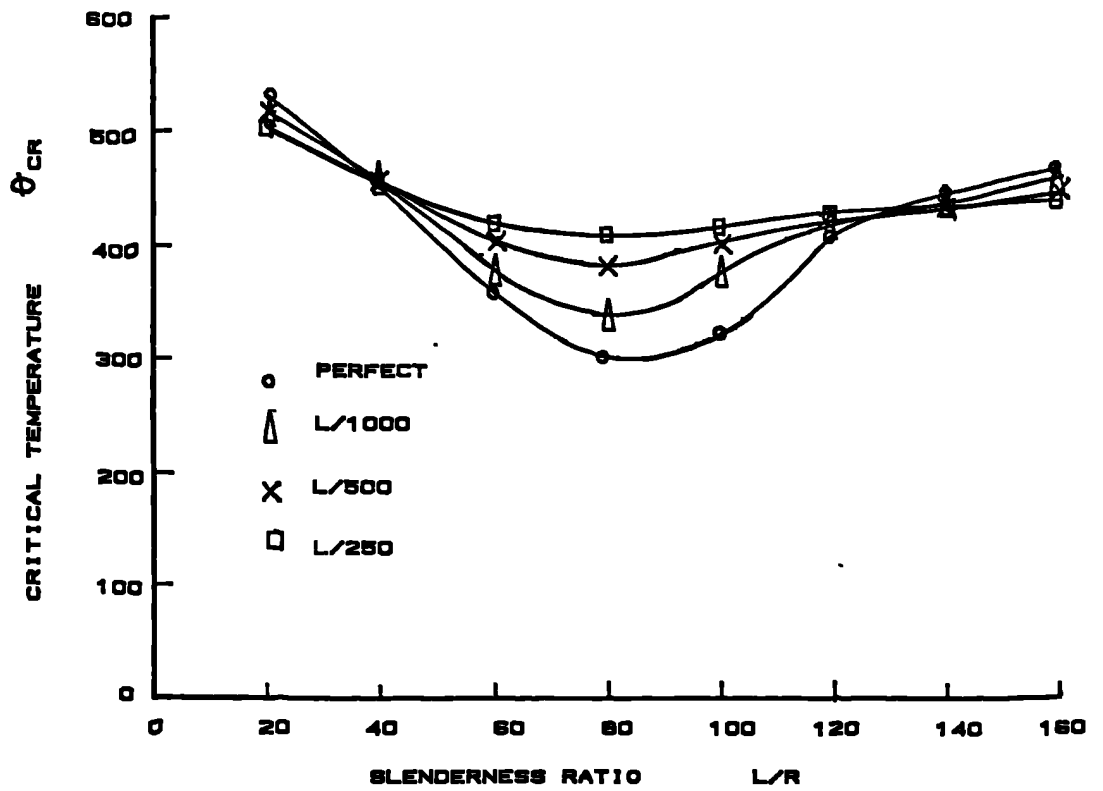


FIG. 7.3 VARIATION OF CRITICAL TEMPERATURE WITH SLENDERNESS RATIO AT INCREASING LEVEL OF INITIAL IMPERFECTION

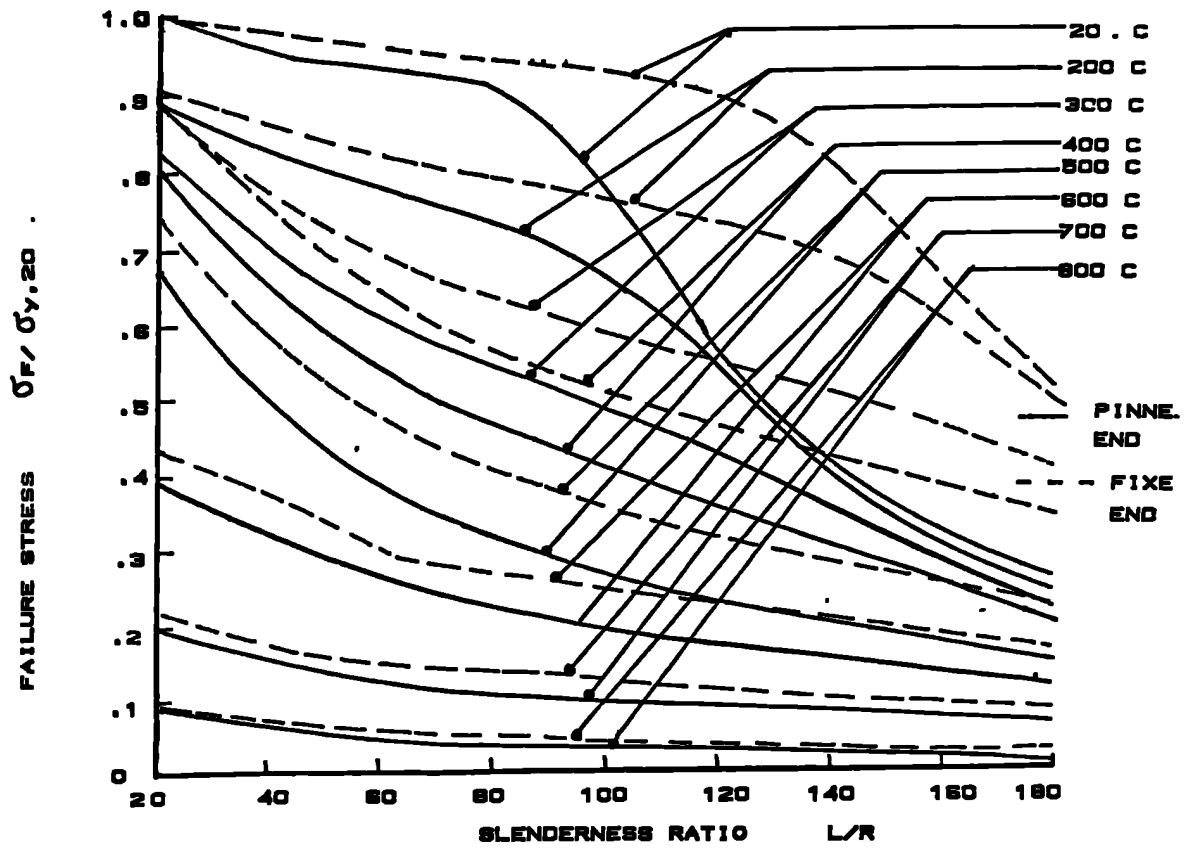


FIG. 7.4 VARIATION OF FAILURE STRESS WITH SLENDERNESS RATIO FOR DIFFERENT END CONDITIONS

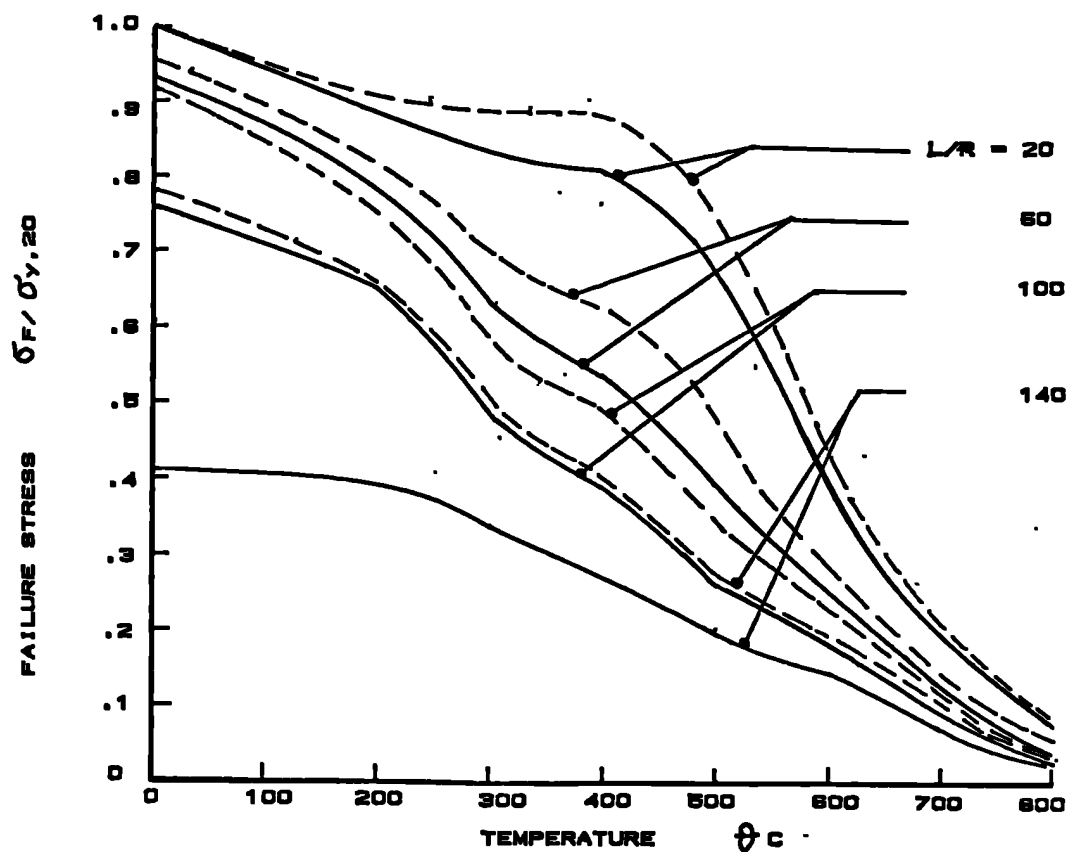


FIG. 7.5 VARIATION OF FAILURE STRESS WITH TEMPERATURE FOR DIFFERENT END CONDITIONS

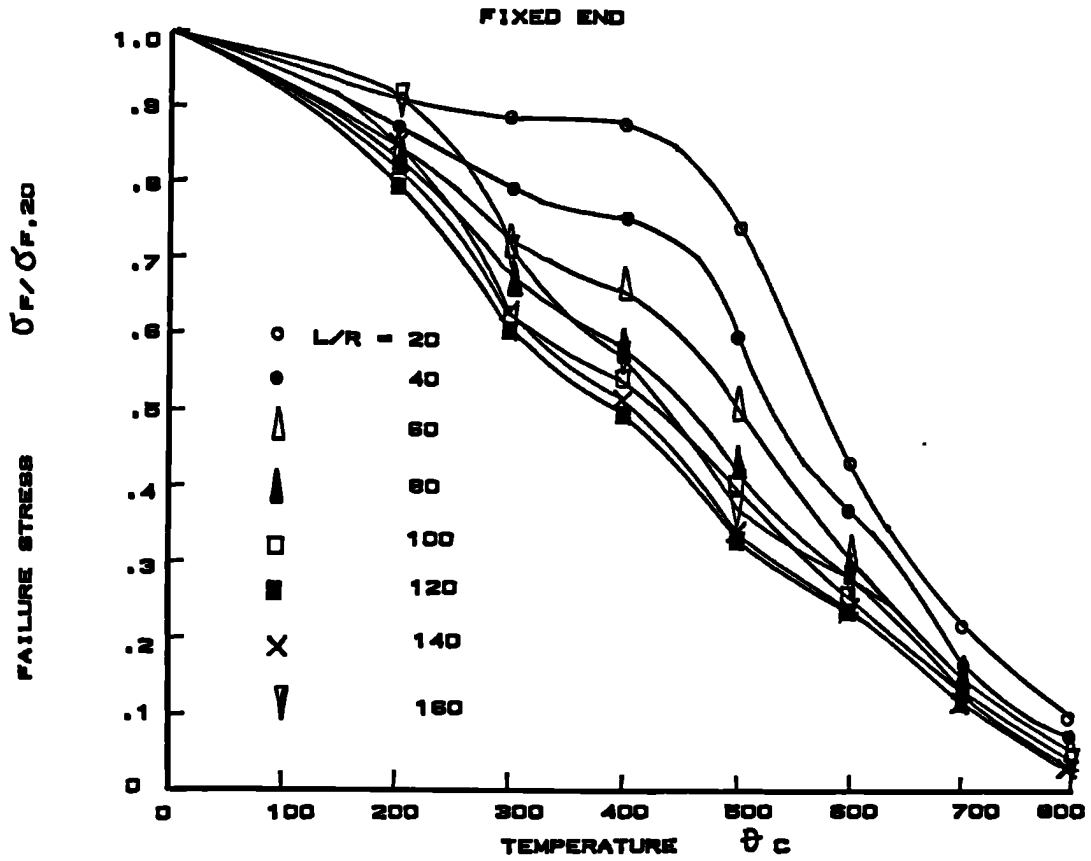


FIG. 7.6 VARIATION OF FAILURE STRESS (RELATIVE TO AMBIENT TEMPERATURE FAILURE STRESS) WITH TEMPERATURE FOR FIXED END CONDITION

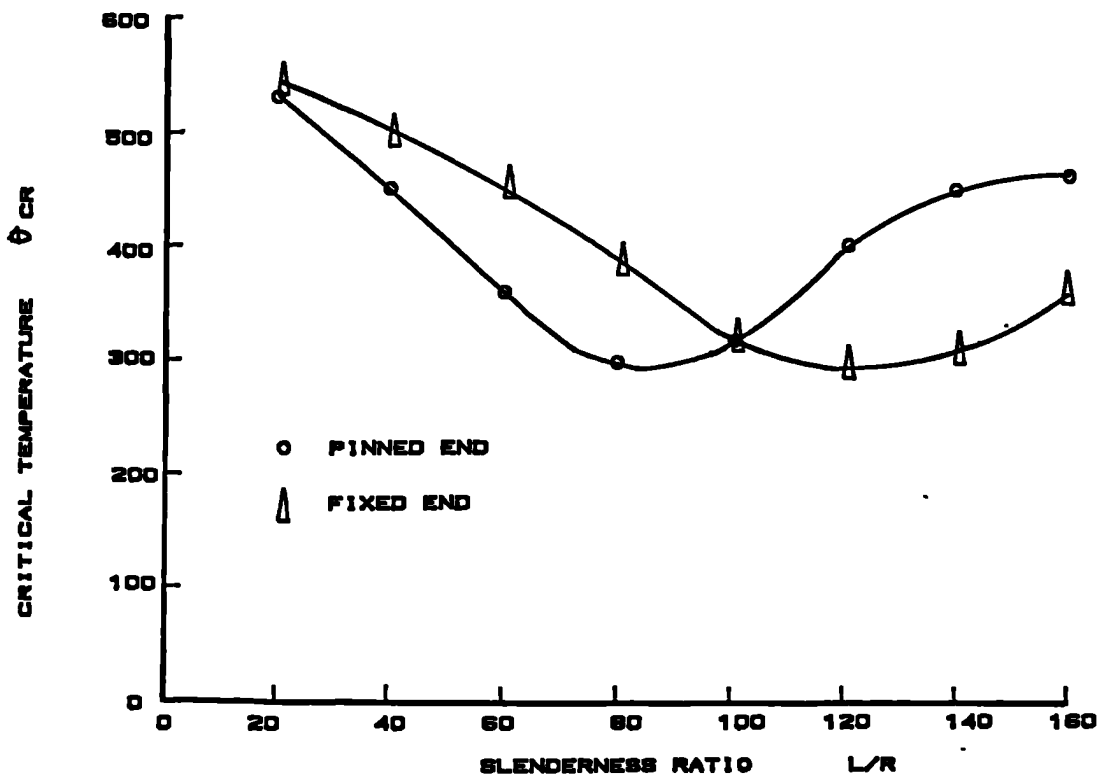


FIG. 7.7 VARIATION OF CRITICAL TEMPERATURE WITH SLENDERNESS RATIO FOR DIFFERENT END CONDITIONS

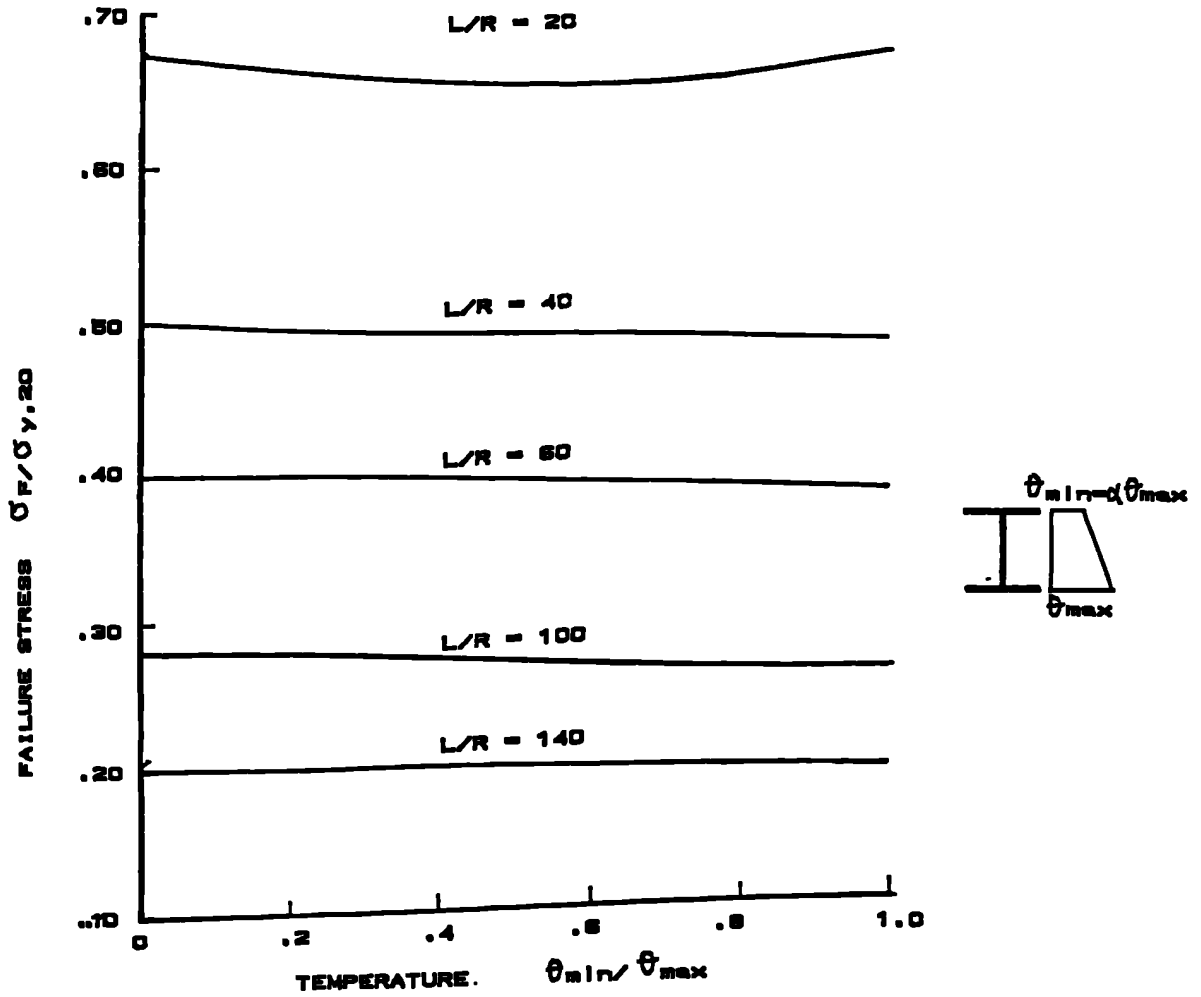


FIG. 7.8 FAILURE STRESS - THERMAL GRADIENT RELATIONSHIP WITH MAXIMUM TEMPERATURE SET AT 500° C

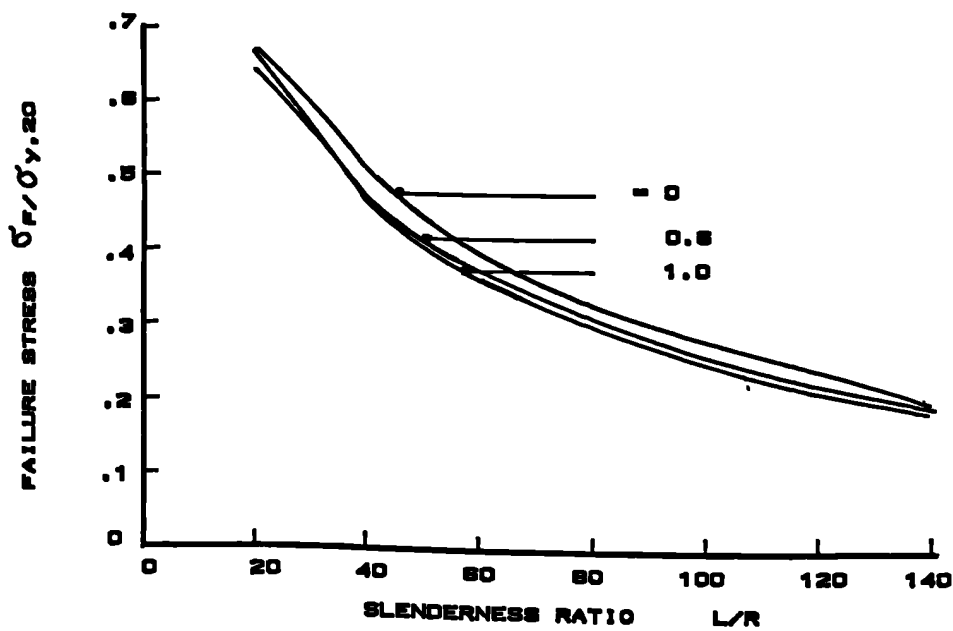


FIG. 7.9 VARIATION OF FAILURE STRESS WITH SLENDERNESS RATIO

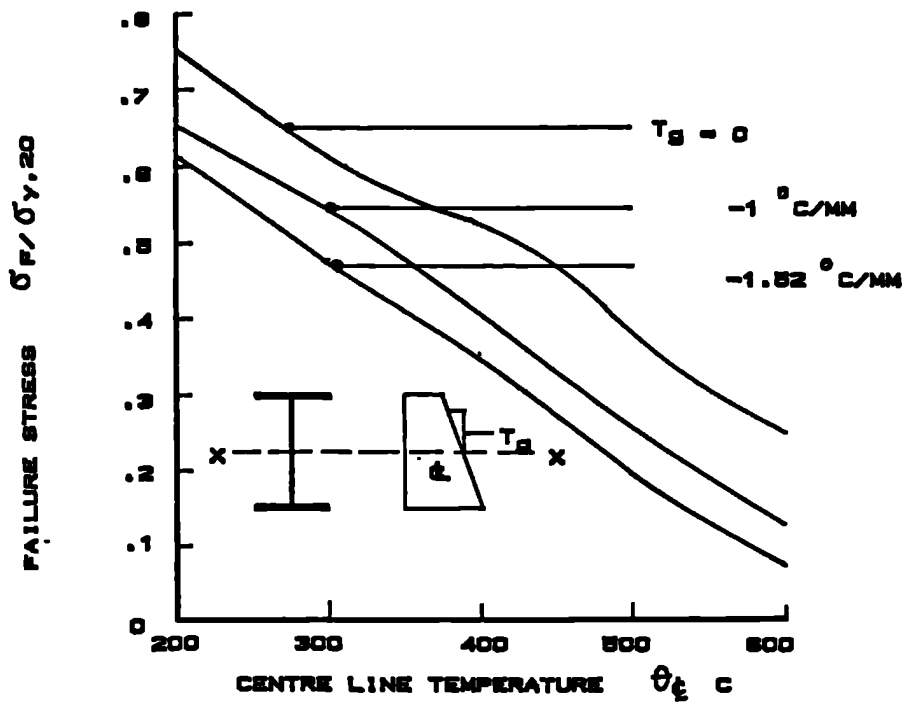


FIG. 7.10 VARIATION OF FAILURE STRESS WITH CENTRE LINE TEMPERATURE AT INCREASING THERMAL GRADIENT

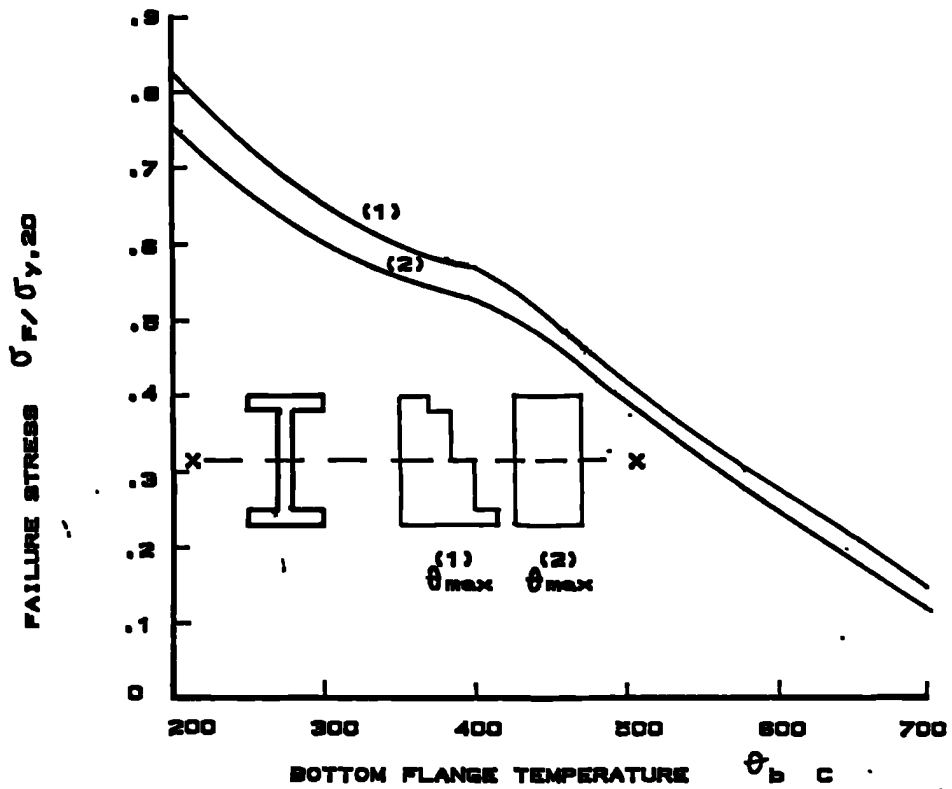


FIG. 7.11 VARIATION OF FAILURE STRESS WITH MAXIMUM TEMPERATURE

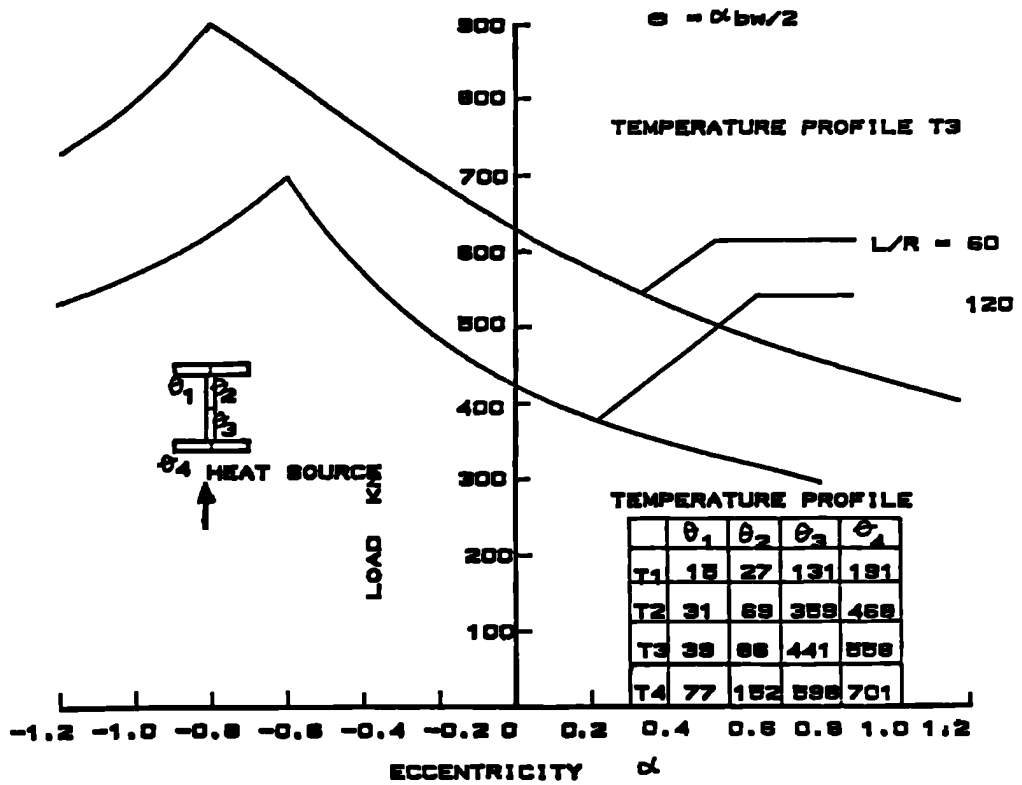


FIG. 7.12 LOAD - ECCENTRICITY OF LOADING RELATIONSHIP WITH THERMAL GRADIENT

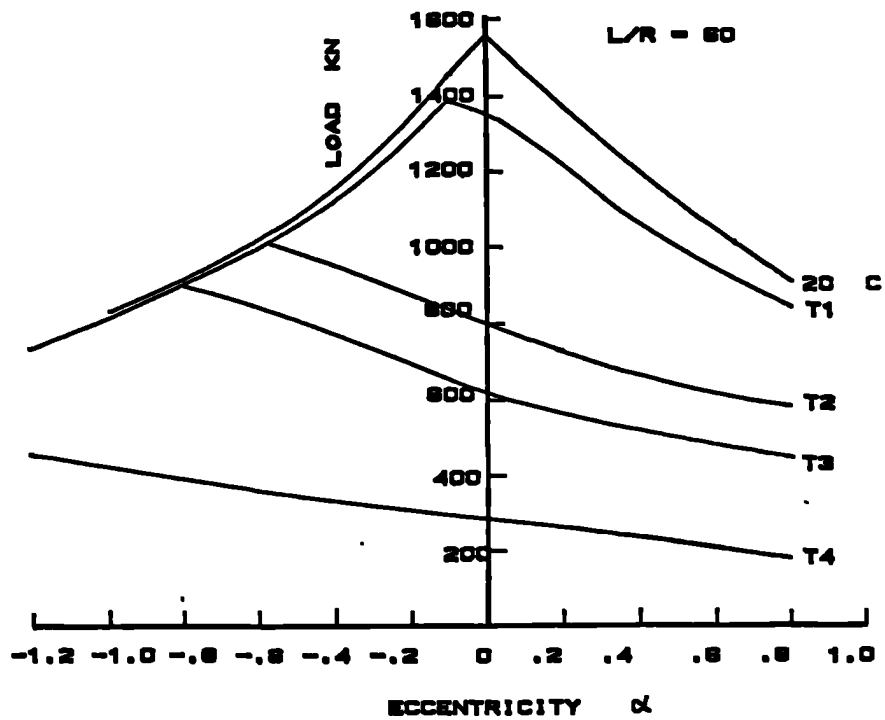


FIG. 7.13 LOAD - ECCENTRICITY OF LOADING RELATIONSHIP AT INCREASING THERMAL GRADIENT

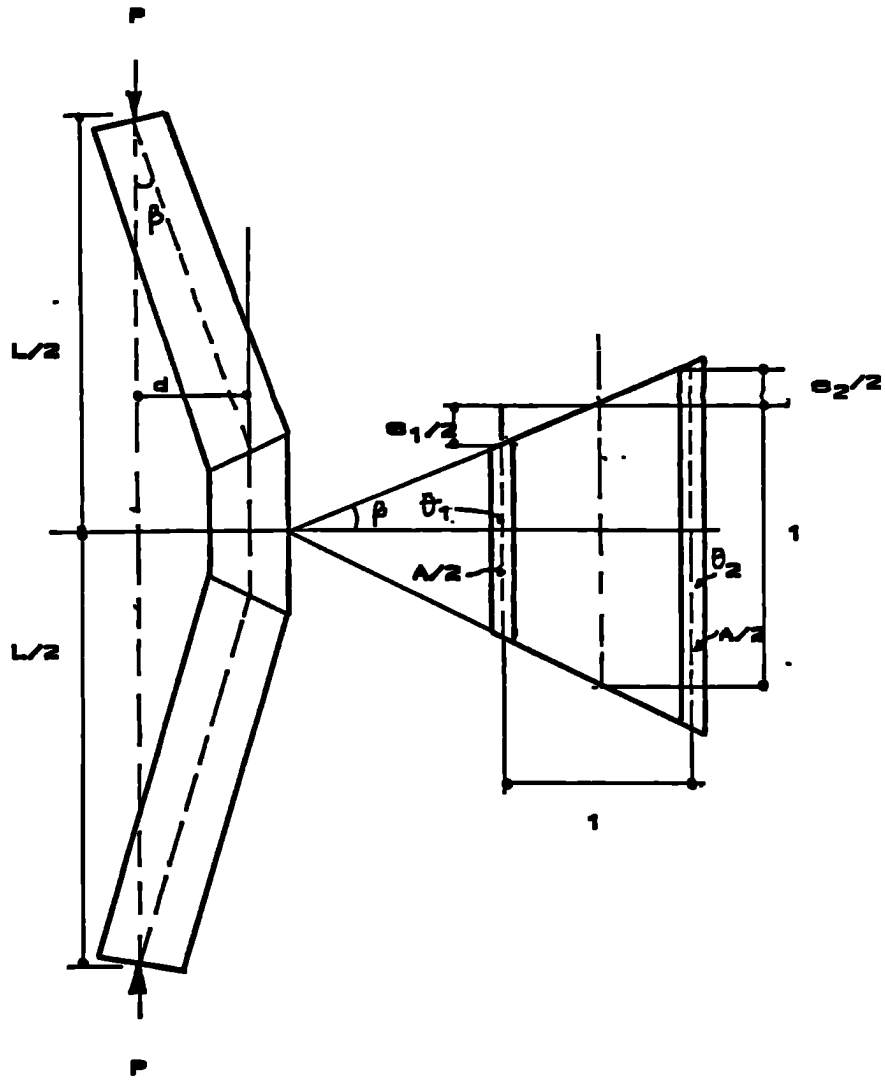


FIG. 7.14 SHANLEY COLUMN MODEL WITH THERMAL GRADIENT

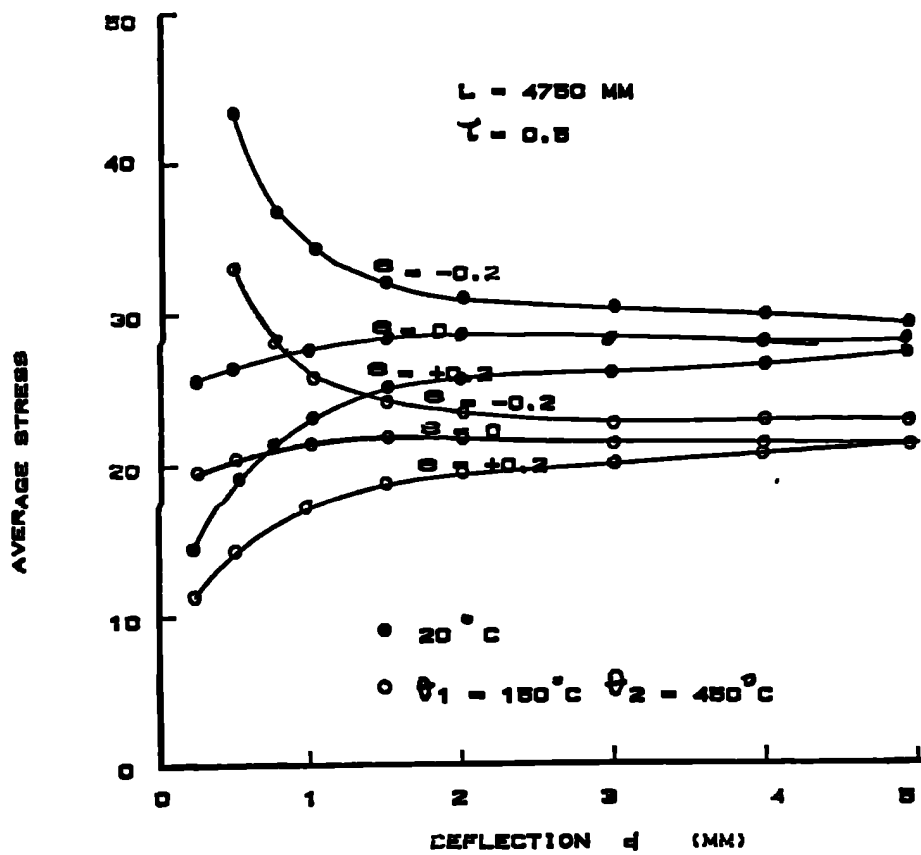


FIG. 7.15 AVERAGE STRESS - DEFLECTION RELATIONSHIP WITH THERMAL GRADIENT AND ECCENTRICITY OF LOADING

Chapter 8

NONLINEAR ANALYSIS OF PLATE USING FLOW THEORY OF PLASTICITY

The finite strip method described previously in Chapter 3 is based on small deflection theory. This limits the analysis to collapse load calculation using material nonlinearity based on deformation theory of plasticity. Since plates can exhibit considerable post-buckling strength the work reported herein is based on large deflection theory using flow theory of plasticity. Although this development is not meant to provide detailed information on the post-buckling behaviour of plates and plate subassemblages, the foundation for the ultimate strength analysis of plates and plate subassemblages is provided for future work.

In the present development the displacement functions for the interactive buckling analysis which satisfy the boundary conditions are

$$\begin{aligned}
U &= \lambda e \left(\frac{1}{2} - \xi \right) + Z_c \kappa \left(\frac{1}{2} - \xi \right)^2 + \sum_{m=2}^r U_r f_r^u(x, y) \\
V &= b v e \left(\eta - \frac{1}{2} \right) + C_v \left(\eta - \frac{1}{2} \right) + \frac{\kappa \lambda}{\pi} \sin \pi \xi \sin \gamma \\
&\quad + \sum_{n=2}^r V_r f_r^v(x, y) \\
W &= -\frac{\kappa \lambda}{\pi} \sin \pi \xi \cos \gamma + \sum_{p=1}^r W_r f_r^w(x, y)
\end{aligned} \tag{8.1}$$

where

$$\begin{aligned}
U_r f_r^u &= (C_1 u_{1m} + C_2 u_{2m}) \sin m \pi \xi \\
V_r f_r^v &= (C_1 v_{1n} + C_2 v_{2n}) \cos n \pi \xi \\
W_r f_r^w &= (C_4 w_{1p} + C_3 \Theta_{1p} + C_6 w_{2p} + C_5 \Theta_{2p}) \sin p \pi \xi
\end{aligned} \tag{8.2}$$

in which

$$\begin{aligned}
\xi &= \frac{x}{\lambda} \\
\eta &= \frac{y}{b} \\
e &= \frac{\text{end shortening}}{\lambda}
\end{aligned} \tag{8.3}$$

b is the strip width

λ is the length of the strip

γ is the angle of the strip relative to the global coordinate system

Z_c is the distance from centroid to the point of load application

κ is the end rotation of the assemblage

and

$$m = 2, 4, \dots$$

$$n = 2, 4, \dots$$

$$p = 1, 3, \dots$$

The C_1, C_2, C_3, C_4, C_5 and C_6 expressions are given in Chapter 3 and U_r, V_r and W_r are the displacement parameters.

The strain vector is obtained from the derivatives of the displacement functions as given by.

$$\begin{aligned}
\epsilon_x &= \frac{\partial U}{\partial x} + \frac{1}{2} \left[\left(\frac{\partial V}{\partial x} \right)^2 - \left(\frac{\partial V_o}{\partial x} \right)^2 \right. \\
&\quad \left. + \left(\frac{\partial W}{\partial x} \right)^2 - \left(\frac{\partial W_o}{\partial x} \right)^2 \right] - z \frac{\partial^2 (W - W_o)}{\partial x^2} \\
\epsilon_y &= \frac{\partial V}{\partial y} - \frac{\partial V_o}{\partial y} + \frac{1}{2} \left[\left(\frac{\partial W}{\partial y} \right)^2 - \left(\frac{\partial W_o}{\partial y} \right)^2 \right] \\
&\quad - z \frac{\partial^2 (W - W_o)}{\partial y^2} \\
\gamma_{xy} &= \frac{\partial U}{\partial y} + \frac{\partial V}{\partial x} - \frac{\partial V_o}{\partial x} + \frac{\partial V}{\partial x} \frac{\partial V}{\partial y} - \frac{\partial V_o}{\partial x} \frac{\partial V_o}{\partial y} \\
&\quad + \frac{\partial W}{\partial x} \frac{\partial W}{\partial y} - \frac{\partial W_o}{\partial x} \frac{\partial W_o}{\partial y} - 2z \frac{\partial^2 (W - W_o)}{\partial x \partial y}
\end{aligned} \tag{8.4}$$

The increment of strain is

$$\begin{aligned}
\Delta \epsilon_x &= \frac{\partial U}{\partial x} + \frac{\partial V}{\partial x} \frac{\partial \Delta V}{\partial x} + \frac{1}{2} \left(\frac{\partial V}{\partial x} \right)^2 \\
&\quad + \frac{\partial W}{\partial x} \frac{\partial \Delta W}{\partial x} + \frac{1}{2} \left(\frac{\partial W}{\partial x} \right)^2 - z \frac{\partial^2 W}{\partial x^2} \\
\Delta \epsilon_y &= \frac{\partial V}{\partial y} + \frac{1}{2} \left(\frac{\partial W}{\partial y} \right)^2 + \frac{\partial W}{\partial y} \frac{\partial \Delta W}{\partial y} - z \frac{\partial^2 W}{\partial y^2} \\
\Delta \gamma_{xy} &= \frac{\partial U}{\partial y} + \frac{\partial V}{\partial x} + \frac{\partial W}{\partial x} \frac{\partial \Delta W}{\partial y} + \frac{\partial W}{\partial y} \frac{\partial \Delta W}{\partial x} \\
&\quad + \frac{\partial W}{\partial x} \frac{\partial W}{\partial y} + \frac{\partial V}{\partial x} \frac{\partial \Delta V}{\partial y} + \frac{\partial V}{\partial y} \frac{\partial \Delta V}{\partial x} \\
&\quad + \frac{\partial V}{\partial x} \frac{\partial V}{\partial y} - 2z \frac{\partial^2 W}{\partial x \partial y}
\end{aligned} \tag{8.5}$$

and the derivatives of the displacement functions are listed in appendix C.

The total strain is given by the sum of the elastic, plastic and thermal strain components.

$$\epsilon_{ij} = \epsilon_{ij}^e + \epsilon_{ij}^p + \epsilon_{ij}^{\theta} \quad (8.6)$$

The incremental strain is

$$\Delta\epsilon_{ij} = \Delta\epsilon_{ij}^e + \Delta\epsilon_{ij}^p + \Delta\epsilon_{ij}^{\theta} \quad (8.7)$$

in which the thermal strain increment is

$$\Delta\epsilon_{ij}^{\theta} = \alpha\Delta\theta \quad (8.8)$$

and

α is the coefficient of thermal expansion (1.4×10^{-5}),

$\Delta\theta$ is the temperature increment,

Considering Prandtl-Reuss associative flow rule the plastic strain increment component is

$$\begin{aligned} \Delta\epsilon_{ij}^p &= \frac{\phi}{3} \frac{\partial(\sigma_e^2)}{\partial\sigma_{ij}} \\ &= \phi S_{ij} \end{aligned} \quad (8.9)$$

where S_{ij} is the deviatoric stress tensor given by

$$S_{ij} = \sigma_{ij} - \delta_{ij}\sigma_{ii} \quad (8.10)$$

in which the hydrostatic stress is given as

$$\sigma_{ii} = \sigma_x + \sigma_y + \sigma_z \quad (8.11)$$

and δ_{ij} is the Kronecker delta. The deviatoric stress can be expressed as

$$\begin{aligned} S_x &= (2\sigma_x - \sigma_y)/3 \\ S_y &= (2\sigma_y - \sigma_x)/3 \\ S_{xy} &= \tau_{xy} \end{aligned} \quad (8.12)$$

The effective stress σ_e^2 is

$$\sigma_e^2 = 3J_2 \quad (8.13)$$

where J_2 is the stress tensor used in von Mises yield condition and is given by

$$J_2 = \frac{1}{3}(\sigma_x^2 + \sigma_y^2 - \sigma_x\sigma_y) + \tau_{xy}^2 \quad (8.14)$$

The stress increment is related to the elastic strain increments by Hooke's law
i.e

$$\begin{aligned} \Delta\sigma_x &= \frac{E_\theta}{(1-\nu^2)}(\Delta\epsilon_x^e + \nu\epsilon_y^e) \\ \Delta\sigma_y &= \frac{E_\theta}{(1-\nu^2)}(\Delta\epsilon_y^e + \nu\epsilon_x^e) \\ \Delta\tau_{xy} &= \frac{E_\theta}{2(1+\nu)}\Delta\gamma_{xy}^e \end{aligned} \quad (8.15)$$

in which E_θ is the effective modulus of elasticity at elevated temperature given in Chapter 3.

The stress-strain relationship for a material undergoing plastic flow can only approximate macroscopically the complicated process of slip taking place within

the crystal lattice. It is usually accepted that the best approximation is obtained using the von Mises yield criterion with its associative Prandtl-Reuss flow rule. This is given as effective stress σ_e .

$$\sigma_e^2 = 3(S_x^2 + S_y^2 + S_x S_y + \tau_{xy}^2) \quad (8.16)$$

The plastic strain increment, ϵ_{ij}^p , is a scalar multiple of the steepest ascent vector of σ_e^2 in the stress space, thus satisfying the requirement of being normal to the yield surface, $\sigma_e^2 = \sigma_y^2$. The factor ϕ in Equation (8.9) must be greater than or equal to zero in order to ensure that the plastic strain increment occurs in the same direction as the corresponding stress deviator.

For an elastic-perfectly plastic material in which yielding occurs when von Mises effective stress reaches the material yield stress, the value of ϕ is obtained from the condition that

$$\Delta(\sigma_e^2) = 0 \quad (8.17)$$

and

$$\begin{aligned} \Delta(\sigma_e^2) &= 2\sigma_x \cdot \Delta\sigma_x + 2\sigma_y \cdot \Delta\sigma_y - \sigma_x \cdot \Delta\sigma_y - \sigma_y \cdot \Delta\sigma_x + 6\tau_{xy} \cdot \Delta\tau_{xy} \\ &= 3S_x \cdot \Delta\sigma_x + 3S_y \cdot \Delta\sigma_y + 6\tau_{xy} \cdot \Delta\tau_{xy} \end{aligned} \quad (8.18)$$

The increment of stress is given by

$$\begin{aligned} \Delta\sigma_x &= \frac{E_\theta}{(1-\nu^2)} (\Delta\epsilon_x + \nu\Delta\epsilon_y - \phi(S_x + \nu S_y) - \Delta\epsilon^\theta(1+\nu)) \\ \Delta\sigma_y &= \frac{E_\theta}{(1-\nu^2)} (\Delta\epsilon_y + \nu\Delta\epsilon_x - \phi(S_y + \nu S_x) - \Delta\epsilon^\theta(1+\nu)) \\ \Delta\tau_{xy} &= \frac{E_\theta}{(1-\nu^2)} \left(\frac{1-\nu}{2} (\Delta\gamma_{xy} - 2\phi\tau_{xy}) \right) \end{aligned} \quad (8.19)$$

Substituting Equation (8.19) into Equation (8.18) results in

$$\frac{3E_\theta}{1-\nu^2}(S_3 - \phi S_4) = 0 \quad (8.20)$$

That is

$$\phi = \frac{S_3}{S_4} \quad (8.21)$$

in which

$$\begin{aligned} S_4 &= S_x^2 + 2\nu S_x S_y + S_y^2 + 2(1-\nu)\tau_{xy}^2 \\ S_3 &= S_1\Delta\epsilon_x + S_2\Delta\epsilon_y + (1-\nu)S_{xy}\Delta\gamma_{xy} - \Delta\epsilon^\theta(1-\nu)(S_x + S_y) \\ S_2 &= S_y + \nu S_x \\ S_1 &= S_x + \nu S_y \end{aligned} \quad (8.22)$$

Substituting Equations (8.21) and (8.22) into Equation (8.19) yields the incremental stress-strain relation.

$$\{\Delta\sigma\} = [F]\{\Delta\epsilon\} + \{\Delta\sigma^\theta\} \quad (8.23)$$

in which the elements of the symmetric elasto-plastic matrix $[F]$ are

$$\begin{aligned} f_{11} &= \frac{E_\theta}{1-\nu^2} \left(1 - \rho \frac{S_1^2}{S_4} \right) \\ f_{22} &= \frac{E_\theta}{1-\nu^2} \left(1 - \rho \frac{S_2^2}{S_4} \right) \\ f_{33} &= \frac{E_\theta}{1-\nu^2} \left(\frac{(1-\nu)}{2} - \rho \frac{((1-\nu)\tau_{xy})^2}{S_4} \right) \\ f_{12} &= \frac{E_\theta}{1-\nu^2} \left(\nu - \rho \frac{S_1 S_2}{S_4} \right) \end{aligned}$$

$$\begin{aligned}
f_{13} &= \frac{E_\theta}{1-\nu^2} \left(-\rho(1-\nu) \frac{S_1 \tau_{xy}}{S_4} \right) \\
f_{23} &= \frac{E_\theta}{1-\nu^2} \left(-\rho(1-\nu) \frac{S_2 \tau_{xy}}{S_4} \right) \\
f_{21} &= f_{12} \\
f_{31} &= f_{13} \\
f_{32} &= f_{23}
\end{aligned} \tag{8.24}$$

and the thermal stress increment $\{\Delta\sigma^\theta\}$ is given by

$$\{\Delta\sigma^\theta\} = \left\{ \begin{array}{l} \left(\frac{S_1}{S_4}(1-\nu)S_\theta - (1+\nu) \right) \Delta\epsilon^\theta \\ \left(\frac{S_2}{S_4}(1-\nu)S_\theta - (1+\nu) \right) \Delta\epsilon^\theta \\ \frac{\tau_{xy}}{S_4}(1-\nu)^2 S_\theta \Delta\epsilon^\theta \end{array} \right\} \tag{8.25}$$

in which

$$S_\theta = S_x + S_y \tag{8.26}$$

$\rho = 1$ when plastic flow occurs, i.e. when $\sigma_e^2 = \sigma_{y,\theta}^2$ and $S_3 > 0$. However, $\rho = 0$ when strain increments are completely elastic i.e. when $\sigma_e^2 < \sigma_{y,\theta}^2$ or when $\sigma_e^2 = \sigma_{y,\theta}^2$ and $S_3 \leq 0$ (elastic unloading from the yield surface). The effective yield stress expression $\sigma_{y,\theta}$ is given in Chapter 3.

In order to incorporate the strain hardening phenomenon the increment in von Mises effective stress $\Delta(\sigma_e^2)$ is no longer zero but a quantity representing the strain hardening function. The increment in the effective stress, $\Delta\sigma_e$, is found by assuming that its rate of change with respect to the effective plastic strain, $\Delta\epsilon^p$, is given by the slope of uniaxial stress versus plastic strain curve ($H' = \frac{d\sigma}{d\epsilon^p}$) at $\sigma = \sigma_e$. Thus

$$H' = \frac{\Delta\sigma_e}{\Delta\epsilon^p} \tag{8.27}$$

The increment in effective plastic strain, $\Delta\epsilon_e^p$, is defined as

$$\begin{aligned}\Delta\epsilon_e^p &= \frac{\{\sigma\} \{\Delta\epsilon\}}{\sigma_e} \\ &= \frac{2}{3}\phi\sigma_e\end{aligned}\quad (8.28)$$

i.e. when

$$\sigma = \sigma_e \quad (8.29)$$

and

$$\begin{aligned}\Delta\epsilon &= \Delta\epsilon^p \\ &= \frac{\phi\partial\sigma_e^2}{3\partial\sigma_e} \\ &= \frac{2}{3}\phi\sigma_e\end{aligned}\quad (8.30)$$

By using geometric relationship that

$$\begin{aligned}H' &= \frac{d\sigma_e}{d\epsilon_e^p} \\ &= \frac{E_\theta E_t(\theta)}{E_\theta - E_t(\theta)} \\ \Delta\sigma_e &= \frac{E_\theta E_t(\theta)}{E_\theta - E_t(\theta)} \Delta\epsilon_e^p\end{aligned}\quad (8.31)$$

where $E_t(\theta)$ is the tangential modulus at elevated temperature obtained from stress-strain-temperature relationship. Substituting Equation (8.30) into Equation (8.31) yields

$$\Delta\sigma_e = \frac{2}{3}\phi\sigma_e \frac{E_\theta E_t(\theta)}{E_\theta - E_t(\theta)} \quad (8.32)$$

But

$$\begin{aligned}\Delta(\sigma_e^2) &= 2\sigma_e \Delta\sigma_e \\ &= \frac{3E_\theta}{1-\nu^2} (S_3 - \phi S_4)\end{aligned}\quad (8.33)$$

Thus

$$\phi = \frac{S_3}{S_5} \quad (8.34)$$

in which

$$S_5 = S_4 + (1 - \nu^2) \frac{4}{9} \sigma_e^2 \frac{E_t(\theta)}{E_\theta - E_t(\theta)} \quad (8.35)$$

By following a similar procedure in establishing an elastic-perfectly plastic material the stress-strain relationship including strain hardening can be established by substituting S_5 for S_4 in the $[F]$ matrix.

Live Energy Function F_e :

The equilibrium of a plate can be specified using an energy formulation. Consider Φ to be the total energy of the plate i.e.

$$\Phi = \Phi^I + \Phi^E \quad (8.36)$$

where

Φ^I is the work done against internal force

Φ^E is the work done by the external forces

The increment of work is

$$\Delta\Phi = \Delta\Phi^I + \Delta\Phi^E \quad (8.37)$$

where

$$\Delta\Phi^I = \int_v \Psi^I dv \quad (8.38)$$

in which

$$\Psi^I = \left\{ \{\sigma\} + \frac{1}{2} \{\Delta\sigma\} \right\}^T \{\Delta\epsilon\} \quad (8.39)$$

and

$$\Delta\Phi^E = \int_{-b/2}^{+b/2} \Psi_1^E dy + \int_{-\lambda/2}^{+\lambda/2} \Psi_2^E dx \quad (8.40)$$

Since uniaxial compression is considered in this analysis only

$$\Psi_1^E = -\lambda \int_e^{e+\Delta e} N_x de \quad (8.41)$$

is evaluated.

Since the value of end shortening, Δe , in any increment is fixed it is independent of the displacement parameters and has no influence on the minimization procedure. Only the internal energy $\Delta\Phi^I$ varies with the displacement parameters. Thus

$$F_e = \Delta\Phi^I \quad (8.42)$$

In the case of biaxial loading the additional energy terms would be included in the definition of F_e and it would no longer be equivalent to the internal energy of the system. This additional potential energy is given by

$$\Delta\Phi_2^E = \int_{-\lambda/2}^{+\lambda/2} \Psi_2^E dx \quad (8.43)$$

where

$$\Psi_2^E = 2 \int_{ve}^{ve+\Delta ve} N_y \cdot dve \quad (8.44)$$

and

$$F_e = \Delta\Phi^I - 2N_y \int_{-\lambda/2}^{+\lambda/2} \Delta ve \cdot dx \quad (8.45)$$

Gradient of F_e

In order to ensure an efficient minimisation procedure the first derivatives of the live energy function, F_e , are required. These are

$$\begin{aligned} \frac{\partial F_e}{\partial \chi_i} &= \frac{\partial(\Delta\Phi^I)}{\partial \chi_i} \\ &= \int_v \frac{\partial(\Psi^I)}{\partial \chi_i} dv \end{aligned} \quad (8.46)$$

where

$$\begin{aligned} \frac{\partial(\Psi^I)}{\partial \chi_i} &= \left\{ \{\sigma\} + \frac{1}{2} \{\Delta\sigma\} \right\}^T \left\{ \frac{\partial(\Delta\epsilon)}{\partial \chi_i} \right\} \\ &+ \frac{1}{2} \left\{ \frac{\partial(\Delta\sigma)}{\partial \chi_i} \right\}^T \{\Delta\epsilon\} \end{aligned} \quad (8.47)$$

in which χ_i are the displacement variables.

The derivatives of the incremental stress-strain relation with respect to χ_i is given with the matrix $[F]$ constant as

$$\left\{ \frac{\partial(\Delta\sigma)}{\partial \chi_i} \right\} = [F] \left\{ \frac{\partial(\Delta\epsilon)}{\partial \chi_i} \right\} \quad (8.48)$$

Thus

$$\begin{aligned}
\left\{ \frac{\partial(\Delta\sigma)}{\partial\chi_i} \right\}^T &= \left\{ \frac{\partial(\Delta\epsilon)}{\partial\chi_i} \right\}^T [F] \{\Delta\epsilon\} \\
&= \left\{ \frac{\partial(\Delta\epsilon)}{\partial\chi_i} \right\}^T \{\Delta\sigma\} \\
&= \{\Delta\sigma\}^T \left\{ \frac{\partial(\Delta\epsilon)}{\partial\chi_i} \right\}
\end{aligned} \tag{8.49}$$

i.e the matrix $[F]$ is symmetric.

This leads to

$$\begin{aligned}
\frac{\partial\Psi^I}{\partial\chi_i} &= \left\{ \{\sigma\} + \frac{1}{2} \{\Delta\sigma\} \right\}^T \left\{ \frac{\partial(\Delta\epsilon)}{\partial\chi_i} \right\} + \frac{1}{2} \{\Delta\sigma\}^T \left\{ \frac{\partial(\Delta\epsilon)}{\partial\chi_i} \right\} \\
&= \left\{ \{\sigma\} + \{\Delta\sigma\} \right\}^T \left\{ \frac{\partial(\Delta\epsilon)}{\partial\chi_i} \right\} \\
&= \{\sigma\}^T \left\{ \frac{\partial(\Delta\epsilon)}{\partial\chi_i} \right\}
\end{aligned} \tag{8.50}$$

The partial derivatives of the incremental strain with respect to the displacement parameters are given in the appendix C.

The computer program originally coded in Fortran 77 by Mofflin[173] was modified. The program utilizes the NAG library routine[174] for unconstrained minimisation of the live energy equation. Details of this approach can be found in the NAG manual.

The modified version was verified by comparing the results obtained on local buckling analysis using both programs. The modified program was found to be as accurate as the original. The stress-strain-temperature relationships were substituted into the program. It has to be pointed out that neither version simulates interactive buckling accurately. It is only local buckling analysis that can be handled effectively. With further work the method could be established

completely. This will prove useful in studying the inelastic behaviour of steel columns in fire.

Due to the lack of time the program could not be used to undertake parametric studies. It is realised that further work has to be done in order to fully establish the method.

Chapter 9

CONCLUSIONS AND RECOMMENDATIONS

The work done in this study is concerned with the development of numerical fire engineering systems and their subsequent use for parametric studies on steel column behaviour in fire. A considerable amount of valuable data has been generated which provides the basis for a better understanding of the behaviour of steel columns in fire.

9.1 Scope of the work

The present work is divided into three main parts. These include a finite strip method which is based on small deflection theory, finite element method and a large deflection finite strip method. In all cases a continuous form of stress-

strain-temperature representation is considered. However, provision is made for any stress-strain-temperature relationship to be included.

The first finite strip method is intended for the inelastic buckling analysis of columns under fire conditions. The analysis is restricted to pinned columns, without initial out-of-straightness. Other structural imperfections such as residual stress could easily be included. The column can buckle in either the overall, local or interactive modes. The material properties are modelled according to deformation theory of plasticity applied to thin plates.

The second part of the present work is based on the finite element approach. This method is capable of handling thermal gradients across the cross-section of a member, and provides a complete load-deformation and temperature-deformation history of columns.

Both methods have been used to study a number of aspects of column behaviour and several interesting points have been observed.

9.1.1 Uniformly heated columns

The general view that uniformly heated columns fail at a temperature of about 550°C is clearly not true for all columns. Columns with different slenderness ratios exhibit different failure temperatures which, in the case of slenderness ratios in the range of $80 \leq l/r \leq 100$, can be as low as 300°C as shown in Fig. 5.4. For stocky and intermediate columns, $20 \leq l/r \leq 80$, the failure temperatures range between 520°C and 300°C, while for columns with slen-

derness ratios, $80 < l/r \leq 160$, the failure temperatures range between 300°C and 510°C.

The non-linear form of the steel material properties at elevated temperature is clearly better represented as a continuous stress-strain-temperature relationship rather than in a bilinear form. The continuous representation has a considerable influence on any column's behaviour while the bilinear form results in identical behaviour for stocky and intermediate columns. However, for more slender columns the discrepancy in buckling predictions using these representations decreases. Using the two approaches the difference between the predicted column behaviour is significant for stocky columns and those with intermediate slenderness ratios, but for very slender columns the bilinear representation seems to give results very close to those of the continuous form.

The ECCS strength expressions always resulted in a very conservative estimate of the failure temperature but the recommendations of CTICM and BS5950 are in close agreement. Using different published guidelines for the stress-strain-temperature characteristics the range of failure temperatures predicted is quite large.

As is to be expected it was found that residual stresses are detrimental to the performance of steel columns in fire. In the absence of any guidance it was assumed that the magnitude of the residual stresses remains constant at increasing temperature. The effect of residual stress clearly depends on its magnitude but is also dependent on the slenderness ratio.

Eccentrically loaded columns, both stocky and intermediate, $l/r \leq 80$, show

improved performance in terms of failure temperature with increasing level of eccentricity of loading. This may not necessarily always be the case if excessive eccentricity is applied. For very slender columns, $l/r \geq 120$, the opposite is the case as the failure temperature decreases with increasing eccentricity of loading.

From the examples considered in the present study it appears that local buckling would not in general constitute a significant problem in the performance of columns in fire. In a situation where ambient - temperature design principles avoid local buckling then its influence appears to be implicitly prevented in fire. It has to be mentioned that further investigation is necessary to verify this observation fully.

In terms of bearing capacity, any of initial out-of-straightness is clearly detrimental to the performance of steel columns in fire as at ambient temperature. However, the failure temperature varies widely with increasing level of initial out-of-straightness. Stocky and very slender columns exhibit a declining failure temperature while columns with intermediate slenderness ratios show improved performance with increasing level of initial out-of-straightness in terms of failure temperature.

As at ambient temperature, columns show improved performance in terms of bearing capacity under fixed end conditions in fire, compared with equivalent pin-ended columns. However, the failure temperatures exhibited by these columns under varying end conditions depend on their slenderness ratios. Both stocky and intermediate columns exhibit higher failure temperatures for the fixed end condition compared with the pinned end condition while for slender

columns the opposite is the case.

9.1.2 Columns under thermal gradients

The blocking in of the web of columns results to symmetrical thermal gradient over the cross-section. The failure temperatures of blocked-in web columns are approximately the same as for bare columns. The major benefit offered by blocking in the web of an H-section column is therefore the reduced rate of temperature increase which accounts for the better fire resistance exhibited by the blocked-in-web columns.

For columns subject to asymmetric non-uniform heating the differential temperature distribution results in a shift of the neutral axis towards the coldest flange. The effect of the higher strength and stiffness of the colder parts is greater than the weakening influence of the induced thermal bowing. The beneficial effect of the variation of strength over the cross-section may be accountable for the improved behaviour exhibited by columns under thermal gradient compared to uniformly heated columns. It should be noted that the consideration of maximum temperature is reasonable in practice. This is particularly true if maximum temperatures are used for the analysis of bare columns, but in a situation where average temperatures are used the opposite is the case. This influences the effect of applied eccentricity of loading depending on its point of application. If non-uniformly heated columns are subject to eccentricity of loading applied along the positive direction of the shifted neutral axis the influence of induced bowing will be reduced.

The third part of the present work is based on the large deflection finite strip method using flow theory of plasticity with von Mises effective stress as a yield condition. The modification to enable elevated temperature structural analysis results in substantial remodelling of the method. Although both local and interactive buckling of plate assemblies are modelled only local buckling analysis could be implemented.

For checking purposes many computer runs of the program for local buckling analysis of stocky columns at ambient temperature were undertaken and compared with the original program results. Elevated temperature computer runs for the same problem were compared with the small deflection finite strip method. The comparison was good but because of time limitation no parametric study could be undertaken.

9.2 Recommendations for future work

Each theory presented herein can be modified in a number of ways for more parametric studies. The first method is complete and exhaustive parametric studies on the column behaviour have been undertaken. However, consideration can be given to other expressions relating strength and stiffness to temperature in order to fully evolve a suitable stress-strain-temperature relationship for steel behaviour in fire.

The finite element method can be modified to include the effect of semi-rigid connections by including experimental moment-rotation characteristics for dif-

ferent connections in the program with adequate provision for calculation of the joint stiffness matrix. This can subsequently be used for parametric studies on the inelastic behaviour of multi-storey frames in fire. In addition some other forms of construction, such as composite structures and beams, can be studied with minimum modification to the program.

The large deflection finite strip method can be used for a full range of parametric studies on the column behaviour in fire with adequate modification to establish the method for interactive buckling analysis.

Finally, in all cases the effect of thermal load on the behaviour of steel columns in fire can be considered.

Generally the present study provides a basis for further research into the behaviour of steel columns in fire. A considerable amount of valuable information has been generated at relatively low cost. This is made possible because of the flexibility of the methods to include the effect of many parameters. It is hoped that better understanding of the behaviour of steel columns in fire could be accomplished using this information. Finally, it is desirable for a more rigorous testing program to be undertaken to validate the theoretical findings.

Bibliography

- [1] Euler L. "De motu vibraorio tympanorum", *Novi Commentari Acad. Petropolit.*, 10(1766), 243-260.
- [2] Bernoulli J. "Essai theorique sur les vibrations de plaques elastiques rectangulaires et libres", *Nova Acta Acad. Petropolit.*, 5(1789), 197-219.
- [3] Bryan G.H. "On the stability of a plane plate under thrusts in its own plane with application on the buckling of the sides of a ship", *Proc. London Math. Soc.*, 1891, p.54.
- [4] Timoshenko S.P. "Einige stabilitatsprobleme der elasticitatstheorie", *Zeitschrift fur Mathematik und Physik*, 1910, p.337.
- [5] Timoshenko S.P. "Sur la stabilite des systemes elastiques", *Ann. des ponts et chaussees*, 13, 496-566, 16, 73-132, 372-412, 1913.
- [6] Reissner H. "Uber die knicksicherheit ebener bleche", *Zentralblatt der Bauverwaltung*, 1909, p.93.
- [7] Bleich F. "Theorie und berechnung der eisernen brucken", *Julius Springer, Berlin* 1924.

- [8] Kollbrunner C.F. "Das Ausbilden des auf Druck beanspruchten Kräftchenwinkels", Mitteilungen Institut für Baustatik, Eidgenössische Technische Hochschule, Zürich, 1935.
- [9] Foppl A. "Vorlesungen über technische Mechanik", vols. 3 and 5, 8th and 3rd ed., B.G. Teubner, Leipzig, 1923.
- [10] Timoshenko S.P. and Gere, J.M. "Theory of elastic stability", 2nd edition, McGraw-Hill, New York, 1961
- [11] Bulson, P.S. "The stability of flat plates", Chatto and Windus, London, 1970.
- [12] Allen, H.G. and Bulson, P.S. "Background to buckling", McGraw-Hill, U.K, 1980
- [13] Kaiser, R. "Rechnerisch und experimentelle Ermittlung der Durchbiegungen und Spannungen von quadratischen Platten bei freier Auflagerung an den Rändern", gleichmäßig verteilter Last und grossen Ausbiegungen, ZAMM p73-98, 1936
- [14] Way S "Uniform loaded, clamped, rectangular plate with large deflection", Proc. 5th Int. Cong. for appl. mech. (Cambridge Mass, 1938), John Wiley and sons, New York p123-128, 1939
- [15] Levy S. "Bending of rectangular plates with large deflections", NACA, TN No 846, 1942
- [16] Wang, C.T. "Nonlinear large deflection boundary-value problems of rectangular plates", NACA, TN, No 1425, 1948

- [17] Basu, A.K. and Chapman, J.C. "large deflection behaviour of transversely loaded rectangular orthotropic plates", Proc. Inst. Civ. Engr., vol 35, 1966
- [18] Levy S. "Bending of rectangular plates with large deflections" NACA 28th Annual Report, TR No 737, p139-157, 1942b
- [19] Woolley R.M, Corrick J.N and Levy S "Clamped long rectangular plate under combined axial load and normal pressure", NACA TN No 1047, 1946
- [20] Timoshenko S.P and Woinowsky-Krieger S. "Theory of plates and shells", 2nd edition, McGraw-Hill, New York, 1959
- [21] Bleich F "Buckling strength of metal structures", McGraw-Hill , New York, 1952
- [22] von Karman, Th: "Festigkeitsprobleme im maschinenbau", Encyclopadie de mathematischen wissenschaften, Teilband IV.4, Teubner, Leipzig 1910, p348-350
- [23] Marguerre K "Zur theorie der gekrummten platten grosser formanderung", Proc 5th Int. Cong. for Applied Mech. (Cambridge Mass, 1938) , John Willey and sons, New York, 93-101, 1939
- [24] Hu P.C, Lundquist E.E and Batdorf S.B "Effect of small deviations from flatness on effective width and buckling of plates in compression", NACA, TN No 1124, 1946

- [25] Coan J.M "Large-deflection theory for plates with small initial curvature loaded in edge compression", Trans. AMSE. Jour. of Applied Mech. p143-151, 1951
- [26] Yamaki N. "Postbuckling behaviour of rectangular plates with small initial curvature loaded in edge compression", Trans. ASME Jour. of Applied Mech. p407-414, 1959
- [27] Bauer L and Reiss E.L "Nonlinear buckling of rectangular plates", New York University Report IMM-316, 1963
- [28] Murray D.W and Wilson E.L "Finite element postbuckling analysis of thin elastic plates", AIAA Jour. vol. 17, No 10, p1915-1920, Oct. 1969
- [29] Vos R.G and Vann W.P "A finite element tensor approach to plate buckling and postbuckling", Int. Jour. for Num. Method in Engg., vol 5 p351-365, 1973
- [30] Crisfield M.A and Puthli R.S "A finite element method applied to the collapse analysis of stiffened box girders diaphragms" Steel plated Struct. Ed. P.J Dowling, J.E Harding and P.A Frieze, Crosby Lockwood Staples, London
- [31] Rojas-Gutierrez R. "Elastic stability of box girder sections ", Ph.D Thesis, University of Sheffield, 1978
- [32] Dwight J.B and Ratcliffe A.T "The strength of thin plates in compression", Symposium on thin-walled steel structures, Swansea, 1967

- [33] Dwight J.B and Moxham K.E "Compressive strength of welded plates",
Int colloquium on stability of struct. under static and dynamic loads,
p462-481, New York
- [34] Little G.H "Plate failure in stiffened steel compression panels", Cam-
bridge University Report No CUED/C-STRUCT/TR 33, 1973
- [35] Dwight J.B and Harrison J.D "Local buckling problems in steel
columns", BWRA Research Report No M9/63, March, 1963
- [36] Dwight J.B and Moxham K.E "Welded steel plates in compression",
Struct. Engineer, vol 47, No 2, p49-66, Feb. 1969
- [37] Little G.H and Dwight J.B "Compressive tests on plates with transverse
welds", Cambridge University Report No CUED/C-STRUCT/TR 31,
1972
- [38] Frieze P.A, Dowling P.J and Hobbs R.E "Ultimate load behaviour of
plates in compression", An Int. Symposium on Steel Plated structure
Imperial College, London, July 1976
- [39] Harding J.E, Hobbs R.E and Neal B.G. "Ultimate load behaviour of
plates under combined direct and shear in-plane loading" , An Int. Sym-
posium on Steel Plated Struct. Imperial College, London, July 1976
- [40] Little G.H. "Rapid analysis of plates collapse by live-energy minimisa-
tion", Int. Jour. Mech. Sci. Vol. 19, p725-744, 1977
- [41] Little G.H "Collapse of rectangular steel plates under uniaxial compres-
sion", The Structural Engineer, vol. 58B, No 3, p45-61 , Sept. 1980

- [42] Crisfield M.A "Large-deflection elasto-plastic buckling analysis of plates using finite elements", TRRL Report LR 593, Crowthorne, 1973
- [43] Ilyushin A.A "Plasticite", Editions Eyrooes, Paris, 1956
- [44] Crisfield M.A "On an approximate yield criterion for thin steel shells", TRRL, Crowthorne, Report LR 658, 1974
- [45] Kaldas M.M and Dickinson S.M "Elastic critical buckling of welded thin steel rectangular plates", Jour. Struct. Mech. 12(2) p199-218, 1984
- [46] Dow R.S and Smith C.S. "Effects of localised imperfections on compressive strength of long rectangular plates", Jour. Constr. Steel Research, 4 p51-76, 1984
- [47] Bradfield C.D and Stonor R.W "Simple collapse analysis of plates in compression", Jour. of Struct. Engg. vol. 110, No 12, p2976-2993, December 1984
- [48] Dawe J.L and Grondin G.Y "Inelastic buckling of steel plates" Jour. of Struct. Engg. vol. 111, No 1 p95-107, January 1985
- [49] Voyiadjis G.Z, Baluch M.H and Chi W.K "Effect of shear and normal strain on plate bending", Jour. of Engineering Mech., vol. 111, No 9, p1130-1143, September 1985
- [50] Mahendran M. and Murray N.W "Elastic buckling analysis of ideal thin-walled structures under combined loading using a finite strip method", Thin-walled Structures 4, p329-362, 1986

- [51] Gradkzi R. and Kowal-Michalska K. "Stability in the elasto-plastic range of rectangular plates subjected to uniaxial compression with unloaded edges clamped", *Thin-walled Structures* 5, p93-109, 1987
- [52] Shanley F.R "Inelastic column theory", *Jour. of Aeronut. Sci.* 14, May 1947
- [53] Bijlaard P.P and Fisher G.P "Column strength of H-sections and square tubes in post buckling range of component plates", *NACA TN 2994*, August, 1953
- [54] Cherry S. "The stability of beams with buckled compression flanges", *The Structural Engineer*, vol. 38, p277-285, 1960
- [55] Skaloud M and Zornerora M "Experimental investigation into the interaction of the buckling of compressed thin-walled columns with the bucking of their plate elements", *Acta Technica, CSAV*, No 4, Prague, Czechoslovakia, 1970
- [56] Goldberg J.E, Bodganoff J.L and Glonz W.D "Lateral and torsional buckling of thin-walled beams", *IABSE* vol. 24, p91-100, 1964
- [57] DeWolf J.T, Pekoz T. and Winter G. "Local and overall buckling of cold-formed members", *Jour. of the Struc. Div. ASCE*, vol. 100, No ST10, p2017-2036, October 1974
- [58] Kalyanaraman V, Pekoz T and Winter G. "Unstiffened compression elements", *Jour. of Struc. Div. ASCE*, vol. 103, No ST9, p1833-1848, September 1977

- [59] Winter G "Strength of thin steel compression flanges", Trans. ASCE vol. 112, paper No 2305, p527-576. 1947
- [60] Winter G "Thin walled structures—Theoretical solutions and test results", preliminary publication of Eight congress, IABSE, p101-112 , 1968
- [61] Kalyanaraman V "Local buckling of cold-formed steel members", Jour. Struc. Div. ASCE, vol. 105 No ST5, p813-828, May 1979
- [62] Stowell E.Z "A unified theory of plastic buckling of columns and plates", NACA TN 1556, 1958
- [63] Gale P.M and Pekoz T "Locally buckled thin-walled columns", Jour. Struc. Engg. vol. 110 n11, p2635-2654, November 1984
- [64] Tsutomu U and Fukumoto Y "Welded box compression members", ASCE Jour. Struc. Eng. vol. 110, No 10, p2457-2470, October 1984
- [65] Gale P.M and Pekoz T.J "Local buckling interaction in cold- formed columns", Jour. Struc. Eng. vol. 113, No 3, p604-620, March 1987
- [66] Lee S.L, Chiew S.P and Shanmugam N.E "Local and overall buckling of steel box column", Steel Struc. Advances, design and construction , Elsevier, 1987
- [67] Longhlan J and Howe D "The influence of local buckling on the behaviour of some thin-walled compression members", Steel Struc. Advances, Design and Construction, Elsevier, 1987
- [68] Yoshida H and Maegawa K "Local and member buckling of H-columns", Jour. Struc. Mech. vol. 6 p1-27, 1978

- [69] Hancock J.G "Nonlinear analysis of thin sections in compression", The University of Sidney, school of civil engineering research report R355, November 1979
- [70] Hancock J.G "Interactive buckling in I-sections", ASCE , Jour. Struc. Div. vol. 107, No 1 p165-179, 1981
- [71] Graves Smith T.R "The ultimate strength of locally buckled columns of arbitrary length", Symposium on Thin-walled steel structures, Swansea, 1967
- [72] Graves Smith T.R "The effect of initial imperfections on the strength of thin-walled box columns", Int. Jour. Mech. Sci. vol.13, p911-925, 1971
- [73] Graves Smith T.R and Sridharan S. "The local collapse of elastic thin-walled columns", Jour. Struc. Mech. vol. 8, No 4, p471-489, 1980
- [74] Little G.H "Local and overall buckling of square box columns", Cambridge University Report No CUED/C-STRUCT/TR 56, 1976
- [75] Srinivasan S. and Ashraf Ali M "Interactive buckling in thin-walled beam-columns", Jour. Eng. Mech. vol. 111, No 12, December 1985
- [76] Rafeal B and Sridharan S "Interactive buckling analysis with finite strips", Int. Jour. Numerical Method Eng. vol. 21, p145-161, 1985
- [77] Hancock J.G and David A.J "Strength tests of thin-walled high strength column", Steel Struc. Advances, Design and Construction, Elsvie, 1987
- [78] BS5950 Pt1, 1985 Structural Use of Steelwork in Building
- [79] AISI, Manual of Steel Construction, 7th ed., N.Y., 1970

- [80] Standards Association of Australia, Steel Structures Code AS1250, 1981
- [81] Encyclopedia of physics, "Elasticity and Plasticity ", Edited by Flugge S., vol. VI, Springer-Verlag, Berlin, 1958
- [82] Bijlaard P.P "Theory and tests on the plastic stability of plates and shells", Jour. Aeron. Sci. 9, p529-541, 1949
- [83] Handleman G.H and Prager W. "Plastic buckling of rectangular plates under edge thrust", Tech. Note, NACA 1530, 1948
- [84] Batdorf S.B "Theories of plastic buckling", Jour. Aero. Sci. 16, p405-408, 1949
- [85] Pearson C.E "Bifurcation criteria and plastic buckling of plates and columns", Jour. Aero. Sci. 7, p417-424, 1950
- [86] Onat E.T and Drucker D.C "Inelastic stability and incremental theories of plasticity", Jour. Aero. Sci. 5, p181-186, 1953
- [87] Hutchinson J.W. and Budiansky B "Analytical and numerical study of the effects of initial imperfection on the inelastic buckling of a column", Buckling of Structures, edited by Budiansky B., p98-105, Springer, Berlin, 1976
- [88] Neal K.W. "Effect of imperfection on the plastic buckling of rectangular plates", ASME, Applied Mech. Div. p115-120, March 1975
- [89] Sanders J.L. 'Plastic stress-strain relations based on linear loading functions", Proc. 2nd U.S Nat. Congr. Applied Mech. p455-460, University of Michigan, Ann Arbor, 1963

- [90] Hutchinson J.W. "Plastic buckling", *Advances in Applied Mech.*, vol. 14, p67-144, 1974
- [91] Yamada Y., Yoshimura N. and Sakurai T. "Plastic stress-strain matrix and its application for the solution of elasto-plastic problems by the finite element method", *Int. Jour. of Mech. Sci.* 10, p343-354, 1968
- [92] Damkilde L. "Elasto-plastic buckling of a finite length cruciform column", *Computer and structure* vol. 21 No 3, p521-528, 1985
- [93] Shrivastara S.C "Inelastic buckling of plates including shear effects", *Int. Jour. Solids Structures* vol. 15, p567-575 , 1979
- [94] Wittrick W.H. "A unified approach to the initial buckling of stiffened panels in compression", *Aero. Quarterly* 19, 1968
- [95] Wittrick W.H. "General sinusoidal stiffness matrices for buckling and vibration analysis of thin flat-walled structures", *Int. Jour. Mech. Sci.* 10, 1968
- [96] Wittrick W.H. and Williams F.H. "A general algorithm for computing natural frequencies of elastic structures", *Quart. Jour. Mech. Appl. Math.* 24 1971
- [97] Williams F.W. and Wittrick W.H. "Computational procedure for a matrix analysis of the stability and vibration of thin flat-walled structures in compression", *Int. Jour. Mech. Sci.* vol. 11, p979-998, 1969
- [98] Wittrick W.H. and Williams F.W. "Buckling and vibration of anisotropic plate assemblies under combined loadings", *Int. Jour. Mech. Sci.* 16, 1974

- [99] Plank R.J. and Wittrick W.H. "Buckling under combined loading of thin flat-walled structures by complex finite strip method", *Int. jour. Num. Method Engg.* 8 1974
- [100] Cheung Y.K. "The finite strip method in structural analysis", Pergamon Press Ltd. 1976
- [101] Loo Y.C. and Cusens A.R. "The finite strip method in bridge engineering", *A viewpoint*, 1978
- [102] Hinton E. "A note on a thick finite strip method for the free vibration of laminated plates", *Earthquake Eng. and Struc. Dynamics*, vol. 4, p511-520, 1976
- [103] Hinton E. "Buckling of initially stressed mindling plates using finite strip method", *Computer and Structure*, vol. 8, p599-607, 1978
- [104] Thanghan P.V. and Reddy D.V. "Stability analysis of skew orthotropic plates by finite strip method", *Computer and Structure*, vol. 8, p599-607, 1978
- [105] Viswanathan A.V. and Tamekumi M. "Elastic buckling analysis for composite stiffened panels and other structures subjected to biaxial in-plane loads", *NASA CR-2216*, 1973
- [106] Williams F.W. "Approximations in complicated critical buckling and free vibration analysis of prismatic plate structures", *Aeronautical Quarterly* 25, 1974
- [107] Plank R.J. and Williams F.W. "Critical buckling of some stiffened panels in compression, shear and bending", *Aero. Quart.*, 25, 1974

- [108] Chan H.C and Cheung Y.K. "Static and dynamic analysis of multi-layered sandwich plates ", Int. Jour. Mech. Sci. vol. 14, p399-406, 1972
- [109] Fukumoto Y., Usami T. and Yamaguchi K. "Inelastic buckling strength of stiffened plates in compression", IABSE proceedings , 1977
- [110] Graves Smith T.R. and Sridharan, S. "A finite strip method for the post-locally buckled analysis of plate structures", Int. Jour. Mech. Sci. vol. 20, p833-842, 1978
- [111] Sridharan S. "Elastic post-buckling behaviour and crinkly collapse of plate structures", Ph.D Thesis, Southampton University, 1978
- [112] Graves Smith T.R. and Sridharan S. "The local collapse of elastic thin-walled columns", Jour. Struct. Mech. Vol. 8, p471-489, 1980
- [113] Fau S.C. "Spline finite strip in structural analysis", Ph.D thesis, University of Hong Kong, 1982
- [114] Cheung Y.K. and Fau S.C. "Static analysis of right box girder bridge by spline finite strip method", Proc. Inst. of Civil Engineers, Pt2, vol. 75, p311-323, 1983
- [115] Fau S.C. and Cheung Y.K. "Analysis of shallow shells by spline finite strip method", Engineering Structure, 5, p255-262, 1983
- [116] Lau S.C.W. and Hancock G.J. "Buckling of thin flat-walled structures by a spline finite strip method", Thin-walled Struct. 4, p269-294, 1986
- [117] Bruce W.G., Williams A.G. and Joseph P. "Plate bending analysis using finite strip-element", Jour. of Struc. Engg., vol. 113, No 6, June 1987

- [118] Bogner F.K., Fox R.L. and Schmidt L.A. "The generation of interrelated compatible stiffness and mass matrices by the use of interpolation formulae", Proc. conf. on Matrix Methods in Struc. Mech., Wright Patterson and Force Base, Ohio, 1965
- [119] Graves Smith T.R., Gierlinski J.T. and Walker B. "A combined finite strip and finite element methods for analysing thin-walled structures", Thin-walled Struc. 3 p163-180, 1985
- [120] ISO, Fire resistance tests-Elements of building construction, International Standard 834, 1975
- [121] Robin Sharples, "The strength of partially exposed steel columns in fire", Sheffield University, M. Phil Thesis, September 1987.
- [122] Lie T.T. and Harmathy T.Z. "A numerical procedure to calculate the temperature of steel columns exposed to fire", National Research Council of Canada, Div. of Building Research, NRCC 12535, Ottawa, 1972
- [123] Bennetts I.D., Proe D.J. and Thomas I.R. "Simulation of the fire testing of structural elements by calculation-thermal response", Steel Constr. Jour. of Australian Instit. of steel construction vol. 19, No 3, February 1986
- [124] Law M. and O'Brient T. "Fire safety of bare external steelwork, Constrado, London
- [125] BS476 Pt8 Test methods and criteria for the resistance of elements of building construction, 1972

- [126] Latham D.J. "Practical fire engineering-The use of unprotected steelwork in building", National Struct. Steel conf.-Development in multi-storey buildings, 1984
- [127] Knublauch E., Rudophi R. and Stanke J. "Theoretische ermittlung der feuerwiderstandslauer vor stahlstutzen und vergleich mit versuchen Teil2, Bestimmung der Kristischen Stahltemperatur, Der Stahlben, 8/74
- [128] European Convention for Constructional steelwork (ECCS) " European recommendation for the fire safety of steel structure", Elsevier scientific publishing Co. Amsterdam, 1983
- [129] Kerstma J., Bijlaard F.S.K. and Twilt L. "Analysis of the gap between the TNO-IBBC buckling curves and the results of full-scale tests", 1979
- [130] Stanke J. "Fenerwidertandsdaner von Stahlstutzen mit behinderter Langsdehnung Bundesanstalt fur Materialprufung, (BAM), Berlin, 1977
- [131] Magnusson S.E., Pettersson O. and Thor J. "Fire engineering design of steel structures" Swedish institute of steel construction , Publication 50, Stockholm, 1976
- [132] Vandamme M. and Janss J. "Buckling of axially loaded steel columns in fire conditions", IABSE proceedings P-43/81
- [133] Janss J. and Minne R. "Buckling of steel columns in fire conditions", Fire Safety Jour. No 4, 1981/82
- [134] European Convention for Constructional Steelwork (ECCS) , European recommendations for steel construction, 1978

- [135] Pettersson O. and Witteveen J. "On the resistance of structural steel elements derived from standard fire tests or by calculation", Fire Safety Jour. No 2, 1979/80
- [136] Olesen F.B. "Fire tests on steel columns", Inst. Building Tech. Structural engineering, Aalborg, Denmark, 1980
- [137] Hoffend F. "Brandverhalten von Stahlstützen bei ausmittiger Lasteinwirkung, Dehnbehinderung ode teilweiser Bekleidung, Sonderforschungsbereich 148, Brandverhalten von Bauteilen. Arbeitsbericht 1978-80, Teil, Tech. Univer.
- [138] Hoffend F., Kordina K. and Meyer-Ottens C. "Nene Prufvorschriften fur Stahlstützen bei Braudprüfungen nach DIN4102 Teil DIN-Milterlung 63, Nr 3 1984
- [139] Hoffend F. and Kordina K. "Versagentemperaturen crit von braudbeanspruchten stahlstützen aus Walzprofilen, Der Stahlbau, 1984
- [140] Aasen Bjorn and Larsen P.K. "Fire simulated tests of high strength steel columns", Steel structures, Advances, Design and Construction, Elsevier, 1987
- [141] Aribert J.M. et Randriantsara C. "Etude du flaubement a des temperatures d'incendie-Action du fluage", Construction Metallique, No 4, 1980
- [142] Fujimoto M., Furumura F. and Ave T. "Creep buckling of steel columns at high temperature ", Report of the Research Laboratory of Engineering Materials, Tokyo Institute of Technology, November 1982

- [143] Fujimoto M., Furumura F., Ave T. and Kim W.J. "Further studies of the creep buckling of steel columns at high temperature" , Report of the Research Laboratory of Engineering Materials, Tokyo Institute of Technology, November 1983
- [144] Alpsten G. "On numerisk simulering av barformagan hos Oisolerade Stalpelare utsatta for brandpaverkan. Nordiska forskningsdagar for stalbyggguad, Stockholm, 1970
- [145] Culver C.G. "Steel column buckling under thermal gradients" ASCE Jour. Struct. Div. ST8, August, 1972
- [146] Culver C.G., Aggarwal V. and Ossenbruggen P.J. "Buckling of steel columns at elevated temperature", ASCE, Jour. Struc. Div., April 1973
- [147] Ossenbruggen P.J., Aggarwal V. and Culver C.G. "Steel column failure under thermal gradients", ASCE, Jour. Struc. Div. April 1973
- [148] Proe D.J., Thomas I.R. and Bennetts I.D. "Simulation of the fire testing of structural elements by calculations-Mechanical response ", Steel Construction Journ. of the Australian Inst. of steel construction , vol. 19, No 4, February 1986
- [149] Method de prevision par le calcul du comportement au des structures en acier-Adoptee par le Groupe de coordination des textes techniques (DTU) Construction Metallique, vol. 13 No 4, December 1976.
- [150] Setti P. "Buckling of axially loaded steel columns with imperfections at elevated temperature", Third Int. Colloquium on stability of metal structures. Preliminary Report CTICM, Paris

- [151] Witteveen J., Twilt L., and Bijlaard F.K.S. "Theoretical and experimental analysis of steel structures at elevated temperatures", IABSE , 10th Congress, Tokyo, Final Report, Zurich, 197
- [152] Witteveen J. and Twilt L., "Behaviour of steel columns under fire actions", Int. Colloquium on column strength, Paris 1972, IABSE, vol. 23
- [153] Eggwertz S. "Creep buckling of steel column at elevated temperatures", IABSE 10th Congress, Tokyo, Preliminary Report, Zurich, 1976
- [154] Harmathy T.Z. "A comprehensive creep model", Trans, ASME Jour. Basic Engineering, 1967
- [155] Randriantsara C. "Etude critique du flambement des poteaux metalliques dans les conditions d'incendie", Thesis INSA, Rennes, 1984
- [156] Proe D.J., Thomas I.R. and Bennetts I.D. "Simulation of the fire testing of structural elements by calculations-Overall behaviour", Steel Construction Jour. of the Australian Instit. of steel construction, vol. 19 No 4, February 1986
- [157] Muzeau J.P. and Lamaire M. "Modele numerique de comportement d'ossature en acier sous forte elevation de temperature", Construction Metallique, No 3, 1980
- [158] Schleich J.B., Dotreppe J.C. and Franssen J.M. "Numerical simulations of fire resistance tests on steel and composite structural elements or frames", Fire Safety Sci.-Proceedings of the first international symposium, October 1985

- [159] Furumora F. and Shinhara Y. "Inelastic behaviour of protected steel columns in fire", Report of the Research Laboratory of Engineering Materials, NO2, Tokyo, 1977
- [160] Witteveen J. "Design methods for fire exposed steel structures", Steel in Building, IABSE-ECCS symposium, Luxemburg, 1985
- [161] Nabil S. Mahmoud, "Inelastic stability of plate structures using finite strip method", Sheffield University, PhD Thesis 1981
- [162] BS5950 Pt8 Draft form of Fire Code for Fire exposed Steel Structures.
- [163] Strymowicz G. and Horsley P.D.M. "Strut behaviour of a new high yield stress structural steel", The structural Engineer, vol. 47 p73-78
- [164] Tebedge N., Chen W. and Tall L. "Experimental studies in column strength of European heavy shapes", International colloquium on column strength, IABSE, Paris, November 1972
- [165] Dibley J.E. "Lateral torsional buckling of I-sections in Grade 55 steel", Proc. of the Inst. of Civil Eng., vol. 43 p599-627
- [166] British Steel Corporation, Report No RSC/7281/1/85
- [167] BS449 Pt.2 1969 The Use of Structural Steel in Building
- [168] Ramberg W. and Osgood W.R., "Description of stress-strain curves by three parameters", NACA Technical Note No 902, 1943
- [169] Al-Zanaty M.H., Murray D.W. and Bjorhorde R., "Inelastic behaviour of multi-storey steel frames", University of Alberta, 1980

- [170] Cooke G., "The structural response of steel I-section members subjected to elevated temperature gradient across the section, The City University, London, September 1987
- [171] British Steel Corporation, Report No SH/RS/3664/6/84/B
- [172] Pifko A. and Isakson G. "A finite element method for the plastic buckling analysis of plates", AIAA Jour. vol. 7 no 10, 1950
- [173] Moffin D.S. "Manual for use of computer program LOBUC", CUED/D-Struct/TR. 105 (1984)
- [174] Numerical Algorithm Group (NAG) manuals.
- [175] Fire resistant steel structures: free-standing blockwork-filled columns and stanchions. Building Research Establishment Digest, December 1986.

Appendix A

For the purpose of completeness the expression for the out-of-plane and in-plane stiffness and stability matrices are given in this appendix.

The out-of-plane stiffness equation is

$$[K_o] = \int_{vol} [B_o]^T [F] [B_o] dvol \quad (A1)$$

in which

$$[B_o] = \begin{bmatrix} z \frac{\pi^2}{\lambda^2} \{Z\}^T \sin \pi \xi \\ -\frac{z}{b^2} \{Z'_{\eta\eta}\}^T \sin \pi \xi \\ \frac{2\pi z}{b\lambda} \{Z'_\eta\}^T \cos \pi \xi \end{bmatrix} \quad (A2)$$

and

$$[F] = \begin{bmatrix} f_{11} & f_{12} & 0 \\ f_{12} & f_{22} & 0 \\ 0 & 0 & f_{33} \end{bmatrix} \quad (A3)$$

The coefficients of the matrix $[F]$ are given in Equation (3.4). Substituting for $[B_o]^T$, $[F]$ and $[B_o]$ in Equation (A1), knowing that

$$\begin{aligned} \int_0^1 \sin^2(\pi \xi) d\xi &= 1.0 \\ \int_0^1 \cos^2(\pi \xi) d\xi &= 1.0 \end{aligned} \quad (A4)$$

and carrying out the integration with respect to z the out-of-plane stiffness matrix $[K_o]$ is

$$\begin{aligned} [K_o] &= \int_0^1 \left[a_4 f_{11} \{Z\} \{Z\}^T - a_5 f_{12} \left[\{Z'_{\eta\eta}\} \{Z\}^T \right. \right. \\ &\quad \left. \left. + \{Z\} \{Z'_{\eta\eta}\}^T \right] + a_6 f_{22} \{Z'_{\eta\eta}\} \{Z'_{\eta\eta}\}^T \right. \\ &\quad \left. + a_7 f_{33} \{Z'\} \{Z'_\eta\}^T \right] d\eta \end{aligned} \quad (A5)$$

Similarly the in-plane stiffness matrix $[K_i]$ is obtained by substituting the $[B_i]$ matrix given by

$$[B_i] = \begin{bmatrix} -\frac{\pi}{\lambda} \{X\}^T \sin \pi \xi \\ \frac{1}{b} \{Y'_\eta\}^T \sin \pi \xi \\ \left(\frac{1}{b} \{X'_\eta\}^T + \frac{\pi}{\lambda} \{Y\}^T \right) \cos \pi \xi \end{bmatrix} \quad (A6)$$

into

$$[K_i] = \int_{vol} [B_i]^T [F] [B_i] dvol \quad (A7)$$

Thus the in-plane stiffness matrix $[K_i]$ is

$$\begin{aligned} [K_i] = & \int_0^1 \left[a_1 f_{11} \{X\} \{X\}^T - a_2 f_{12} \left[\{Y'_\eta\} \{X\}^T \right. \right. \\ & + \left. \left. \{X\} \{Y'_\eta\}^T \right] + a_3 f_{22} \{Y'_\eta\} \{Y'_\eta\}^T \right. \\ & + f_{33} \left[a_3 \{X'_\eta\} \{X'_\eta\}^T + a_2 \left[\{Y\} \{X'_\eta\}^T \right. \right. \\ & + \left. \left. \{X'_\eta\} \{Y\}^T \right] + a_1 \{Y\} \{Y\}^T \right] d\eta \end{aligned} \quad (A8)$$

The constants in the stiffness equations (Equations (A5) and (A8)) are

$$\begin{aligned} a_1 &= \pi^2 b \frac{t}{b} \\ a_2 &= \pi t \\ a_3 &= \lambda \frac{t}{b} \\ a_4 &= \frac{\pi^4 b t^3}{12 \lambda^3} \\ a_5 &= \frac{\pi^2 t^3}{12 \lambda b} \\ a_6 &= \frac{\lambda t^3}{12 b^3} \\ a_7 &= \frac{\pi^2 t^3}{3 b \lambda} \end{aligned}$$

The out-of-plane stability matrix $[S_o]$ is

$$[S_o] = \int_{vol} [B_{so}] \{\sigma\}^T dvol \quad (A9)$$

and the $[B_{so}]$ matrix is given by:

$$[B_{so}] = \begin{bmatrix} \frac{1}{\lambda^2} [N'_{o,\xi}]^T [N'_{o,\xi}] \\ \frac{1}{b^2} [N'_{o,\eta}]^T [N'_{o,\eta}] \\ \frac{1}{b\lambda} \{ [N'_{o,\eta}]^T [N'_{o,\xi}] [N'_{o,\xi}]^T [N'_{o,\eta}] \} \end{bmatrix} \quad (A10)$$

Substituting the expressions for $[B_{so}]$ and $\{\sigma\}^T$ into the out-of-plane stability matrix $[S_o]$ and considering only uniaxial compression i.e $\sigma_y = \tau_{xy} = 0$ results in

$$[S_o] = \int_0^1 \int_0^1 \int_{-t/2}^{+t/2} \frac{b\sigma_x}{\lambda} [N'_{o,\xi}]^T [N'_{o,\xi}] dz d\xi d\eta \quad (A11)$$

where

$$[N_o] = \{ \{Z\}^T \sin \pi \xi \}^T \quad (A12)$$

Differentiating $[N_o]$ with respect to ξ yields

$$[N'_{o,\xi}] = \pi \{ \{Z\}^T \cos \pi \xi \}^T \quad (A13)$$

and

$$[N'_{o,\xi}]^T = \pi \{ \{Z\}^T \cos \pi \xi \} \quad (A14)$$

Substituting Equations (A13) and (A14) into Equation (A11), carrying out the integration with respect to z and ξ , and taking note of the conditions of Equation (A4) then out-of-plane stability matrix is

$$[S_o] = \frac{bt\pi^2}{\lambda} \int_0^1 \sigma_x \{Z\} \{Z\}^T d\eta \quad (A15)$$

Similarly the in-plane stability matrix $[S_i]$ is

$$[S_i] = \int_0^1 \int_0^1 \int_{-t/2}^{+t/2} \frac{b\sigma_x}{\lambda} [N_{i,\xi}]^T [N_{i,\xi}] dz d\xi d\eta \quad (A16)$$

where

$$[N_i] = [\{X\}^T \cos \pi\xi \quad \{Y\}^T \sin \pi\xi] \quad (A17)$$

Differentiating $[N_i]$ with respect to ξ yields

$$[N'_{i,\xi}] = \pi[-\{X\}^T \sin \pi\xi \quad \{Y\}^T \cos \pi\xi]^T \quad (A18)$$

and

$$[N'_{i,\xi}]^T = \pi[-\{X\} \sin \pi\xi \quad \{Y\} \cos \pi\xi]^T \quad (A19)$$

Substituting the expressions for $[N'_{i,\xi}]^T$ and $[N'_{i,\xi}]$ into Equation (A16) and noting the condition in Equation (A4) while integrating with respect to z and ξ gives the in-plane stability matrix $[S_i]$ given by:

$$[S_i] = \frac{bt\pi^2}{\lambda} \int_0^1 \sigma_z[\{X\} \{X\}^T + \{Y\} \{Y\}^T] d\eta \quad (A20)$$

The integration of both the stiffness and stability matrices is accomplished numerically by using Simpson's rule or the Gaussian integration method.

Appendix B

In order to evaluate the tangential stiffness, $(K_T)_{ij}$, the expressions for e_{1j} , e_{2j} and e_{3j} must be defined. These expressions are given as follows;

$$\begin{aligned}
 e_{1j} = & [1 + U'_0] \frac{\partial N}{\partial q_j} + N \frac{\partial U'_0}{\partial q_j} - V''_0 \frac{\partial M}{\partial q_j} - M \frac{\partial V''_0}{\partial q_j} \\
 & + \left[\frac{K\pi C_z}{l} \frac{V'_0}{\sqrt{1 - (V'_0)^2}} + K S_z \frac{V''_0}{(1 - (V'_0)^2)^{\frac{3}{2}}} \right] \frac{\partial N}{\partial q_j} \\
 & + N \left[\frac{K\pi C_z}{l} \left(\frac{1}{\sqrt{1 - (V'_0)^2}} + \frac{(V'_0)^2}{(1 - (V'_0)^2)^{\frac{3}{2}}} \right) \right. \\
 & \left. + 3K S_z \frac{V'_0 V''_0}{(1 - (V'_0)^2)^{\frac{3}{2}}} \right] \frac{\partial V'_0}{\partial q_j} + N K S_z \frac{1}{(1 - (V'_0)^2)^{\frac{3}{2}}} \frac{\partial V''_0}{\partial q_j} \quad (B1)
 \end{aligned}$$

$$\begin{aligned}
 e_{2j} = & \frac{\partial A_2}{\partial q_j} \\
 = & V'_0 \frac{\partial N}{\partial q_j} + N \frac{\partial V'_0}{\partial q_j} \\
 & - \frac{V'_0 V''_0}{\sqrt{1 - (V'_0)^2}} \left(2 + \frac{(V'_0)^2}{1 - (V'_0)^2} \right) \frac{\partial M}{\partial q_j} \\
 & - M \left[\frac{V'_0}{\sqrt{1 - (V'_0)^2}} \left(2 + \frac{(V'_0)^2}{1 - (V'_0)^2} \right) \frac{\partial V''_0}{\partial q_j} \right. \\
 & \left. + \frac{V''_0}{\sqrt{1 - (V'_0)^2}} \left(2 + \frac{3(V'_0)^4}{(1 - (V'_0)^2)^2} + \frac{5(V'_0)^2}{1 - (V'_0)^2} \right) \frac{\partial V'_0}{\partial q_j} \right] \\
 & + \frac{V'_0 V''_0}{1 - (V'_0)^2} \left[1 + \frac{(V'_0)^2}{1 - (V'_0)^2} \right] \frac{\partial M^*}{\partial q_j} \\
 & + M^* \left[\frac{2V'_0 V''_0}{1 - (V'_0)^2} \left(1 + \frac{(V'_0)^2}{1 - (V'_0)^2} \right) \frac{\partial V''_0}{\partial q_j} \right. \\
 & \left. + \frac{(V''_0)^2}{1 - (V'_0)^2} \left(1 + \frac{4(V'_0)^4}{(1 - (V'_0)^2)^2} + \frac{5(V'_0)^2}{1 - (V'_0)^2} \right) \frac{\partial V'_0}{\partial q_j} \right] \\
 & + \left[3K S_z (1 + U'_0) \frac{V'_0 V''_0}{(1 - (V'_0)^2)^{\frac{3}{2}}} - \frac{K\pi C_z}{l} (1 + U'_0) \right. \\
 & \left. \left(\frac{1}{\sqrt{1 - (V'_0)^2}} + \frac{V'_0}{(1 - (V'_0)^2)^{\frac{3}{2}}} \right) \right]
 \end{aligned}$$

$$\begin{aligned}
& - \frac{K^2 \pi^2 C_z^2}{l^2} \left(\frac{V'_0}{1 - (V'_0)^2} + \frac{(V'_0)^3}{(1 - (V'_0)^2)^2} \right) \\
& - \frac{K^2 \pi C_z S_z}{2l} \left(\frac{V''_0}{(1 - (V'_0)^2)^2} + \frac{4(V'_0)^2 V''_0}{(1 - (V'_0)^2)^3} \right) \\
& - 3K^2 S_z^2 \frac{(V''_0)^2 V'_0}{(1 - (V'_0)^2)^4} - \frac{K \pi C_z}{l} \left] \frac{\partial N}{\partial q_j} \right. \\
& + 3K S_z \frac{V'_0 (V''_0)^2}{(1 - (V'_0)^2)^{\frac{5}{2}}} \frac{\partial M}{\partial q_j} + N \left[3K S_z \frac{V'_0 V''_0}{(1 - (V'_0)^2)^{\frac{5}{2}}} \right. \\
& - \left. \frac{K \pi C_z}{l} \left(\frac{1}{\sqrt{1 - (V'_0)^2}} + \frac{V'_0}{(1 - (V'_0)^2)^{\frac{3}{2}}} \right) \right] \frac{\partial U'_0}{\partial q_j} \\
& + N \left[3K S_z (1 + U'_0) \left(\frac{V''_0}{(1 - (V'_0)^2)^{\frac{5}{2}}} + \frac{5(V'_0)^2 V''_0}{(1 - (V'_0)^2)^{\frac{7}{2}}} \right) \right. \\
& - \left. \frac{K \pi C_z}{l} (1 + U'_0) \left(\frac{V'_0}{1 - (V'_0)^2} + \frac{1}{(1 - (V'_0)^2)^{\frac{3}{2}}} \right) \right. \\
& + \left. \frac{3(V'_0)^2}{(1 - (V'_0)^2)^{\frac{5}{2}}} \right] - \frac{K^2 \pi^2 C_z^2}{l^2} \left(\frac{1}{1 - (V'_0)^2} \right. \\
& + \left. \frac{4(V'_0)^2}{(1 - (V'_0)^2)^2} + \frac{4(V'_0)^4}{(1 - (V'_0)^2)^3} \right) \\
& - \frac{K^2 \pi C_z S_z}{l} \left(\frac{6V'_0 V''_0}{(1 - (V'_0)^2)^3} + \frac{12(V'_0)^3 V''_0}{(1 - (V'_0)^2)^4} \right) \\
& - 3K^2 S_z^2 \left(\frac{(V'_0)^2}{(1 - (V'_0)^2)^4} + \frac{8(V''_0)^2 (V'_0)^2}{(1 - (V'_0)^2)^5} \right) \left] \frac{\partial V'_0}{\partial q_j} \right. \\
& + N \left[3K S_z (1 + U'_0) \frac{V'_0}{(1 - (V'_0)^2)^{\frac{5}{2}}} - \frac{K^2 \pi C_z S_z}{l} \left(\frac{1}{2(1 - (V'_0)^2)^2} \right. \right. \\
& + \left. \left. \frac{2(V'_0)^2}{(1 - (V'_0)^2)^3} \right) - 6K^2 S_z^2 \frac{V'_0 V''_0}{(1 - (V'_0)^2)^4} \right] \frac{\partial V''_0}{\partial q_j} \\
& + 3K S_z M \left[\frac{(V''_0)^2}{(1 - (V'_0)^2)^{\frac{5}{2}}} + \frac{5(V'_0)^2 (V''_0)^2}{(1 - (V'_0)^2)^{\frac{7}{2}}} \right] \frac{\partial V'_0}{\partial q_j} \\
& + 6M K S_z \frac{V'_0 V''_0}{(1 - (V'_0)^2)^{\frac{5}{2}}} \frac{\partial V''_0}{\partial q_j} \tag{B2}
\end{aligned}$$

$$\begin{aligned}
e_{3j} &= \frac{\partial A_3}{\partial q_j} \\
&= - \left[1 + U'_0 + \frac{(V'_0)^2}{\sqrt{1 - (V'_0)^2}} \right] \frac{\partial M}{\partial q_j} + V''_0 \left[1 + \frac{(V'_0)^2}{1 - (V'_0)^2} \right] \frac{\partial M^*}{\partial q_j}
\end{aligned}$$

$$\begin{aligned}
& - M \left[\frac{\partial U'_o}{\partial q_j} + \frac{V'_o}{\sqrt{1 - (V'_o)^2}} \left(2 + \frac{(V'_o)^2}{1 - (V'_o)^2} \right) \frac{\partial V'_o}{\partial q_j} \right] \\
& + M^* \left[\left(1 + \frac{(V'_o)^2}{1 - (V'_o)^2} \right) \frac{\partial V''_o}{\partial q_j} \right. \\
& + \left. \frac{2V'_o V''_o}{1 - (V'_o)^2} \left(1 + \frac{(V'_o)^2}{1 - (V'_o)^2} \right) \frac{\partial V'_o}{\partial q_j} \right] \\
& + \left[\frac{K^2 \pi C_z S_z}{2l} \frac{V'_o}{(1 - (V'_o)^2)^2} + K^2 S_z^2 \frac{V''_o}{(1 - (V'_o)^2)^3} \right. \\
& - \left. K S_z (1 + U'_o) \frac{V''_o}{(1 - (V'_o)^2)^{\frac{3}{2}}} \right] \frac{\partial N}{\partial q_j} \\
& - \left[K S_z \frac{V''_o}{(1 - (V'_o)^2)^{\frac{3}{2}}} (1 + V''_o) \right] \frac{\partial M}{\partial q_j} \\
& - N K S_z \frac{V''_o}{(1 - (V'_o)^2)^{\frac{3}{2}}} \frac{\partial U'_o}{\partial q_j} + N \left[\frac{K^2 \pi C_z S_z}{2l} \right. \\
& \left. \left(\frac{1}{(1 - (V'_o)^2)^2} + \frac{4(V'_o)^2}{(1 - (V'_o)^2)^3} \right) \right. \\
& + \left. K^2 S_z^2 \frac{6V'_o V''_o}{(1 - (V'_o)^2)^4} - K S_z (1 + U'_o) \frac{3V'_o V''_o}{(1 - (V'_o)^2)^{\frac{3}{2}}} \right] \frac{\partial V'_o}{\partial q_j} \\
& + N \left[K^2 S_z^2 \frac{1}{(1 - (V'_o)^2)^3} - K S_z (1 - U'_o) \frac{1}{(1 - (V'_o)^2)^{\frac{3}{2}}} \right] \frac{\partial V''_o}{\partial q_j} \\
& - M \left[K S_z \frac{3V'_o V''_o}{(1 - (V'_o)^2)^{\frac{3}{2}}} (1 + V''_o) \right] \frac{\partial V'_o}{\partial q_j} \\
& - K S_z \frac{1}{(1 - (V'_o)^2)^{\frac{3}{2}}} M [1 + 2V''_o] \frac{\partial V''_o}{\partial q_j} \tag{B3}
\end{aligned}$$

On substitution of these equations into Equation (6.36) the tangential stiffness coefficients can be obtained upon numerical integration. This is accomplished by using the Gaussian integration technique.

Incremental stress resultants:

The incremental stress resultants $\frac{\partial N}{\partial q_j}$, $\frac{\partial M}{\partial q_j}$ and $\frac{\partial M^*}{\partial q_j}$ can be evaluated from Equations (6.50). The b_{1j} , b_{2j} and b_{3j} components in the incremental stress

resultants are

$$\begin{aligned}
b_{1j} = & [1 + U'_o] \frac{\partial U'_o}{\partial q_j} + V'_o \frac{\partial V'_o}{\partial q_j} \\
& - \left[\frac{K\pi C_z}{l} \frac{V'_o}{\sqrt{1 - (V'_o)^2}} + K S_z \frac{V''_o}{(1 - (V'_o)^2)^{\frac{3}{2}}} \right] \frac{\partial U'_o}{\partial q_j} \\
& - \left[\frac{K\pi C_z}{l} (1 + U'_o) \left(\frac{1}{\sqrt{1 - (V'_o)^2}} + \frac{(V'_o)^2}{(1 - (V'_o)^2)^{\frac{3}{2}}} \right) \right. \\
& + 3K S_z (1 + U'_o) \frac{V'_o V''_o}{(1 - (V'_o)^2)^{\frac{5}{2}}} - \frac{K^2 \pi^2 C_z^2}{2l^2} \\
& \left. \left(\frac{1}{1 - (V'_o)^2} + \frac{2(V'_o)^2}{(1 - (V'_o)^2)^2} \right) \right. \\
& - \left. \frac{K^2 \pi C_z S_z}{2l} \left(\frac{V''_o}{(1 - (V'_o)^2)^2} + \frac{4(V'_o)^2 V''_o}{(1 - (V'_o)^2)^{\frac{3}{2}}} \right) \right. \\
& - \left. 3K^2 S_z^2 \frac{(V''_o)^2 V'_o}{(1 - (V'_o)^2)^4} - \frac{K\pi C_z}{l} \right] \frac{\partial V'_o}{\partial q_j} \\
& - \left[K S_z (1 + U'_o) \frac{V''_o}{(1 - (V'_o)^2)^{\frac{3}{2}}} - \frac{K^2 \pi C_z S_z}{2l} \frac{V'_o}{(1 - (V'_o)^2)^2} \right. \\
& \left. - K^2 S_z^2 \frac{V''_o}{(1 - (V'_o)^2)^3} \right] \frac{\partial V''_o}{\partial q_j} \tag{B4}
\end{aligned}$$

$$\begin{aligned}
b_{2j} = & V''_o \frac{\partial U'_o}{\partial q_j} + \frac{V'_o V''_o}{\sqrt{1 - (V'_o)^2}} \left[2 + \frac{(V'_o)^2}{1 - (V'_o)^2} \right] \frac{\partial V'_o}{\partial q_j} \\
& + \left[1 + U'_o + \frac{(V'_o)^2}{\sqrt{1 - (V'_o)^2}} \right] \frac{\partial V''_o}{\partial q_j} \\
& - 3K S_z \frac{V'_o (V''_o)^2}{(1 - (V'_o)^2)^{\frac{5}{2}}} \frac{\partial V'_o}{\partial q_j} - \left[K S_z \frac{V''_o}{(1 - (V'_o)^2)^{\frac{3}{2}}} \right. \\
& \left. + K S_z \frac{(V''_o)^2}{(1 - (V'_o)^2)^{\frac{3}{2}}} \right] \frac{\partial V''_o}{\partial q_j} \tag{B5}
\end{aligned}$$

$$\begin{aligned}
b_{3j} = & \frac{V'_o (V''_o)^2}{1 - (V'_o)^2} \left[1 + \frac{(V'_o)^2}{1 - (V'_o)^2} \right] \frac{\partial V'_o}{\partial q_j} \\
& + V''_o \left[1 + \frac{(V'_o)^2}{1 - (V'_o)^2} \right] \frac{\partial V''_o}{\partial q_j} \tag{B6}
\end{aligned}$$

The evaluation of the stress resultants is achieved by using a continuous stress-strain-temperature relationship of a Ramberg-Osgood type. Details of the

numerical calculation of the incremental stress resultants can be found in the INSTAF manual.

Appendix C

Derivatives of displacement functions:

The derivatives of the displacement functions are

$$\begin{aligned}
 \frac{\partial U}{\partial x} &= -e - 2\frac{Z_c}{\lambda}\kappa\left(\frac{1}{2} - \xi\right) + U_r\frac{\partial f_r^u}{\partial x} \\
 \frac{\partial U}{\partial y} &= U_r\frac{\partial f_r^u}{\partial y} \\
 \frac{\partial V}{\partial x} &= \kappa\cos\pi\xi\sin\gamma + V_r\frac{\partial f_r^v}{\partial x} \\
 \frac{\partial V}{\partial y} &= ve + \frac{C_v}{b} + V_r\frac{\partial f_r^v}{\partial y} \\
 \frac{\partial W}{\partial x} &= -\kappa\cos\pi\xi\cos\gamma + W_r\frac{\partial f_r^w}{\partial x} \\
 \frac{\partial^2 W}{\partial x^2} &= \frac{\kappa\pi}{\lambda}\sin\pi\xi\cos\gamma + W_r\frac{\partial^2 f_r^w}{\partial x^2} \\
 \frac{\partial W}{\partial y} &= W_r\frac{\partial f_r^w}{\partial y} \\
 \frac{\partial^2 W}{\partial y^2} &= W_r\frac{\partial^2 f_r^w}{\partial y^2} \\
 \frac{\partial^2 W}{\partial x\partial y} &= W_r\frac{\partial^2 f_r^w}{\partial x\partial y}
 \end{aligned} \tag{C1}$$

Derivatives of strain increment:

In order to evaluate the gradient of the live energy function with respect to the displacement parameters the strain increment derivatives with respect to the displacement parameters have to be evaluated first. The partial derivatives of the strain increment are

$$\left\{ \frac{\partial(\Delta\epsilon)}{\partial\chi_i} \right\} = \frac{\partial(\Delta\epsilon)}{\partial\{U_r V_r W_r \kappa C_v\}} \tag{C2}$$

where

$$\left\{ \frac{\partial\Delta\epsilon}{\partial U_r} \right\} = \left\{ \begin{array}{c} \frac{\partial f_r^u}{\partial x} \\ 0 \\ \frac{\partial f_r^u}{\partial y} \end{array} \right\}$$

$$\begin{aligned}
\left\{ \frac{\partial \Delta \epsilon}{\partial V_r} \right\} &= \left\{ \begin{array}{c} \left(\frac{\partial \Delta V}{\partial x} + \frac{\partial V}{\partial x} \right) \frac{\partial f_r^u}{\partial x} \\ \left(1 + \frac{\partial \Delta V}{\partial y} + \frac{\partial V}{\partial y} \right) \frac{\partial f_r^u}{\partial y} + \left(\frac{\partial \Delta V}{\partial x} + \frac{\partial V}{\partial x} \right) \frac{\partial f_r^u}{\partial y} \end{array} \right\} \\
\left\{ \frac{\partial \Delta \epsilon}{\partial W_r} \right\} &= \left\{ \begin{array}{c} \left(\frac{\partial \Delta W}{\partial x} + \frac{\partial W}{\partial x} \right) \frac{\partial f_r^w}{\partial x} - z \frac{\partial^2 f_r^w}{\partial x^2} \\ \left(\frac{\partial \Delta W}{\partial y} + \frac{\partial W}{\partial y} \right) \frac{\partial f_r^w}{\partial y} - z \frac{\partial^2 f_r^w}{\partial y^2} \\ \left(\frac{\partial \Delta W}{\partial y} + \frac{\partial W}{\partial y} \right) \frac{\partial f_r^w}{\partial x} + \left(\frac{\partial \Delta W}{\partial x} + \frac{\partial W}{\partial x} \right) \frac{\partial f_r^w}{\partial y} - 2z \frac{\partial^2 f_r^w}{\partial x \partial y} \end{array} \right\} \\
\left\{ \frac{\partial \Delta \epsilon}{\partial \kappa} \right\} &= \left\{ \begin{array}{c} \frac{2Z_c}{\lambda} \left(\frac{1}{2} - \xi \right) + \cos \pi \xi \sin \gamma \left(\frac{\partial \Delta V}{\partial x} + 2 \frac{\partial V}{\partial x} \right) \\ - \cos \pi \xi \cos \gamma \left(\frac{\partial \Delta W}{\partial x} + 2 \frac{\partial W}{\partial x} \right) - z \frac{\pi}{\lambda} \sin \pi \xi \cos \gamma \\ 0 \\ \cos \pi \xi \sin \gamma \left(1 + \frac{\partial \Delta V}{\partial y} + 2 \frac{\partial V}{\partial y} \right) \\ - \cos \pi \xi \cos \gamma \left(\frac{\partial \Delta W}{\partial y} + 2 \frac{\partial W}{\partial y} \right) \end{array} \right\} \\
\left\{ \frac{\partial \Delta \epsilon}{\partial C_v} \right\} &= \left\{ \begin{array}{c} 0 \\ \frac{1}{b} \left(\frac{\partial \Delta V}{\partial x} + 2 \frac{\partial V}{\partial x} \right) \end{array} \right\} \quad (C3)
\end{aligned}$$

Gradient of live energy:

The gradient of the function F_e is

$$\begin{aligned}
\frac{\partial F_e}{\partial U_r} &= \frac{\partial \Delta \Phi^I}{\partial U_r} \\
&= \int_v \left(\sigma_x \frac{\partial f_r^u}{\partial x} + \tau_{xy} \frac{\partial f_r^u}{\partial y} \right) dv \\
&= \int_A \left(N_x \frac{\partial f_r^u}{\partial x} + N_{xy} \frac{\partial f_r^u}{\partial y} \right) dA \\
\frac{\partial F_e}{\partial V_r} &= \frac{\partial \Delta \Phi^I}{\partial V_r} \\
&= \int_v \left(\sigma_x \left(\frac{\partial \Delta V}{\partial x} + \frac{\partial V}{\partial x} \right) \frac{\partial f_r^v}{\partial x} + \sigma_y \frac{\partial f_r^v}{\partial y} \right. \\
&\quad \left. + \tau_{xy} \left(\left(1 + \frac{\partial \Delta V}{\partial y} + \frac{\partial V}{\partial y} \right) \frac{\partial f_r^v}{\partial x} + \left(\frac{\partial \Delta V}{\partial x} + \frac{\partial V}{\partial x} \right) \frac{\partial f_r^v}{\partial y} \right) \right) dv \\
&= \int_A \left(\left(N_x \left(\frac{\partial \Delta V}{\partial x} + \frac{\partial V}{\partial x} \right) + N_{xy} \left(1 + \frac{\partial \Delta V}{\partial y} + \frac{\partial V}{\partial y} \right) \right) \frac{\partial f_r^v}{\partial x} \right.
\end{aligned}$$

$$\begin{aligned}
& + \left(N_y + N_{xy} \left(\frac{\partial \Delta V}{\partial x} + \frac{\partial V}{\partial x} \right) \right) \frac{\partial f_r^v}{\partial y} \Big) dA \\
\frac{\partial F_c}{\partial W_r} &= \frac{\partial \Delta \Phi^I}{\partial W_r} \\
&= \int_v \left(\sigma_x \left(\left(\frac{\partial \Delta W}{\partial x} + \frac{\partial W}{\partial x} \right) \frac{\partial f_r^w}{\partial x} - z \frac{\partial^2 f_r^w}{\partial x^2} \right) \right. \\
&+ \sigma_y \left(\left(\frac{\partial \Delta W}{\partial y} + \frac{\partial W}{\partial y} \right) \frac{\partial f_r^w}{\partial y} - z \frac{\partial^2 f_r^w}{\partial y^2} \right) \\
&+ \tau_{xy} \left(\left(\frac{\partial \Delta W}{\partial y} + \frac{\partial W}{\partial y} \right) \frac{\partial f_r^w}{\partial x} + \left(\frac{\partial \Delta W}{\partial x} + \frac{\partial W}{\partial x} \right) \frac{\partial f_r^w}{\partial y} \right. \\
&\left. \left. - 2z \frac{\partial^2 f_r^w}{\partial x \partial y} \right) \right) dv \\
&= \int_A \left(\left(N_x \left(\frac{\partial \Delta W}{\partial x} + \frac{\partial W}{\partial x} \right) + N_{xy} \left(\frac{\partial \Delta W}{\partial y} + \frac{\partial W}{\partial y} \right) \right) \frac{\partial f_r^w}{\partial x} \right. \\
&+ \left(N_y \left(\frac{\partial \Delta W}{\partial y} + \frac{\partial W}{\partial y} \right) + N_{xy} \left(\frac{\partial \Delta W}{\partial x} + \frac{\partial W}{\partial x} \right) \right) \frac{\partial f_r^w}{\partial y} \\
&\left. - \left(M_x \frac{\partial^2 f_r^w}{\partial x^2} + M_y \frac{\partial^2 f_r^w}{\partial y^2} + 2M_{xy} \frac{\partial^2 f_r^w}{\partial x \partial y} \right) \right) dA \\
\frac{\partial F_c}{\partial \kappa} &= \frac{\partial \Delta \Phi^I}{\partial \kappa} \\
&= \int_v \left(\sigma_x \left(2 \frac{Z_c}{\lambda} \left(\frac{1}{2} - \xi \right) + \cos \pi \xi \sin \gamma \left(\frac{\partial \Delta V}{\partial x} + 2 \frac{\partial V}{\partial x} \right) \right. \right. \\
&+ \left. \left. - \cos \pi \xi \cos \gamma \left(\frac{\partial \Delta W}{\partial x} + 2 \frac{\partial W}{\partial x} \right) - z \frac{z}{\lambda} \sin \pi \xi \cos \gamma \right) \right. \\
&+ \tau_{xy} \left(\cos \pi \xi \sin \gamma \left(1 + \frac{\partial \Delta V}{\partial y} + 2 \frac{\partial V}{\partial y} \right) \right. \\
&\left. \left. - \cos \pi \xi \cos \gamma \left(\frac{\partial \Delta W}{\partial y} + 2 \frac{\partial W}{\partial y} \right) \right) \right) dv \\
&= \int_A \left(N_x 2 \frac{Z_c}{\lambda} \left(\frac{1}{2} - \xi \right) + \left(N_x \left(\frac{\partial \Delta V}{\partial x} + 2 \frac{\partial V}{\partial x} \right) \right. \right. \\
&+ \left. \left. N_{xy} \left(1 + \frac{\partial \Delta V}{\partial y} + 2 \frac{\partial V}{\partial y} \right) \right) \cos \pi \xi \sin \gamma \right. \\
&+ \left(N_x \left(\frac{\partial \Delta W}{\partial x} + 2 \frac{\partial W}{\partial x} \right) + N_{xy} \left(\frac{\partial \Delta W}{\partial y} + 2 \frac{\partial W}{\partial y} \right) \right) (-\cos \pi \xi \cos \gamma) \\
&+ \left. M_x \left(-\frac{\pi}{\lambda} \sin \pi \xi \cos \gamma \right) \right) dA
\end{aligned}$$

$$\begin{aligned}
\frac{\partial F_c}{\partial C_v} &= \frac{\partial \Delta \Phi^I}{\partial C_v} \\
&= \int_v \left(\sigma_v \frac{1}{b} + \tau_{xy} \left(\frac{1}{b} \left(\frac{\partial \Delta V}{\partial x} + 2 \frac{\partial V}{\partial x} \right) \right) \right) dv \\
&= \int_A \left(\left(N_y + N_{xy} \left(\frac{\partial \Delta V}{\partial x} + 2 \frac{\partial V}{\partial x} \right) \right) \frac{1}{b} \right)
\end{aligned} \tag{C4}$$

where

$$\begin{aligned}
\frac{\partial f_r^u}{\partial x} &= \frac{m\pi}{\lambda} ((1 - \eta)u_{1m} + \eta u_{2m}) \cos \pi m \xi \\
\frac{\partial f_r^u}{\partial y} &= \frac{1}{b} (-u_{1m} + u_{2m}) \sin \pi m \xi \\
\frac{\partial f_r^v}{\partial x} &= -\frac{n\pi}{\lambda} ((1 - \eta)v_{1n} + \eta v_{2n}) \sin n\pi \xi \\
\frac{\partial f_r^v}{\partial y} &= \frac{1}{b} (-v_{1n} + v_{2n}) \cos n\pi \xi \\
\frac{\partial f_r^w}{\partial x} &= \frac{p\pi}{\lambda} \left((1 - 3\eta^2 + 2\eta^3)w_{1p} + (\eta - 2\eta^2 + \eta^3)b\Theta_{1p} \right. \\
&\quad \left. + (3\eta^2 - 2\eta^3)w_{2p} + (\eta^3 - \eta^2)b\Theta_{2p} \right) \cos p\pi \xi \\
\frac{\partial^2 f_r^w}{\partial x^2} &= -\left(\frac{p\pi}{\lambda} \right)^2 \left((1 - 3\eta^2 + 2\eta^3)w_{1p} + (\eta - 2\eta^2 + \eta^3)b\Theta_{1p} \right. \\
&\quad \left. + (3\eta^2 - 2\eta^3)w_{2p} + (\eta^3 - \eta^2)b\Theta_{2p} \right) \sin p\pi \xi \\
\frac{\partial f_r^w}{\partial y} &= \left((-6\eta + 6\eta^2) \frac{w_{1p}}{b} + (1 - 4\eta + 3\eta^2)\Theta_{1p} \right. \\
&\quad \left. + (6\eta - 6\eta^2) \frac{w_{2p}}{b} + (3\eta^2 - 2\eta)\Theta_{2p} \right) \sin p\pi \xi \\
\frac{\partial^2 f_r^w}{\partial y^2} &= \left((-6 + 12\eta) \frac{w_{1p}}{b^2} + (-4 + 6\eta) \frac{\Theta_{1p}}{b} \right. \\
&\quad \left. + (6 - 12\eta) \frac{w_{2p}}{b^2} + (6\eta - 2) \frac{\Theta_{2p}}{b} \right) \sin p\pi \xi \\
\frac{\partial^2 f_r^w}{\partial x \partial y} &= \frac{p\pi}{\lambda} \left((-6\eta + 6\eta^2) \frac{w_{1p}}{b} + (1 - 4\eta + 3\eta^2)\Theta_{1p} \right. \\
&\quad \left. + (6\eta - 6\eta^2) \frac{w_{2p}}{b} + (3\eta^2 - 2\eta)\Theta_{2p} \right) \cos p\pi \xi
\end{aligned} \tag{C5}$$

where

u_{1m} , u_{2m} , v_{1n} , v_{2n} , w_{1p} , Θ_{1p} , w_{2p} and Θ_{2p} are the displacement and rotation parameters.